Analyse morphologique et biomécanique de l'épaule et du membre supérieur des enfants avec une paralysie obstétricale du plexus brachial : impact sur les thérapeutiques

Christelle Pons

UNIVERSITE BIOLOGIE BRETAGNE SANTE LOIRE

UBO
Université de Bretagne Occidentale

THESE DE DOCTORAT DE

L'UNIVERSITE
DE BRETAGNE OCCIDENTALE
COMUE UNIVERSITE BRETAGNE LOIRE

ECOLE DOCTORALE N° 605
Biologie Santé
Spécialité : *Analyse et traitement de l'information et des images médicales*

Par
Christelle PONS

Analyse morphologique et biomécanique de l'épaule et du membre supérieur des enfants avec une paralysie obstétricale du plexus brachial: impact sur les thérapeutiques.

Thèse présentée et soutenue à Brest, le 5 décembre 2018
Unité de recherche : LaTIM INSERM UMR 1101

Rapporteurs avant soutenance :

Laurence CHEZE	Professeur, Université Lyon 1
Franck FITOUSSI	Professeur, Université Pierre et Marie Curie

Composition du Jury :

Laurence CHEZE	Professeur, Université Lyon 1
Franck FITOUSSI	Professeur, Université Pierre et Marie Curie
Présidente du Jury Marie-Agnès GIROUX-METGES	Professeur, Université Bretagne Loire
Raphael GROSS	Maître de conférences, Université Bretagne Loire
Directeur de Thèse Sylvain BROCHARD	Professeur, Université Bretagne Loire
Co-Directrice de Thèse Valérie BURDIN	Professeur, Institut Mines Telecom

Remerciements

Merci à toutes celles et ceux qui m'ont soutenue durant ces quatre années de thèse.

Merci à Sylvain Brochard, Professeur à l'université Bretagne Loire, directeur de thèse, qui a accepté depuis plus de 8 ans de m'aider dans ma formation scientifique et médicale. Son enthousiasme à toute épreuve associée à une rigueur non négociable m'impressionneront toujours. Merci à lui pour sa patience, sa disponibilité et son soutien.

Merci à Valérie Burdin, Professeure à l'Insitut Mines Telecom, directrice de thèse, pour sa bienveillance, sa disponibilité et son aide qui m'a été particulièrement utile lors des questionnements sur la segmentation.

Merci au Professeure Laurence Chèze, Professeure à l'Université Lyon 1, qui avait déjà été rapporteur pour mon mémoire de master 2, d'avoir accepté d'être à nouveau rapporteur pour cette thèse et membre du jury. Votre expertise en biomécanique de l'épaule enrichira ce travail.

Merci au Professeur Franck Fitoussi, Professeur à l'Université Pierre et Marie Curie d'avoir accepté d'être rapporteur et membre de jury. La lecture et l'évaluation de ce travail par un chirurgien orthopédique est un honneur.

Merci au Professeure Marie Agnes Giroux Metges et au Docteur Raphael Gross qui m'ont fait l'honneur d'accepter d'être membre du jury.

Merci aux membres de l'équipe du LaTIM qui m'ont aidée lors des différents travaux de cette thèse, Mathieu Lempereur, Bhushan Borotikar, Pierre-Henri Conze, Marc Garetier, Douraied Ben Salem et Asma Salhi.

Merci à l'équipe américaine du FAB pour la collaboration enrichissante lors de mon master 2 et de ma thèse.

Merci à toutes les personnes ayant accepté de participer au projet POPBtox, investigateurs, chef de projet, attachée de recherche clinique (Dauphou Eddi, Mélanie Pelouin, Nathaly Quintero, Marianne Alison, Grégoire le Gal, Madeleine Aslan, Jennifer Bastien, Gilles Dautel, Floriane Colin, Marion Delpont, Bruno Dohin, Marie Agnes Galloy, Vincent Gautheron, Salem Hassan Al Khoury, Pascal Jehanno , Mélanie Kaas, Olivier Prodhomme, Mélanie Porte, Anne Gaelle Py, Helène Rauscent, Emilie Rumilly, Katherine Sanchez Barr, Catherine Tréguier, Philippe Violas).

Merci à l'équipe médicale et paramédicale de Ty Yann d'avoir accepté mes présences en pointillé et mes défaillances d'organisation ces derniers mois, avec une pensée spéciale pour Laetitia, Agathe, Valentine et France.

Enfin merci à mes amis et ma famille, à mes deux petits bonshommes et à Thomas.

Table des matières

Introduction synthétique

Le plexus brachial est un plexus nerveux situé à la base du cou ayant pour principale fonction l'innervation du membre supérieur. Les fibres nerveuses qui forment le plexus brachial sont issues des rameaux ventraux des nerfs spinaux cervicaux et thoraciques (de C5 à T1).
La paralysie obstétricale du plexus brachial (POPB) est une parésie d'un ou des deux membres supérieurs causée le plus souvent par un étirement excessif des racines nerveuses du plexus brachial lors d 'une naissance difficile. Les racines C5 et C6, innervant majoritairement l'épaule, sont les plus fréquemment touchées.
La majorité des parésies est temporaire. La récupération neurologique est toutefois absente ou incomplète dans environ 20% des cas. Les enfants avec une atteinte nerveuse plus grave garderont des séquelles à vie comprenant une perte de force, une perte de mobilité passive et active impactant les activités de vie quotidienne.

L'épaule permet l'orientation dans l'espace du membre supérieur. Elle comprend cinq articulations (articulations gléno-huémrale, sterno-costo-claviculaire, acromio-claviculaire, scapulo-thoracique et sous deltoidienne). Sa mobilité doit être la plus importante possible pour que la préhension se fasse dans un espace maximisé. Cette mobilité est en grande partie autorisée par l'articulation gléno-humérale. Chez les enfants avec POPB sans récupération complète, l'atteinte de l'épaule et plus particulièrement de l'articulation gléno-humérale, est la principale cause de morbidité. L'atteinte des muscles mobilisant l'articulation gléno-humérale est à l'origine d'une diminution de leur force et de la limitation de la mobilité active et passive de cette articulation impactant la mobilité de l'ensemble du membre supérieur. Cette atteinte musculaire est également à l'origine d'un changement au niveau des contraintes mécaniques s'exerçant sur l'articulation gléno-humérale à l'origine de sa déformation tridimensionnelle. Cette déformation, bien décrite et connue, gêne à son tour le fonctionnement musculaire et le mouvement.

Chez ces enfants avec POPB, les principaux objectifs thérapeutiques sont la récupération maximale de la motricité, la lutte contre les rétractions musculaires et les déformations

articulaires pour l'obtention d'une bonne mobilité du membre supérieur. Une attention spécifique est portée à l'épaule.

La compréhension précise de l'atteinte des muscles de l'épaule ainsi que de l'organisation du mouvement dans cette population pourrait permettre d'améliorer les thérapeutiques proposées.

L'exploration clinique de l'atteinte des muscles gléno-huméraux et des limitations de la mobilité de l'épaule et de l'ensemble du membre supérieur, n'est pas suffisante pour cet objectif. Elle ne permet en effet pas d'obtenir des données quantifiées et précises sur l'atteinte individuelle des muscles et sur la limitation du mouvement.
Dans un objectif de compréhension plus précise du fonctionnement de l'épaule et de l'ensemble du membre supérieur chez l'enfant avec POPB et d'orientation des choix thérapeutiques, d'autres explorations telles que l'IRM et l'analyse quantifiée du mouvement peuvent compléter l'examen clinique. L'IRM permet l'obtention de données quantitatives sur la morphologie de chaque muscle, notamment leur forme et leur volume liés à la fonction musculaire. L'analyse quantifiée du mouvement permet la décomposition des mouvements dans chaque articulation pour une tâche donnée et peut évaluer la performance du mouvement.

La contribution que nous soumettons dans ce document **porte sur l'évaluation de l'atteinte des muscles de l'épaule** ainsi que sur **l'analyse du mouvement des membres supérieurs chez l'enfant avec POPB sans récupération complète**. Après une introduction générale du contexte présentant la paralysie obstétricale du plexus brachial, les problématiques rencontrées dans cette pathologie et les thérapeutiques proposées, **les chapitres ont été regroupés par thématique de recherche**. Le chapitre II porte sur **l'étude morphologique musculaire en IRM** et présente une contribution de **3 articles**. Le chapitre III porte sur l'analyse du mouvement des membres supérieurs et fait l'objet de **l'article 4** qui fournit des précisions sur les propriétés métrologiques des techniques permettant de quantifier les volumes et formes musculaires chez des enfants avec développement typique et chez des enfants avec POPB. A partir des résultats des chapitres II et III, le chapitre IV présente une discussion des perspectives d'exploration du fonctionnement de l'épaule chez l'enfant en particulier une segmentation

automatique développée par notre équipe est présentée en annexe 3. Enfin, fort de ces réflexions, un **essai thérapeutique de prévention précoce de la déformation musculo-squelettique** faisant l'objet de **l'article 5** est proposé dans le chapitre V.

I Contexte

1 Anatomie de l'épaule et du membre supérieur

Les éléments anatomiques préalables à la compréhension de nos travaux sont présentés ci-dessous.

Le membre supérieur est constitué de trois segments : bras, avant-bras et main. Il est relié au tronc par l'épaule. Le coude relie le bras à l'avant-bras et le poignet relie l'avant-bras à la main *(figure 1)*.

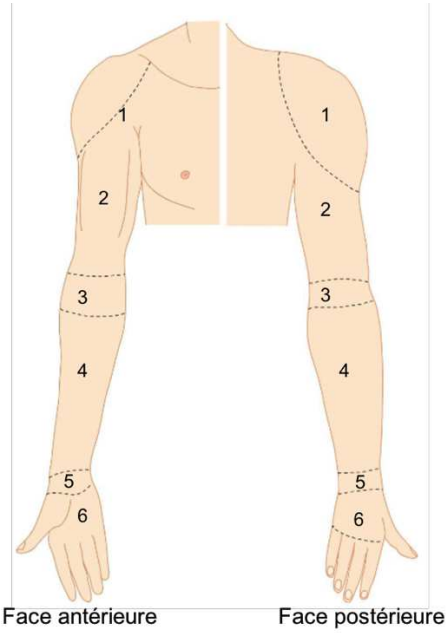

Figure 1 : le membre supérieur
1 : épaule, 2 : bras, 3 : coude, 4 : avant-bras, 5 : poignet, 6 : main

Cette section ne repose pas sur une revue complète de la littérature. Elle est basée sur les références (Kamina et Gouazé 2009; Kapandji et Tubiana 2005; Netter 2015; Forro et Lowe 2018). Étant donné les conséquences importantes de l'atteinte du plexus brachial au niveau de l'épaule et plus spécifiquement de l'articulation gléno-humérale chez les enfants avec POPB, les chapitres en lien seront plus particulièrement développés.

1.1 Les os

1.1.1 La clavicule

La clavicule est un os court, cylindrique située entre le sternum et la scapula. Vue de dessus, elle dessine un S italique.

1.1.2 La scapula

La scapula (*figure 2*) est un os de forme triangulaire avec 2 faces (antérieure et postérieure), 3 bords (latéral, médial et supérieur) et 3 angles (supérieur, inférieur et externe). Au niveau de l'angle externe, en regard de l'humérus, se trouve une surface articulaire, appelée glène. Elle est orientée en dehors, en avant et légèrement vers le haut (Ohl et al. 2012). Sa concavité est moins marquée que celle de la tête humérale (Kapandji et Tubiana 2005). La glène est presque plane favorisant l'amplitude des mouvements de l'articulation gléno-humérale. La face antérieure de la scapula est concave et appliquée contre le thorax alors que la face postérieure est plutôt convexe. Aux trois quarts supérieurs de la face postérieure se trouve l'épine de la scapula qui divise la face postérieure en 2 : la fosse sus-épineuse et la fosse sous épineuse. L'acromion est le prolongement de l'épine de la scapula qui va s'articuler avec la clavicule. Il forme une arcade avec le processus coracoïde. La scapula se situe le plus souvent en regard de la 1ère à la 7ème côte.

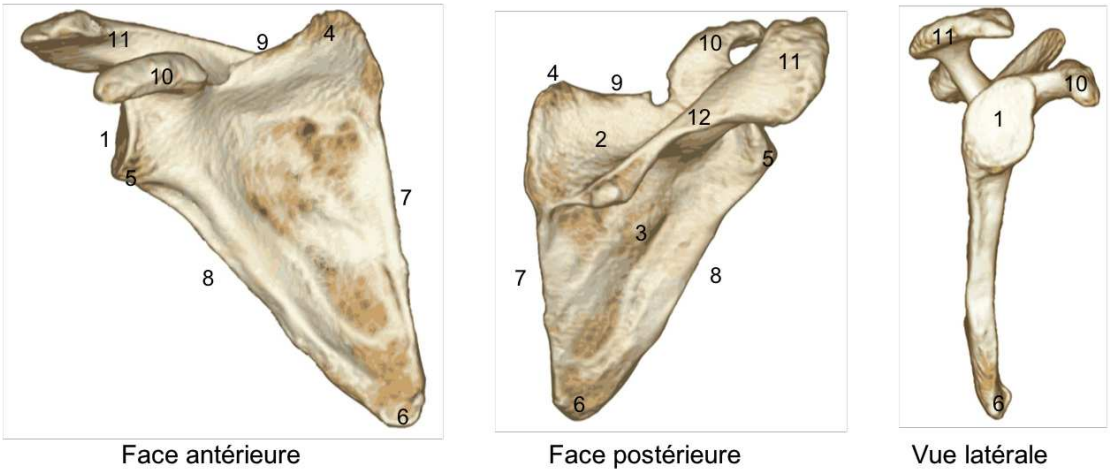

Figure 2 : Repères anatomiques de la scapula

1 : glène, 2 : fosse sus épineuse, 3 : fosse sous épineuse, 4 : angle supérieur, 5, angle latéral, 6 : angle inférieur, 7 : bord médial, 8 : bord latéral, 9 : bord supérieur, 10 : processus coracoïde, 11 : acromion, 12 : épine de la scapula.
https://www.imaios.com/fr/e-Anatomy/Membres/Membre-superieur-Schemas

1.1.3 L'humérus

L'humérus (*figure 3*) est un os long qui s'articule dans son extrémité supérieure (tête humérale) avec la glène de l'omoplate et dans son extrémité inférieure avec le radius et l'ulna. La tête humérale est orientée en haut, en dedans et en arrière. On l'assimile à un tiers de sphère (Kapandji et Tubiana 2005). Les muscles péri-articulaires viennent s'insérer sur 2 saillies : le tubercule mineur en avant et le tubercule majeur en dehors. Au niveau de l'extrémité inférieure, on retrouve la palette humérale et deux points facilement palpables : l'épicondyle médial et l'épicondyle latéral.

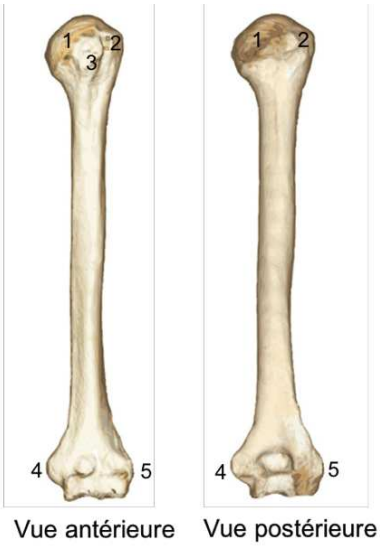

Figure 3 : Repères anatomiques de l'humérus
1 : tête humérale, 2 : tubercule majeur, 3 : tubercule mineur, 4 : épicondyle médial, 5 : épicondyle latéral
https://www.imaios.com/fr/e-Anatomy/Membres/Membre-superieur-Schemas

1.1.4 Le radius

Le radius est l'os antéro latéral de l'avant-bras. C'est un os long qui s'articule en haut avec l'humérus, en haut et en dedans avec l'ulna, en bas avec l'ulna et le carpe. Son corps est plus volumineux en bas. Il présente une courbure permettant le mouvement de prono-supination. Au niveau de l'extrémité inférieure, le processus styloïde radial est facilement palpable.

1.1.5 L'ulna

L'ulna est l'os postéro médial de l'avant-bras. C'est un os long qui s'articule en haut avec l'humérus, en haut et en dehors avec le radius, latéralement avec le radius et en bas avec le ligament intra articulaire qui s'articule lui-même avec le carpe. Au niveau de l'extrémité inférieure, le processus styloïde ulnaire est facilement palpable.

1.1.6 Os de la main et du poignet

La main est formée de 27 os constants répartis en 3 groupes : le carpe, le métacarpe et les phalanges.

1.2 Les articulations

1.2.1 Complexe articulaire de l'épaule

L'épaule est le complexe articulaire le plus mobile de l'organisme. Elle comprend **cinq articulations mécaniquement liées** (*Figure 4)*. On compte trois articulations vraies : gléno-humérale, sterno-costo-claviculaire, acromio-claviculaire et deux articulations physiologiques (espaces de glissement) : scapulo-thoracique et sous deltoidienne (Kapandji et Tubiana 2005).

Dans le premier groupe (articulations anatomiques) on retrouve :
- **l'articulation gléno-humérale**. C'est une enarthrose, composée par la tête humérale et la glène de la scapula dont la concavité est peu marquée et renforcée par le bourrelet glénoidien. Son appareil capsulo-ligamentaire est suffisamment lâche pour permettre sa grande mobilité. Une **participation musculaire** est nécessaire pour assurer la coaptation des deux surfaces articulaires dans toutes les positions.
- l'articulation sterno-costo-claviculaire. C'est l'élément de jonction articulaire du membre supérieur au squelette axial.
- l'articulation acromio-claviculaire. C'est le seul élément reliant la scapula au reste du squelette axial.

Dans le deuxième groupe (articulations physiologiques) on retrouve :

- **l'articulation scapulo-thoracique**. C'est un **espace de glissement** de la scapula sur la cage thoracique. Cet espace est constitué d'une interface de plusieurs tissus mous. Cette articulation est très liée mécaniquement aux articulations acromio-claviculaire et sternoclaviculaire.

- l'articulation sous acromiale est la connexion entre l'arcade coraco-acromiale et la tête humérale. Cette articulation est mécaniquement liée à la gléno-humérale.

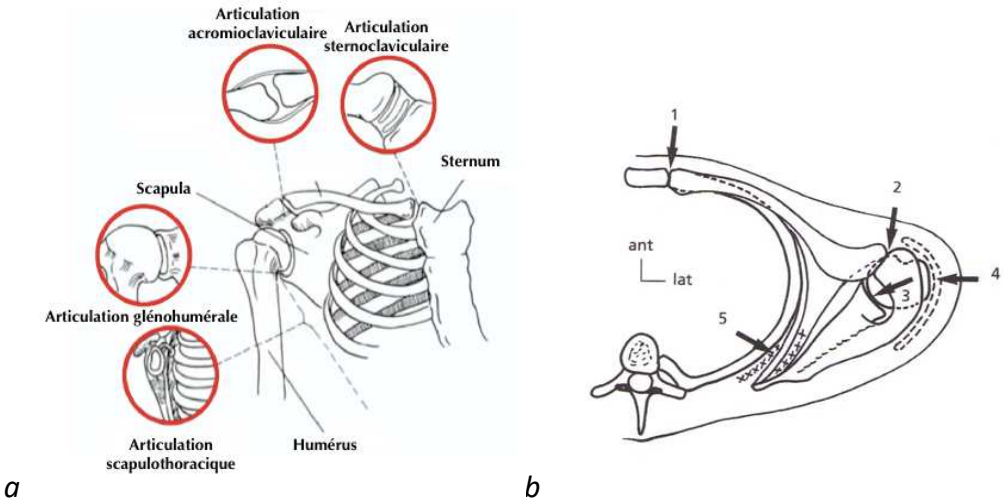

Figure 4
a : Les 3 os et 4 des articulations du complexe de l'épaule. L'articulation sous acromiale peut être considérée comme une articulation physiologique supplémentaire.
b : Vue supérieure des articulations du complexe de l'épaule, montrant en particulier en 5 l'espace de glissement scapulo-thoracique (1 : sternoclaviculaire, 2 : acromio-claviculaire, 3: scapulohumérale, 4 : sous acromiale)
(Issu de Dufour, 2005)

La **mobilité de l'épaule doit être la plus importante possible** pour que la préhension se fasse dans un espace maximisé. L'épaule est, avec ses 3 axes de travail et ses 3 degrés de liberté articulaire, le complexe le plus mobile de l'organisme.

Les mouvements principaux du complexe de l'épaule (*figure 5*) peuvent être décomposés en:

- flexion qui élève le bras vers l'avant
- extension, qui porte le bras en arrière
- adduction, qui rapproche le bras de l'axe du corps
- abduction, qui élève le bras sur le côté
- rotation interne, qui correspond à une rotation autour de l'axe huméral vers l'intérieur
- rotation externe, qui correspond à une rotation autour de l'axe huméral vers l'extérieur.

Les mouvements de flexion-extension, abduction-adduction et rotation interne-externe permettent l'orientation de l'humérus par rapport au thorax dans les trois plans de l'espace et autorisent le mouvement de circumduction de l'épaule (Veeger et van der Helm 2007). Lors de ces différents mouvements, les cinq articulations fonctionnent simultanément et dans des proportions variables (Veeger et van der Helm 2007; Hurov 2009).

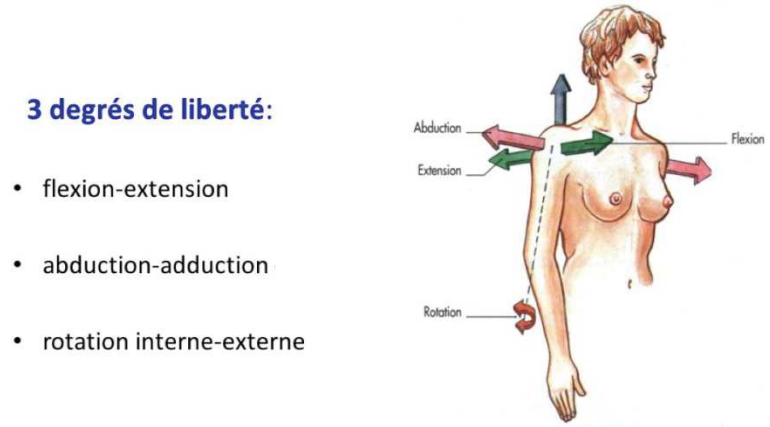

Figure 5 : les mouvements globaux de l'épaule
https://slideplayer.fr/slide/171630

Au niveau de l'articulation scapulo-thoracique, si l'on considère le système de coordonnées locales défini par l'International Society of Biomechanics (ISB), le mouvement le plus important de la scapula est sa **rotation latérale autour d'un axe antéro-postérieur** (medial-lateral rotation). La rotation selon l'axe vertical s'appelle **protraction** (sens antihoraire) et **rétraction** (sens horaire) (internal/external rotation). Le mouvement de la scapula autour d'un axe frontal est appelé **tilt antéropostérieur**. La bascule est antérieure lorsque l'angle inférieur de la scapula s'éloigne du thorax (Figure 6).

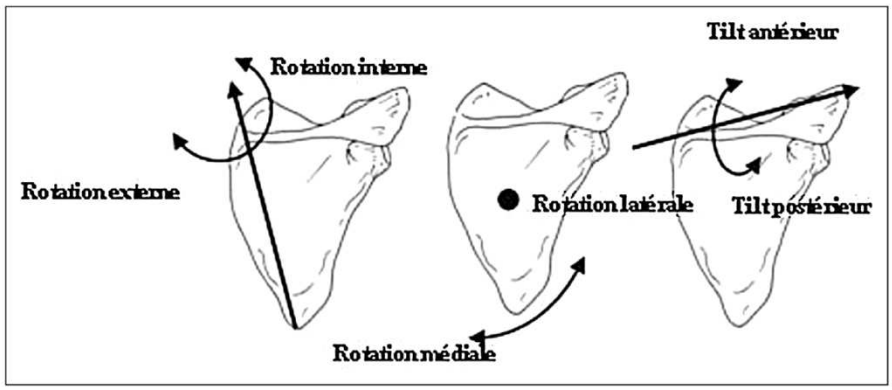

Figure 6 : mouvements de l'articulation scapulo-thoracique
(Issu de Nguyen C, 2015)

Au niveau de l'articulation gléno-humérale, la morphologie de la tête humérale et de la glène, qui ont une forme similaire mais des rayons de courbures différents, facilite les mouvements amples (Veeger et van der Helm 2007; Hurov 2009). Les contractions coordonnées des muscles de l'épaule assurent le centrage dynamique de la tête de l'humérus dans la glène (Veeger et van der Helm 2007; Hurov 2009).

Le mouvement scapulo-huméral ou gléno-huméral peut se décomposer en :

- abduction physiologique qui est l'écartement dans le plan de la scapula (c'est à dire environ 45°)
- flexion-extension qui s'effectue dans un plan perpendiculaire au plan de la scapula.
- rotations axiales qui s'effectuent dans le plan transversal

L'international society of biomechanics (ISB) déconseille d'utiliser les termes de flexion et d'abduction car en fonction de l'ordre de la séquence (abduction/flexion ou flexion/ abduction) les résultats ne sont pas les mêmes. Il propose la décomposition par les rotations suivantes : plan d'élévation, élévation humérale et rotation axiale (Figure 7).

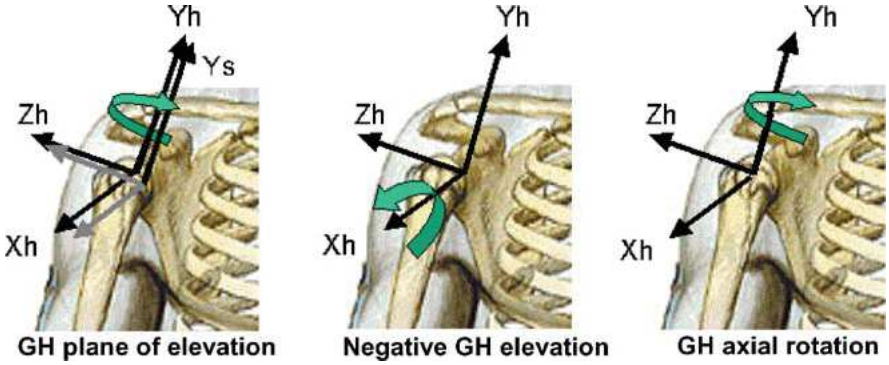

Figure 7 : Définition des mouvements gléno-huméraux.
(Issu de Wu G, 2005)

1.2.2 Articulations du coude

Le coude est composé de trois articulations ayant la même cavité articulaire : l'articulation huméro-ulnaire, l'articulation huméro-radiale et l'articulation radio-ulnaire proximale.

Les articulations huméro-ulnaire et huméro-radiale interviennent dans les mouvements de flexion extension de coude.

Les articulations radio-ulnaire proximale et distale, unissant respectivement les épiphyses proximales et distales, toutes deux trochoïdes, permettent des mouvements de rotation : la pronation et la supination.

1.2.3 Articulations du poignet

Les mouvements de la main sur l'avant-bras font intervenir de nombreuses articulations solidaires entre elles, comprenant l'articulation radio-carpienne et les articulations intercarpiennes (proximales, distales et médio-carpiennes).

Le poignet possède 3 degrés de liberté. Les mouvements de flexion extension se déroulent davantage dans l'articulation radio-carpienne. Les mouvements d'abduction-adduction se déroulent principalement dans l'articulation médio-carpienne. Des rotations légères se produisent dans l'articulation médio-carpienne.

1.2.4 Articulations de la main

Elles comprennent les articulations carpo-métacarpiennes, métacarpo-phalangiennes et interphalangiennes.

1.3 Les muscles

1.3.1 Muscles intervenant dans la mobilité du membre supérieur

Certains muscles du dos naissent du rachis et se terminent soit sur la ceinture du membre supérieur, soit sur l'humérus. Ils comprennent un groupe superficiel comprenant les muscles trapèze et grand dorsal et un groupe profond avec les muscles élévateurs de la scapula, petit rhomboïde et grand rhomboïde.

De même certains muscles du thorax se terminent sur la ceinture du membre supérieur ou sur l'humérus. Il s'agit des muscles grand pectoral, petit pectoral, subclavier et dentelé antérieur.

Les muscles de l'épaule naissent de la ceinture du membre supérieur et se terminent sur l'humérus. Ils comprennent 6 muscles : les muscles deltoïde, supraépineux, infraépineux, petit

rond, grand rond et subscapulaire *(figure 8)*. Les muscles supraépineux, infraépineux, et subscapulaire forment la coiffe des rotateurs. Avec le muscle grand pectoral, ces muscles seront ci-dessous appelés muscles gléno-huméraux du fait de leur rôle important dans la mobilisation de l'articulation gléno-humérale.

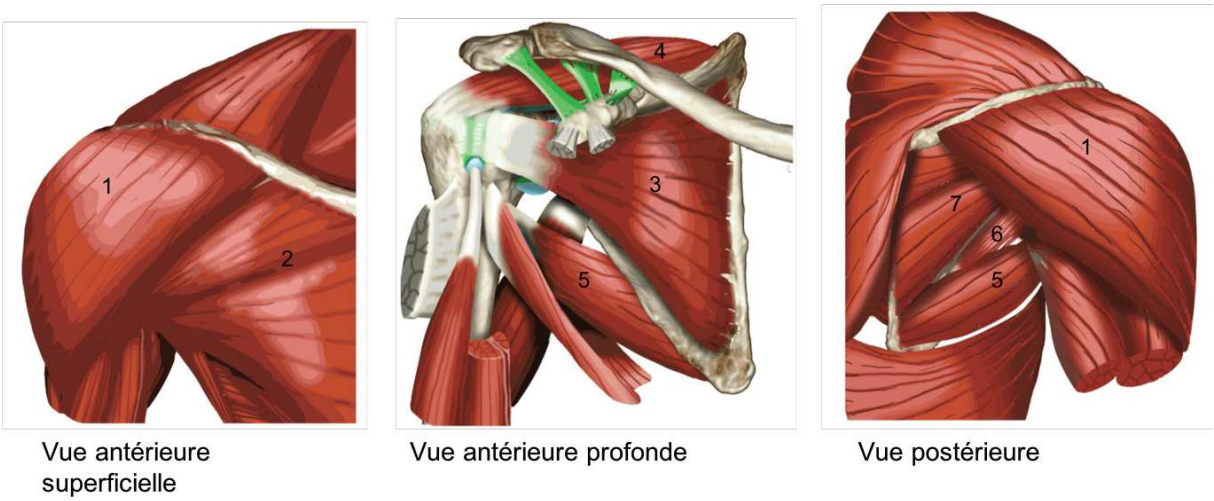

Figure 8 : muscles de l'épaule
1 : deltoïde, 2 : grand pectoral, 3 : subscapulaire, 4 : supraépineux, 5 : grand rond, 6 : infraépineux
https://www.imaios.com/fr/e-Anatomy/Membres/Membre-superieur-Schemas

Les muscles du bras comprennent deux groupes : un groupe antérieur comprenant les muscles biceps brachial, coraco-brachial et brachial et un groupe postérieur constitué du muscle triceps brachial.

Au niveau de l'avant-bras, la partie antérieure comprend 4 plans. Son plan superficiel comprend 4 muscles : les muscles brachio-radial, rond pronateur, fléchisseur radial du carpe, long palmaire et fléchisseur ulnaire du carpe. On retrouve ensuite les plans des muscles fléchisseurs superficiels et profonds des doigts. Enfin, le plan profond comprend les muscles supinateur et carré pronateur.

Les muscles postérieurs de l'avant-bras sont organisés en un plan superficiel comprenant les muscles long extenseur radial du carpe, court extenseur radial du carpe, extenseur commun des doigts, extenseur du petit doigt, extenseur ulnaire du carpe et anconé. Le plan profond est destiné essentiellement au pouce.

Enfin les muscles de la main comprennent 3 groupes, non détaillés ici : les muscles de l'éminence thénar destinés au pouce, les muscles de l'éminence hypothénar destinés au petit doigt et le groupe intermédiaire annexé à tous les doigts.

1.3.2 Fonction musculaire

Par leur contraction, les muscles ont un rôle dans la stabilité statique et dynamique des articulations.

Leur rôle dans la **stabilité statique** relève de la contraction musculaire isométrique durant laquelle la force musculaire équilibre une résistance.

Leur rôle dans la **stabilité dynamique** relève de la contraction musculaire isotonique qui provoque un mouvement de rotation du muscle (ou moment de la force musculaire). En fonction de leur **bras de levier**, les muscles seront dans une position plus ou moins favorable pour mobiliser l'articulation (J. M. M. Brown et al. 2007). Le bras de levier d'une force par rapport à un axe de rotation est la distance entre la ligne d'action de la force et l'axe de rotation *(figure 9)*. Le bras de levier varie en fonction de la position de l'articulation. La **ligne d'action** d'un muscle est la direction dans laquelle la force de ce muscle est appliquée. On peut distinguer les muscles mobilisateurs principaux, les muscles synergiques et les muscles antagonistes. Les **mobilisateurs principaux** (« prime movers ») sont activés précocement lors d'un mouvement et ont des fibres musculaires avec des lignes d'action proches de la direction du mouvement prévu avec un moment de force agoniste. Les **muscles synergiques** sont activés plus tardivement lors du mouvement et ont des lignes d'action légèrement divergentes par rapport à celles des mobilisateurs principaux mais conservent un moment de force agoniste. Les **muscles antagonistes** sont activés plus tardivement lors du mouvement et ont des lignes d'action dans des directions opposées à celle du mouvement, à l'origine d'un moment de force antagoniste (Wickham et Brown 1998; J. M. M. Brown et al. 2007). Des segments musculaires d'un même muscle peuvent avoir des rôles différents dans la mobilisation d'une articulation (J. M. M. Brown et al. 2007). En fonction de la position et de l'amplitude du mouvement réalisé, les bras de levier peuvent varier *(figure 9)*. Un muscle peut donc être impliqué uniquement dans une partie du mouvement (Hurov 2009).

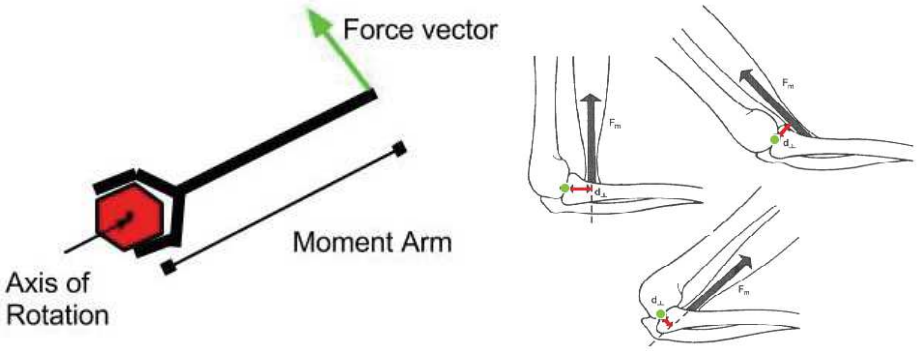

Figure 9 : bras de levier
A gauche : définition d'un bras de levier (moment arm)
https://stressoverstrain.wordpress.com/tag/torque/
A droite : illustration au niveau de l'épaule, le bras de levier change en fonction de la position. Il apparaît en rouge. La ligne d'action est la direction de la flèche noire.
http://oregonstate.edu/instruct/exss323/Angular_Kinetics/elbowmomentarm.htm

Par exemple, au niveau de l'articulation gléno-humérale, les muscles principalement impliqués dans chaque mouvement en tant que mobilisateurs principaux sont (J. M. M. Brown et al. 2007; Kuechle et al. 1997, 2000) :

- flexion : deltoïde antérieur, supraépineux, grand pectoral
- extension : deltoïde postérieur, grand rond, grand dorsal
- abduction : supra épineux, deltoïde
- adduction : grand pectoral, grand dorsal
- rotation interne : subscapulaire, grand pectoral
- rotation externe : infraépineux, petit rond

Les fonctions mobilisatrices principales de chaque muscle sont rapportées dans l'annexe 1.

1.4 Le plexus brachial

Le plexus brachial est un plexus nerveux situé à la base du cou. Il a pour principale fonction **l'innervation du membre supérieur**. Les fibres nerveuses qui forment le plexus brachial sont issues des rameaux ventraux des nerfs spinaux cervicaux et thoraciques (de **C5 à T1**) (Kattan et Borschel 2011; Bayot et Elzeftawy 2018).

Le plexus brachial s'organise successivement en **racines, troncs, divisions, faisceaux, branches terminales et nerfs périphériques** (Kattan et Borschel 2011) (*figure 10*).

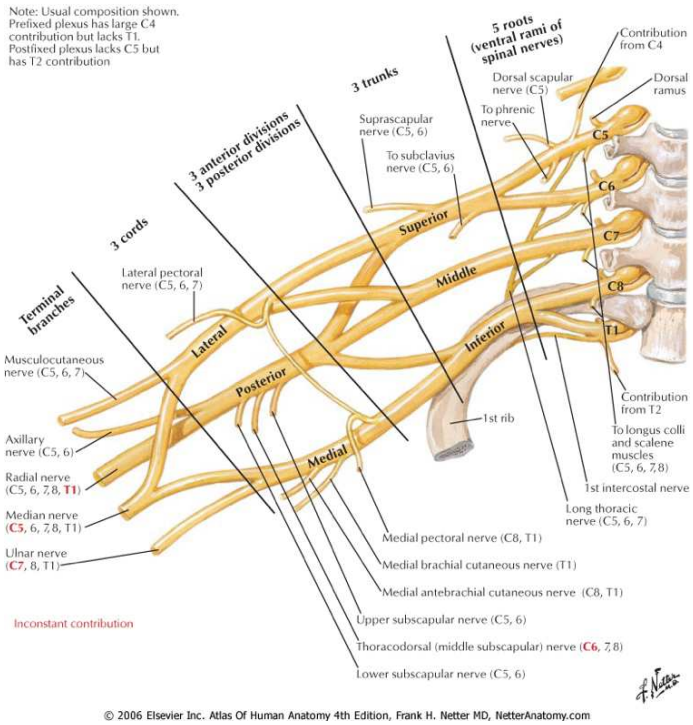

Figure 10 : le plexus brachial

Le plus souvent

- Les racines C5 et C6 fusionnent pour former le tronc supérieur du plexus brachial, la racine C7 est seule à l'origine du tronc moyen et les racines C8 et T1 fusionnent pour former le tronc inférieur
- Chacun de ces troncs se divise ensuite en une branche dorsale et une branche ventrale
- Les trois branches dorsales se réunissent pour former le faisceau postérieur. Les branches ventrales des troncs supérieur et moyen se réunissent pour former le faisceau latéral. La branche ventrale du tronc inférieur devient le faisceau médial.
- Les trois faisceaux forment le nerf musculo cutané, le nerf médian, le nerf ulnaire, le nerf radial et le nerf axillaire.

Différents **nerfs collatéraux** émergent des racines nerveuses, troncs et faisceaux. Ainsi, les racines donnent le nerf scapulaire dorsal issu de C5 ; le nerf thoracique long issu de C5, C6 ; et le premier nerf intercostal (T1). Le tronc supérieur donne le nerf supra-scapulaire et le nerf subclavier. Le faisceau latéral donne le nerf pectoral latéral. Le faisceau médial donne le nerf pectoral médial, les nerfs cutanés médiaux du bras et de l'avant-bras. Le faisceau postérieur donne le nerf subscapulaire supérieur, le nerf thoraco-dorsal et le nerf subscapulaire inférieur.

Le tableau en annexe 1 rapporte l'innervation des muscles intervenant dans la mobilité du membre supérieur (épaule coude poignet).

2 La paralysie obstétricale du plexus brachial

La paralysie obstétricale du plexus brachial (POPB) est une parésie d'un membre supérieur chez le bébé secondaire à une lésion du plexus brachial à la naissance.

2.1 Description de la maladie

La paralysie obstétricale du plexus brachial a une incidence estimée à **1.4/1000 naissances** (Chauhan, Blackwell, et Ananth 2014). Les facteurs de risque de POPB sont maternels (obésité, gain de poids excessif durant la grossesse, diabète, âge avancé), fœtaux (poids de naissance élevé), et liés à l'accouchement (accouchement par voie basse et plus particulièrement accouchement par le siège, dystocie des épaules, travail prolongé, utilisation de forceps et/ou de ventouse) (Mollberg et al. 2005; Okby et Sheiner 2012; Weizsaecker, Deaver, et Cohen 2007).

Les lésions obstétricales du plexus brachial sont le plus souvent causées par **un étirement excessif des racines nerveuses**, soit lors d'une traction sur la tête, soit lors d'une traction du membre supérieur (Abid 2016). La lésion du plexus brachial peut survenir de l'origine de la moelle épinière aux branches terminales (Kattan et Borschel 2011). Du fait de la complexité du plexus brachial, il existe une **grande diversité de combinaisons théoriques** de lésions au sein des éléments constituant le plexus brachial (Yang 2014). Les racines C5 et C6 sont les plus fréquemment touchées, éventuellement en association avec la racine C7. Le plexus complet est moins souvent atteint (Abid 2016; Zafeiriou et Psychogiou 2008). Les lésions proximales sont appelées « lésions pré-ganglionnaires » ou « avulsion de racine ». Les lésions plus distales sont appelées « lésions post-ganglionnaires ». Différents types d'atteintes nerveuses peuvent survenir dans ce cas : neurotmésis, axonotomésis et neurapraxie (Raducha et al. 2017; Abid 2016) (*figure 11*). Une **parésie du membre supérieur** survient avec atteinte des muscles en fonction de leur innervation radiculaire et de la gravité de la lésion des racines nerveuses.

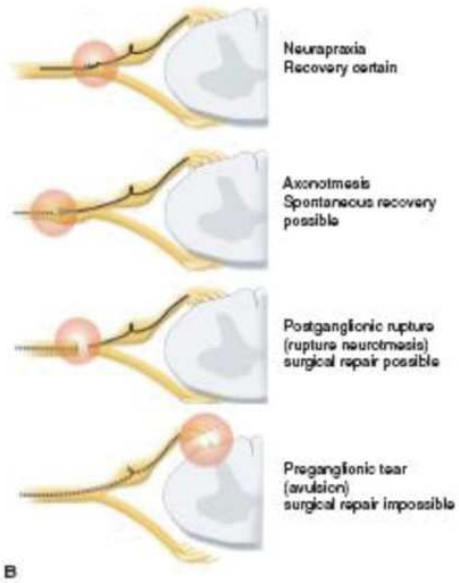

Figure 11 : Atteinte nerveuse du plexus brachial
Séquence de lésions nerveuses allant de l'avulsion, au neurotmesis, à la neurapraxie.
https://obgynkey.com/brachial-plexus-birth-palsy-microsurgery/

Narakas et Birch (Narakas 1987; Al-Qattan et al. 2009) ont proposé une classification en fonction de la présentation clinique :

- groupe I (C5-C6) avec parésie au niveau de l'épaule et du biceps, correspondant à l'atteinte la plus fréquente ; ce groupe est aussi appelé paralysie d'Erb
- groupe II (C5-C7) avec parésie au niveau de l'épaule, du biceps et des extenseurs de l'avant-bras
- groupe III (C5-T1) avec parésie complète du membre supérieur
- groupe IV avec parésie complète du membre supérieur et syndrome de Horner (associant un myosis, un ptosis et une anhydrose localisée).

La paralysie de Kumpke (C8-T1) est rare, avec parésie du poignet et de la main.

La majorité des parésies est temporaire. La récupération neurologique est **absente ou incomplète dans environ 20% des cas** (Chauhan, Blackwell, et Ananth 2014). La localisation de l'atteinte nerveuse (supérieure, inférieure, complète) et son importance (avulsion, rupture) conditionnent le pronostic de récupération (Zafeiriou et Psychogiou 2008; Yang 2014).

Les enfants avec une atteinte nerveuse plus grave garderont des **séquelles** comprenant, au sens de la classification internationale du fonctionnement (CIF), des **déficiences, une limitation des activités, des restrictions de participation et une réduction de la qualité de vie**

(Figure 12). Les déficiences seront majoritairement secondaires à l'atteinte musculo-squelettique avec une perte de force, une perte de mobilité passive et active. Les limitations des activités et restrictions de participation sont en lien avec la diminution de mobilité du membre supérieur et les conséquences esthétiques (Julka et Vander Have 2011; Zafeiriou et Psychogiou 2008; Sarac et al. 2013; Hulleberg et al. 2014; Squitieri et al. 2013; Bae, Waters, et Zurakowski 2008; Butler et al. 2017). Ainsi, les enfants pourront présenter des difficultés à l'écriture ou seront gênés dans leur participation aux activités sportives nécessitant des préhensions bimanuelles.

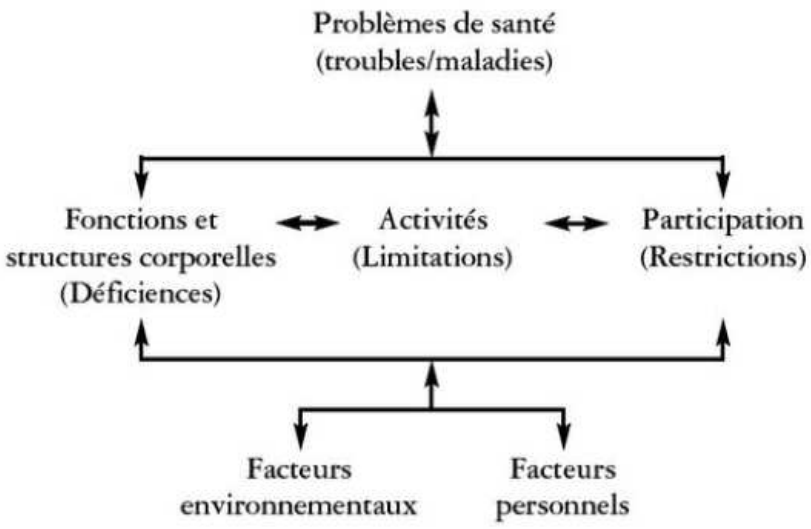

Figure 12 : Classification internationale du fonctionnement, du handicap et de la santé (CIF)
Les déficiences : désignent des problèmes dans la fonction organique où la structure anatomique tel qu'un écart ou une perte importante.
Les activités : désignent l'exécution d'une tâche ou d'une action par une personne.
La participation désigne l'implication d'une personne dans une situation de vie réelle.
Les limitations d'activités désignent les difficultés que rencontre une personne dans l'exécution d'activité.
Les restrictions de participation : désignent les problèmes qu'une personne peut rencontrer dans son implication dans une situation réelle.

2.2 Atteinte musculo-squelettique de l'épaule des enfants avec POPB

Chez les enfants avec POPB, les **conséquences musculo-squelettiques** de l'atteinte du plexus brachial et de la dénervation sont majeures au niveau de l'épaule et persistent à l'âge adulte (Partridge et Edwards 2004; Hulleberg et al. 2014). L'atteinte de l'épaule est la **principale cause de morbidité** dans cette population (Michael L. Pearl 2009; Julka et Vander Have 2011; Bahm et al. 2007; Sibinski et al. 2010; van Gelein Vitringa et al. 2009; Peter M. Waters et al. 2009; P. M. Waters, Smith et Jaramillo 1998).

Au niveau de l'épaule, on retrouve le plus souvent une rétraction en rotation interne ou une limitation importante des amplitudes articulaires passives en rotation externe, une limitation des amplitudes articulaires de l'épaule plus modérée dans les autres degrés de liberté, une diminution de force et des amplitudes articulaires actives.

2.2.1 Cercle vicieux de la déformation musculo-squelettique

Du fait de leur innervation, les muscles gléno-huméraux (Shenaq et al. 2005) sont systématiquement affectés chez les enfants avec POPB sans récupération complète. L'atteinte des muscles est à l'origine d'un **changement au niveau des contraintes mécaniques** s'exerçant sur l'articulation gléno-humérale et d'une déformation tridimensionnelle de celle-ci. Cette déformation gêne à son tour le fonctionnement musculaire et le mouvement. L'ensemble forme un cercle vicieux *(figure 13)*.

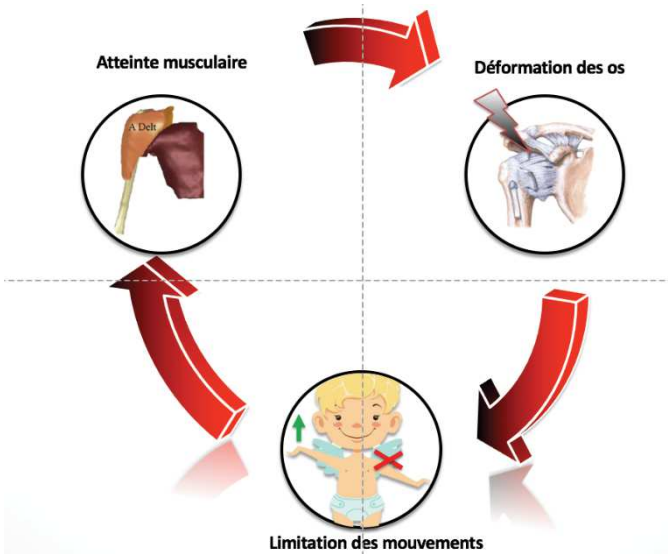

Figure 13 : cercle vicieux de l'atteinte de l'épaule chez les enfants avec POPB

2.2.2 Atteinte musculaire

La dénervation induit des modifications morphologiques et structurelles, physiologiques, métaboliques et biochimiques des muscles (Midrio 2006) ayant pour principale conséquence une altération de leurs propriétés contractiles. La diminution des sollicitations mécaniques, du fait de la parésie affectant l'ensemble du membre supérieur, a également des conséquences propres telles qu'une atrophie, ou un changement de composition des muscles

avec altération de leurs propriétés fonctionnelles (Clark, Cook et Ploutz-Snyder 2007; Giroux-Metges et al. 2005).

Chez l'enfant avec POPB, les études évaluant l'atteinte musculaire avaient le plus souvent pour objectif principal l'étude de l'impact de cette atteinte dans la genèse de la déformation osseuse *(figure 14)*. Dans ces études, **l'atteinte du muscle subscapulaire** est prédominante, avec une **atrophie marquée** (Hogendoorn et al. 2010; van Gelein Vitringa et al. 2009; Van Gelein Vitringa et al. 2011; Pöyhiä et al. 2005). La **structure histologique** de ce muscle est retrouvée altérée avec une augmentation de la raideur des fibres musculaires, une surface des fibres et une longueur sarcomérique plus faibles par rapport à des muscles du membre supérieur de sujets sans pathologie neuromusculaire, expliquant la rétraction en rotation interne d'épaule chez ces enfants (Einarsson et al. 2008). Une **atrophie notable du muscle infraépineux** est également montrée (van Gelein Vitringa et al. 2009; Van Gelein Vitringa et al. 2011; Pöyhiä et al. 2005). Les muscles deltoïde, grand pectoral et supra-épineux ont été peu étudiés, ils semblaient davantage préservés (Peter M. Waters et al. 2009; Van Gelein Vitringa et al. 2011; van Gelein Vitringa et al. 2009; Pöyhiä et al. 2005). Des corrélations entre les atteintes musculaires individuelles des muscles subscapulaire et infraépineux et la déformation osseuse de l'articulation gléno-humérale mesurée dans le plan axial (rétroversion de la glène, subluxation de l'humérus) ont été retrouvées (Hogendoorn et al. 2010; Pöyhiä et al. 2005; Van Gelein Vitringa et al. 2011; Peter M. Waters et al. 2009). Le muscle grand pectoral, à l'origine d'un déséquilibre musculaire entre les rotateurs internes et externes pourrait également être impliqué dans la genèse de la déformation osseuse (Peter M. Waters et al. 2009).

Différentes études traitant de l'atteinte musculaire ont été réalisées **chez l'animal**, notamment la souris ou le rat, chez lesquels des paralysies du plexus brachial ou des dénervations musculaires peuvent être réalisées lors d'expérimentations juste après la naissance. Chez ces animaux, une **dégénérescence musculaire avec infiltration graisseuse**, en lien avec une dysrégulation dans l'expression des gènes myogéniques et adipogènes (Das et al. 2011; H. M. Kim et al. 2010) est montrée suite à une dénervation du muscle supra-épineux. Des **déséquilibres musculaires** entre les rotateurs internes et externes (subscapulaire et infraépineux) et une perturbation de la croissance musculaire dans la genèse de la

déformation de l'articulation gléno-humérale se mettent en place. Ils sont à l'origine d'une **diminution des possibilités de rotation externe passive** d'épaule et d'une modification des contraintes mécaniques exercées sur l'os ayant pour conséquence la genèse de la déformation de l'articulation gléno-humérale (Soldado et al. 2014; Tatara et al. 2014). Ces études étant réalisées chez l'animal, leurs conclusions sont à interpréter avec précaution chez l'enfant avec POPB (Soldado et al. 2012).

Deux études, réalisées par une même équipe, ayant pour objectif principal de mieux comprendre les facteurs musculaires impliqués dans la genèse de la déformation, ont utilisé des modélisations biomécaniques de l'épaule (Crouch et al. 2014; Cheng et al. 2015). **Sept muscles** (infraépineux, subscapulaire, grand dorsal, chef long du biceps, deltoïde antérieur, grand pectoral, chef long du triceps) ont été identifiés comme pouvant produire une augmentation de la force postérieure s'appliquant sur l'articulation gléno-humérale et favorisant la rétroversion de la glène ainsi que la subluxation postérieure de la tête humérale (Crouch et al. 2014). **L'association des déséquilibres musculaires et de la perturbation de la croissance** de ces muscles aurait l'impact le plus fort, comparé au déséquilibre musculaire seul ou à la perturbation de la croissance isolée. Des implications pour la prise en charge des enfants avec POPB en étaient déduites. Ces études présentaient toutefois certaines limites. Tout d'abord, le modèle utilisait des données anatomiques provenant d'études caractérisant l'épaule chez l'adulte (Holzbaur, Murray, et Delp 2005). De plus, seul le plan transversal était considéré dans le raisonnement. Enfin, dans les modélisations, les atteintes simulées étaient les mêmes pour chaque muscle.

Chez l'enfant avec POPB, une dégénérescence des muscles d'importance variable suite à la dénervation survient. **L'atteinte du couple subscapulaire-infraépineux, de même que la perturbation de la croissance et les modifications de l'architecture du muscle subscapulaire sont des points clés dans la pathologie de l'épaule des enfants avec POPB.** Ces éléments sont impliqués dans la rétroversion de la glène et la migration postérieure de la tête de l'humérus. La majorité des études a cependant étudié un nombre restreint de muscles. **Les déséquilibres de forces et la perturbation des mouvements de l'épaule dans les trois plans de l'espace** (Brochard, Alter, et Damiano 2014), (paragraphe 2.3)**, la déformation tridimensionnelle de l'articulation gléno humérale** (Brochard et al. 2016; Frich, Schmidt et Torfing 2017) **et le**

potentiel impact de nombreux muscles dans la genèse de cette déformation dans les études de simulation (Cheng et al. 2015; Crouch et al. 2014) **sont des éléments montrant l'intérêt de chercher une atteinte plus globale des muscles de l'épaule et des déséquilibres dans les couples agonistes-antagonistes.** Une meilleure connaissance de l'atteinte de l'ensemble des muscles de l'épaule pourrait ainsi aider à la compréhension plus globale des limitations du mouvement et de la déformation tridimensionnelle de l'épaule.

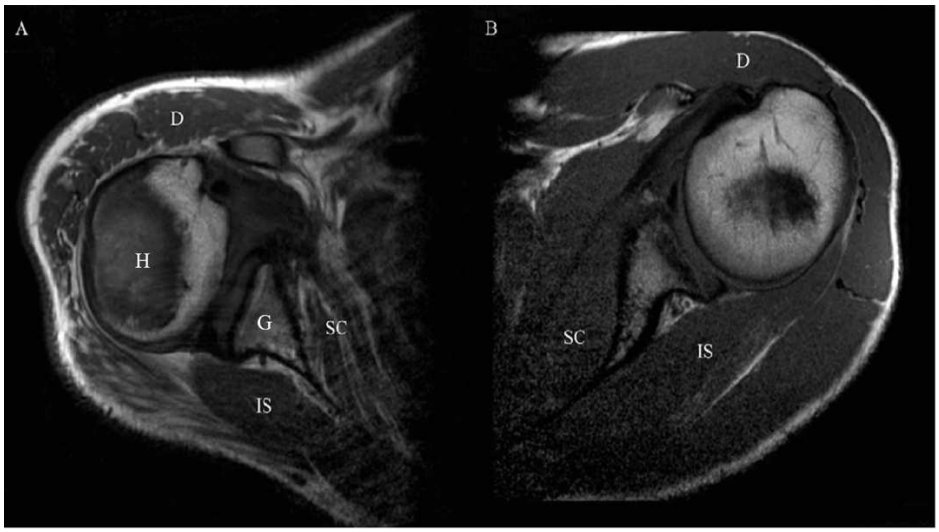

Figure 14 : Atteinte des muscles gléno-huméraux en IRM, déformation gléno-humérale associée
Coupes transversales T1 des épaules d'un enfant avec atteinte du plexus brachial droit
A : épaule atteinte, B : épaule non atteinte, D : deltoide, SS : subscapulaire, IS : infraépineux, G : glène, H : humérus.
(Issu de Hogendoorn S 2010).

2.2.3 Atteinte osseuse

Les déformations osseuses de l'articulation gléno-humérale (*figure 15*) surviennent **très précocement** dans les mois suivant la naissance (van der Sluijs et al. 2004; Van Gelein Vitringa et al. 2011; Greenhill et al. 2018; Iorio et al. 2015), principalement chez les enfants ayant une atteinte haute de plexus brachial (Bhardwaj et al. 2013; Hogendoorn et al. 2010). Ces déformations ont été étudiées dans de nombreux articles et sont désormais bien décrites (Bahm et al. 2007; Moukoko et al. 2004; Van der Sluijs et al. 2004; Van Gelein Vitringa et al. 2011; Van der Sluijs et al. 2001; Brochard et al. 2016; Frich, Schmidt et Torfing 2017; Eismann et al. 2015). Elles sont caractérisées par un **excès de rétroversion de la glène, une orientation vers le bas et une déformation de celle-ci, une migration postérieure, inférieure et médiale de la tête humérale** allant progressivement vers la luxation complète *(figure 15)* (Bahm et al.

2007; Moukoko et al. 2004; Van der Sluijs et al. 2004; Van Gelein Vitringa et al. 2011; Van der Sluijs et al. 2001; Brochard et al. 2016; Frich, Schmidt et Torfing 2017; Eismann et al. 2015).

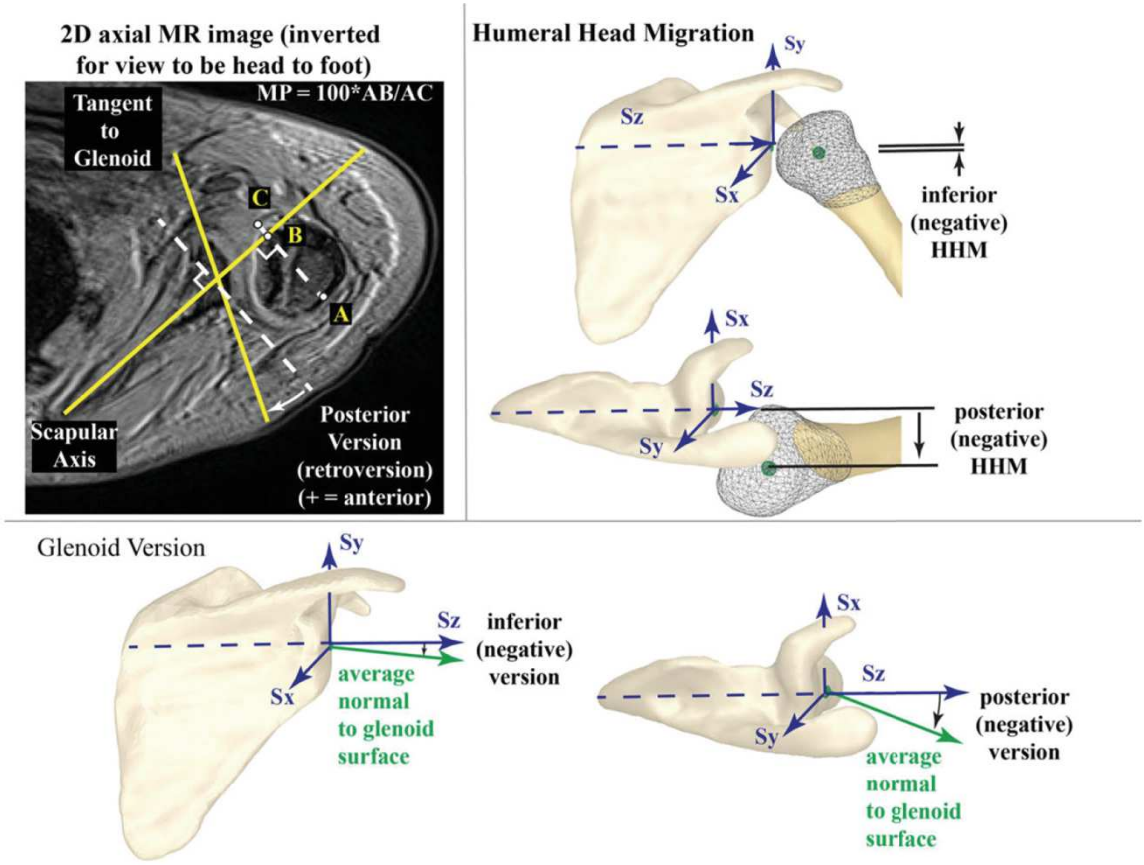

Figure 15 : Déformation de l'articulation gléno-humérale chez l'enfant avec POPB en IRM, bidimensionnelle et tridimensionnelle
En haut à gauche: coupe transversale IRM d'une épaule déformée chez un enfant avec POPB.
En haut à droite : migration de la tête humérale en arrière et en bas chez le même enfant.
En dessous : version glénoidienne avec orientation de la glène en arrière et en bas chez le même enfant.
(Issu de Brochard S, 2016)

2.3 Perturbation du mouvement chez les enfants avec POPB

La diminution de la fonction musculaire avec la perte de force suite à la dénervation, l'altération de la croissance et de la structure des muscles mais également les déformations osseuses, qui à leur tour limitent l'action des muscles du fait de la modification de leurs bras de levier (Peter M. Waters 2005; Hultgren et al. 2013; Kirkos et al. 2005; Nath et Paizi 2007) ont pour conséquence une **perturbation des mouvements du membre supérieur** atteint, de façon prédominante au niveau de l'**épaule** (Mayfield et al. 2017; Iorio et al. 2015; Talbert et al. 2011; Mosqueda et al. 2004; Russo et al. 2014). Dans certains travaux, une **participation**

centrale avec un phénomène d' « apraxie développementale » pourrait participer à cette perturbation du mouvement (Colon, Vredeveld et Blaauw 2007; Boylan et Fouladvand 2001; Anguelova et al. 2017)

Cette perturbation du mouvement est le principal facteur à l'origine des **limitations d'activité et restrictions de participation dans cette population**. La majorité des enfants avec POPB est décrite comme indépendante pour la plupart des activités de vie quotidiennes (s'habiller, faire sa toilette, s'alimenter) mais ces activités peuvent être ressenties comme difficiles par les enfants (Van der Holst et al. 2017; Hulleberg et al. 2014). Certaines tâches peuvent être particulièrement compliquées à effectuer, comme mettre le bras dans la manche d'un pull ou coincer un pull à l'arrière du pantalon pour les jeunes enfants, boutonner chez les enfants plus âgés (Sundholm, Eliasson, et Forssberg 1998; Spaargaren et al. 2011). La participation à certains sports peut s'avérer délicate (Sarac et al. 2013). La **dextérité du membre supérieur** atteint des enfants avec POPB mais également du membre supérieur sain est moins bonne que celle d'enfants présentant un développement typique (Aktaş et al. 2018; Immerman et al. 2012; Matthews 2018).

Chez les enfants avec POPB, l'épaule a été étudiée spécifiquement. **D'importantes limitations dans les amplitudes de mouvements dans les trois plans de l'espace au niveau de l'articulation gléno-humérale** (Herisson et al. 2017; Russo et al. 2014; Duff, Dayanidhi, et Kozin 2007), avec une très forte **limitation des mouvements en rotation externe** ont été décrites. La perturbation des mouvements de l'épaule du fait de la rétraction en rotation interne est à l'origine d'une modification des forces s'exerçant sur l'articulation gléno-humérale (Kleiber et al. 2013). Cette modification des forces durant le mouvement pourrait avoir à son tour un impact sur la **déformation osseuse** (Kleiber et al. 2013).

L'interdépendance du fonctionnement des articulations entre elles, mise en évidence dans cette population par la perturbation du rythme scapulo-huméral (Herisson et al. 2017; Russo et al. 2014; Duff, Dayanidhi, et Kozin 2007) avec une augmentation de la mobilité de la scapula pour compenser la limitation de mobilité de l'articulation gléno-humérale, montre l'intérêt d'une évaluation de l'ensemble des articulations du membre supérieur (Holzbaur, Murray et Delp 2005) chez ces enfants. Cela permettrait chez les enfants avec POPB une meilleure

compréhension des **stratégies de mouvement du membre supérieur** avec visualisation des **perturbations en lien avec l'atteinte du plexus brachial**, notamment au niveau de l'épaule, mais aussi des **éventuelles compensations** mises en place dans les articulations sus et sous-jacentes. Cela pourrait ainsi aider à la **compréhension des limitations d'activité** objectivées chez ces enfants et à l'orientation dans les propositions de prises en charge thérapeutiques.

2.4 Évaluation biomécanique et fonctionnelle des enfants avec POPB

L'examen clinique recherche la présence de **déformations, spécificités de positionnement et évalue la mobilité passive et active** de l'ensemble des articulations du membre supérieur (Michael L. Pearl 2009). Il est complété par une évaluation de **l'utilisation du membre supérieur** atteint de l'enfant au quotidien, des limitations d'activité, et des restrictions de participation (Sundholm, Eliasson et Forssberg 1998).

L'évaluation de la motricité passive consiste en l'examen des amplitudes articulaires passives dans les trois plans de l'espace. Pour l'évaluation de la motricité active, différentes échelles semi-quantitatives, facilement réalisables en consultation, sont utilisables. Elles permettent de standardiser l'examen du membre supérieur de l'enfant avec POPB. L'Active Movement Scale (AMS) (Curtis et al. 2002; Clarke et Curtis 1995) *(figure 16)* dans laquelle un score est donné aux groupes musculaires au niveau de l'ensemble du membre supérieur (rotateurs internes, extenseurs d'épaule, …) pour chaque mouvement en fonction de leur réalisation avec ou sans pesanteur et sur plus ou moins de la moitié de l'amplitude articulaire complète du mouvement évalué, le score de Toronto ou le British Medical Research Council Muscle Grading System (A. Bialocerkowski, O'shea et Pin 2013; Sarac et al. 2015) ont pour objectif d'évaluer la force. L'échelle de Mallet est très souvent utilisée (A. Bialocerkowski, O'shea et Pin 2013) *(figure 16)* pour évaluer les amplitudes actives du membre supérieur. Dans cette échelle, l'enfant doit réaliser différentes tâches (rotation externe, abduction, main à la bouche…) sélectionnées pour identifier les mouvements difficiles chez l'enfant avec POPB, notamment au niveau de l'épaule. La cotation se fait en utilisant un score allant de 1 à 5 (la cotation 5 représente un mouvement normal).

With gravity eliminated:
No contraction 0
Contraction without movement 1
Movement <½ of ROM 2
Movement >½ of ROM 3
Full movement 4
Against gravity:
Movement <½ of ROM 5
Movement >½ of ROM 6
Full movement 7

Clarke HM, Curtis CG. An approach to obstetrical brachial plexus injuries. Hand Clin. 1995, 11: 563–80. ROM - Range of Motion

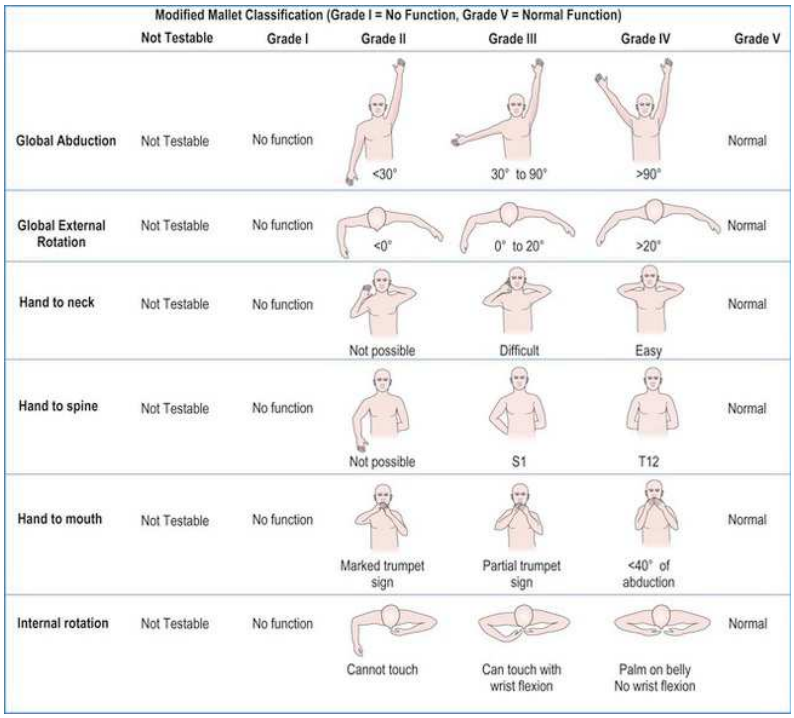

Figure 16 : exemples d'échelles d'évaluation des amplitudes articulaires actives
Au-dessus : échelle AMS, en dessous : échelle de Mallet modifiée

En pratique, les enfants avec POPB sont évalués principalement avec l'examen clinique. Les décisions thérapeutiques chez ces enfants sont réalisées principalement avec cet examen clinique. Il présente cependant certaines limites (Talbert et al. 2011):

- il ne permet pas d'obtenir des **données quantitatives**
- lors de la cotation des échelles, il existe un **risque d'erreur systématique** pour la notation de certains items, notamment chez le jeune enfant (A. Bialocerkowski, O'shea et Pin 2013; A. E. Bialocerkowski et Galea 2006)
- la **décomposition en sous items et l'individualisation des facteurs individuels** affectés sont limités.

Dans un objectif de compréhension plus précise du fonctionnement de l'épaule et de l'ensemble du membre supérieur chez l'enfant avec POPB et d'orientation des choix thérapeutiques, d'autres explorations telles que l'IRM et l'analyse quantifiée du mouvement peuvent compléter l'examen clinique. Ces explorations ne sont pas employées en pratique clinique courante mais sont utilisées actuellement dans un cadre de recherche.

Dans le cadre du questionnement sur l'atteinte musculaire des muscles gléno-huméraux, **l'IRM de l'épaule** semble particulièrement intéressante (Bahm et al. 2007; Pöyhiä et al. 2007; Peter M. Waters et al. 2009). En effet, cette technique d'imagerie non irradiante et non invasive permet l'évaluation quantitative de chaque muscle, dont l'accès individuel est impossible en clinique du fait de la complexité anatomique et fonctionnelle de l'épaule. L'IRM est largement utilisée dans l'évaluation morphologique du système locomoteur car la morphologie y est très en lien avec la fonctionnalité. Différents éléments morphologiques (volume, …) liés à la fonction musculaire sont mesurables et quantifiables pour chaque muscle en IRM et représentent un intérêt dans l'étude et la compréhension de l'atteinte des muscles chez les enfants avec POPB.

L'évaluation du mouvement de l'épaule mais aussi de l'ensemble du membre supérieur chez l'enfant avec POPB, est impossible de manière précise avec le seul examen clinique y compris avec l'utilisation d'échelles (A. E. Bialocerkowski et Galea 2006; A. Bialocerkowski, O'shea et Pin 2013). **L'analyse quantifiée du mouvement** permet la décomposition des mouvements dans chaque articulation pour une tâche donnée, et à l'aide des paramètres spatio-temporels, peut évaluer la performance du mouvement. Elle a une place spécifique pour la quantification du mouvement chez les enfants avec POPB et l'évaluation des interventions thérapeutiques (Russo et al. 2014; Fitoussi et al. 2009).

2.4 Traitements chez l'enfant avec POPB

La récupération de la motricité, la **lutte contre les rétractions musculaires et déformations articulaires pour l'obtention d'une bonne mobilité du membre supérieur** sont les objectifs thérapeutiques chez les enfants avec POPB (Shenaq et al. 2005; Peter M. Waters 2005). Une **attention spécifique est portée à l'épaule** (Julka et Vander Have 2011). A son niveau, le

maintien de la mobilité active et passive, la lutte contre les déséquilibres de force, le maintien de la congruence scapulo-humérale et la prévention de l'installation de changements dysplasiques permanents sont des objectifs thérapeutiques prioritaires.

2.4.1 Rééducation

Des thérapies rééducatives peuvent être proposées tout au long de la vie de l'enfant présentant une POPB initialement pour favoriser la récupération puis pour limiter les séquelles chez les enfants qui n'auront pas une récupération complète de leur pathologie. Elles sont le plus souvent réalisées en première ligne et complétées si nécessaire par d'autres prises en charge.

Dès quelques semaines de vie, une **prise en charge rééducative précoce est recommandée**, afin de favoriser la récupération du membre supérieur atteint, **faciliter la fonction de ses muscles** et **prévenir les complications** à type de rétractions des tissus mous et déformations articulaires et osseuses survenant rapidement au niveau de l'épaule (Bialocerkowski 2005; Justice D 2015; Philandrianos 2011; DiTaranta P 2004; Verchere 2014; Smith 2018). Elle peut consister en des exercices doux à type de mobilisations passives, stimulation de la mobilisation active, exercices à domicile, mise en place d'orthèses (Bialocerkowski 2005, Justice D 2015, Philandrianos 2011, di Taranto P 2004). Le maintien des amplitudes articulaires en **rotation externe** lors des mobilisations et avec les orthèses est particulièrement ciblé.

Chez l'enfant plus âgé n'ayant pas récupéré complètement, des rééducations peuvent être proposées, afin de **maintenir les amplitudes articulaires actives et passives ainsi que la force**, dans un contexte chirurgical (pré ou post opératoire) ou en dehors (Safoury et al. 2017; Yilmaz et al. 2018; Rasmussen et al. 2013).

En parallèle de ces prises en charge ayant pour objectif premier de limiter les déficiences à type de limitations d'amplitudes articulaires passives et actives au niveau articulaire, des **thérapies proposant un travail plus global** de l'ensemble du membre supérieur ont également été rapportées chez l'enfant conservant des séquelles de sa POPB. Des programmes globaux de rééducation à la maison (S. H. Brown et al. 2015) ou des programmes

de type contrainte induite visant à améliorer la fonction du membre supérieur et les limitations d'activité ont été proposés (Buesch et al. 2010; Vaz et al. 2010).

Il est actuellement difficile d'évaluer l'efficacité de ces interventions rééducatives du fait du faible niveau de preuve des études actuelles avec le plus souvent absence de groupe contrôle.

2.4.2 Chirurgies nerveuses précoces

Dans les cas les plus graves, chez les bébés avec POPB, des **microchirurgies de reconstruction nerveuse** sont proposées précocement **si la récupération est insuffisante** (Peter M. Waters 2005; Zafeiriou et Psychogiou 2008; Michael L. Pearl 2009; Smith et al. 2018). Elles consistent en des transferts nerveux, greffes nerveuses ou combinaison des deux (Smith et al. 2018; Pondaag et Malessy 2014) permettant une amélioration clinique des possibilités de mouvements actifs (Smith et al. 2018; Pondaag et Malessy 2014). Les indications sont claires dans les atteintes complètes du plexus sans récupération à quelques semaines de vie avec intervention envisagée dès 3-4 mois de vie (Ruchelsman et al. 2009; Pondaag et Malessy 2014; Smith et al. 2018; Raducha et al. 2017). **La place et le moment des chirurgies nerveuses chez les enfants présentant des atteintes incomplètes** (groupes Narakas I et II) **sont davantage discutés** du fait de la difficulté à estimer la récupération spontanée chez ces enfants (Pondaag et Malessy 2014; Ruchelsman et al. 2009; Abid 2016).

2.4.3 Chirurgies secondaires musculo-squeletiques

Chez les **enfants plus âgés** n'ayant pas récupéré complètement et présentant d'importantes limitations d'amplitudes articulaires **pour lesquels la prise en charge rééducative est insuffisante ou a échoué**, des interventions chirurgicales « **interventions chirurgicales secondaires** » sont proposées afin d'améliorer **les possibilités de mouvements** dans ces directions et de limiter **le cercle vicieux de la déformation osseuse** (Peter M. Waters 2005; Michael L. Pearl 2009; Ruchelsman, Grossman et Price 2011; Julka et Vander Have 2011). Au niveau de l'épaule, elles consistent en une réduction de luxation de la tête humérale et en des gestes au niveau des tissus mous. Dans ces gestes au niveau des tissus, les muscles sont ciblés. Chez les enfants présentant des limitations d'amplitude articulaires en rotation externe et

abduction, des techniques à type **de libération de rétraction(s) musculaire(s), ou transferts musculaires** sont utilisées, visant à rétablir les longueurs musculaires et améliorer les déséquilibres musculaires (Michael L. Pearl 2009; Ozben et al. 2011; Hultgren et al. 2013; Louden et al. 2013; Hultgren et al. 2014; Greenhill et al. 2018; Michael L. Pearl et al. 2006; Kozin et al. 2010). Les muscles les plus fréquemment ciblés sont les muscles subscapulaires, grand dorsal et grand rond ainsi que grand pectoral. Ces chirurgies, réalisées à l'âge de 6 mois pour les plus précoces permettent une amélioration des amplitudes articulaires actives en abduction et rotation externe, un arrêt de progression voire une amélioration de la déformation, mais également une amélioration des activités et de la qualité de vie (Hoffer, Wickenden et Roper 1978; Peter M. Waters 2005; Kozin et al. 2006; Cohen et al. 2010; Van der Holst et al. 2015).

Lorsque la déformation osseuse est trop avancée, sans efficacité suffisante des gestes au niveau des tissus mous, des **gestes osseux** (triangle tilt surgery, ostéotomie de rotation humérale, correction de l'orientation de la glène) sont proposés afin d'améliorer la mobilité dans les amplitudes articulaires faisant défaut et impactant l'utilisation du membre supérieur chez l'enfant (Michael L. Pearl 2009; Dodwell et al. 2012). Des chirurgies secondaires sont également possibles au niveau des autres articulations du membre supérieur (Costil, Romana, et Fitoussi 2018).

2.4.4 Injections de toxine botulinique

Les toxines botuliniques ont une **action sur la synapse neuromusculaire** à la base de leur utilisation thérapeutique. Injectée dans un muscle, la toxine botulinique de type A bloque la libération de l'acétylcholine au niveau de la jonction neuromusculaire (Vidal 2015). Les effets de la toxine sont réversibles (Poulain, Popoff et al. 2008). La toxine botulinique a été de plus en plus utilisée ces dernières années dans le traitement de la POPB en association avec la rééducation, les orthèses ou les chirurgies (Ruchelsman, Grossman et al. 2011). Elle est utilisée dans cette pathologie pour **lutter contre les déséquilibres musculaires**. Au niveau de l'épaule, les muscles rotateurs internes sont ciblés et injectés afin de limiter le déséquilibre de force en faveur de ces muscles. Des résultats positifs sur les amplitudes articulaires passives et actives de cette articulation ainsi que sur les capacités fonctionnelles sont mis en évidence dans des études de faible puissance (Grossman, Price et al. 2003; Basciani and Intiso 2006; DeMatteo,

Bain et al. 2006; Gobets, Beckerman et al. 2010; Shin, Shin et al. 2014). Ces injections pourraient avoir une place dans la prévention de la subluxation ou luxation postérieure de l'épaule (Ezaki, Malungpaishrope et al. 2010, Greenhill DA 2016) et favoriser la simplification des interventions chirurgicales secondaires (Ezaki, Malungpaishrope et al. 2010; Michaud, Louden et al. 2014, Greenhill DA 2016).

3 Synthèse de l'introduction

Chez les enfants avec paralysie obstétricale du plexus brachial sans récupération complète, **l'atteinte de l'épaule** est la principale cause de morbidité. En effet, les lésions nerveuses impliquent quasi systématiquement les racines C5 et C6, innervant les muscles de l'épaule, avec un impact particulièrement important au niveau des **muscles de l'articulation gléno-humérale**. Cette atteinte musculaire, d'importance variable selon les muscles, a pour conséquence la **déformation osseuse très précoce** de l'articulation gléno-humérale. Ces deux éléments, atteinte musculaire et déformation osseuse, sont à **l'origine d'une perturbation du mouvement de l'épaule**. Cette perturbation du mouvement de l'épaule a, à son tour, un impact sur les forces exercées sur l'articulation gléno-humérale et sur l'ensemble de la motricité du membre supérieur de l'enfant avec POPB *(Figure 12)*. **Le maintien de la mobilité passive et active de l'épaule et de l'ensemble du membre supérieur, la conservation de l'intégrité de l'articulation gléno-humérale sont des objectifs majeurs dans la prise en charge de l'enfant avec POPB**.

Les **muscles gléno-huméraux sont au cœur de la pathologie de l'épaule**, à la fois pour leur rôle dans la déformation de l'articulation et dans la limitation des mouvements. Ils sont ciblés dans les prises en charge rééducatives et interventions chirurgicales. **Une meilleure connaissance de leur atteinte apparaît comme un point clé pour améliorer la compréhension** des conséquences de l'atteinte musculaire sur la déformation tridimensionnelle de l'épaule et la limitation de la mobilité du membre supérieur.

Le simple examen clinique ne permet pas la connaissance anatomique et fonctionnelle précise des muscles de l'épaule chez l'enfant avec un développement typique et chez les enfants présentant une pathologie de l'épaule.

L'IRM, en donnant accès à différents éléments morphologiques (volume, …) liés à la fonction musculaire, **représente un moyen d'exploration de l'anatomie fonctionnelle de l'épaule** chez l'enfant.

Chez les enfants avec POPB, l'examen morphologique des muscles en IRM, pourrait permettre de donner un accès à la compréhension de l'atteinte individuelle et à la fonction spécifique des muscles gléno-huméraux et ainsi guider les développements thérapeutiques.

La suite du document repose sur la présentation des 5 publications issues de ces travaux.
Le chapitre II présente **des travaux sur 3** aspects ayant fait l'objet de **publications** :

- **Quantifier le volume et la forme des muscles** squelettiques chez l'homme en utilisant l'IRM : revue systématique de validité et fiabilité (Quantifying skeletal muscle volume and shape in humans using MRI : a systematic review of validity and reliability)
- **Volume des muscles** de l'épaule chez l'enfant et **relation à la force**, étude cas témoin pilote (In vivo pediatric shoulder muscle volumes and their relationship to 3D strength)
- **Atrophie des muscles** de l'épaule, **relation avec la perte de force** chez les enfants avec POPB (Shoulder muscle atrophy and its relation to strength loss in obstetrical brachial plexus palsy).

Etant donné l'impact direct des limitations de mouvement sur les activités et la participation chez ces enfants, la connaissance et la **compréhension des spécificités de leurs mouvements** au niveau de l'épaule mais aussi de l'ensemble du membre supérieur ainsi que l'évaluation de leurs performances sont nécessaires. Le chapitre III présente une quatrième publication scientifique qui consiste en une étude cas-témoin :

- Caractéristiques du **mouvement tridimensionnel du membre supérieur** chez les **enfants avec paralysie obstétricale du plexus brachial** et enfants avec développement typique (Three-dimensional upper limb movement characteristics in children with brachial plexus birth palsy).

L'association de ces travaux, visant à mieux comprendre le fonctionnement de l'épaule et du mouvement du membre supérieur chez l'enfant avec POPB, et des éléments physiopathologiques déjà connus et présentés dans l'introduction, sont à l'origine de **discussions autour de perspectives d'exploration de l'épaule et du membre supérieur ainsi que de perspectives thérapeutiques** développées dans les chapitre IV et V. **Un essai thérapeutique est proposé dans un cinquième article** :

- Efficacité et sécurité des injections intramusculaires précoces de toxine botulinique pour prévenir la déformation de l'épaule chez les bébés atteints de paralysie obstétricale du plexus brachial (POPB-TOX), un essai contrôlé randomisé : protocole de l'étude (Effectiveness and safety of early intramuscular botulinum toxin injections

to prevent shoulder deformity in babies with obstetrical brachial plexus palsy (POPB-TOX), a randomized controlled trial : study protocol)..

II. Etude morphologique musculaire en IRM

La force développée par un muscle est influencée par certains **paramètres morphologiques** (Lieber et Fridén 2000; Cormie, McGuigan et Newton 2011). Les paramètres tels que la surface de section physiologique ou anatomique, le volume musculaire, l'angle de pennation, la longueur de la fibre musculaire ou le bras de levier sont d'importants éléments pour l'évaluation de la **performance du mouvement humain** (Lieber et Fridén 2000). **L'architecture musculaire peut changer** lors d'une altération de l'utilisation des muscles, lors d'une pathologie ou lorsque les contraintes varient, modifiant ainsi ses propriétés fonctionnelles (Lieber et Fridén 2000; Kubo et al. 2003; Tate et al. 2006; C. I. Morse et al. 2005).

L'**IRM** est largement utilisée dans **l'évaluation morphologique du système locomoteur**. Elle permet d'identifier les lésions musculaires, les quantifier et donne des informations sur leur composition (Fleckenstein et al. 1991; Theodorou et Kakitsubata 2012). Elle permet également la **mesure quantitative du volume musculaire** et de la surface de section anatomique chez les sujets sains et présentant des pathologies du muscle (Vanmechelen, Shortland et Noble 2017; Valentin et al. 2015). Des **corrélations** de ces deux mesures évaluées en IRM avec la **force** ont été montrées dans différentes populations (Akagi et al. 2009; Mathur et al. 2008; Fukunaga et al. 2001; Vidt et al. 2012). La corrélation plus forte entre le volume musculaire mesuré en IRM et la force permet de recommander l'utilisation de cette technique plutôt que la mesure simple de la surface de section (Fukunaga et al. 2001; Akagi et al. 2009; Blazevich et al. 2009; Vidt et al. 2016; Tonson et al. 2008; Mathur et al. 2008). L'importance de ces corrélations était variable en fonction des populations, avec par exemple des corrélations moins fortes lors du vieillissement, dans l'enfance ou dans certaines pathologies (Akagi et al. 2009; Kanehisa et al. 1994).

L'étude des volumes des muscles en IRM est ainsi utilisée en pratique clinique pour le diagnostic et le suivi des maladies neuromusculaires (Jenkins et al. 2013; Godi et al. 2016), l'évaluation de certains traitements (E. X. Wu et al. 2008). L'étude des volumes et des formes des muscles est également utilisée en recherche pour améliorer la compréhension de certains symptômes ou maladies (Kaick et al. 2010; Engstrom et al. 2007).

L'accès au volume musculaire et à ses changements par l'IRM, étant donné ses possibles relations avec la fonction musculaire, représente un intérêt fort dans le cadre de la compréhension de l'atteinte musculaire au niveau de l'épaule chez les enfants avec POPB.

1 Article 1 : Quantification des volumes et des formes des muscles squelettiques chez l'homme en IRM : revue systématique de validité et fiabilité.

De nombreuses **techniques de mesure, manuelles et/ou automatiques** peuvent être utilisées en IRM pour **quantifier les volumes musculaires**. Leur utilisation est conditionnée par deux facteurs : la **qualité de mesure** (ou propriétés métrologiques) et les **aspects pragmatiques en relation avec leur utilisation**, notamment le temps nécessaire pour réaliser la mesure (Rodary, Pezet-Langevin et Kalifa 2001).

Les propriétés métrologiques d'un outil de mesure comprennent trois principaux aspects : la validité (« validity »), la fiabilité ou reproductibilité (« reliability ») et la sensibilité au changement (« responsiveness ») (Mokkink et al. 2010; Rodary, Pezet-Langevin et Kalifa 2001; Brink et Louw 2012).

La **validité** représente la capacité de l'outil à évaluer spécifiquement ce qu'il cherche à mesurer. Différents types de validité peuvent être distingués. La validité de contenu (« content validity ») évaluant le degré selon lequel l'élément mesuré est un reflet adéquat de l'élément à mesurer et la validité de critère (« criterion validity ») estimant le degré selon lequel l'instrument testé est un reflet exact de l'instrument gold standard sont pertinents à retenir dans le cadre du travail ci-dessous (Mokkink et al. 2010). Dans le cadre de la mesure de volume musculaire en IRM, la validité de contenu pourra être testée en estimant le volume d'un muscle sur un examen IRM puis en mesurant le volume réel de ce même muscle après dissection. La validité de critère pourra être déterminée en comparant l'estimation d'un même volume musculaire par la technique de mesure testée et la technique de mesure de référence en IRM.

La **fiabilité** représente la capacité de l'outil à rapporter les mêmes résultats, sans erreur de mesure, lors de l'évaluation d'un même élément dans des situations similaires. On peut distinguer : la fiabilité test-retest qui évalue la stabilité des résultats d'une mesure lors de plusieurs tests pour un même élément, la fidélité intra-examinateur qui correspond à l'accord entre plusieurs mesures prises par un même observateur pour l'évaluation d'un même élément, et la fidélité inter examinateur qui correspond à l'accord entre plusieurs mesures réalisées par différents observateurs pour l'évaluation d'un même élément (Mokkink et al. 2010; Rodary, Pezet-Langevin et Kalifa 2001; Brink et Louw 2012). Dans le cadre de la mesure de volume musculaire en IRM, une bonne fiabilité test-retest montrera une stabilité des résultats dans l'estimation d'un même volume musculaire sur deux examens IRM réalisés avec les mêmes paramètres mais à deux occasions différentes. Une bonne fidélité intra examinateur retrouvera des estimations proches pour un même volume musculaire sur le même examen par un même examinateur mais avec des mesures à plusieurs reprises. Une bonne fidélité inter-examinateur retrouvera des estimations proches pour un même volume musculaire sur le même examen avec des mesures réalisées par deux examinateurs différents. La **sensibilité au changement** évalue la capacité de l'instrument à mesurer les variations du phénomène mesuré (Beaton et al. 2001).

Dans la revue systématique « Quantifying skeletal muscle volume and shape in humans using MRI : a systematic review of validity and reliability », l'objectif principal était de **rapporter la validité et la fiabilité des techniques** utilisées pour estimer les volumes musculaires squelettiques et les formes musculaires tridimensionnelles à partir des données d'IRM dans les muscles sains et pathologiques. Les objectifs secondaires étaient de déterminer la **faisabilité** de ces techniques et de proposer des recommandations pour les recherches futures.

Cet article est proposé ici dans sa version acceptée dans la revue Plos One le 8 novembre 2018. Les appendices seront trouvés en annexe 2.

Quantifying skeletal muscle volume and shape in humans using MRI: a systematic review of validity and reliability

Christelle Pons[1, 2*¶],; Bhushan Borotikar[2&]; Marc Garetier[2,3]; Valérie Burdin[2,4]; Douraied Ben Salem[2,5,6], Mathieu Lempereur[2,5,7 &]; Sylvain Brochard[1,2,5,7¶]

[1]Pediatric rehabilitation department, Fondation ILDYS, Brest, France

[2]Laboratoire de Traitement de l'Information Médicale, INSERM U1101, Brest, France

[3]Radiology department, **hôpital d'Instruction des Armées Clermont-Tonnerre, Brest, France**

[4]IMT Atlantique, Brest, France

[5]Université de Bretagne Occidentale, Brest, France

[6] Radiology department, CHRU de Brest, Brest, France

[7]PMR department, CHRU de Brest, Hopital Morvan, Brest, France

¶ These authors contributed equally to this work

& These authors also contributed equally to this work.

*Corresponding Author :

E-mail: christelle.ponsbecmeur@ildys.org

Abstract

Aims: The aim of this study was to report the metrological qualities of techniques currently used to quantify skeletal muscle volume and 3D shape in healthy and pathological muscles.

Methods: A systematic review was conducted (Prospero CRD42018082708). PubMed, Web of Science, Cochrane and Scopus databases were searched using relevant keywords and inclusion/exclusion criteria. The quality of the articles was evaluated using a customized scale.

Results: Thirty articles were included, 6 of which included pathological muscles. Most evaluated lower limb muscles. Partially or completely automatic and manual techniques were assessed in 10 and 24 articles, respectively. Manual slice-by-slice segmentation reliability was good-to-excellent (n=8 articles) and validity against dissection was moderate to good(n=1). Manual slice-by-slice segmentation was used as a gold-standard method in the other articles. Reduction of the number of manually segmented slices (n=6) provided good to excellent validity if a sufficient number of appropriate slices was chosen. Segmentation on one slice (n=11) increased volume errors. The Deformation of a Parametric Specific Object (DPSO) method (n=5) decreased the number of manually-segmented slices required for any chosen level of error. Other automatic techniques combined with different statistical shape or atlas/images-based methods (n=4) had good validity. Some particularities were highlighted for specific muscles. Except for manual slice by slice segmentation, reliability has rarely been reported.

Conclusions: The results of this systematic review help the choice of appropriate segmentation techniques, according to the purpose of the measurement. In healthy populations, techniques that greatly simplified the process of manual segmentation yielded greater errors in volume and shape estimations. Reduction of the number of manually segmented slices was possible with appropriately chosen segmented slices or with DPSO. Other automatic techniques showed

promise, but data were insufficient for their validation. More data on the metrological quality of techniques used in the cases of muscle pathology are required.

Introduction

The volume and shape of a muscle are strongly related to its function [1–4]. Structural differences between muscles, which result from different muscle fibre architecture, are good predictors of force generation capacity [1]. Physiological cross-sectional area is the major determinant of joint torque [1]. Muscle volume, which is closely related to physiological cross sectional area, was shown to be strongly connected with joint torque in both healthy and pathological populations [2–5]. Changes in muscle volumes and shapes may be normal, such as hypertrophy after a strengthening program, or atrophy associated with ageing [6,7]. Changes can also be pathological due to neuromuscular disease or injury [5,8,9].

Assessment of muscle volume and shape is essential for both clinical practice and research. Measurement of muscle volume facilitates surveillance of neuromuscular disease progression [10,11] and the effects of treatments [12,13], as well as being useful for diagnostic purposes [14,15]. Muscle shapes can be used to distinguish between pathologies [16,17] and modelling individual muscles can be useful when planning surgery [18], evaluating changes over time [6,19] and in order to improve the understanding of particular symptoms or diseases [16,17,20–22].

Magnetic resonance imaging (MRI) is the gold-standard technique for the evaluation of muscle volumes and three-dimensional (3D) shapes, and is used as a reference to validate other imaging techniques for this purpose [23,24]. Many manual and automatic segmentation techniques have been developed for the estimation of muscle volumes and 3D shapes from MRI data [25–29]. However, despite the widespread use of these measurements in both clinical practice and

research, to date neither their metrological qualities nor their feasibility for use in routine practice have been specifically reviewed.

Knowledge of the validity and reliability of measurement methods is essential when choosing a technique in order to ensure an accurate interpretation of the results [30,31]. Validity is the degree to which a technique measures what it is intended to measure, and the extent to which the values obtained are similar to the true values. Reliability is the extent to which a technique yields the same results over repeated trials in stable study subjects [31,32]. Techniques that are easy to use may lack validity or reliability whereas techniques that are valid and reliable are not always feasible for use in a research or clinical setting if they are too time-consuming. It may thus be necessary to compromise between (I) the metrological accuracy required and (II) practical considerations of usage.

The main aim of this systematic review was to report the validity and reliability of techniques used to estimate skeletal muscle volumes and 3D muscle shapes based on MRI data in healthy and pathological muscles in humans. The secondary aims were to determine the feasibility of those techniques and to provide recommendations for future research.
Our first hypothesis was that manual slice by slice segmentation would have good metrological properties but would need a large amount of time. The second was that while providing valid and reliable results, automatic segmentation techniques would require less time.

Materials and methods

This systematic review adheres to the PRISMA guidelines. A PRISMA checklist was completed (S1 Table) and the review protocol was published in Prospero (CRD42018082708).

Database search and selection process

Articles were identified through a comprehensive search of the following online bibliographic databases: PubMed, Web of Science, The Cochrane Library and Scopus. In order to ensure the search was exhaustive, the following Medical Subject Headings (MeSH) and keyword combinations were used (I) MRI, magnetic resonance imaging, (II) muscle, skeletal muscle, muscul* (III) (keywords relating to segmentation) volum*, cross sectional area, three dimension*, 3D, shape, segmentation, organ size and (IV) (keywords relative to metrological properties) reliability, reproducibility, repeatability, validity, accuracy, measur*, metrologic*, validation stud*. Search strings were formulated and tailored to the search syntax of each database to ensure a common search strategy (S1 Text). Neither publication year nor language limits were imposed. The last search was performed in January 2018.

Inclusion criteria were: I) studies in which the main aim was to describe and/or evaluate a method to determine skeletal muscle (or functional groups) volume and/or shape using MRI data, II) the study was on human subjects and III) the study included an evaluation of the metrological qualities of the method. Studies that evaluated head and neck muscles or that evaluated muscle groups that were not functionally grouped [33,34] and conference papers were excluded. Articles that compared ultrasonography (USG) with MRI to evaluate MRI validity were also excluded [35]. The references of the selected articles were screened to complete the review process. The titles, abstracts and whole texts of the articles identified by the search were independently evaluated by two examiners (CP and ML). Any disagreements were resolved by discussion between the two examiners.

Quality assessment of selected studies

Since no standardized tools exist to determine the quality of articles in the field of radiology, a customized quality assessment scale was developed from other scales in the literature [36,37].

The aim of the scale was to assess both the intrinsic quality of each article (maximum score 30) and the metrological qualities of the method evaluated (maximum score 11). The total score was named the Q score and was out of 100. The first (quality) part of the scale was based on previously published quality checklists for systematic reviews as well as scales for the assessment of the quality of studies included in systematic reviews. Those scales included questions relating to study design and quality of the reporting of methodologies and results [38–40], for example “were the aims clearly stated” or “was the description of patient recruitment clear” (S2 Table). The second (metrological) part of the scale was based on published scales that were specifically designed for the evaluation of metrological studies in other fields than radiology [31,36,37,41,42]. It included questions such as “was concurrent validity evaluated?” or “Was the gold standard measure described ?”. The grades for the questions ranged from 0 to 2. This scale was only used for the purposes of the present study. The quality rating was carried out independently by two examiners (CP and BB) and disagreements were resolved by consensus.

Data extraction and analysis

Information regarding the samples included, muscles evaluated, magnetic field strengths and MRI protocols used were collected from each article. The technique evaluated, the reference technique used, operators and outcome measures (validity, reliability and feasibility) were also recorded (table 1 and S3 Table). In this paper, validity refers to the concept of concurrent validity [31] and reliability refers to the correlations between different measurements within the same stable subject, as well as the measurement error [30,43]. To assess the validity and reliability of the results reported in each article, the following values were considered: standard error of the estimate (SEE) and root mean square error (RMSE), values > 10% = poor, 5 - 10% = moderate, 1 - 5% = good and < 1% = excellent. The same limits were used for the coefficient of variation. Mean differences, results > 5% = poor, 2 - 5% = moderate, 1 - 2% = good and <

1% = excellent. For mean distances, results with distances > 6 mm = poor, 3 - 6 mm = moderate, 1 - 3 mm = good and < 1 mm = excellent. Intraclass correlation coefficients (ICC) and r^2 values from 0 - 0.49 = poor, 0.5 - 0.69 = moderate, 0.7 - 0.89 = good and > 0.9 = excellent [44]. The same limits were used for the Dice similarity index(DSI). DSI is the size of the overlap of the two segmentations divided by the total size of the two objects. If different statistical analyses were available in the same study, the worst results were primarily used for the classification. Although we acknowledge that there is no reference or reported recommendation for this categorization, it was used to provide clarity and to standardize the hierarchy of the results reported in the selected articles. The results for validity and reliability were also extracted as they were reported in each original article (S4 Table). When similar evaluations were carried out, for example a bilateral psoas evaluation in a healthy subject using the same technique for each side [45], only the poorest values of validity or reliability were reported. Technique feasibility was determined as the time required for manual segmentation to be carried out or from the time needed to run automatic techniques.

Table 1 : Description of the segmentation techniques and methodology of the articles included

	Muscles evaluated	reference technique	technique (methodology and volume/shape calculation)	optimization of the acquisition for targeted error	operators		Outcome measures		Statistical analysis
					number, qualification and experience	reliability study design	volume/ 3D shape		
Albracht 2008 [52]	GM, GL, SO	slice by slice manual segmentation, volume using 3D shape	single slice manual segmentation (CSAmax), muscle length (ML) obtained using full muscle reconstruction and shape factor (p)determined in a group with untrained and trained persons, volume: p* CSAmax* ML	-	-	-	volume	concurrent validity	volume RMSE
Amabile 2017 [53]	QL, ES, GlMa, GlMe, GlMi, AddOP, VLI, VM, TFL, RF, Gra, Sar, BFS, BLF, SM, ST, grouped in spine extensors/flexors, hip extensors/flexors, knee extensors/flexors, both sides	3D reconstruction, segmentation using parametric shape deformation and image processing (DPSO method)	- use of ACSAmax and muscle length (ML) obtained using full muscle reconstruction and shape factor (p), volume: p* ACSAmax* ML - reduced MRI set method: model using the DPSO method, with 5 segmented slices, volume predicted from a multilinear regression	-	-	-	volume	concurrent validity	volume RMSE
Andrews 2015 [65]	Gra, Sar, BFL, RF, ST, BFS, SM, VI, VM, Add, VL, left side	slice by slice manual segmentation	interactive segmentation using shape priors + statistical shape model	image preprocessing (linear transformation)	1, physical therapist, expert	-	3D shape	concurrent validity	DSI, mean Surf D

Barnouin 2014[46]	RF, VI, VL, VM, Qua, both sides	-	slice by slice manual segmentation, volume: muscle tissue area * interslice distance	-	2, trained	-	volume	inter rater reliability (muscle volume estimation, muscle individual contribution)	ICC, Student, mean diff
Barnouin 2015 [47]	RF, VI, VL, VM, both sides	slice by slice manual segmentation, volume: cylinder method	- slice by slice manual segmentation, volume: cone method/ 3d-order polynomial regression/ 4th-order polynomial regression '- manual segmentation of a reduced number of slices , volume: cylinder/ cone method/ 3d-order polynomial regression/ 4th-order polynomial regression	-	-	-	volume	concurrent validity, comparison between methods	ANOVA, mean diff, CV
Belavy 2011 [55]	RF, VM, VL, VI, Sar, Gra,Add M, Add L, BFL, BFS,ST, SM, GL, GM, So+FHL, TP, FDL, Per LBT, TA +EDL + EHL, left side	slice by slice manual segmentation, volume: linear interpolation	manual segmentation of a reduced number of slices, selection of the segmented slices with 5 algorithms including subalgorithms with various number of slices (1-largest CSA and the sum of the 3,6,9 … largest CSA measurement/ 2-largest CSA with immediately adjacent CSAs/ 3-same as 2 except every second images taken/ 4- method using CSA at 30, 40, 50, 80%/ 5- most proximal CSA with every 2d, 3d, 4th... CSA measurements), volume: linear interpolation	number of slices chosen: % within 0.5% of the reference % change in muscle volume; variability of the % change in muscle size same or less than that of the variability of the reference % change in muscle volume.	1, NR	-	volume change	concurrent validity	Pearson correlation coefficient r, mean percentage change

Elliot 1997 [66]	GM, GL, So	-	image based segmentation + manual segmentation, volume: addition of the number of voxels	correction algorithm for partial volume effect	2, trained	-	volume	inter rater reliability	correlation coefficient, max diff
Eng 2007 [54]	PT (10times), ECRB (10 times), EPL (10 times), FCU (7 times), BR (6 times)	dissection	manual segmentation in the 3 planes, volume: addition of the number of voxels	-	2, NR	-	volume	concurrent validity, inter rater reliability	ICC, mean diff
Engstrom 2011 [67]	QL, Ps, ESM, both sides	slice by slice manual segmentation	atlas based + statistical shape based segmentation	image preprocessing (bias field correction, partial volume interpolation)	1, expert (for manual segmentation)		'3D shape	concurrent validity	DSI, TC, mean Surf D
Jolivet 2014 [68]	RF, VLMI, Sar, TFL, BFS, BFL, ST, ST, Gra	slice by slice manual segmentation, volume: using 3D shape	segmentation using parametric shape deformation and image processing, improvements (improved DPSO technique: semi automatic contouring, automatic adjustements of the intermediate contours)	number of slices chosen to obtain an error <5%/ <5mm	-	-	volume, 3D shape	concurrent validity	point-to-surface distance 2*RMSE
Kim 2017 [29]	Sspi	thresholding and manual post-processing	image based and shape based segmentation, volume: accumulation of the 2D contours, Laplacian smoothing process	-	2, experts	-	3D shape	concurrent validity	DSI, Accuracy = (RP+ RN)/(RP+ E N+ E P+ RN), mean Surf D, Max Surf D
Lehtinen 2003 [56]	Sspi,Ssca, Ispi+Tmin	slice by slice manual segmentation, volume: calculated by the software	- single slice manual segmentation (at the Y-shaped position), volume: calculated by the software '- manual segmentation of 2 slices (at the Y-shaped position and at a defined more medial position), volume: calculated by the software	-	2, orthopaedic surgeons	each operator contoured muscles 3 times on 3 days	volume	concurrent validity, intra and inter rater reliability	Student, mean diff, 2SD, CV

Le Troter 2016 [48]	RF, VI, VM, VL, Qua, right side	slice by slice manual segmentation, volume: cone method	- atlas based segmentation (semi automated) '- atlas based segmentation (fully automated)	-	1, experienced	-	volume, 3D shape	concurrent validity, repeatability, evaluation of affine and non linear registration methods, and fusion methods	ICC, CV, DSI, FNVF, FPVF, MVSF
				[53]					
Lund 2002 [49]	TA+EDL+EHL, left side	slice by slice manual segmentation, volume: cylinder method	- slice by slice manual segmentation, volume: NR - slice by slice manual segmentation, volume: cone method '- manual segmentation of 8 slices, volume: cylinder method '- manual segmentation of 8 slices, volume: cone method	number of slices chosen: to have < 10% difference/ reference volume	2, NR	manual segmentation of 13 slices equally distributed 3 times by one operator, 1 time by another	volume	concurrent validity (reduced number of slices), intra and inter rater reliability using 13 slices, comparison between methods	ICC, ANOVA, mean diff, 2SD
Marcon 2015 [9]	Qua	manual segmentation of a reduced number of slices (every third slice), volume: NR	- single slice manual segmentation (at 25cm above the knee joint), volume: NR	slice at 25cm (rather than slice at 15 and 20cm) chosen: to have the minimal SEE	1, musculoskeletal radiology fellow	operator repeated the every third slice manual segmentation	volume	concurrent validity (single slice), intra rater reliability (every 3d slice manual segmentation)	ICC, SEE
Mersmann 2014 [57]	GM, GL, SO, TS, right side	slice by slice manual segmentation, volume: integral of the CSA along the muscle length	single slice manual segmentation (CSA max), muscle length (ML) obtained using full muscle reconstruction and shape factor (p) determined in a group with untrained and trained persons, volume: p* ACSAmax* ML	-	-	-	volume	concurrent validity	r^2, ANOVA, volume RMSE

Mersmann 2015 [58]	VL, VM, VI, one side	slice by slice manual segmentation, volume: integral of the CSA along the muscle length	single slice manual segmentation (CSA max), muscle length (ML) obtained using full muscle reconstruction and shape factor (p), determined in a group with untrained and trained persons, volume: p* ACSAmax* ML	-	-	-	volume	concurrent validity	coefficient of determination r^2, ANOVA, volume RMSE
Moal 2014 [59]	Add BLM, BF, ES, GlMa, GlMe, GlMi, Gra, Il, Obl, Ps, QL, RA, RF, Sar, SMT, TFL, VLI, VM	slice by slice manual segmentation (T1 images), volume using 3D shape	segmentation using parametric shape deformation and image processing (DPSO)	-	3 experienced operators	3 operators made 3 T1 reconstruction and 3 Fat reconstruction (using DPSO method)	'volume, 3D shape	- intra rater reliability and inter rater reliability of the DPSO method for T1 and fat images '- concurrent validity of the DPSO method for T1 and fat images with reference method	Student, mean diff, SD, CV, point to surface distance 2*RMSE

Morse 2007 [60]	Qua, VL, VM, VI, RF, right side	slice by slice manual segmentation, volume: muscle tissue area * interslice distance	- 1/single slice manual segmentation (CSAmax), muscle length (ML) with US, volume: equation using ML and ACSA max '- 2/ single slice manual segmentation (CSA at 40% from the distal end of the femur), regression equation to estimate the maximum muscle cross-sectional area, muscle length (ML) with US, volume: equation using ML and ACSA max '- 3/same method as 2/ with CSA at 50% '- 4/same method as 2/ with CSA at 60%	-	1 (measures made 3 times, average recorded)	-	volume	concurrent validity	r^2, SEE, mean diff, 1.96SD
Nordez 2009 [27]	Qua (VL+VI+VM+RF)	slice by slice manual segmentation, volume using 3D shape.	- manual segmentation of a reduced number of slices (3-21), volume: cone method, '- manual segmentation of a reduced number of slices (3-21), volume: Cavalieri formula '- manual segmentation of a reduced number of slices, cubic spline interpolation to estimate missing CSAs '- manual segmentation of a reduced number of slices (3-21), volume: DPSO	number of slices chosen to obtain an error<=1.1%	2, NR	1st operator outlined all the slices a second time on different days.	volume	intra rater reliability and inter rater reliability for the reference technique, concurrent validity , comparison between methods	ICC, ANOVA, Student, mean diff, 1.96SD

Popadic 2011 [50]	TB, both sides	slice by slice manual segmentation, volume: cone method	- single slice manual segmentation (CSA max), humerus length (HL), volume: equation using CSAmax, humerus length (HL), BMI '- single slice manual segmentation (CSA max), humerus length (HL), volume: equation using CSAmax, HL '- single slice manual segmentation (CSA 50%), humerus length (HL), volume: equation using CSA50%, HL '- single slice manual segmentation (CSA 60%), humerus length (HL), volume: equation using CSA 60%, HL	-	-	-	volume, volume change	concurrent validity muscle volume, muscle volume change)	adjusted r^2, RSE
Skorupska 2016 [61]	Pir, GlMi, GlMe, GlMa, both sides	-	slice by slice manual segmentation, volume: addition of the voxels and multiplication by the voxel dimension	-	2 physical therapists, 3/0 years of experience, trained	-	volume	inter rater reliability	ICC
Smeulders 2010 [62]	FCU, ECU, right side	-	slice by slice manual segmentation, volume: muscle tissue area * interslice distance	-	2, NR	1st operator repeated the evaluation of the first dataset, each observer evaluated both datasets	volume	intra rater reliability, inter rater reliability, repeatability	ICC, Student, mean diff, CV, SDD

Springer 2012 [48]	GlMe, GlMi, OE, both sides	-	slice by slice manual segmentation, volume: NR	-	2, NR	2d operator repeated the evaluation of all datasets after an interval of 4 weeks.	volume	intra rater reliability, inter rater reliability	Student, mean diff, 1.96SD, CV
Sudhoff 2009 [63]	SM, ST, BFS, BFL, Sar, TFL, Gra, VLI, VM, RF, GM, GL	slice by slice manual segmentation (T1 images), volume: using 3D shape	segmentation using parametric shape deformation and image processing (DPSO)	number of slices chosen to obtain an error<5%	2, NR	-	volume, 3D shape	concurrent validity, inter rater reliability	ICC, mean diff, SD, point to surface distance error, point to surface distance 2*RMSE
Tingart 2003 [25]	Sspi,Ssca, Ispi+Tmin	dissection, water displacement	slice by slice manual segmentation, volume: muscle tissue area * interslice distance	-	3, NR	each operator contoured muscles 3 times on 3 days	volume	concurrent validity, intra rater reliability, inter rater reliability	Pearson r^2, mean diff, SD, CV
Tracy 2003 [26]	Qua, trained side	slice by slice manual segmentation, volume: cone method	- manual segmentation of a reduced number of slices (every 2nd/ 4th/ 6ty/ 8th/ 10th section), volume: cone method '- single slice manual segmentation (CSAmax), volume: univariate regression	-	1, NR	-	volume, volume change	concurrent validity (muscle volume, muscle volume change after training)	r^2, SEE, mean diff, 2SD
Valentin 2015 [45]	ES, M, RA, Ps both sides	-	slice by slice manual segmentation, volume: muscle tissue area * interslice distance	-	2, novice (received training)	new analysis made 2 weeks later if low/ moderate agreement between assessors on the 1st evaluation	volume	inter rater reliability	ICC, mean diff, 2SD

Vanmechelen 2017 [51]	GM, SOL, TA, RF, SM, ST, left side	slice by slice manual segmentation, volume: muscle tissue area * slice thickness	single slice manual segmentation, muscle length (ML) obtained using full muscle reconstruction and form factor (FF), volume: ((ACSAmax* ML)-Offset)*FF	-	-	-	volume	concurrent validity	r^2, SEE
Yamauchi 2017 [28]	VL, VM, VI, RF, SM, ST, BFS, BFL, painful side	slice by slice manual segmentation, volume: muscle tissue area * interslice distance	-single slice manual segmentation at different femoral length levels, femoral length (FL), volume: regression equations which varied for each muscle '- use of muscle thickness at different femoral length levels and femoral length (FL), volume: regression equations which varied for each muscle	Use of the CSA at 60% from the distal end of the femur and muscle thickness at 50% of the distal end of the femur to have the best correlations with MV	1, trained image analyst	-	volume	concurrent validity	SEE

NR: not reported,
ICC: intraclass correlation coefficient, mean diff: mean difference, SD: standard deviation, CV: coefficient of variation, SDD: smallest detectable difference, RMSE: root mean square error, SEE: standard error of the estimate, DSI: Dice similarity index, mean surf D: mean surface distance, max surf D: maximal surface distance, TC: Tannimoto coefficient, FNVF: false negative volume fraction, FPVF: false positive volume fraction, MVSF: muscle volume similarity fraction
RF: rectus femoris, VI: vastus intermedius, VL: vastus lateralis, VM : vatsus medialis, Qua : quadriceps, Pir : Piriformis, GlMi : Gluteus Minimus, GlMe : Gluteus Medius, GlMa : Gluteus Maximus, FCU: flexor carpi ulnaris, ECU: extensor carpi ulnaris, Sspi: Supraspinatus, Ssca: Subscapularis, Ispi+Tmin: Infraspinatus and Teres minor, ES: Erector Spinae, M: multifidus, RA: rectus abdominis, Ps: Psoas, Sar: Sartorius, Gra: Gracilis, AddM: Adductor Magnus, Add L: Adductor longus, BFL: Biceps Femoris Long head, BFS: Biceps Femoris Short head, ST: Semi Tendinosus, SM: Semi Membranosus, GL: Gastrocnemius Lateralis, GM: Gastrocnemius Medialis, So+FHL: Soleus and flexor hallucis longus, TP: Tibialis Posterior, FDL: flexor digitorum longus, Per LBT: Peroneus (Longus, Brevis, Tertius), TA+EDL+EHL: tibialis anterior and extensor digitorum longus and extensor hallucis longus, So: Soleus, TS: triceps surae, TB: triceps brachii, TA: Tibialis Anterior, VLMI: Vastus Lateralis and Medius and Intermedius, TFL: tensor Fascia Lata, Add BLM: adductor (brevis, longus, magnus), Il: Iliacus , Obl: Obliquus (transversus abdominis, internus and externus obliquus), QL: Quadratus Lumborum, VLI: Vastus Lateralis and Intermedius together, VLMI: Vastus Lateralis and Medialis and Intermedius, BF: Biceps Femoris, SMT: Semi Membranosus and Tendinosis, ESM : erector spinae and multifidus, PT: pronator teres, ECRB : Extensor Carpi Radialis Brevis, EPL : Extensor Pollicis Longus, Br : Brachioradialis

Results

Selection process

The literature search identified 2160 citations in PubMed, 324 citations in the Cochrane Library, 3911 citations in Scopus, 2302 citations in Web of Science. After removing duplicates, 4631 remained. After screening titles and abstracts, 86 articles were found to be potentially eligible. Finally, 30 met the inclusion criteria and were included (Fig 1).

Fig 1: flow chart

Quality assessment

The mean Q score of the articles included was 64.1/100 (SD: 9.7). The primary aim of seventeen articles was to determine the metrological properties of a measurement technique. Ten articles had a score above 70/100 [9,27,28,45–51], fifteen articles had a score between 60 and 70/100 [25,26,52–64] and five articles had a score below 60/100 [29,65–68]. Details of the scores of each article are provided in S2 Table.

Description of Studies

The methodological characteristics (samples, designs and measurement methods) of each article are presented in table 1 and S3 Table.

The articles included primarily focused on segmentation techniques. Manual techniques (including slice by slice cross sectional area (CSA) segmentation, segmentation of CSA in a reduced number of slice(s), segmentation of CSA on one slice and muscle length use) were evaluated in twenty-four articles [9,25–28,45–58,60–64] and partially or completely automatic segmentation techniques (deformation of a parametric specific object, semi-automated and automated atlas-based, image-based and shape-based, atlas-based and statistical shape-based,

and interactive-segmentation using shape priors and statistical shape modelling methods) were evaluated in ten articles [27,29,48,53,59,64–68].

Muscle volume was evaluated in twenty-six articles [9,25–28,45–54,56–64,66,68], changes in muscle volume were evaluated in three articles [26,50,55] and 3D shapes were evaluated in seven articles [29,48,59,64,65,67,68].

Seventeen articles included only healthy subjects [26,27,45–50,52,53,57–60,62,64,67] and six included subjects with a muscular pathology of which five were on adults with: low back pain, total unilateral arthroplasty, anterior cruciate ligament reconstruction, chronic obstructive pulmonary disease or knee osteoarthritis [9,28,61,63,65]; the fifth article was on children with cerebral palsy [51]. Three articles evaluated cadavers [25,54,56].

Forty different muscles were examined: upper limb muscles were assessed in six articles [25,29,50,54,56,62] and lower limb muscles in twenty-four articles [9,26–28,45–49,51–53,55,57–61,63–68]. The rectus femoris muscle was the most frequently evaluated (n=13 articles). Different functional groups were used (n=18 articles). For example, for the quadriceps, it could be considered as a whole, or groupings could be made between vastus lateralis and intermedius or vastus lateralis, medialis and intermedius, or all the muscles could be segmented separately.

With regards to MRI parameters, 1.5T scanners were the most frequently used (n=22 articles), T1 weighted sequences were used in twenty four articles and 3D sequences were used in seven articles [9,29,46,47,52,54,66]. Axial slices were the most frequently segmented.

Manual techniques (table 1 and 2, S3 S4 and S5 Tables)

Slice by slice CSA segmentation

Estimation of muscle volume using slice-by-slice CSA segmentation was evaluated in 11 articles (Range Q score: 61-73, mean Q score: 68.5 [25,27,45–49,61–64]). Slice thicknesses varied between 1.5mm [25] and 10 mm [45]. In seven of those articles, there were no gaps

between slices [25,27,46,47,49,61,64]. After segmentation, seven different calculation methods were used to estimate muscle volume.

Moderate to good validity was found between manual slice-by-slice CSA segmentation and measurements from cadavers (n=1 article, [25]). Intra-rater reliability was good to excellent (n=4 [25,27,62,63]). Inter-rater reliability was moderate to good (n=8 [25,27,44,45,60–63]). Test retest reliability was good (n=2, [48,62]). Results were less reliable for external obturator volume [63] or gluteus minimus volume. Results for quadriceps volume were more reliable than results for the individual muscles that constitute it [27,46,48,64]. In articles that included both healthy and pathological muscles, results were more reliable for healthy muscles than pathological muscles [61,63]. Mean differences of less than 1% were found between different methods of volume estimation (cone, cylinder, 3^{rd} and 4^{th} order polynomial regression equations) (n=2, [47,49]).

49 **Table 2: Evidence of validity and reliability by technique and by muscle**

		slice-by-slice CSA segmentation	CSA segmentation on a reduced number of slices	CSA segmentation/ muscle thickness using a single slice and muscle length	CSA segmentation on a single slice	deformation of a parametric specific object (DPSO)	deformation of a parametric specific object (DPSO) , reduced MRI set method	other automatic methods
supraspinatus	validity	++ [25]	+ (2 MSS) [56]		+ [56]			++++ [29]
	intraR	+++ [25]	+++ (2 MSS) [56]		+++ [56]			
	interR	+++ [25]	+++ (2 MSS) [56]		+++ [56]			
subscapularis	validity	++ [25]	++ (2 MSS) [56]		+ [56]			
	intraR	+++ [25]	+++ (2 MSS) [56]		+++ [56]			
	interR	+++ [25]	+++ (2 MSS) [56]		+++ [56]			
infraspinatus + teres minor	validity	++ [25]	++ (2 MSS) [56]		++ [56]			
	intraR	+++ [25]	+++ (2 MSS) [56]		+++ [56]			
	interR	+++ [25]	++ (2 MSS) [56]		+++ [56]			
triceps brachii	validity			++ [50]				
flexor carpi ulnaris	intraR	++++ [62]						
	interR	+++ [62]						
extensor carpi ulnaris	intraR	+++ [62]						
	interR	++ [62]						
quadratus lumborum	validity			+ [53]		++ (Dixon)/ +++ (T1) (18%MSS) [59]		+++ [67]
	intraR					+++ (18%MSS) [59]		
	interR					+++ (18%MSS) [59]		
erector spinae	validity			++ [53]		++ (Dixon)/ +++ (T1) (15% MSS) [59]		
	intraR					+++ (15% MSS) [59]		
	interR	+++ [45]				+++ (15% MSS) [59]		
multifidus	interR	++ [45]						
rectus abdominis	validity					++ (Dixon)/ +++ (12% MSS) (T1) [59]		
	intraR					+++ (12% MSS) [59]		
	interR	+ [45]				++ (12% MSS) [59]		
psoas	validity					++ (Dixon)/ +++ (T1) (10% MSS) [59]		+++ [67]
	intraR					+++ (10% MSS) [59]		
	interR	+++ [45]				+++ (10% MSS) [59]		
erector spinae and multifidus	validity							+++ [67]
	interR	+++ [45]						
gluteus medius	validity			++ [53]		++ (Dixon)/ +++ (T1) (25% MSS) [59]		
	intraR	+++ [63]				+++ (25% MSS) [59]		

	interR	+++ [61] + [63]				++ (25% MSS) [59]		
gluteus minimus	validity			+ [53]		++ (Dixon)/ +++ (T1) (30% MSS) [59]		
	intraR	+ (P) / ++ (H) [63]				++ (30% MSS) [59]		
	interR	+++ [61] + [63]				++ (30% MSS) [59]		
external obturator	intraR	++ [63]						
	interR	+ [63]						
gluteus maximus	validity			++ [53]		++ (Dixon)/ +++ (T1) (18% MSS) [59]		
	intraR					+++ (18% MSS) [59]		
	interR	+++ [61]				+++ (18% MSS) [59]		
piriformis	interR	+++ [61]						
iliacus	validity					++ (Dixon)/ +++ (T1) (25% MSS) [59]		
	intra reliab					+++ (25% MSS) [59]		
	inter reliab					+++ (25% MSS) [59]		
obliquus	validity					++ (Dixon)/ +++ (T1) (20% MSS) [59]		
	intraR					+++ (20% MSS) [59]		
	interR					+++ (20% MSS) [59]		
spine flexors	validity						++ [53]	
spine extensors	validity						+ [53]	
hip flexors	validity						++ [53]	
hip extensors	validity						++ [53]	
rectus femoris	validity		++++ (alg 2, 9 MSS) [55] + to +++ (depending of nr of MSS) [47]	+++ [51] ++ [60] + (CSA/thickness) [28] +++ [53]		++ (Dixon)/ +++ (T1) (13% MSS) [59] ++ (6 MSS) [64] ++ (improved DPSO, 5 MSS) [68]		+ (fully)/ +++ (semi) [48] +++ [65]
	intraR					+++ (13% MSS) [59] ++ 6 MSS)[64]		
	interR	++ (1 subject) [64] ++ [46] +++ [48]				+++ (13% MSS) [59]		
vastus lateralis	validity		+ to +++ (depending of nr of MSS) [47]	+++ (58) +++ [60] + (thickness)/ ++ (CSA) [60]				+ (fully)/ +++ (semi) [48] +++ [65]
	interR	++ [48] ++ [46]						
vastus medialis	validity		+ to +++ (depending of nr of MSS) [47]	++ [53] +++ [60] ++ (58) + (thickness)/ ++ (CSA) [60]		++ (Dixon)/ +++ (T1) (15% MSS) [59] ++ (7 MSS) [64]		+++ (fully and semi) [48] +++ [65]
	intraR					+++ (15% MSS) [59] ++ (7 MSS) [64]		

	interR	++ [46] ++ (1 subject) [64] +++ [48]				+++ (15% MSS) [59]		
vastus intermedius	validity	++++ Barnouin 2015	+ to +++ (depending of nr of MSS) [47]	++ (58) ++ [60] + (thickness)/ ++ (CSA) [60]				+ (fully)/ +++ (semi) [48] +++ [65]
	interR	+++ [46] +++ [48]						
vastus lateralis and intermedius	validity			+++ [53]		++ (Dixon)/ +++ (T1) (15% MSS) [59] ++ (7 MSS) [63]		
	intraR					+++ (15% MSS) [59] +++ (7 MSS) [63]		
	interR	++ (1 subject) [64]				+++ (15% MSS) [59]		
vastus lateralis and medialis and intermedius	validity		++++ (alg 3, 3 MSS) [55]			++ (improved DPSO, 5 MSS) [68]		
quadriceps	validity		++ to ++++ (depending of nt of MSS) [26] + to +++ (depending of nt of MSS) [47] +++ to ++++ (depending of volume calculation method, 5 to 12 MSS) [27]	+ to ++ (CSA at different levels) [60]	++ [26] ++ (9)	++++ [27]	++ [53]	
	intraR	++++ [27]						
	interR	+++ [48] ++ [46] ++++ [27]	+++ (9)					
sartorius	validity		++++ (alg 3, 7 MSS) [55]	+++ [53]		++ (Dixon)/ +++ (T1) (10% MSS) [59] ++ (7 MSS) [64] ++ (improved DPSO, 5 MSS) [68]		+++ [65]
	intraR					+++ (10% MSS) [59] + (7 MSS) [64]		
	interR	+ (1 subject) [64]				+++ (10% MSS) [59]		
tensor fascia lata	validity			++ [53]		++ (Dixon)/ +++ (T1) (15%MSS) [59] ++ (6 MSS) [64] ++ (improved DPSO, 4 MSS) [68]		
	intraR					+++ (15%MSS) [59] ++ (6 MSS) [64]		
	interR	++ (1 subject) [64]				+++ (15%MSS) [59]		
biceps femoris short head	validity		++++ (all) [55]	++ [53] + [60]		++ (8 MSS) [64] ++ (improved DPSO, 5 MSS) [68]		+++ [65]
	intraR					+ (8 MSS) [63]		

	interR	+ (1 subject) [64]						
biceps femoris long head	validity		++++ (all) [55]	++ [53] + [60]		+++ (6 MSS) [64] ++ (improved DPSO, 4 MSS) [68]		+++ [65]
	intraR					+ (6 MSS) [64]		
	interR	++ (1 subject) [64]						
biceps femoris	validity					++ (Dixon)/ +++ (T1) (12% MSS) [59]		
	intraR					+++ (12% MSS) [59]		
	interR					+++ (12% MSS) [59]		
semi tendinonsis	validity		++++ (alg 2, 11 MSS) [55]	++ [53] + [60] ++ [51]		++ (6 MSS) [64] ++ (improved DPSO, 6 MSS) [68]		+++ [65]
	intraR					+ (6 MSS) [64]		
	interR	++ (1 subject) [64]						
semi membranosus	validity		++++ (all) [55]	++ [53] + [60] ++ [51]		++ (6 MSS) [64] ++ (improved DPSO, 5 MSS) [68]		+++ [65]
	intraR					+ (6 MSS) [64]		
	interR	++ (1 subject) [64]						
gracilis	validity		++++ (all) [55]	++ [53]		++ (Dixon)/ +++ (T1) (10% MSS) [59] ++ (7 MSS) [64] ++ (improved DPSO, 4 MSS) [68]		+++ [65]
	intraR					+++(10% MSS) [59] + (7 MSS) [64]		
	interR	+ (1 subject) [64]				+++ (10% MSS) [59]		
AddOP	validity			++ [53]				
add longus	validity		++++ (alg 2, 3 MSS) [55]					
add magnus	validity		++++ (alg 2, 1 MSS) [55]					
semi membranosus and tendinosis	validity					++ (Dixon)/ +++ (T1) (11%MSS) [59]		
	intraR					+++ (11%MSS) [59]		
	interR					+++ (11%MSS) [59]		
adductor (brevis, longus, magnuas)	validity					++ (Dixon)/ +++ (T1) (20%MSS) [59]		
	intraR					+++ (20%MSS) [59]		
	interR					+++ (20%MSS) [59]		
adductor	validity							+++ [65]
knee flexors	validity						++ [53]	
knee extensors	validity						++ [53]	
gastrocnemius medialis	validity		++++ (alg 2, 2 MSS) [55]	++ [52] ++ [51] +++ [57]		++ (8 MSS) [64]		

	interR	++ (1 subject) [64]						
gastrocnemius lateralis	validity		++++ (alg 2, 7 MSS) [55]	+ [52]		++ (6 MSS) [64]		
	intraR					+ (6 MSS) [64]		
	interR	++ (1 subject) [64]						
soleus	validity		++++ (alg 2, 4 MSS) [55]	++ [52] ++ [51] ++ [57]				
tibialis posterior	validity		++++ (alg 2, 12 MSS) [55]					
peroneus (Longus, Brevis, Tertius)	validity		++++ (alg 3, 7 MSS) [55]					
tibialis anterior + extensor digitorum longus + extensor hallucis longus	validity		++++ (alg 3, 10 MSS) [55] ++++ (8 MSS) [49]					
	intraR		+++ 13 slices [49]					
	interR		++ 13 slices [49]					
flexor digitorum longus	validity		++++ (alg 2, 7 MSS) [55]					
tibialis anterior	validity			++ [51]				

IntraR: intra rater reliability, interR: inter rater reliability

Excellent, good, moderate and poor metrological qualities are represented by ++++, +++, ++ and + signs respectively

CSA segmentation on a reduced number of slices

Estimation of muscle volume using CSA segmentation on a reduced number of slices was evaluated in 6 articles (Range Q score: 66-73; mean Q score: 70.2 [9,26,27,47,49,55]). The choice of slices for segmentation was based on different elements, such as the number of slices [27,49], interslice distance [9,26,47,55], specific characteristics of the slices (for example slices with largest CSA, or slices taken in a specific part of the muscle [55]). Six different methods of volume estimation were reported: the cylinder method [49], the cone method [26,27,49], the Cavalieri method [27], cubic spline interpolation [27], and 3rd and 4th order polynomial equations [47]. Comparison between segmentation data from techniques using a reduced number of slices and slice-by-slice segmentation (n=5 [26,27,47,49,55]) showed that validity varied from poor to excellent. Validity was excellent when a sufficient number of slices was segmented Reducing the number of slices systematically increased the error. The number and the choice of slices to segment and the choice of volume calculation method to obtain a pre-determined error was specific to each muscle. The method of CSA segmentation on a reduced number of slices had moderate to good intra and inter-rater reliability ICC (n=2 [9,49]).

CSA segmentation or muscle thickness using a single slice and muscle length

Eight articles evaluated the use of CSA segmentation or muscle thickness using a single slice and muscle length to estimate muscle volume (Range Q scores: 61-78; mean Q score: 67.4) [50–53,57,58,60]. For the measurements, either the slice with the greatest CSA [51–53,57,58,60], or slices taken at specific locations (for example at 50% of the bone length) [28,50,60] were used. To estimate muscle volumes, equations using muscle length, CSA and shape factors were used. The validity of these methods was evaluated by comparing with slice-by-slice manual segmentation in all the studies but one. Results showed that validity ranged from poor to good, but was mostly moderate (n=8 [50–53,57,58,60]). The smallest errors were found for CSA measured at 60% from the distal end of the femur or humerus for the quadriceps,

knee flexors and triceps brachialis (n=3 [28,50,60]), and using muscle thickness at 50% of the femur for the quadriceps (n=1 [28]). Some muscle volumes appeared to be more difficult to obtain with CSA segmentation using a single slice, such as gluteus minimus and quadratus lumborum, for which validity was poor. No studies evaluated reliability.

CSA segmentation on a single slice without muscle length

Estimation of muscle volume using CSA segmentation on a single slice without muscle length was evaluated in three articles (Range Q score: 68-72; mean Q score: 69.3 [9,26,56]). Specific slices were chosen, either the one with the largest CSA [26] or those taken at specific locations [9,56]. Manual slice-by-slice segmentation was used as the control reference to evaluate validity, and showed that it was poor to moderate (n=3 [9,26,56]). Poor results were found for supraspinatus, and subscapularis muscles [56]. Intra and inter-rater reliability were good (n=1 [56]).

Automatic segmentation techniques (table 1 and 2, S3 S4 and S5 Tables)

Deformation of a parametric specific object method with manual segmentation

Estimation of muscle volume and/or 3D shape using the deformation of a parametric specific object (DPSO) method with manual segmentation was evaluated in five articles (Range Q score: 46-71; mean Q score: 62.2 [27,53,59,64,68]).This technique involves manual contouring on a reduced set of images, followed by a parametric shape-based interpolation combined with a kriging technique in order to obtain a surface model without using the intermediate slices [68,69]. Validity was moderate to good compared to slice-by-slice manual segmentation (n=4 [27,59,64,68]). Reducing the number of slices increased the error (n=1 [53]). Reliability was poor to good depending on the muscle (n=2, [59,64]). The number of manually segmented slices

306 required to obtain a pre-determined error was specific to each muscle. A larger number of slices
307 was necessary for gluteus minimus, gluteus medius, obliquus and iliacus.
308
309 ## Other automatic segmentation techniques
310 Four other methods to estimate 3D muscle shapes were evaluated: semi-automated and
311 automated atlas-based segmentation [48], image-based and shape-based segmentation [29],
312 atlas-based and statistical shape-based segmentation [67], and interactive-segmentation using
313 shape priors and statistical shape modelling [65] (Range Q scores: 49-73: mean Q score: 55.5).
314 Andrews et al. used a probabilistic shape representation called generalized log-ratio
315 representation that included adjacency information along with a rotationally invariant random
316 forest boundary detector to automatically segment thigh muscles [65]. Kim et al. used an active
317 contour segmentation method with a level sets approach to automatically extract supraspinatus
318 muscle from an MR image [29]. Engstrom et al., used a statistical shape model (SSM) to
319 automatically segment quadratus lumborum [67]. During the fitting process, the deformable
320 SSM was constrained using probabilistic MR atlases. Le Trotter et al. used a multi-atlas based
321 automatic segmentation method to quantify the volume of the quadriceps femoris muscle group
322 [48]. Validity against slice by slice manual segmentation was moderate to excellent and most
323 of the results showed good validity. No studies of reliability were found.
324
325 # Technique feasibility (S4 Table)
326 The duration of segmentation was evaluated in eight studies [25,26,46,56,59,64–66]. Use of a
327 reduced number of slices to obtain muscle volume divided segmentation time by 4, use of only
328 one or two slices divided segmentation time by 26 and 15, respectively [56]. Use of the DPSO
329 method to evaluate 3D shape halved the time taken in one article [59] and divided it by 12 in
330 another [27]. Using automatic segmentation methods, one article reported that the time-to-run,

without human interaction, was about 50 minutes per image [65]. No other studies evaluated feasibility.

Discussion

This review included 30 articles which primarily focused on segmentation techniques. It has reported currently available evidence for the metrological qualities of manual and automatic segmentation techniques that estimate muscle volume and shape, and the feasibility of their use in a clinical or research setting. The majority of studies reviewed included healthy subjects, evaluated lower limb muscles and used slice-by-slice manual segmentation as the gold-standard reference. Greater errors in volume and shape estimation were found to be produced by methods that simplified and shortened the manual segmentation process. Sufficient evidence was available to support the validity of the DPSO technique. A lack of robust studies meant that other automatic segmentation techniques could not be validated but the evidence currently available was considered to be encouraging and further work on these methods is indicated. Some particularities for specific muscles and segmentation techniques were highlighted.

Metrological qualities of manual and automatic techniques

Manual segmentation techniques

Slice-by-slice manual segmentation was the most evaluated technique but its validity was only evaluated in one study (on rotator cuff muscles). As slice-by-slice manual segmentation is widely used as a reference method, further studies are warranted to confirm its validity. With regards to reliability, results varied among muscles. The use of different volume calculation methods did not seem to change the errors, indicating that errors found between measurements were likely related to segmentation. The quality of the results was lower for deep muscles such as gluteus minimus and for muscles whose boundaries are unclear, such as the individual

muscles of the quadriceps. Identifying their external borders appears challenging. To limit these segmentation errors, we believe that it is essential that standardized procedures using clear anatomical landmarks per muscle are developed and implemented [46]. Despite the fact that few studies evaluated image acquisition methods, they appear to be key for the limitation of segmentation errors [70]. Regarding the studies that compared data from subjects with healthy or pathological muscles, the weaker reliability for pathological muscles could be attributed to shape changes and boundaries that are more difficult to identify [65]. Slice-by-slice manual segmentation is also time-consuming, hence it cannot be easily used in clinical practice.

Techniques based on the manual segmentation of a reduced number of slices reached good to excellent validity when a sufficient number of slices was segmented. The appropriate number of slices varied among muscles. For most, fewer than half of the total number of slices need to be manually segmented, with slice thicknesses of 10 mm and interslice distances of 5 mm, allowing shorter processing time, whilst maintaining an almost equivalent level of performance compared to slice by slice segmentation. Results can further be improved by the choice of appropriate slices to segment [55]. Errors in volume estimation can however occur when the number of segmented slices is reduced [26,27,47,49,55]. We were unable to determine any general rules based on muscle shape or the size, thus further studies are required to assess these methods in muscles that were not evaluated in this systematic review, especially upper limb and trunk muscles. Lastly, important differences between volume calculation methods were also highlighted. For example, the cone method was inappropriate for fusiform muscles [27,47].

Use of even faster techniques, such as the segmentation of a single slice with or without muscle length, could be associated with a loss of precision. Because of their speed of realization, these techniques can be used in clinical practice if the aim is, for example, to estimate the degree of muscle loss in diseases that causes severe atrophy, where differences of more than 10% in

volume would normally be expected. Special attention must however be paid when using these methods for non-fusiform muscles. Although the guidelines used for the choice of each slice were detailed for each technique, there was little reliability evaluations. It has been previously reported that the optimal location of measurements can be difficult to both define and reproduce [61] thus there is a potential for errors to occur from manual CSA segmentation. Further studies are warranted to evaluate reliability.

Automatic segmentation techniques

The DPSO method, which involves automatic segmentation of intermediate slices, had good validity if enough slices were manually segmented. For non-fusiform and small muscles, a greater number of slices has to be manually segmented to maintain good accuracy. If this method is found to be reliable, it could be used in association with manual techniques to reduce the number of manually segmented slices and help save time. Further studies are warranted to determine which technique is the most accurate and fast between manual segmentation of a reduced number of slices with different volume estimation methods and manual segmentation with DPSO [27]. The results could differ depending on the muscles, because of their specific shapes and localizations.

The validity of the other four partially or completely automatic techniques analysed (semi-automated and automated atlas-based segmentation, image based and shape-based segmentation, atlas based and statistical shape-based segmentation) could not be confirmed in this review due to the small number of low-quality studies currently available, however it is important to note that results were encouraging. These techniques appeared to be promising in terms of validity. High quality, additional metrological studies are thus needed to validate them. Each technique had its own characteristics: segmentation using generalized log-ratio representation transformation can impose soft constraints whereas deformable statistical shape

models and atlas-based segmentations use hard constraints. However, the generalized log-ratio representation method cannot effectively delineate pose variability as against the other techniques and thus requires image pre-processing as an additional step. Thus, some techniques may be more appropriate than others depending on the muscles and their properties and on the characteristics of the population (children, persons with muscle pathology etc.). Other findings indicated that techniques, such as random-walk segmentation [71,72], wavelet-based segmentation [73], or deep learning-based segmentation [74] should additionally be investigated further to determine if they could provide rapid, accurate, valid and reliable measurements of muscle volume and shape for use in routine clinical practice.

Pathological muscles

Methods to estimate skeletal muscle volumes and/or 3D muscle shapes using MRI data are used clinically for diagnosis [14], to evaluate the effects of treatment [12], and as an aid to preoperative planning [18]. In the case of muscle pathologies, changes in muscle shape and signal occur because of muscle degeneration, which can render identification of muscle boundaries in MRI difficult (due to fatty and fibrous infiltration) [16,17]. Modification of the anatomical landmarks used for CSA segmentation, of techniques that are based on shape factors, and of volume estimation methods may therefore be required. This is, however, currently unknown due to a lack of studies that have evaluated pathological muscles. This finding suggested that specific metrological studies are required depending on the pathology being investigated in order to avoid measurement errors and that caution must be applied when extrapolating the results of techniques used in healthy muscles to those with pathologies.

Image acquisition

The MRI protocol used to acquire images can have a huge impact on segmentation outcomes [70]. The studies included in this review mostly used T1 weighted sequences, suggesting that

these anatomical sequences are appropriate for segmentation because of their ability to provide good quality images of the muscles, to distinguish the margins between them and because of their capacity to contrast bones from muscle [9,27,29,64]. However other sequences could also be used and differences in metrological properties between sequences were shown in one article [59]. No other studies compared different sequences in the articles included. Thus, data regarding the validity of the different sequences are warranted [59]. Regarding the issue of 2D or 3D acquisition, of the seven articles which used 3D sequences, none showed that 3D sequences yielded better results than 2D sequences. Most of them evaluated manual segmentation techniques. Since 3D sequences take longer to acquire, have lower contrast and are more sensitive to susceptibility and B0 inhomogeneities [75], there was no evidence to recommend 3D acquisition for manual segmentation. Continuous slice acquisition, allowing muscle tracking, might be an interesting method [55]. The size of the muscle should be considered in determining the resolution to use to avoid partial volume artefacts [49,66]. A greater resolution is needed for small muscles. We suggest the use of a T1 sequence, 2D acquisition with continuous slices between 1 and 10mm thick, oriented in an orthogonal way to the large axis of the muscles, with a resolution that avoids partial volume effects. However, the paucity of data in the articles included in the systematic review does not allow strong recommendations to be made. Lastly, no data are currently available to show the effect of MRI scanner and coil type on data acquisition and the quality of metrological parameters, despite the fact that all of these elements could impact on the accuracy and reliability of the muscle volume and shape [54,65,76,77]. Further studies are therefore warranted to clarify these issues.

The feasibility of MRI can be limited by the availability of MRI scanners and the cost of MRI devices and assessments. Thus, some other techniques, for example using ultrasonography, could be interesting to estimate skeletal muscle volumes and 3D muscle shapes [78].

Improving future metrological study methodology

We believe future work should include evaluation of test-retest reliability since we found only two articles that assessed this [48,62]. Test retest reliability refers to the extent to which the rating of one sample of individuals by one observer on two or more separate occasions using the same test yields similar results, with all test conditions remaining as constant as possible [31]. This is of high importance because factors such as patient positioning could impact on the accuracy and reliability of the muscle volume and shape as determined using MRI [54,65,76,77]. The second evaluation of great importance in future work is responsiveness. Responsiveness refers to the quality of a measure when showing changes [32], and is also a very important quality for the evaluation of neuromuscular disease progression [10,11] and the effects of treatment [12,50]. We were unable to report on the responsiveness of techniques in the present review as it was only evaluated in two articles.

Furthermore, precise reporting of the statistical analysis method employed is essential for metrological studies. As a result of the work undertaken in this review we recommend that the following evaluations are included as standard in future work, in addition to the usual analyses of correlation to improve the internal validity, on measurement technique studies [30,79]. The first evaluation we recommend is measurement error. In order to demonstrate the reliability of a technique, the standardized error of measurement, including limits of agreement or smallest detectable change [30], should be known as they indicate whether the observed difference is due to a true change in muscle volume or size, or if it is simply a measurement error.

Limitations

When considering our findings and recommendations, it is important to note that the strength of any conclusions depends on the quality of the original articles [43]. The articles were rated as moderate to good quality, however only two included statistical power calculations, reducing the conclusions that can be drawn from the results. This aspect of study design should be included in all future studies into this topic. A second limitation of this study is the heterogeneity

of source material included, in particular the different MRI parameters used in the studies and the different muscles evaluated prevented pooled analysis from being carried out and complicated the synthesis of the results. Regarding MRI, even when the same sequences were used, the parameters remained heterogeneous since they were device-dependent. Regarding muscles, some muscles have been the focus of many studies, whilst others have been neglected. Clinicians and researchers should bear this in mind when using a technique that has not been previously evaluated for the muscle in question. The results of this study are therefore only relevant for the methods of estimation of muscle volume and shape evaluated by the studies included, and must be generalised with caution to other methods and other muscles. Finally, the statistical methods employed by the different studies also varied considerably which, in turn, further prevented more definite conclusions from being drawn in this review. The different statistical methods used to report concurrent validity (including r^2, ICC, Dice Similarity Index), Tannimoto coefficient, mean differences, SD, SEE, RMSE and point-to-surface distance) and reliability (such as ICC, mean differences, RMSE, coefficient of variation and standard deviation) limited the synthesis of the data with a quantitative pooled analysis. Future work should aim to overcome as far as possible such diversity in order to both strengthen results as well as improving the generalisability of findings across different methods.

Conclusion

The results of this systematic review provide a rationale for the choice of appropriate segmentation techniques depending on the muscle, the need for precision and the available time. Such uses could include diagnosis of a disease, evaluation of a treatment response, monitoring of disease progression or measurement for research purposes. Further research is required to confirm the validity of manual slice-by-slice segmentation and automatic techniques, except for DPSO for which there is sufficiently strong supporting evidence. The reliability of most techniques in current use also needs to be confirmed, except for manual slice-by-slice

segmentation, which has been shown to be sufficiently reliable (if time consuming). Studies to evaluate different MRI protocols are warranted. Specific studies in pathological muscles are also needed to enable the proper application of such techniques in routine clinical practice.

Acknowledgements

We sincerely thank Johanna Robertson and Jennifer Dandrea Palethorpe for the English revision. We sincerely thank Elisabeth Bruyant, Sebastien Kerdraon and Vincent Josse for their help relating to MRI techniques.

References

1. Lieber RL, Fridén J. Functional and clinical significance of skeletal muscle architecture. Muscle Nerve. 2000 Nov 1;23(11):1647–66.
2. Fukunaga T, Miyatani M, Tachi M, Kouzaki M, Kawakami Y, Kanehisa H. Muscle volume is a major determinant of joint torque in humans. Acta Physiol Scand. 2001 Aug;172(4):249–55.
3. Holzbaur KRS, Delp SL, Gold GE, Murray WM. Moment-generating capacity of upper limb muscles in healthy adults. J Biomech. 2007;40(11):2442–9.
4. Trappe SW, Trappe TA, Lee GA, Costill DL. Calf muscle strength in humans. Int J Sports Med. 2001 Apr;22(3):186–91.
5. Pons C, Sheehan FT, Im HS, Brochard S, Alter KE. Shoulder muscle atrophy and its relation to strength loss in obstetrical brachial plexus palsy. Clin Biomech Bristol Avon. 2017 Oct;48:80–7.
6. Narici MV, Maganaris CN, Reeves ND, Capodaglio P. Effect of aging on human muscle architecture. J Appl Physiol Bethesda Md 1985. 2003 Dec;95(6):2229–34.
7. Mathur S, Takai KP, Macintyre DL, Reid D. Estimation of thigh muscle mass with magnetic resonance imaging in older adults and people with chronic obstructive pulmonary disease. Phys Ther. 2008 Feb;88(2):219–30.
8. Layec G, Venturelli M, Jeong E-K, Richardson RS. The validity of anthropometric leg muscle volume estimation across a wide spectrum: from able-bodied adults to individuals with a spinal cord injury. J Appl Physiol Bethesda Md 1985. 2014 May 1;116(9):1142–7.
9. Marcon M, Ciritsis B, Laux C, Nanz D, Nguyen-Kim TDL, Fischer MA, et al. Cross-sectional area measurements versus volumetric assessment of the quadriceps femoris muscle in patients with anterior cruciate ligament reconstructions. Eur Radiol. 2015 Feb;25(2):290–8.
10. Jenkins TM, Burness C, Connolly DJ, Rao DG, Hoggard N, Mawson S, et al. A prospective pilot study measuring muscle volumetric change in amyotrophic lateral sclerosis. Amyotroph Lateral Scler Front Degener. 2013 Sep;14(5–6):414–23.
11. Godi C, Ambrosi A, Nicastro F, Previtali SC, Santarosa C, Napolitano S, et al. Longitudinal MRI quantification of muscle degeneration in Duchenne muscular dystrophy. Ann Clin Transl Neurol. 2016 Aug;3(8):607–22.

12. Wu EX, Tang H, Tong C, Heymsfield SB, Vasselli JR. In vivo MRI quantification of individual muscle and organ volumes for assessment of anabolic steroid growth effects. Steroids. 2008 Apr;73(4):430–40.
13. Popadic Gacesa JZ, Kozic DB, Dragnic NR, Jakovljevic DG, Brodie DA, Grujic NG. Changes of functional status and volume of triceps brachii measured by magnetic resonance imaging after maximal resistance training. J Magn Reson Imaging JMRI. 2009 Mar;29(3):671–6.
14. Koltzenburg M, Yousry T. Magnetic resonance imaging of skeletal muscle. Curr Opin Neurol. 2007 Oct;20(5):595–9.
15. Andersen H, Gjerstad MD, Jakobsen J. Atrophy of foot muscles: a measure of diabetic neuropathy. Diabetes Care. 2004 Oct;27(10):2382–5.
16. Kaick O van, Hamarneh G, Ward AD, Schweitzer M, Zhang H. Learning Fourier descriptors for computer-aided diagnosis of the supraspinatus. Acad Radiol. 2010 Aug;17(8):1040–9.
17. HajGhanbari B, Hamarneh G, Changizi N, Ward AD, Reid WD. MRI-based 3D shape analysis of thigh muscles patients with chronic obstructive pulmonary disease versus healthy adults. Acad Radiol. 2011 Feb;18(2):155–66.
18. Blemker SS, Delp SL. Three-dimensional representation of complex muscle architectures and geometries. Ann Biomed Eng. 2005 May;33(5):661–73.
19. de Boer MD, Maganaris CN, Seynnes OR, Rennie MJ, Narici MV. Time course of muscular, neural and tendinous adaptations to 23 day unilateral lower-limb suspension in young men. J Physiol-Lond. 2007 Sep 15;583(3):1079–91.
20. Belavy DL, Ohshima H, Bareille M-P, Rittweger J, Felsenberg D. Limited effect of fly-wheel and spinal mobilization exercise countermeasures on lumbar spine deconditioning during 90 d bed-rest in the Toulouse LTBR study. Acta Astronaut. 2011 Oct;69(7–8):406–19.
21. Engstrom CM, Walker DG, Kippers V, Mehnert AJH. Quadratus lumborum asymmetry and L4 pars injury in fast bowlers: a prospective MR study. Med Sci Sports Exerc. 2007 Jun;39(6):910–7.
22. Inan M, Alkan A, Harma A, Ertem K. Evaluation of the gluteus medius muscle after a pelvic support osteotomy to treat congenital dislocation of the hip. J Bone Jt Surg-Am Vol. 2005 Oct;87A(10):2246–52.
23. Tothill P, Stewart AD. Estimation of thigh muscle and adipose tissue volume using magnetic resonance imaging and anthropometry. J Sports Sci. 2002 Jul;20(7):563–76.
24. Nakatani M, Takai Y, Akagi R, Wakahara T, Sugisaki N, Ohta M, et al. Validity of muscle thickness-based prediction equation for quadriceps femoris volume in middle-aged and older men and women. Eur J Appl Physiol. 2016 Dec;116(11–12):2125–33.
25. Tingart MJ, Apreleva M, Lehtinen JT, Capell B, Palmer WE, Warner JJP. Magnetic resonance imaging in quantitative analysis of rotator cuff muscle volume. Clin Orthop. 2003 Oct;(415):104–10.
26. Tracy BL, Ivey FM, Jeffrey Metter E, Fleg JL, Siegel EL, Hurley BF. A more efficient magnetic resonance imaging-based strategy for measuring quadriceps muscle volume. Med Sci Sports Exerc. 2003 Mar;35(3):425–33.
27. Nordez A, Jolivet E, Südhoff I, Bonneau D, de Guise JA, Skalli W. Comparison of methods to assess quadriceps muscle volume using magnetic resonance imaging. J Magn Reson Imaging JMRI. 2009 Nov;30(5):1116–23.
28. Yamauchi K, Yoshiko A, Suzuki S, Kato C, Akima H, Kato T, et al. Estimation of individual thigh muscle volumes from a single-slice muscle cross-sectional area and muscle thickness using magnetic resonance imaging in patients with knee osteoarthritis. J Orthop Surg Hong Kong. 2017 Dec;25(3):2309499017743101.
29. Kim S, Lee D, Park S, Oh K-S, Chung SW, Kim Y. Automatic segmentation of supraspinatus from MRI by internal shape fitting and autocorrection. Comput Methods Programs Biomed. 2017 Mar;140:165–74.

30. de Vet HCW, Terwee CB, Knol DL, Bouter LM. When to use agreement versus reliability measures. J Clin Epidemiol. 2006 Oct;59(10):1033–9.
31. Brink Y, Louw QA. Clinical instruments: reliability and validity critical appraisal. J Eval Clin Pract. 2012 Dec;18(6):1126–32.
32. Mokkink LB, Terwee CB, Patrick DL, Alonso J, Stratford PW, Knol DL, et al. The COSMIN study reached international consensus on taxonomy, terminology, and definitions of measurement properties for health-related patient-reported outcomes. J Clin Epidemiol. 2010 Jul;63(7):737–45.
33. Brunner G, Nambi V, Yang E, Kumar A, Virani SS, Kougias P, et al. Automatic quantification of muscle volumes in magnetic resonance imaging scans of the lower extremities. Magn Reson Imaging. 2011 Oct;29(8):1065–75.
34. Mitsiopoulos N, Baumgartner RN, Heymsfield SB, Lyons W, Gallagher D, Ross R. Cadaver validation of skeletal muscle measurement by magnetic resonance imaging and computerized tomography. J Appl Physiol Bethesda Md 1985. 1998 Jul;85(1):115–22.
35. Esformes JI, Narici MV, Maganaris CN. Measurement of human muscle volume using ultrasonography. Eur J Appl Physiol. 2002 May;87(1):90–2.
36. Borotikar B, Lempereur M, Lelievre M, Burdin V, Ben Salem D, Brochard S. Dynamic MRI to quantify musculoskeletal motion: A systematic review of concurrent validity and reliability, and perspectives for evaluation of musculoskeletal disorders. PloS One. 2017;12(12):e0189587.
37. Pons C, Rémy-Néris O, Médée B, Brochard S. Validity and reliability of radiological methods to assess proximal hip geometry in children with cerebral palsy: a systematic review. Dev Med Child Neurol. 2013 Dec;55(12):1089–102.
38. Whiting P, Rutjes AWS, Reitsma JB, Bossuyt PMM, Kleijnen J. The development of QUADAS: a tool for the quality assessment of studies of diagnostic accuracy included in systematic reviews. BMC Med Res Methodol. 2003 Nov 10;3:25.
39. Downs SH, Black N. The feasibility of creating a checklist for the assessment of the methodological quality both of randomised and non-randomised studies of health care interventions. J Epidemiol Community Health. 1998 Jun;52(6):377–84.
40. von Elm E, Altman DG, Egger M, Pocock SJ, Gøtzsche PC, Vandenbroucke JP, et al. The Strengthening the Reporting of Observational Studies in Epidemiology (STROBE) Statement: guidelines for reporting observational studies. Int J Surg Lond Engl. 2014 Dec;12(12):1495–9.
41. Lempereur M, Brochard S, Leboeuf F, Rémy-Néris O. Validity and reliability of 3D marker based scapular motion analysis: a systematic review. J Biomech. 2014 Jul 18;47(10):2219–30.
42. Terwee CB, Mokkink LB, Knol DL, Ostelo RWJG, Bouter LM, de Vet HCW. Rating the methodological quality in systematic reviews of studies on measurement properties: a scoring system for the COSMIN checklist. Qual Life Res Int J Qual Life Asp Treat Care Rehabil. 2012 May;21(4):651–7.
43. Mokkink LB, Terwee CB, Knol DL, Stratford PW, Alonso J, Patrick DL, et al. The COSMIN checklist for evaluating the methodological quality of studies on measurement properties: a clarification of its content. BMC Med Res Methodol. 2010 Mar 18;10:22.
44. Atkinson G, Nevill AM. Statistical methods for assessing measurement error (reliability) in variables relevant to sports medicine. Sports Med Auckl NZ. 1998 Oct;26(4):217–38.
45. Valentin S, Yeates TD, Licka T, Elliott J. Inter-rater reliability of trunk muscle morphometric analysis. J Back Musculoskelet Rehabil. 2015;28(1):181–90.
46. Barnouin Y, Butler-Browne G, Voit T, Reversat D, Azzabou N, Leroux G, et al. Manual segmentation of individual muscles of the quadriceps femoris using MRI: a reappraisal. J Magn Reson Imaging JMRI. 2014 Jul;40(1):239–47.
47. Barnouin Y, Butler-Browne G, Moraux A, Reversat D, Leroux G, Behin A, et al.

658 Comparison of Different Methods to Estimate the Volume of the Quadriceps Femoris Muscles
659 Using MRI. J Med Imaging Health Inform. 2015 Oct;5(6):1201–7.
660 48. Le Troter A, Fouré A, Guye M, Confort-Gouny S, Mattei J-P, Gondin J, et al. Volume
661 measurements of individual muscles in human quadriceps femoris using atlas-based
662 segmentation approaches. Magma N Y N. 2016 Apr;29(2):245–57.
663 49. Lund H, Christensen L, Savnik A, Boesen J, Danneskiold-Samsøe B, Bliddal H. Volume
664 estimation of extensor muscles of the lower leg based on MR imaging. Eur Radiol. 2002
665 Dec;12(12):2982–7.
666 50. Popadic Gacesa J, Dragnic NR, Prvulovic NM, Barak OF, Grujic N. The validity of
667 estimating triceps brachii volume from single MRI cross-sectional area before and after
668 resistance training. J Sports Sci. 2011 Mar;29(6):635–41.
669 51. Vanmechelen IM, Shortland AP, Noble JJ. Lower limb muscle volume estimation from
670 maximum cross-sectional area and muscle length in cerebral palsy and typically developing
671 individuals. Clin Biomech Bristol Avon. 2017 Nov 14;51:40–4.
672 52. Albracht K, Arampatzis A, Baltzopoulos V. Assessment of muscle volume and
673 physiological cross-sectional area of the human triceps surae muscle in vivo. J Biomech. 2008
674 Jul 19;41(10):2211–8.
675 53. Amabile C, Moal B, Chtara OA, Pillet H, Raya JG, Iannessi A, et al. Estimation of
676 spinopelvic muscles' volumes in young asymptomatic subjects: a quantitative analysis. Surg
677 Radiol Anat. 2017;39(4):393–403.
678 54. Eng CM, Abrams GD, Smallwood LR, Lieber RL, Ward SR. Muscle geometry affects
679 accuracy of forearm volume determination by magnetic resonance imaging (MRI). J Biomech.
680 2007;40(14):3261–6.
681 55. Belavý DL, Miokovic T, Rittweger J, Felsenberg D. Estimation of changes in volume
682 of individual lower-limb muscles using magnetic resonance imaging (during bed-rest). Physiol
683 Meas. 2011 Jan;32(1):35–50.
684 56. Lehtinen JT, Tingart MJ, Apreleva M, Zurakowski D, Palmer W, Warner JJP. Practical
685 assessment of rotator cuff muscle volumes using shoulder MRI. Acta Orthop Scand. 2003
686 Dec;74(6):722–9.
687 57. Mersmann F, Bohm S, Schroll A, Arampatzis A. Validation of a simplified method for
688 muscle volume assessment. J Biomech. 2014 Apr 11;47(6):1348–52.
689 58. Mersmann F, Bohm S, Schroll A, Boeth H, Duda G, Arampatzis A. Muscle shape
690 consistency and muscle volume prediction of thigh muscles. Scand J Med Sci Sports. 2015
691 Apr;25(2):e208-213.
692 59. Moal B, Raya JG, Jolivet E, Schwab F, Blondel B, Lafage V, et al. Validation of 3D
693 spino-pelvic muscle reconstructions based on dedicated MRI sequences for fat-water
694 quantification. Irbm. 2014 Jun;35(3):119–27.
695 60. Morse CI, Degens H, Jones DA. The validity of estimating quadriceps volume from
696 single MRI cross-sections in young men. Eur J Appl Physiol. 2007 Jun;100(3):267–74.
697 61. Skorupska E, Keczmer P, Łochowski RM, Tomal P, Rychlik M, Samborski W.
698 Reliability of MR-Based Volumetric 3-D Analysis of Pelvic Muscles among Subjects with Low
699 Back with Leg Pain and Healthy Volunteers. PloS One. 2016;11(7):e0159587.
700 62. Smeulders MJC, van den Berg S, Oudeman J, Nederveen AJ, Kreulen M, Maas M.
701 Reliability of in vivo determination of forearm muscle volume using 3.0 T magnetic resonance
702 imaging. J Magn Reson Imaging JMRI. 2010 May;31(5):1252–5.
703 63. Springer I, Müller M, Hamm B, Dewey M. Intra- and interobserver variability of
704 magnetic resonance imaging for quantitative assessment of abductor and external rotator
705 muscle changes after total hip arthroplasty. Eur J Radiol. 2012 May;81(5):928–33.
706 64. Südhoff I, de Guise JA, Nordez A, Jolivet E, Bonneau D, Khoury V, et al. 3D-patient-
707 specific geometry of the muscles involved in knee motion from selected MRI images. Med Biol
708 Eng Comput. 2009 Jun;47(6):579–87.
709 65. Andrews S, Hamarneh G. The Generalized Log-Ratio Transformation: Learning Shape

and Adjacency Priors for Simultaneous Thigh Muscle Segmentation. IEEE Trans Med Imaging. 2015 Sep;34(9):1773–87.
66. Elliott MA, Walter GA, Gulish H, Sadi AS, Lawson DD, Jaffe W, et al. Volumetric measurement of human calf muscle from magnetic resonance imaging. Magma N Y N. 1997 Jun;5(2):93–8.
67. Engstrom CM, Fripp J, Jurcak V, Walker DG, Salvado O, Crozier S. Segmentation of the quadratus lumborum muscle using statistical shape modeling. J Magn Reson Imaging JMRI. 2011 Jun;33(6):1422–9.
68. Jolivet E, Dion E, Rouch P, Dubois G, Charrier R, Payan C, et al. Skeletal muscle segmentation from MRI dataset using a model-based approach. Comput Methods Biomech Biomed Eng Imaging Vis. 2014 Feb 17;2.
69. Jolivet E, Daguet E, Bousson V, Bergot C, Skalli W, Laredo JD. Variability of hip muscle volume determined by computed tomography. Biocybern Biomed Eng. 2009 Feb;30(1):14–9.
70. Wang L, Chitiboi T, Meine H, Günther M, Hahn HK. Principles and methods for automatic and semi-automatic tissue segmentation in MRI data. Magma N Y N. 2016 Apr;29(2):95–110.
71. Baudin PY, Azzabou N, Carlier PG, Paragios N. Prior knowledge, random walks and human skeletal muscle segmentation. Med Image Comput Comput-Assist Interv MICCAI Int Conf Med Image Comput Comput-Assist Interv. 2012;15(Pt 1):569–76.
72. Baudin P-Y, Goodman D, Kumrnar P, Azzabou N, Carlier PG, Paragios N, et al. Discriminative parameter estimation for random walks segmentation. Med Image Comput Comput-Assist Interv MICCAI Int Conf Med Image Comput Comput-Assist Interv. 2013;16(Pt 3):219–26.
73. Essafi S, Langs G, Paragios N. Hierarchical 3D diffusion wavelet shape priors. In: 2009 IEEE 12th International Conference on Computer Vision. 2009. p. 1717–24.
74. Liu F, Zhou Z, Jang H, Samsonov A, Zhao G, Kijowski R. Deep convolutional neural network and 3D deformable approach for tissue segmentation in musculoskeletal magnetic resonance imaging. Magn Reson Med. 2017 Jul 21;
75. Fallah F, Machann J, Martirosian P, Bamberg F, Schick F, Yang B. Comparison of T1-weighted 2D TSE, 3D SPGR, and two-point 3D Dixon MRI for automated segmentation of visceral adipose tissue at 3 Tesla. Magma N Y N. 2017 Apr;30(2):139–51.
76. Fischmann A, Morrow JM, Sinclair CDJ, Reilly MM, Hanna MG, Yousry T, et al. Improved anatomical reproducibility in quantitative lower-limb muscle MRI. J Magn Reson Imaging JMRI. 2014 Apr;39(4):1033–8.
77. Melke GS de F, Costa ALF, Lopes SLP de C, Fuziy A, Ferreira-Santos RI. Three-dimensional lateral pterygoid muscle volume: MRI analyses with insertion patterns correlation. Ann Anat Anat Anz Off Organ Anat Ges. 2016 Nov;208:9–18.
78. Nakatani M, Takay Y, Wakahara T, Sugisaki N, Ohta M, Kawakami Y, Fukunaga T, Kanehisa H. Validity of muscle thickness-based prediction equation for quadriceps femoris volume in middle-aged and older men and women. Eur J Appl Physiol. 2016 Dec;116(11-12):2125-2133.
79. Mokkink LB, Terwee CB, Patrick DL, Alonso J, Stratford PW, Knol DL, et al. The COSMIN checklist for assessing the methodological quality of studies on measurement properties of health status measurement instruments: an international Delphi study. Qual Life Res. 2010 May;19(4):539–49.

L'ensemble des étapes nécessaires à l'estimation d'un volume musculaire est rapporté dans ce travail, comprenant les données concernant l'acquisition des images et éventuellement le post processing, les données relatives aux techniques de segmentation à partir des images acquises et les techniques utilisées pour les calculs de volume une fois la segmentation réalisée. Une grande diversité de protocoles était retrouvée pour chacune de ces étapes.
Il y avait de plus une variété notable dans les muscles évalués et dans les groupements musculaires réalisés. Les populations différaient également selon les articles (sujets sains, sujets pathologiques, cadavres).
L'ensemble de ces paramètres, associé à la variabilité des tests statistiques utilisés, rendait les **comparaisons entre les études complexes** et ne permettait pas la réalisation d'une **méta-analyse.** En effet, les études étaient trop **hétérogènes** en termes de population, type de technique testée et qualité méthodologique et n'auraient pas pu conduire à des résultats précis par technique et par muscle, limitant ainsi l'intérêt de l'étude.

Dans le contexte particulier de l'**enfant**, les résultats de ce travail sont à utiliser avec **précaution**. En effet, une seule étude incluse dans la revue systématique concernait les enfants (Vanmechelen, Shortland et Noble 2017). Du fait d'éventuelles différences morphologiques au niveau des muscles (modification du contraste musculaire en IRM (Bottomley et al. 1984) de la forme musculaire et du cartilage de croissance (Khanna et Thapa 2009), des spécificités pour l'acquisition des images en IRM puis pour la segmentation pourraient exister. De même, une **vigilance** particulière est à avoir pour **l'étude du muscle pathologique**. Les quelques données retrouvées laissaient présager une fiabilité plus faible des mesures chez des sujets avec une prothèse de hanche et rachialgiques (Springer et al. 2012; Skorupska et al. 2016).

L'évaluation métrologique se limitait à la validité dans la moitié des études. **La fidélité test-retest et la sensibilité au changement** sont des propriétés importantes à considérer dans une perspective de suivi de population pédiatrique. Dans le cadre spécifique du suivi longitudinal d'enfants présentant une POPB, avec évaluation du bénéfice d'une thérapeutique, l'évaluation de ces deux propriétés apparait indispensable afin de pouvoir écarter une erreur de mesure dans l'interprétation des résultats.

Les techniques de **segmentation automatiques** apparaissent très prometteuses, du fait de la réduction ou disparition du temps de segmentation manuelle, avec des perspectives d'utilisation en recherche mais peut-être également en pratique clinique dans l'avenir. De **nouvelles études métrologiques** sont indispensables afin de confirmer cette hypothèse pour les techniques décrites dans les articles inclus dans la revue systématique. Lors de l'utilisation de certaines techniques de segmentation automatiques, des prérequis sont cependant nécessaires et à prendre en compte, comme la nécessité d'avoir une base de données d'entraînement (Le Troter et al. 2016; Engstrom et al. 2011).

Pour la **mesure des volumes des muscles gléno-huméraux chez les enfants** à developpement typique et présentant une POPB, aucune donnée métrologique n'était disponible dans la littérature concernant les techniques adaptées pour les muscles, deltoïde, grand pectoral et grand rond chez l'enfant. Pour les muscles de la coiffe des rotateurs, les techniques simples de segmentation apparaissaient insuffisamment précises dans deux des articles inclus (Tingart et al. 2003; Lehtinen et al. 2003). Le faible nombre d'examens, la présence de muscles de formes et tailles différentes, la possibilité d'artefacts respiratoires au niveau du muscle pectoral, les difficultés attendues pour délimiter les muscles du fait de la dégénérescence musculaire (chez les enfants avec POPB) étaient des éléments en faveur du choix d'une **technique de segmentation manuelle précise**. Une technique de segmentation manuelle sur un grand nombre de coupes, avec une fréquence de segmentation variant en fonction de la taille et de la complexité des muscles évalués, pour répondre aux objectifs de précision mais aussi de faisabilité a été choisie.

2 Article 2 : Morphologie musculaire en IRM et fonction des muscles de l'épaule chez l'enfant sain

Chez les enfants, le **fonctionnement typique de l'épaule** reste peu exploré. Peu d'éléments descriptifs de l'épaule sont disponibles dans cette population au niveau musculaire. Les connaissances anatomiques provenant **d'études cadavériques adultes** leur sont appliquées bien qu'aucun élément ne permette de le justifier. Des différences morphologiques au niveau des muscles entre des populations d'âges différents ont déjà été constatées (Tate et al. 2006; Kubo et al. 2003; Akagi et al. 2009). Des variations en fonction de l'âge et des muscles de la distribution musculaire et une évolution de la relation force volume en fonction des âges et selon les sexes ont été montrées dans différentes régions anatomiques chez l'enfant (Kanehisa et al. 1995; Deighan et al. 2006; Kanehisa et al. 1994; Pitcher et al. 2012; Wood et al. 2004). Ainsi, au niveau de l'épaule, la croissance pourrait se faire de manière inhomogène en fonction des groupes musculaires, entraînant un équilibre entre les muscles agonistes et antagonistes différents de celui de l'adulte et la relation entre l'architecture musculaire et la genèse de force pourrait être plus faible chez les enfants.

Définir le fonctionnement de l'épaule chez les enfants à développement typique et connaitre sa « normalité » représente un enjeu. En effet, la bonne connaissance de ses spécificités anatomiques et de son fonctionnement normal est une étape préalable à l'identification et à la compréhension des dysfonctionnements présents chez les enfants présentant des pathologies de l'épaule, comme les enfants avec POPB.
L'étude IRM, non invasive et non irradiante, permettant la visualisation de l'ensemble des structures de l'épaule ainsi que la **mesure quantifiée des volumes musculaires**, semble particulièrement intéressante dans ce cadre.

Dans cette première étude, l'objectif principal était d'établir une **base de données pédiatrique sur les volumes des muscles de l'épaule et leur distribution,** dans une population regroupant des enfants d'âges, de tailles et de genres divers. L'objectif secondaire était **d'associer les**

volumes musculaires de l'épaule aux moments articulaires isométriques volontaires maximaux produits dans les différents degrés de liberté de l'épaule.

Le travail réalisé consistait en 1/ à la participation aux choix de de la méthodologie de segmentation, de répartition des muscles en groupes fonctionnels, de méthodologie de division du deltoide, des statistiques, en 2/ à la segmentation manuelle des muscles, en 3/ à la relecture de l'article principalement écrits par le premier et le dernier auteurs.

Journal of Biomechanics 47 (2014) 2730–2737

Contents lists available at ScienceDirect

Journal of Biomechanics

journal homepage: www.elsevier.com/locate/jbiomech
www.JBiomech.com

In vivo pediatric shoulder muscle volumes and their relationship to 3D strength

Hyun Soo Im [a], Katharine E. Alter [a,b], Sylvain Brochard [a,c,d], Christelle Pons [c], Frances T. Sheehan [a,*]

[a] Functional and Applied Biomechanics Section, Rehabilitation Medicine Department, National Institutes of Health, Bethesda, MD, USA
[b] Mt Washington Pediatric Hospital, Baltimore, MD, USA
[c] Rehabilitation Medicine Department, University Hospital of Brest, Brest, France
[d] LaTIM, INSERM U1101, Brest, France

ARTICLE INFO

Article history:
Accepted 28 April 2014

Keywords:
Torque
MRI
Children
Reliability
Rotator cuff
Injury

ABSTRACT

In the pediatric shoulder, injury and pathology can disrupt the muscle force balance, resulting in severe functional losses. As little data exists pertaining to *in vivo* pediatric shoulder muscle function, musculoskeletal data are crucially needed to advance the treatment of pediatric shoulder pathology/injury. Therefore, the purpose of this study was to develop a pediatric database of *in vivo* volumes for the major shoulder muscles and correlate these volumes with maximum isometric flexion/extension, internal/external rotation, and abduction/adduction joint moments. A methodology was developed to derive 3D shoulder muscle volumes and to divide the deltoid into sub-units with unique torque producing capabilities, based on segmentation of three-dimensional magnetic resonance images. Eleven typically developing children/adolescents (4F/7M, 12.0 ± 3.2 years, 150.8 ± 16.7 cm, 49.2 ± 16.4 kg) participated. Correlation and regression analyses were used to evaluate the relationship between volume and maximum, voluntary, isometric joint torques. The deltoid demonstrated the largest ($30.4 \pm 1.2\%$) and the supraspinatus the smallest ($4.8 \pm 0.5\%$) percent of the total summed volume of all six muscles evaluated. The anterior and posterior deltoid sections were $43.4 \pm 3.9\%$ and $56.6 \pm 3.9\%$ of the total deltoid volume. The percent volumes were highly consistent across subjects. Individual muscle volumes demonstrated moderate-high correlations with torque values (0.70–0.94, $p < 0.001$). This study presents a comprehensive database documenting normative pediatric shoulder muscle volume. Using these data a clear relationship between shoulder volume and the torques they produce was established in all three rotational degrees-of-freedom. This study furthers the understanding of shoulder muscle function and serves as a foundation for evaluating shoulder injury/pathology in the pediatric/adolescent population.

1. Introduction

Shoulder stability and function are predominantly maintained by a balance of muscle forces (Ackland and Pandy, 2011; Boettcher et al., 2010; Otis et al., 1994). As such, congenital conditions (e.g., brachial plexus palsy (Kozin et al., 2010) and cerebral palsy (Abel et al., 2003; Brochard et al., 2012)) can cause muscle imbalances and skeletal deformities, resulting in functional losses in both the pediatric and adult populations. Sports related injuries, which have been viewed as primarily adult issues, are now becoming prominent in pediatric populations as participation in high-level competitive sports is taking place at earlier ages (Davis, 2010; Emery, 2006). Unfortunately, much of the existing knowledge regarding shoulder function originates from adult cadaver and modeling studies. Since evidence suggests that children may not be scaled versions of adults (Neu et al., 2002; Tonson et al., 2008), *in vivo* pediatric shoulder musculoskeletal data are needed to enhance the understanding of typical shoulder function and improve the management and treatment of pediatric shoulder pathology/injury.

Although it is well accepted that an individual muscle's volume can predict its force generating capacity (Akagi et al., 2009; Blazevich et al., 2009; Fukunaga et al., 2001), establishing this relationship for the shoulder presents unique challenges. Specifically, the largest shoulder muscle (deltoid) has multiple lines of action, which enables it to generate torques on humerus in opposite directions (Ackland and Pandy, 2011; Brown et al., 2007; Kuechle et al., 2000). Specifically, the anterior deltoid segments produce

* Correspondence to: National Institutes of Health, Building 10 CRC RM 1-1469, 10 Center Drive MSC 1604, Bethesda, MD 20892-1604, USA. Tel.: +1 301 451 7585; fax: +1 301 451 7536.
E-mail address: fsheehan@cc.nih.gov (F.T. Sheehan).

http://dx.doi.org/10.1016/j.jbiomech.2014.04.049
0021-9290/

humeral flexion torque, while the posterior segments produce humeral extension torque. Likewise, but to a lesser degree, the deltoid is capable of ad/abduction and internal/external rotation torques. Thus, it is difficult to relate the volume of the deltoid to its ability to generate a torque in a specific direction. This has resulted in a paucity of data with regard to the shoulder muscle volume–torque relationship. To evaluate the full three-dimensional (3D) muscle volume–torque relationship an *in vivo* methodology is needed for separating the deltoid into sub-units with non-antagonist torque producing capabilities. Currently, the volume–torque relationship has been evaluated for only one of the three rotational degrees of freedom (DOF_R), ab/adduction (Audenaert et al., 2009; Holzbaur et al., 2007; Vidt et al., 2012). The pediatric shoulder muscle volume–torque relationship has not been quantified. Rather, individual shoulder muscle cross-sectional areas have been used to evaluate hypertrophy with training (Pitcher et al., 2012) and functional losses with pathological atrophy (Poyhia et al., 2005).

Therefore, the primary purpose of this study was to establish a normative pediatric database of shoulder muscle volume and its distribution, spanning a range of ages, sizes, and genders. The deltoid, pectoralis major, teres minor/infraspinatus, teres major/lattisimus dorsi, supraspinatus, and subscapularis were evaluated. The secondary purpose was to associate shoulder muscle volumes with the maximum voluntary isometric joint moments they produce in all three DOF_R. To accomplish these two purposes, an *in vivo* methodology for splitting the deltoid into functional sub-units was developed. The inter-rater reliability of obtaining pediatric muscle volumes and creating deltoid sub-units was evaluated.

2. Methods

Fourteen typically developing children/adolescents were recruited for this IRB (National Institute of Child Health and Human Development, intramural) approved study. A legal guardian or subject over 18 years of age provided written consent. Additionally, each subject under 18 years of age provided written assent. A pediatric physiatrist performed a history and physical. Potential subjects with active or historical upper limb pathology/injury or known contraindications to MR imaging were removed from the study. Three children declined MR imaging after enrollment and withdrew, leaving a cohort of seven males and four females (Table 1).

2.1. MR acquisition

Each participant was given time to become accustomed to the scanner. The subject was placed supine on the plinth of a 3T MR scanner (Verio: Siemens, Germany). To optimize the signal- and contrast-to-noise ratios, the dominant shoulder was positioned at the MR isocenter. In addition, standard cardiac flex coils were positioned anterior, posterior, and lateral to the shoulder. The arm was placed as close to anatomical position as possible with the forearm pronated for comfort. Sandbags were placed alongside the arm and a large supportive strap was gently secured around the coils and chest. A T1-gradient recalled echo sequence was acquired for the dominant shoulder. With the exception of the in-plane field of view, all scanning parameters were held constant across subjects ($416 \times 312 \times 192$ pixels, slice thickness 1.2 mm, TR=16.6 ms, TE=5.1 ms, imaging time=4 min 22 s). This slight variation in the in-plane resolution across subjects (0.55 mm × 0.55 mm–0.63 mm × 0.63 mm) enabled higher resolution for smaller subjects.

Table 1
Subject data. Top: cohort demographic and anthropomorphic data. Abbreviations: BMI=body mass index; SD=standard deviation.

Subject	Gender	Dominant arm	Age (years)	Height (cm)	Weight (kg)	BMI	Weight category[a]
1	M	R	13.8	157.5	74.3	29.9	Obese
2	M	R	14.5	180.3	72.0	22.1	Normal
3	M	R	11.4	159.0	40.5	16.0	Normal
4	M	R	7.3	131.0	23.9	13.9	Normal
5	M	R	11.1	130.0	44.6	26.4	Obese
6	M	R	9.2	142.2	47.3	28.2	Obese
7	M	R	13.7	151.8	64.9	18.2	Under
8	F	R	8.7	127.0	26.3	23.4	Obese
9	F	R	10.8	152.4	45.5	16.3	Normal
10	F	R	18.7	165.1	49.5	19.6	Normal
11	F	L	12.4	162.6	53.1	20.1	Normal
		Mean	12.0	150.8	49.2	21.3	
		SD	3.2	16.7	16.4	5.2	

[a] Centers for Disease Control categorization based on BMI.

2.2. MR image processing

Individual muscle volumes were quantified from 3D muscle models, derived by segmenting the MR data (Fig. 1) in MIPAV (NIH, Bethesda, MD). Segmentation guidelines were established in a preliminary dataset. An image magnification factor of six was used to achieve greater precision. Muscle segmentations began and ended with at least five consecutive MR image slices. To maximize efficiency without sacrificing accuracy, every slice was not segmented in the mid-belly of the muscles. For the shortest muscle (supraspinatus), every other slice was segmented in the mid-belly. For the mid-length muscles (infraspinatus/teres minor, subscapularis, and teres major) every fourth slice was segmented in the mid-belly. For the longest muscles (deltoid and pectoralis major) every sixth slice was segmented in the mid-belly. Segmentation was guided by tracking minor changes in area through the "skipped" slices and by visualizing muscle fascial planes, origins, and insertions in a tri-planar view (MIPAV). Segmentation propagation direction was inferior to superior. The segmentation process created a point cloud delineating the outer edge of the muscle (Fig. 1). This point cloud was imported into Geomagic (Research Triangle Park, NC) and a surface was wrapped to the points without smoothing filters. Any errors in the wrapping (e.g., holes in the surfaces, overlapping surfaces areas, etc.) were manually corrected. The final muscle volume was recorded. Each muscle's volume was also reported as a percent volume of the total summed volume of the six muscles measured.

The deltoid, pectoralis major (PM), supraspinatus, and subscapularis were segmented as individual muscles. The infraspinatus and teres minor were segmented as one muscle (I-tm) because they have analogous functions and the fascial boundaries between them are often indistinct (Lehtinen et al., 2003; Portney and Watkins, 2009; Talbert et al., 2011; Van Gelein Vitringa et al., 2011). Using a similar rationale, the teres major (TM) was segmented assuming its distal border was at the level of the most distal scapula point. In doing so, a small portion of the latissimus dorsi was included in the TM volume. The latissimus dorsi was not separately segmented, as it was not fully captured in taller subjects. The research team was blinded to the subject's demographics throughout the analysis phase.

2.3. Assigning muscles to functional groups

Muscle function was categorized (Table 2) based on moment arm data from studies that used an identical testing position (Brown et al., 2007; Kuechle et al., 1997, 2000). Muscles with moment arms greater than 3 mm in a selected torque direction were defined as contributors to that direction. This was a qualitative decision based on the fact that a 4 mm moment arm was ~10% of the largest moment arm (Table 2). Although the TM is often reported as an adductor, currently it was not categorized as such, as it has an adductor moment arm less than 3 mm with the shoulder flexed to 90° (Kuechle et al., 1997).

2.4. Splitting the deltoid into functional compartments

To quantify the deltoid volume and associate it with the primary torques it produces, the deltoid was split into two segments (Fig. 2) based on the seven functionally independent segments defined by Brown et al. (2007). Neither a full seven-way split nor a three-way split (Klepps et al., 2004; Lorne et al., 2001) was used based on the results of a preliminary study, which demonstrated that it was not feasible to reliably identify the fascial planes for these splits in the MR images. Attempting to do so resulted in inconsistent segmental volumes across subjects that did not match well with the previous data (Brown et al., 2007; Peterson and Rayan, 2011). The anterior segment, which combined the anterior three sections of the seven-segment model (Fig. 2), was considered a flexor; whereas the posterior section, which combined the posterior four sections (Fig. 2) was considered an extensor. The entire deltoid was considered an abductor, as only the smallest segment of the seven-segment deltoid model (closest to the spinal column) produces adduction (Brown et al., 2007). Although they were minor torques of the deltoid, internal and external rotation were assigned to the anterior and posterior deltoid (Kuechle et al., 2000).

The deltoid was divided using a 2D slice plane, defined by three points (S1, S2, and D; Fig. 3). S1 and S2 were the medial and lateral borders of the fascial plane between the deltoid segments at the level of the mid-acromioclavicular joint (Wickham and Brown, 1998). To ensure that the correct border had been defined, the four intramuscular tendons posterior to the bicipital groove (Sakoma et al., 2011) were identified in an image at the superior aspect of the humeral head. The

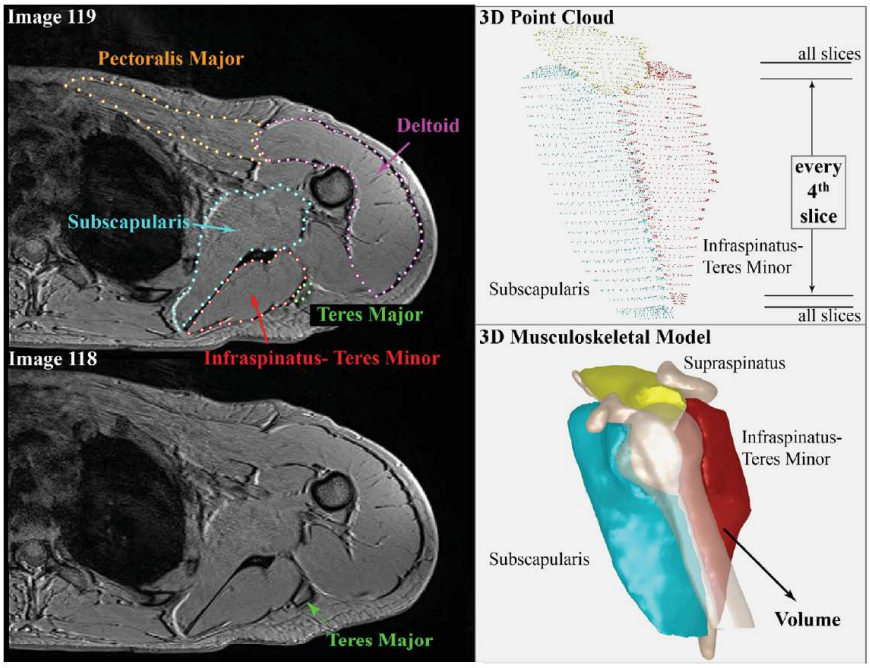

Fig. 1. Segmentation. Left column: images 118 and 119 are ~18.4% and ~18.8% of the humeral length distal from the superior aspect of the humeral head. For this subject (same subject depicted in Fig. 3) the images resolution is 0.6 mm × 0.6 mm × 1.2 mm. In this location, the area of the pectoralis major, subscapularis, deltoid, and I-tm demonstrate minimal change between slices. As these images contain the superior aspect of the teres major, there is a rapid change in its area. For this reason every slice was segmented for at least five slices representing the origin and insertion of the muscle but the segmentation was not done for every slice in the mid-belly of the muscle. Top right: the segmentation generates an individual point cloud for each muscle (yellow: supraspcapularis, red: I-tm, and blue: subscapularis). Bottom right: a 3D surface was wrapped to the point cloud. After manual correction of any minor errors in the model, the volume was calculated. Note that the humerus is shown slightly transparent in order to highlight the scapula. (For interpretation of the references to color in this figure legend, the reader is referred to the web version of this article.)

third most posterior tendon (AP tendon, Fig. 3) represented the border between the anterior and posterior segments. If this tendon did not communicate with the fascial plane defined by points S1 and S2, the images were re-evaluated until agreement was reached. Point D was defined as the center of the fascial plane dividing the deltoid segments just proximal to the deltoid's distal humeral insertion (segments D3 and D5, Figs. 2 and 3). As a final check, the separation of the deltoid segments was visualized on a sagittal reconstruction of the 3D axial image set.

2.5. Reliability of muscle volumes

To test the inter-rater reliability, two investigators independently analyzed the volumes for the I-tm and supraspinatus, along with the anterior, posterior, and total deltoid. These muscles were chosen to represent a variety of shapes, sizes, depths, and functions. Intra-class correlation coefficients (ICCs), using a two-way mixed effects model, were computed. The muscle volumes were acquired, using the identical protocol, for the unimpaired, dominant arm of ten children/ adolescents (six boys and four girls) with unilateral brachial plexus palsy. This cohort had similar demographics (age= 12.1 ± 3.3 years, height=157.8 ± 20.9 cm, and weight=51.5 ± 17.3 kg) to the typically developing children/adolescents of the main study.

2.6. Maximum isometric torque measures

Identical to a previous study (Brochard et al., 2014, in press) maximum voluntary isometric joint torques (strength) were measured by a physician for all three DOF_R using a hand-held dynamometer (Jtech Commander powertrack II). Subjects were assessed in six functional directions. Testing position, testing order (flexion, abduction, external rotation, internal rotation, adduction, and extension), and verbal instructions were standardized. All torque measures were acquired with the subject lying on a plinth and the shoulder in the anatomic position, with one exception. To maximize reliability, max-adduction strength was measured with the subject prone and the humerus in 90° of flexion. For internal/external rotation assessments, a strap was used to stabilize the upper-arm against the body. Subjects first conducted a sub-maximal contraction as a practice/warm-up. Three trials of maximal voluntary isometric contractions were performed in each direction, while subjects were encouraged to push as hard as they could with the shoulder without moving or displacing the elbow from its rest position. Only trials lasting for at least three seconds were accepted. Subjects rested for ten seconds between trials and a minimum of one minute between different directions.

2.7. Statistics

The 3D volumes of the six muscles, along with the anterior and posterior deltoid volumes, were correlated (Pearson's) with the strength (SPSS ver19, IBM, Armonk, NY). A multivariate regression analysis was performed to determine if using the individual volumes of a functional group as independent variables (Table 2) could better predict the maximum isometric joint torques. p-value < 0.05 was considered significant.

3. Results

In this pediatric database, the largest total volume (summed volume of all six muscles) was three and a half times greater than the smallest (273.2–943.8 cm^2). The deltoid demonstrated the largest percent volume of the six muscles segmented (Table 3, 30.4 ± 1.2%) and the supraspinatus demonstrated the smallest (Table 3, 4.7 ± 0.5%). The percent volumes were highly consistent across subjects, with coefficients of variation ranging from 0.038 (deltoid) to 0.107 (supraspinatus) and a correlation between each individual muscle and the total muscle volume ranging from 0.937 to 0.996 (Fig. 4).

The anterior and posterior deltoid sections were 43.4 ± 3.9% and 56.6 ± 3.9% of the total deltoid volume (Table 3). If defined as a percent of the total shoulder muscle volume these deltoid sub-sections demonstrated consistency similar to all other muscles.

The individual muscle volumes were moderately to strongly correlated with maximum voluntary isometric joint torques (Table 2, max r-values for each torque direction ranged from

Table 2
Pearson correlation coefficients and regression values for muscle volume–torque relationship. Correlation and regression coefficients (columns 5 and 6) between the maximum isometric torque produced in specific directions (column 1) and the individual muscle volumes for selected muscles (column 2) are presented. Muscles identified as torque contributors to a given direction were labeled as primary, secondary, or minor (column 4). These categorizations were largely based on moment arms (column 3) from relevant studies, but other factors such as size and clinical knowledge were considered in assigning a role. Abbreviations: PM – Pectoralis Major, TM – Teres Major, I-tm – Infraspinatus/Teres Minor.

Torque direction	Muscle	Moment arm (mm)	Role	r-value	r^2-value
Flexion	Anterior deltoid	15.9[a]	Primary	0.885	0.784
	Supraspinatus	7[b]	Primary	0.819	0.670
	PM	10[b]	Primary	0.853	0.728
	I-tm	4[b]	Minor	**0.919**	**0.844**
Extension	Posterior deltoid	45.4[a]	Primary	**0.937**	**0.878**
	TM	38[b]	Primary	0.891	0.794
Abduction	Supraspinatus	19[b]	Primary	0.701	0.492
	Total deltoid	19.5[a]	Primary	0.784	0.614
	I-tm	19[b]	Secondary	**0.806**	**0.649**
Adduction	PM	21[b]	Primary	0.772	0.596
	Subscapularis	8[b]	Minor	**0.832**	**0.693**
Internal rotation	Subscapularis	22.5[c]	Primary	0.750	0.562
	PM	20 [c]	Secondary	0.772	0.591
	Anterior deltoid	6[c]	Minor	0.780	0.608
	TM	7.5[c]	Minor	**0.789**	**0.623**
External rotation	I-tm	24[c]	Primary	**0.929**	**0.863**
	Posterior Deltoid	5[c]	Minor	0.895	0.800

[a] Volume weighted moment arms (Brown et al., 2007).
[b] Kuechle et al., 1997.
[c] Kuechle et al., 2000.

0.789–0.937 ($p<0.001$)). Therefore, 62–91% of the maximum isometric torque could be predicted from single muscle volumes. Using multivariate regression analyses improved the predictability for external rotation only ($r^2=0.94$ $p<0.001$).

The maximum voluntary isometric joint torques were strongly correlated with each other. The torques in antagonistic directions (flexion/extension, internal/external, abduction/adduction) had correlation coefficients ranging from 0.866 to 0.951 ($p<0.001$). The correlation of each torque with the torques in orthogonal directions ranged from 0.844 to 0.966 ($p<0.001$).

The inter-rater reliability for generating muscle volumes was excellent (ICC=0.993–0.999), well above the level required for "clinical relevance" (Portney and Watkins, 2009). The average inter-rater differences were -0.9 ± 4.5 cm^3, 2.2 ± 2.1 cm^3, and -1.0 ± 2.3 cm^3 (-0.4%, 2.1%, and -2.8%) for the entire deltoid, infraspinatus, and supraspinatus. Quantifying the anterior and posterior deltoid segments demonstrated excellent inter-rater reliability (ICC=0.970 and 0.989 $p<0.001$). The average inter-rater differences were -6.5 ± 12.1 cm^3, and 6.0 ± 9.8 cm^3 (-6.4% and 4.3%).

4. Discussion

This study presents a comprehensive database documenting normative pediatric shoulder muscle volume. Using these data an association between muscle volume and strength was established in all three DOF_R. The methodology for reliably splitting the *in vivo* deltoid volume into subgroups with unique torque producing abilities is important for further research, as it simplifies the evaluation of a muscle with multiple actions. Fortunately, the application of this methodology is not limited to pediatric data, but should be directly applicable to adult data as well. Thus, both the methodologies developed and the databases established within this study will likely advance the understanding of shoulder injury, pathology, and overuse by facilitating functional-based analyses in both the pediatric and adult populations.

Despite the diverse spectrum of ages and sizes, the muscle volume distribution remained consistent across individual subjects. Hence, this normative pediatric muscle database could be beneficial for estimating shoulder muscle volumes, particularly when such data are difficult to obtain. For example, acquiring MR data for children often requires anesthesia (Halliday and Kelleher, 2013; Usher and Kearney, 2003), yet such a risk is difficult to justify for research purposes. This database also provides a baseline to which atrophic (e.g., children with cerebral palsy or brachial plexus palsy) or hypertrophic (e.g., overuse) muscle volumes can be compared.

The relative distribution of shoulder muscles in children appears to be consistent with adults (Fig. 5) with a few notable exceptions. In this pediatric cohort the deltoid occupies a relatively smaller, and the rotator cuff muscles (supraspinatus, subscapularis, and I-tm) a relatively larger, percentage of the shoulder muscle volume (Holzbaur et al., 2007; Peterson and Rayan, 2011; Vidt et al., 2012). The differences in muscle distribution, albeit small, between the current pediatric and previous adult cohorts, combined with the documented humeral shape changes during development (Edelson, 2000; Sheehan et al., 2014) indicate that caution must be used when applying results from adult modeling and experimental studies to pediatric populations.

The concept that muscle volumes are predictive of maximum isometric torques was supported by the moderate to strong regression coefficients. The differences in regression coefficients across muscles of a functional group (Table 2) were quite small, a likely result of the strong association between muscle volumes. The results expand upon the current knowledge of the *in vivo* relationship between shoulder muscle volume and strength by establishing these relationships for all cardinal planes. The inability to fully explain the variance in maximum voluntary isometric joint torques was anticipated, as numerous other factors (e.g., moment arm values, specific tension, fiber length, and pennation angles) also influence a muscle's ability to generate torque. As these parameters are most often derived from cadaveric studies, such data for the pediatric shoulder are unavailable. In addition, these parameters can vary across the muscles of the shoulder. Thus, the quantified volume–torque relationship defines the relationship between a single muscle's volume and the torque it can produce, which will likely be useful in evaluating the effects of muscle atrophy/hypertrophy in the production of torque. The conclusions of this study in no manner imply that the muscle volume alone can quantify differences in strength across different muscles (Ward et al., 2006; Zajac, 1992).

The abduction/adduction regression coefficients matched well with literature values (Audenaert et al., 2009; Vidt et al., 2012) but tended to be smaller. This difference may have arisen from the fact that the overall volume was fairly evenly distributed across genders in the current study (Fig. 4) but in a past study (Vidt et al., 2012), the average female volume was ~18 standard deviations less than the average male volume. This large difference in volume between the male and female populations likely create a correlation that was stronger for the entire population, but weaker within the sub-populations.

The fact that the multivariate regression analysis improved the prediction of only one (external rotation) of the six joint torques indicates that the relationship between individual muscle volumes and torque may be more relevant than the relationship between the summed muscle volumes within a functional group and its

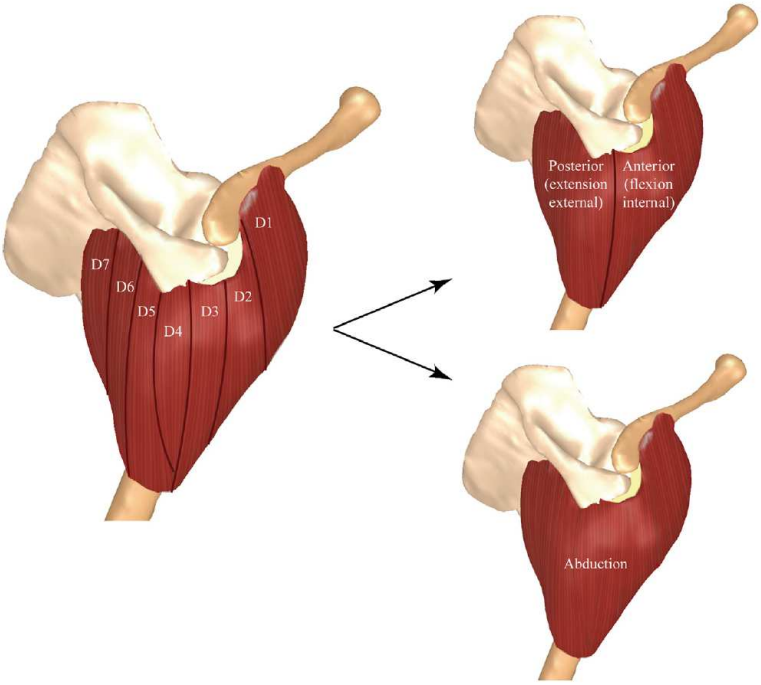

Fig. 2. Deltoid functional divisions. Left: previous studies have provided evidence that the deltoid is comprised of seven unique functional groups. Based on the quantification of moment arms, Brown et al. (2007) defined these segments as flexors-abductors (D1–D3), extensors-abductors (D4–D6), and extensor-adductors (D7). The internal-external rotation moment arms were not reported. The study of Sakoma et al. (2011) also supported this division into seven segments (defined as A1, A2, A3, M1, P1, P2, and P3, which roughly matched D1–D7). The origins of segments D6, D7, D3, and D1 are isolated to the scapular spine, the acromion process, and the clavicle, respectively. The origins of D4 and D2 span the acromion and either the spinal process or the clavicle. Top Right: The anterior (D1–D3) and posterior (D4–D7) segments were assigned to the flexion-internal rotation and the extension-external rotation functional groups, respectively. Bottom right: the entire deltoid volume was considered an abductor since the volume of D7, which contributed to adduction, was negligible compared to the entire deltoid.

corresponding torque (Holzbaur et al., 2007). Performing a regression based on the summed volume assumes that the multiplicative coefficient for each muscle volume is a constant. This constant accounts for the moment arm, specific tension, and pennation angle of each muscle. There can be no expectation that it would be constant across muscles of a functional group. In addition, the colinearity amongst the volumes created a bias against improving the single regressions with a multivariate regression.

The cross-correlation between joint torques was expected as shoulder function requires a high level of dynamic interaction between co-contracting muscles. Thus, the shoulder's capacity to produce force in one direction is balanced by a reciprocal capacity to produce force in the opposite direction.

It is well accepted that the deltoid is functionally capable of producing moments on the humerus in opposing directions. Dividing the deltoid based on the seven-segment deltoid model (Brown et al., 2007) provided clear guidance for assigning extension, flexion, and abduction to the segments. Compared to these torques, the deltoid's ability to produce internal/external rotation is minor and these moment arms have only been reported based on three-segment models (Ackland et al., 2008; Otis et al., 1994). The anterior deltoid is an internal rotator, whereas the posterior deltoid is an external rotator, but the mid-deltoid has been reported as being both an internal (Ackland and Pandy, 2011) and external (Otis et al., 1994) rotator. As the seven-segment model can be converted to the commonly used three-segment model by combining segments (anterior=D1+D2, mid=D3+D4, and posterior=D5+D6+D7, Fig. 2), the current two-segment deltoid allocated a small portion of the mid-deltoid to the anterior and posterior segments, forming a compromise across past studies. A more realistic 3D curved plane defining the boundary between sections D3 and D4 was not used since identifying it in the mid-belly was difficult and time-consuming. In a preliminary dataset, a comparison of the segmental volumes derived using the 2D and 3D slice planes demonstrated small volumetric differences.

Although the current methodology deviated slightly from the three-segment deltoid model (Klepps et al., 2004; Lorne et al., 2001), it enabled the deltoid to be reliably divided into sub-units with unique torque producing abilities. This methodology is pivotal to establishing the *in vivo* volume–torque relationship for all three DOF_R. More importantly, it opens a rich path for research into injury, pathology, and hypertrophy in both pediatrics and adult populations. For example, in obstetrical brachial plexus palsy, external rotation and extension torque weakness have been documented (Kozin et al., 2010). Yet, the contribution of deltoid atrophy to this weakness may have been masked by a reliance on evaluating the entire deltoid (Hogendoorn et al., 2010; Van Gelein Vitringa et al., 2011).

In this pediatric cohort, the anterior deltoid was a smaller percentage (43.4%) of the entire deltoid relative to the limited available adult cadaver data. For a single adult cadaver, the anterior–posterior deltoid split was 50.7–49.2% (Wickham and Brown, 1998). For five adult cadavers it was approximately 46.5–52.5% (Peterson and Rayan, 2011). This may indicate a differential development of the functional sub-units within the deltoid. To more fully explore this issue, future work is needed to establish *in vivo* adult segmental volumes.

This study confirms that the process of deriving muscle volumes from MR images in children/adolescents is as reliable as in adults, if not more so. The inter-rater reliability matched that of

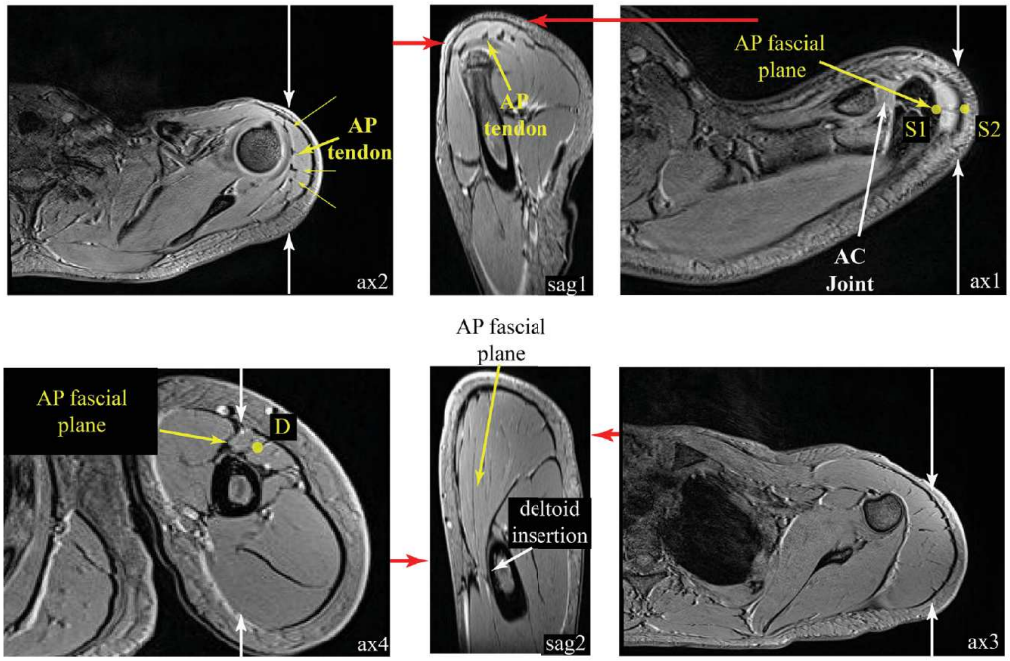

Fig. 3. Defining the three points of the anterior–posterior deltoid slice plane. Both rows present two axial images whose locations are defined by the horizontal arrows extending to the center sagittal image. Similarly, the location of the central sagittal image is indicated on the right and left axial images using vertical arrows. Note that ax1 and ax4 have been enlarged and cropped for better visualization. Top row: the proximal two points defining the 2D slice plane were defined in the axial image at the level of the acromioclavicular joint (ax1). To ensure that the fascial plane dividing the anterior and posterior deltoids (AP fascial plane) had been located, the intramuscular tendons (as defined by Sakoma et al. (2011)) were identified in an axial image at the superior aspect of the humeral head. The "AP tendon" marks the division between the anterior and posterior deltoids. This tendon was followed back to image ax1 to ensure that it communicated with the AP fascial plane. Bottom Row: Just superior to the distal insertion of the posterior deltoid, the AP fascial plane was identified and the center of this plane was the 3rd point. A 3D plane outlining the fascial plane could not be used because the fascial plane in the mid-belly of the deltoid was often indistinguishable, as can be seen in ax3.

Table 3
Muscle volume, strength, and physical measures for each subject.

Muscle Volumes (cm^3)										*Strength (N.m)*						*Physical Measurements (mm)*		
Subject	**Total Deltoid**	**Ant. Deltoid**	**Pos. Deltoid**	**PM**	**TM**	**Sub**	**I-tm**	**Supra**	**Total**	**Flex**	**Ext**	**Abd**	**Add**	**IR**	**ER**	**Hum. Length**	**Epi. Width**	**Sca. Length**
1	286.2	134.5	151.8	240.4	123.2	143.8	115.5	34.8	943.8	57.2	37.7	59.3	41.1	43.4	22.2	282.5	61.1	115.6
2	251.8	119.2	132.6	210.8	125.5	116.8	104.1	43.5	852.6	45.8	34.8	36.9	32.9	27.7	19.1	333.2	56.9	122.0
3	155.2	62.9	92.3	140.5	81.2	67.9	66.2	29.9	540.7	16.0	13.2	18.9	18.9	13.7	7.4	292.8	44.3	111.0
4	86.7	33.3	53.5	57.0	33.4	43.2	38.7	14.1	273.2	8.4	9.2	5.7	7.0	4.4	4.0	225.7	37.9	86.9
5	136.4	57.9	78.4	96.2	61.0	64.9	64.1	22.4	444.9	17.2	15.4	18.4	22.0	11.6	9.4	259.0	49.2	109.4
6	221.6	95.4	126.2	146.9	81.5	110.9	100.7	35.5	697.1	41.2	33.9	47.9	33.9	30.3	23.1	267.7	56.4	105.7
7	277.8	129.2	148.6	225.1	103.8	137.7	111.6	38.1	894.0	30.6	32.0	21.8	20.1	17.9	17.4	340.4	56.0	120.9
8	157.7	56.8	100.9	101.3	59.5	79.8	76.6	23.5	498.5	27.8	18.5	18.0	21.6	12.1	10.2	251.2	51.8	95.1
9	80.5	38.4	42.1	58.1	38.8	49.9	36.2	13.0	276.6	7.5	10.6	12.8	10.1	7.5	6.7	220.1	40.7	91.7
10	145.9	62.9	83.0	125.9	71.0	76.1	62.0	22.1	503.0	21.3	20.0	15.4	16.5	10.6	7.7	262.5	54.2	106.8
11	239.4	109.0	130.4	176.2	95.1	128.5	97.9	37.8	774.8	34.8	29.2	29.2	33.6	12.2	16.9	305.1	55.4	115.5
Mean	185.4	81.8	103.6	143.5	79.4	92.7	79.4	28.6	609.0	28.0	23.1	25.8	23.4	17.4	13.1	276.4	51.3	107.3
SD	73.3	36.7	37.3	63.8	30.8	36.0	28.3	10.2	238.0	15.8	10.6	16.1	10.7	11.7	6.8	39.2	7.4	11.7
Distribution	30.4%	43.4%[a]	56.6%[a]	23.1%	13.1%	15.4%	13.2%	4.8%										
SD	1.2%	3.9%[a]	3.9%[a]	2.2%	1.2%	1.4%	1.1%	0.5%										

Abbreviations: SD – standard deviation, Ant. – Anterior, Pos. – Posterior, PM – Pectoralis Major, TM – Teres Major, I-tm – Infraspinatus/Teres Minor, Sub – Subscapularis, Supra – Supraspinatus, Flex – Flexion, Ext – extension, Abd – Abduction, Add – Adduction, IR – Internal Rotation, ER – External Rotation, Hum – Humeral, Epi – Epicondylar, Sca – Scapular.

[a] The distribution of the anterior and posterior deltoid is relative to the total deltoid volume. The distribution for all other muscles is relative to the summed volumes of the total deltoid, PM, TM, sub, I-tm, and supra. The Hum. Length, Epi. Width, and Sca. Length are defined as the distance between the most superior and inferior aspects of the humerus, the medial and lateral edges of the humeral epicondyles, and the Trigonum Spinae Scapulae and the Angulus Inferior, as measured from MR images.

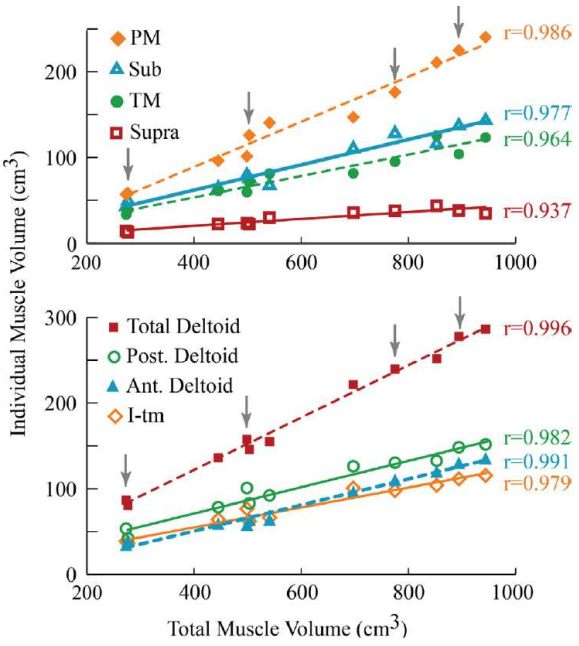

Fig. 4. Individual muscle volume relative to total muscle volume. All correlations had a p-value < 0.001. The gray arrows mark the data from the female subjects. Abbreviations: PM – Pectoralis Major, Sub – Subscapularis, TM – Teres Major, Supra – Supraspinatus, Post. – Posterior, Ant. – Anterior, I-tm – Infraspinatus/Teres Minor.

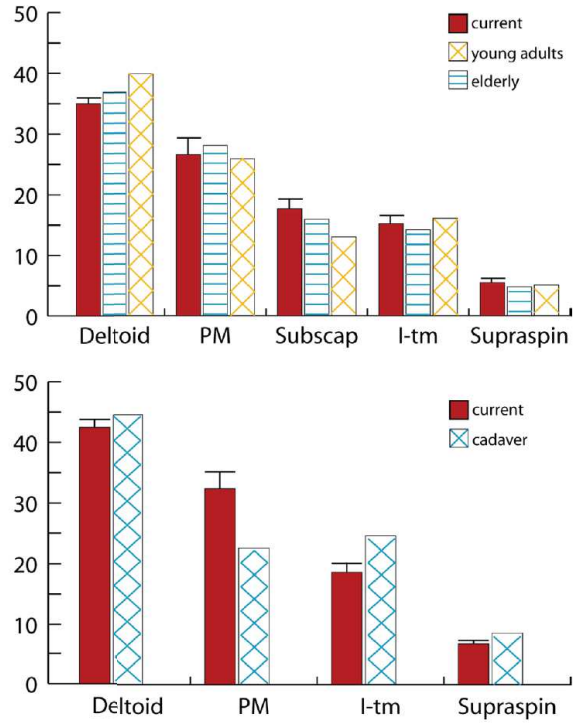

Fig. 5. Comparison of the muscle volume distribution. The distribution was calculated based on only the muscles that overlapped between studies. TOP: Comparison to past *in vivo* studies in young adults and elders (Holzbaur et al., 2007; Vidt et al., 2012). Bottom: to past cadaver study (Peterson and Rayan, 2011). As Peterson and Rayan (2011) reported average masses, the percent volumes were based on the assumption that muscle density was constant across muscles. Note: the distributions are slightly different than those listed in Table 3 since the set of muscles used for the total volume was dependent on the data available in the previous studies. Although measured, the volume of the teres major was not included in the above figures because it was calculated differently than had been done previously. Abbreviations: PM –Pectoralis Major, Subscap – Subscapularis, Supraspin – Supraspinatus, I-tm – Infraspinatus/Teres Minor.

Tingart et al. (2003) but the average difference (−0.4%) was lower than the 4% reported for the intra-rater reliability of the deltoid (Holzbaur et al., 2007). The higher percent differences (6.4% and 4.3%) for the anterior and posterior deltoid segments arose primarily from a single subject with −40.2 and a 31.2 cm^3 difference in segment volumes between observers. Advancements in MR technology have provided higher resolution and stronger MR units (3-T) with larger bores, allowing optimal subject placement and increased signal-to-noise ratios. This enabled the voxel resolution for the current study (0.36–0.48 mm^3) to be two times better than the data acquired by Tingart et al. (2003). Thus, the current accuracy is likely equivalent to or better than the 2–4% accuracy reported in this previous study.

While the present study is the largest and most comprehensive database documenting the relationship between pediatric shoulder muscle volume and strength, the cohort is still objectively small, and thus a limitation of the study. For this reason, the full individual dataset is provided so that future experimental and modeling studies can use the current data as a foundation. In the current pediatric database, it was not feasible to create a "gold standard" to evaluate the methodology for dividing the deltoid. Therefore, the exact accuracy of this methodology remains unknown.

This study quantified 3D, *in vivo* shoulder muscle volumes and their association with strength in a normative pediatric population. The potential for asserting definitive conclusions with regard to shoulder muscle function, particularly differences between the pediatric and adult shoulders, is predicated on expanding the normative database quantitatively (i.e., additional subjects) and qualitatively (i.e., broader sample of characteristics). The current data provides a reference for clinicians and researchers investigating pediatric shoulder pathology. This information is useful in identifying muscle imbalances and tailoring interventions to specific muscles and functions.

Conflict of interest

None.

Acknowledgments

The authors would like to thank Diane Damiano, PhD, Christopher Hollingsworth, Lindsay Curatalo, Christopher Stanley, and Lauri Ohlrich for their help and support in the work. In addition, we would like to thank the Radiology Department, headed by Dr. David Bluemke at the Clinical Center of the National Institutes of Health. This work was funded by the Intramural Research Program of the National Institutes of Health Clinical Center, Bethesda, MD, USA. Drs. Brochard and Pons were supported by an award from the University Hospital of Brest, the French Society of Physical Medicine and Rehabilitation (SOFMER), and the French Society of Research in Children with Disabilities (SFERHE). All work for this study was done under protocol number 03-CC-0060, approved by the Institutional Review Board of the National Institute of Child Health and Human Services.

References

Abel, M.F., Damiano, D.L., Blanco, J.S., Conaway, M., Miller, F., Dabney, K., Sutherland, D., Chambers, H., Dias, L., Sarwark, J., Killian, J., Doyle, S., Root, L., LaPlaza, J., Widmann, B., Snyder, B., 2003. Relationships among musculoskeletal

impairments and functional health status in ambulatory cerebral palsy. J. Pediatr. Orthop. 23, 535–541.
Ackland, D.C., Pak, P., Richardson, M., Pandy, M.G., 2008. Moment arms of the muscles crossing the anatomical shoulder. J. Anat. 213, 383–390.
Ackland, D.C., Pandy, M.G., 2011. Moment arms of the shoulder muscles during axial rotation. J. Orthop. Res. 29, 658–667.
Akagi, R., Takai, Y., Ohta, M., Kanehisa, H., Kawakami, Y., Fukunaga, T., 2009. Muscle volume compared to cross-sectional area is more appropriate for evaluating muscle strength in young and elderly individuals. Age Ageing 38, 564–569.
Audenaert, E.A., De Roo, P.J., Mahieu, P., Cools, A., Baelde, N., D'Herde, K., Verdonk, R., 2009. Deltoid muscle volume estimated from ultrasonography: in vitro validation and correlation with isokinetic abduction strength of the shoulder. Med. Biol. Eng. Comput. 47, 557–563.
Blazevich, A.J., Coleman, D.R., Horne, S., Cannavan, D., 2009. Anatomical predictors of maximum isometric and concentric knee extensor moment. Eur. J. Appl. Physiol. 105, 869–878.
Boettcher, C.E., Cathers, I., Ginn, K.A., 2010. The role of shoulder muscles is task specific. J Sci. Med Sport/Sports Med. Aust. 13, 651–656.
Brochard, S., Alter, K.E., Damiano, D.L., 2014. Shoulder strength profiles in children with and without brachial plexus palsy. Muscle Nerve (In press).
Brochard, S., Lempereur, M., Mao, L., Remy-Neris, O., 2012. The role of the scapulo-thoracic and gleno-humeral joints in upper-limb motion in children with hemiplegic cerebral palsy. Clin. Biomech. 27, 652–660.
Brown, J.M., Wickham, J.B., McAndrew, D.J., Huang, X.F., 2007. Muscles within muscles: coordination of 19 muscle segments within three shoulder muscles during isometric motor tasks. J. Electromyogr. Kinesiol. 17, 57–73.
Davis, K.W., 2010. Imaging pediatric sports injuries: upper extremity. Radiol. Clin. N. Am. 48, 1199–1211.
Edelson, G., 2000. The development of humeral head retroversion. J. Shoulder Elb. Surg. 9, 316–318.
Emery, K.H., 2006. Imaging of sports injuries of the upper extremity in children. Clin. Sports Med. 25, 543–568 (viii).
Fukunaga, T., Miyatani, M., Tachi, M., Kouzaki, M., Kawakami, Y., Kanehisa, H., 2001. Muscle volume is a major determinant of joint torque in humans. Acta Physiol. Scand. 172, 249–255.
Halliday, M., Kelleher, J., 2013. Question 1: is sedation necessary for MRI in an infant? Arch. Dis. Child. 98, 825–828.
Hogendoorn, S., van Overvest, K.L., Watt, I., Duijsens, A.H., Nelissen, R.G., 2010. Structural changes in muscle and glenohumeral joint deformity in neonatal brachial plexus palsy. J. Bone Joint Surg. Am. 92, 935–942.
Holzbaur, K.R., Murray, W.M., Gold, G.E., Delp, S.L., 2007. Upper limb muscle volumes in adult subjects. J. Biomech. 40, 742–749.
Klepps, S., Auerbach, J., Calhon, O., Lin, J., Cleeman, E., Flatow, E., 2004. A cadaveric study on the anatomy of the deltoid insertion and its relationship to the deltopectoral approach to the proximal humerus. J. Shoulder Elb. Surg. 13, 322–327.
Kozin, S.H., Boardman, M.J., Chafetz, R.S., Williams, G.R., Hanlon, A., 2010. Arthroscopic treatment of internal rotation contracture and glenohumeral dysplasia in children with brachial plexus birth palsy. J. Shoulder Elb. Surg. 19, 102–110.
Kuechle, D.K., Newman, S.R., Itoi, E., Morrey, B.F., An, K.N., 1997. Shoulder muscle moment arms during horizontal flexion and elevation. J. Shoulder Elb. Surg. 6, 429–439.
Kuechle, D.K., Newman, S.R., Itoi, E., Niebur, G.L., Morrey, B.F., An, K.N., 2000. The relevance of the moment arm of shoulder muscles with respect to axial rotation of the glenohumeral joint in four positions. Clin. Biomech. 15, 322–329.
Lehtinen, J.T., Tingart, M.J., Apreleva, M., Zurakowski, D., Palmer, W., Warner, J.J., 2003. Practical assessment of rotator cuff muscle volumes using shoulder MRI. Acta Orthop. Scand. 74, 722–729.
Lorne, E., Gagey, O., Quillard, J., Hue, E., Gagey, N., 2001. The fibrous frame of the deltoid muscle. Its functional and surgical relevance. Clin. Orthop. Relat. Res. 386, 222–225.
Neu, C.M., Rauch, F., Rittweger, J., Manz, F., Schoenau, E., 2002. Influence of puberty on muscle development at the forearm. Am. J. Physiol. Endocrinol. Metab. 283, E103–107.
Otis, J.C., Jiang, C.C., Wickiewicz, T.L., Peterson, M.G., Warren, R.F., Santner, T.J., 1994. Changes in the moment arms of the rotator cuff and deltoid muscles with abduction and rotation. J. Bone Joint Surg. Am. 76, 667–676.
Peterson, S.L., Rayan, G.M., 2011. Shoulder and upper arm muscle architecture. J. Hand Surg. Am. 36, 881–889.
Pitcher, C.A., Elliott, C.M., Williams, S.A., Licari, M.K., Kuenzel, A., Shipman, P.J., Valentine, J.P., Reid, S.L., 2012. Childhood muscle morphology and strength: alterations over six months of growth. Muscle Nerve 46, 360–366.
Portney, L., Watkins, M., 2009. Statistical measures of reliability, Foundations of Clinical Research Applications to Practice.
Poyhia, T.H., Nietosvaara, Y.A., Remes, V.M., Kirjavainen, M.O., Peltonen, J.I., Lamminen. A.E., 2005. MRI of rotator cuff muscle atrophy in relation to glenohumeral joint incongruence in brachial plexus birth injury. Pediatr. Radiol. 35, 402–409.
Sakoma, Y., Sano, H., Shinozaki, N., Itoigawa, Y., Yamamoto, N., Ozaki, T., Itoi, E., 2011. Anatomical and functional segments of the deltoid muscle. J. Anat. 218, 185–190.
Sheehan, F.T., Brochard, S., Behnam, A., Alter, K.E., 2014. Three-dimensional humeral morphological alterations and atrophy associated with obstetrical brachial plexus palsy. J. Shoulder Elb. Surg. 23, 708–719.
Talbert, R.J., Michaud, L.J., Mehlman, C.T., Kinnett, D.G., Laor, T., Foad, S.L., Schnell, B., Salisbury, S., 2011. EMG and MRI are independently related to shoulder external rotation function in neonatal brachial plexus palsy. J. Pediatr. Orthop. 31, 194–204.
Tingart, M.J., Apreleva, M., Lehtinen, J.T., Capell, B., Palmer, W.E., Warner, J.J., 2003. Magnetic resonance imaging in quantitative analysis of rotator cuff muscle volume. Clin. Orthop. Relat. Res. 415, 104–110.
Tonson, A., Ratel, S., Le Fur, Y., Cozzone, P., Bendahan, D., 2008. Effect of maturation on the relationship between muscle size and force production. Med. Sci. Sports Exerc. 40, 918–925.
Usher, A., Kearney, R., 2003. Anesthesia for magnetic resonance imaging in children: a survey of Canadian pediatric centres. Can. J. Anaesth. 50, 425.
Van Gelein Vitringa, V.M., Jaspers, R., Mullender, M., Ouwerkerk, W.J., Van Der Sluijs, J.A., 2011. Early effects of muscle atrophy on shoulder joint development in infants with unilateral birth brachial plexus injury. Dev. Med. Child Neurol. 53, 173–178.
Vidt, M.E., Daly, M., Miller, M.E., Davis, C.C., Marsh, A.P., Saul, K.R., 2012. Characterizing upper limb muscle volume and strength in older adults: a comparison with young adults. J. Biomech. 45, 334–341.
Ward, S.R., Hentzen, E.R., Smallwood, L.H., Eastlack, R.K., Burns, K.A., Fithian, D.C., Friden, J., Lieber, R.L., 2006. Rotator cuff muscle architecture: implications for glenohumeral stability. Clin. Orthop. Relat. Res. 448, 157–163.
Wickham, J.B., Brown, J.M., 1998. Muscles within muscles: the neuromotor control of intra-muscular segments. Eur. J. Appl. Physiol. Occup. Physiol. 78, 219–225.
Zajac, F.E., 1992. How musculotendon architecture and joint geometry affect the capacity of muscles to move and exert force on objects: a review with application to arm and forearm tendon transfer design. J. Hand Surg. Am. 17, 799–804.

Différentes difficultés méthodologiques ont été rencontrées pour ce travail.

Dans le travail ci-dessus, une **séquence anatomique avec des coupes très fines**, a été choisie. Des vérifications de la justesse de la segmentation sur les coupes axiales étaient possibles dans les plans sagittal et frontal. Une technique de segmentation manuelle sur un grand nombre de coupes était utilisée. Les **évaluations de fidélité inter-examinateur retrouvaient d'excellents résultats sur trois muscles** laissant présager de bonnes qualités métrologiques pour cette technique. Malgré l'absence de segmentation de toutes les coupes, **15 heures au minimum** étaient nécessaires pour réaliser les segmentations manuelles puis la reconstruction d'une épaule unique, ne permettant pas d'utiliser cette technique sur des populations beaucoup plus larges ou en pratique clinique.

Afin **d'établir des groupes fonctionnels des muscles** intervenant dans chacun des mouvements de l'articulation gléno-humérale, **les bras de levier** déterminés à partir d'études cadavériques chez les adultes **ont été utilisés** avec une méthode de « tendon excursion » permettant de s'affarnchir de la détermination du centre de rotation de l'articulation gléno-humérale. Ils sont à l'origine d'un biais dans le raisonnement pour l'étude de la relation volume-force et sont une limite pour cette étude.

Enfin, le **muscle deltoïde**, du fait de son organisation tridimensionnelle entourant l'épaule, **présente des actions différentes** en fonction des chefs musculaires avec pour certains chefs des actions antagonistes (J. M. M. Brown et al. 2007). De ce fait, **une technique de division** en deux parties **a été proposée**. Sa fidélité inter-examinateur était très satisfaisante mais sa validité reste à prouver. De même, son utilisation dans des images autres que celles obtenues pour ce travail, avec une séquence différente par exemple, sera à explorer.

Malgré ces difficultés méthodologiques, ce travail a permis de recueillir les **premières données de volumes des muscles de l'articulation gléno-humérale** ainsi que leur **distribution** spécifique dans une population d'enfants avec développement typique. **Des corrélations moyennes à fortes entre les volumes musculaires et la force ont pu être établies** dans toutes les directions du mouvement et avec l'ensemble des muscles intervenant dans la genèse de force dans les différentes directions, confirmant l'intérêt de l'étude morphologique des

muscles de l'épaule en IRM chez l'enfant. **Ces premières données vont pouvoir servir de données de référence dans les études** incluant des enfants présentant des pathologies de l'épaule, comme les **enfants avec POPB**.

Des études similaires à celle présentée ci-dessus proposant une étude des volumes musculaires et de leur relation à la force dans des **groupes d'enfants par âge et sexe** pourrait permettre d'évaluer l'impact de la croissance sur l'anatomie et le fonctionnement de l'épaule chez l'enfant à développement typique et potentiellement d'affiner cette première base de données.

Erratum : Des erreurs se sont glissées dans le tableau 1 (calcul de l'IMC), la version exacte est présentée ci-dessous

.

subject	gender	dominant arm	age (years)	height (cm)	wieght (kg)	BMI	weight category
1	M	R	13,8	157,5	74,3	30,0	obese
2	M	R	14,5	180,3	72,0	22,1	normal
3	M	R	11,4	159,0	40,5	16,0	normal
4	M	R	7,3	131,0	23,9	13,9	normal
5	M	R	11,1	130,0	44,6	26,4	obese
6	M	R	9,2	142,2	47,3	23,4	obese
7	M	R	13,7	151,8	64,9	28,2	obese
8	F	R	8,7	127,0	26,3	16,3	normal
9	F	R	10,8	152,4	45,5	19,6	normal
10	F	R	18,7	165,1	49,5	18,2	normal
11	F	L	12,4	162,6	53,1	20,1	normal

3 Article 3 : Morphologie musculaire en IRM et fonction musculaire de l'épaule chez l'enfant avec paralysie obstétricale du plexus brachial

Bien que les **muscles** soient au cœur de la pathologie de l'épaule chez les enfants avec POPB, leur **atteinte reste imparfaitement connue**.

En IRM, la **morphologie et notamment la trophicité des muscles scapulo-huméraux** de l'enfant avec POPB sans récupération neurologique complète a été étudiée dans **cinq articles** (Pöyhiä et al. 2005; van Gelein Vitringa et al. 2009; Peter M. Waters et al. 2009; Hogendoorn et al. 2010; Van Gelein Vitringa et al. 2011) afin d'établir un lien entre les déformations osseuses et l'atteinte musculaire.

Dans ces travaux, la trophicité des muscles de l'épaule était explorée avec des **techniques de segmentation simples**, telles que l'épaisseur de section maximale ou la surface de section anatomique du muscle mesurées sur une coupe unique. Dans le cadre du muscle pathologique de l'enfant, ces techniques utilisant une coupe unique ne sont cependant pas validées. Elles **ne sont pas adaptées à des muscles avec des formes non fusiformes spécifiques comme le deltoide.** Enfin, du fait de l'atrophie, des déformations du muscle peuvent être suspectées. L'ensemble est en faveur d'une évaluation du muscle dans son ensemble par une technique de segmentation précise (Lehtinen et al. 2003)(Article 1).

Seul un **petit nombre de muscles était étudié**, principalement les muscles subscapulaire et infraépineux. Cependant ce ne sont ni les seuls muscles du couple rotation interne/externe (Kuechle et al. 2000; Ackland, Keynejad, et Pandy 2011), ni les seuls muscles à intervenir dans la stabilisation et la mobilisation de l'épaule (paragraphe 2.2.2).

Les corrélations entre la trophicité musculaire et les déformations osseuses étaient établies sans que **le lien entre la trophicité musculaire et la force**, en lien avec les contraintes mécaniques s'exerçant sur l'articulation gléno-humérale, ne soit connu dans cette population (Dysart, Harkness et Herbison 1989; M. L. Pearl et Edgerton 1998). Les corrélations connues pour l'enfant à développement typique et présentées ci-dessus ne pouvaient pas être utilisées

étant donné le caractère pathologique des muscles chez les enfants avec POPB, présentant une infiltration graisseuse et un changement de leur architecture (Einarsson et al. 2008; Hogendoorn et al. 2010) modifiant possiblement leurs propriétés contractiles.

Cette étude « atrophie des muscles de l'épaule, relation avec la perte de force chez l'enfant avec POPB » visait à mieux évaluer l'atteinte musculaire des muscles gléno huméraux. Son **objectif principal** était de quantifier le profil et la gravité de **l'atrophie musculaire des muscles gléno-huméraux** chez les enfants présentant une POPB en utilisant une technique de segmentation manuelle sur un grand nombre de coupes permettant la considération du muscle dans son ensemble. Ses objectifs secondaires étaient de **quantifier l'équilibre entre les volumes musculaires agonistes et antagonistes**, ainsi que de déterminer la **relation volume force** au niveau de l'épaule dans cette population.

Clinical Biomechanics 48 (2017) 80–87

Contents lists available at ScienceDirect

Clinical Biomechanics

journal homepage: www.elsevier.com/locate/clinbiomech

Shoulder muscle atrophy and its relation to strength loss in obstetrical brachial plexus palsy

Christelle Pons[a], Frances T. Sheehan[b,*], Hyun Soo Im[b], Sylvain Brochard[c], Katharine E. Alter[b]

[a] Rehabilitation Medicine Department, University Hospital of Brest, 2 Avenue Foch, 29609 Brest Cedex, France
[b] Functional and Applied Biomechanics Section, Rehabilitation Medicine Department, National Institutes of Health, 9000 Rockville Pike, Bethesda, MD 20892, USA
[c] LaTIM, INSERM U1101, 2 Avenue Foch, 29200 Brest, France

ARTICLE INFO

Keywords:
Obstetrical brachial plexus palsy
Children
Muscle volume
MRI
Strength
Shoulder

ABSTRACT

Background: Treatment/prevention of shoulder muscle strength imbalances are major therapeutic goals for children with obstetrical brachial plexus palsy. The study aims were to characterize muscle atrophy in children/adolescents with unilateral obstetrical brachial plexus palsy, to quantify the agonist-antagonist muscle volume balance and the association between muscle volume and strength.

Methods: Eight boys and four girls (age = 12.1, standard deviation = 3.3) participated in this case-control study. Three-dimensional magnetic resonance images of both shoulders were acquired. The unimpaired shoulder served as a reference. Volumes of deltoid, pectoralis major, supraspinatus, infraspinatus, teres major, subscapularis were calculated based on 3D models, derived through image segmentation. Maximal isometric torques were collected in six directions.

Findings: All the major muscles studied were significantly atrophied. The teres major demonstrated the biggest difference in atrophy between groups (51 percentage points), the pectoralis major was the least atrophied (23 percentage points). The muscle volume distribution was significantly different between shoulders. Muscle volume could predict maximal voluntary isometric torques, but the regression coefficients were weaker on the impaired side (72% to 91% of the strength could be predicted in the uninvolved side and 24% to 90% in the involved side and external rotation strength could not be predicted).

Interpretation: This study demonstrates muscle atrophy varied across all the main shoulder muscles of the glenohumeral joint, leading to significant muscle volume imbalances. The weaker coefficients of determination on the impaired side suggest that other variables may contribute to the loss of strength in addition to atrophy.

1. Introduction

Obstetrical brachial plexus palsy (OBPP) is one of the most common birth injuries, with an incidence around 1.5 per 1000 births (Chauhan et al., 2014). While many injuries are transient, 18–34% of patients have long-term or permanent impairments/disability (Chauhan et al., 2014; Hoeksma et al., 2004; Lagerkvist et al., 2010). The upper (C5C6) and/or middle (C7) trunks of the brachial plexus and their distal elements are the most commonly injured elements (Lagerkvist et al., 2010). These nerve injuries lead to varying degrees of muscle denervation in shoulder girdle muscles (prime movers and scapular stabilizers), inducing a complex profile of muscle atrophy and force imbalances between agonist and antagonist muscle pairs (Brochard et al., 2014). The combined effects of shoulder muscle force imbalances, weakness, and joint pathology can severely diminish a child's functional use of their arm and/or hand for activities of daily living and other tasks.

Although the primary interventional goals when treating OBPP related impairments is to improve function by minimizing force imbalances across the shoulder muscles, there are little data defining the pattern or severity of muscle atrophy in children/adolescents with OBPP either individually or as a group. Studies evaluating atrophy in OBPP have typically used qualitative assessments (Hogendoorn et al., 2010; Pöyhiä et al., 2005), substituted cross-sectional areas for volumes (Eismann et al., 2015; Pöyhiä et al., 2005; Ruoff et al., 2012; Waters et al., 2009), or defined the volume using only a portion of the muscle (Van Gelein Vitringa et al., 2009; Van Gelein Vitringa et al., 2011). Additionally, these studies evaluated a limited subset of shoulder muscles, primarily the subscapularis and infraspinatus (Pöyhiä et al., 2005; Talbert et al., 2011; Van Gelein Vitringa et al., 2009; Van Gelein Vitringa et al., 2011; Waters et al., 2009). Therefore, the full extent and pattern of shoulder muscle atrophy in OBPP is not well established. The

* Corresponding author at: Rehabilitation Medicine, National Institutes of Health, 6707 Democracy Blvd., Suite 856, Bethesda, MD 20817, USA.
E-mail address: fsheehan@cc.nih.gov (F.T. Sheehan).

http://dx.doi.org/10.1016/j.clinbiomech.2017.07.010
Received 24 February 2017; Accepted 26 July 2017

lack of information related to the pectoralis major (PM) and teres major (TM) is a major deficit when developing treatments for children with OBPP, as these muscles are often targeted for lengthening, transfer procedures (Kirkos et al., 2005; Kozin et al., 2010; Odeh and Odeh, 2015; Ozben et al., 2011; Ozturk et al., 2010) or botulinum toxin injections (Ezaki et al., 2010; Michaud et al., 2014). Thus, a more complete understanding of the pattern and degree of muscle atrophy across shoulder muscles in patients with OBPP is needed to improve interventional outcomes.

An understanding of the volume-torque relationship in children/adolescents with OBPP will provide valuable patient-specific information, including the optimal target muscles for a given procedure. For example, Aydin and colleagues (Aydın et al., 2011) state that a preoperative examination should determine whether the muscle being transferred has sufficient power to justify the procedure. Yet, it is not possible to directly measure the power of an individual muscle. A recent study in typically developing children/adolescents established the relationship between shoulder muscle volume and torque in all three rotational degrees of freedom (Im et al., 2014). However, the *in vivo* relationship between muscle volume and torque has not been established in children with OBPP. A direct relationship between muscle volume and strength may not exist in these children, as other factors, such as glenohumeral deformity (Brochard et al., 2016) or fatty infiltration (Hogendoorn et al., 2010), may alter the relationship.

The primary purpose of this study was to quantify the pattern and severity of muscle atrophy of the major shoulder muscles (anterior deltoid, posterior deltoid, PM, TM, combined infraspinatus and teres minor, subscapularis, and supraspinatus) in the involved, relative to the uninvolved, shoulder in children/adolescents with unilateral OBPP using a 3D magnetic resonance (MR) based methodology. The secondary purposes were to quantify the agonist-antagonist muscle volume balance and determine if the maximum voluntary isometric joint moment in all three degrees of freedom could be predicted by the muscle volumes using a multiple regression analysis. As this study set out to evaluate the muscle volume to torque relationship, it was known from the outset that an older population, inclusive of children with previous surgical interventions, would be targeted. Thus, a separate analysis addressed if muscle atrophy and volume distribution was different in individuals with and without previous reconstructive surgery. In support of these purposes, the inter-rater reliability of obtaining muscle volumes in children/adolescents with OBPP was evaluated.

2. Methods

Data from an ongoing IRB (National Institute of Child Health and Human Development, intramural, MD, USA) approved study (Brochard et al., 2014; Brochard et al., 2016; Im et al., 2014; Sheehan et al., 2014) formed the basis of this case-controlled study. Sixteen children/adolescents with unilateral OBPP were recruited as a sample of convenience. A legal guardian or subject over 18 years of age provided written consent. Written assent was obtained from subject's under 18 years of age. The exclusion criteria were: 1) < 30° active flexion and abduction, 2) other neurological problems (*e.g.*, cerebral palsy, arthrogryposis), 3) contraindications for MR imaging, and 4) shoulder surgery and/or botulinum toxin injections within the 6 months prior to inclusion. A pediatric physiatrist performed a history and physical examination. Data were included only if a complete three-dimensional MR dataset was available for both shoulders. The final cohort consisted of eight boys and four girls [age = 12.1 (SD 3.3) years, height = 155.9 (SD 20.8) cm, 52.6 (SD 17.9) kg] with five of these children having had past surgical interventions (Supplementary material 1).

The MR data were acquired as a subset of a previous study (Sheehan et al., 2014), but the muscle volume was not analyzed as part of that study. Each participant was placed supine on the scanning bed of a 3 T MR scanner (Verio: Siemens, Germany). A flexible cardiac coil was placed posterior to the shoulder while its pair was wrapped around the subject's shoulder and chest. The arm was in a neutral position with the hand pronated. A T1-gradient recalled echo sequence was independently acquired for each shoulder, enabling optimal shoulder position relative to the MR unit. Neither sedation nor anesthesia was used. The imaging parameters, based on recommended parameters for denervated muscle (Kamath et al., 2008; Menashe et al., 2015), were held constant for each subject (416 × 312 × 192 pixels, slice thickness = 1.2 mm, TR = 16.6 ms, TE = 5.1 ms, imaging time = 4 min 22 s). The in-plane resolution varied from 0.55 mm × 0.55 mm to 0.63 mm × 0.63 mm across subjects, allowing for finer resolution in smaller subjects. The minimum scan volume ranged from the inferior scapular angle to 5 mm proximal of the acromion superior edge and from the lateral edge of the arm to the mid-spine. Throughout data processing the research team was blinded to the subjects' identity and side of impairment.

The 3D volume calculation was carried out as previously done (Im et al., 2014). The muscles of interest were manually segmented using MIPAV (Medical Image Processing Analysis and Visualization, Bethesda, MD, USA). The first and last five images containing a specific muscle were always used in segmentation. In the belly of the muscle every other, every fourth, or every sixth slice was used, based on the length of the muscle. Segmentation was guided by tracking minor area changes through the "skipped" images and using a tri-planar view to identify the muscular fascial planes, origins, and insertions. In cases of severe atrophy, segmentations were allowed to deviate from the uniform slice separation to more precisely capture the volume. The infraspinatus and teres minor were segmented as a single muscle (infraspinatus-teres minor (I-tm)). Similarly, the distal border of the TM was assumed to be at the level of the most distal scapular point, resulting in a small portion of the latissimus dorsi being included within the TM volume.

From the segmentation, a three-dimensional model (Fig. 1) of each muscle was created (Geomagic, Research Triangle Park, NC, Morrisville, USA). Smoothing filters were not used and minor modeling errors (*e.g.*, overlapping surfaces, holes) were manually corrected. Muscle volume was computed from the 3D model. The deltoid was split into functional segments, based on previous work in typically developing children (Im et al., 2014), and the volume of its functional sub-sections were quantified.

Each subject's contralateral shoulder was used as a control for the involved side. The atrophy was defined as the ratio of muscle volume from the involved side relative to that of the uninvolved side for each muscle. The proportional volumes of each muscle were obtained by dividing the corresponding volumes by the total muscle volume of the six muscles volumes quantified. These proportional volumes defined the muscle volume distribution. The ratio of agonist to antagonist muscle volume was computed for both shoulders in each of the three movement planes. The external rotation muscle group was the I-tm, the internal rotation group was the subscapularis and PM. The extensor group was the posterior deltoid and TM. The flexor group was the PM, supraspinatus, and the anterior deltoid. The abduction group was the entire deltoid, I-tm, and supraspinatus. The adductor group was the PM and subscapularis (Table 1).

Functional groups (Table 1) were determined based on moment arms from *in vitro* adult studies that used identical testing positions (Brown et al., 2007; Kuechle et al., 1997; Kuechle et al., 2000). Muscles with a moment arm greater than 6 mm in a specific torque direction were considered as contributors to that torque. This qualitative cut-off was slightly higher than our previous study (Im et al., 2014) due to the potential alteration in moment arms secondary to the bone deformities and humeral head migration in OBPP (Brochard et al., 2016). This resulted in the entire deltoid being considered an abductor, its anterior segment a flexor, and its posterior segment an extensor (Brown et al., 2007).

Two investigators independently assessed inter-rater reliability of calculating the muscle volumes from MR images in fifteen randomly

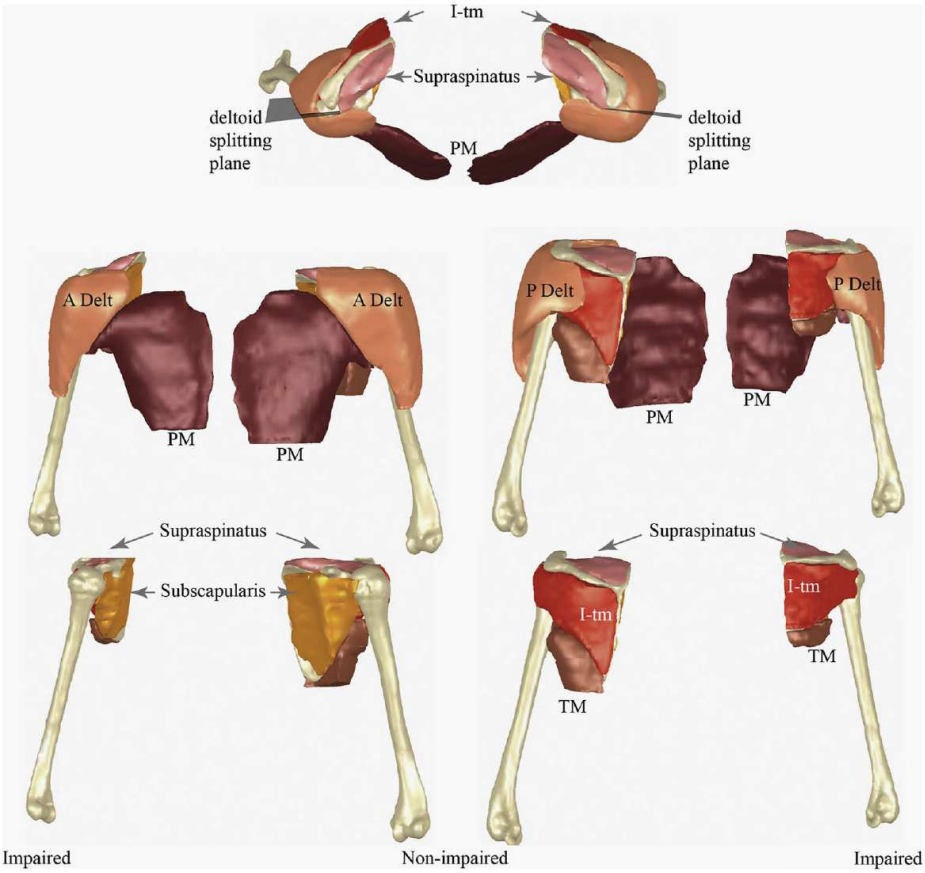

Fig. 1. Comparison of muscle volumes between sides for a single subject. The musculoskeletal models are both from a single male subject (subject 2). This subject has a Narakas score of 3 and a Mallet of 15. Top row is a superior to inferior view (involved arm on the right of the image), the left column provides an anterior to posterior view (involved side on the left of the image), and the right column provides a posterior view (involved arm on the right side of the image). For the bottom four images the identical scale is used. The identical scale is used in the top two images. Thus, the smaller muscle and bone volumes seem for the involved side are a result of atrophy/hypotrophy and are not a scaling artefact. The 3D MR images were acquired independently for both arms, as per the protocol, but used the identical resolution. Thus, the pose of each arm relative to each the other was based on a visual approximation and not a true anatomical position.

selected shoulders (five affected and 10 healthy shoulders) for three of the six muscles evaluated (deltoid, supraspinatus and I-tm). In total the volumes of 45 muscles were segmented twice. The selected muscles represented a diversity of shapes, sizes, depths, and functions. The reliability of calculating the anterior and posterior deltoid volume was quantified.

As part of a previous study (Brochard et al., 2014), maximal voluntary isometric joint torques were acquired in all three degrees of freedom using a hand held dynamometer (JTech Commander PowerTrack II). The position of the child, dynamometer, and observer; the order of the torque production (flexion, abduction, external rotation, internal rotation, adduction, and extension); and verbal encouragement cues were standardized. Children rested at least 10 s between trials and at least 1 min between directions. The highest maximal voluntary isometric torque value produced in three trials was used for the multiple regression analysis.

An *a priori* power analysis, based on a Wilcoxon paired test, determined that at least 10 subjects were required ($\alpha = 0.05$ and

Table 1
Adjusted coefficient of determination (R^2) for muscle volume-torque relationship.

Torque direction	Muscle	Moment arm (mm)	R^2 value	
			Involved	Uninvolved
Flexion	Anterior Deltoid	15.9 (Brown et al., 2007)	0.60	0.87
	Supraspinatus	7 (Kuechle et al., 1997)	–	0.81
	PM	10 (Kuechle et al., 1997)	0.90	0.78
Extension	Posterior deltoid	45.4 (Brown et al., 2007)	0.37	0.89
	TM	38 (Kuechle et al., 1997)	0.86	0.86
Abduction	Supraspinatus	19 (Kuechle et al., 1997)	0.24	0.83
	Total deltoid	19.5 (Brown et al., 2007)	0.45	0.86
	I-tm	19 (Kuechle et al., 1997)	0.58	0.81
Adduction	PM	21(Kuechle et al., 1997)	0.80	0.83
	Subscapularis	8 (Kuechle et al., 1997)	0.44	0.72
Internal rotation	Subscapularis	22.5 (Kuechle et al., 2000)	0.46	0.76
	PM	20 (Kuechle et al., 2000)	0.88	0.82
External rotation	I-tm	24 (Kuechle et al., 2000)	–	0.91

Muscles were identified as torque contributors to a given direction based on published moment arm data (Brown et al., 2007; Kuechle et al., 1997; Kuechle et al., 2000). R^2 values are presented when $P < 0.05$.
Abbreviations: I-tm = infraspinatus-teres minor, PM = pectoralis major, TM = teres major.

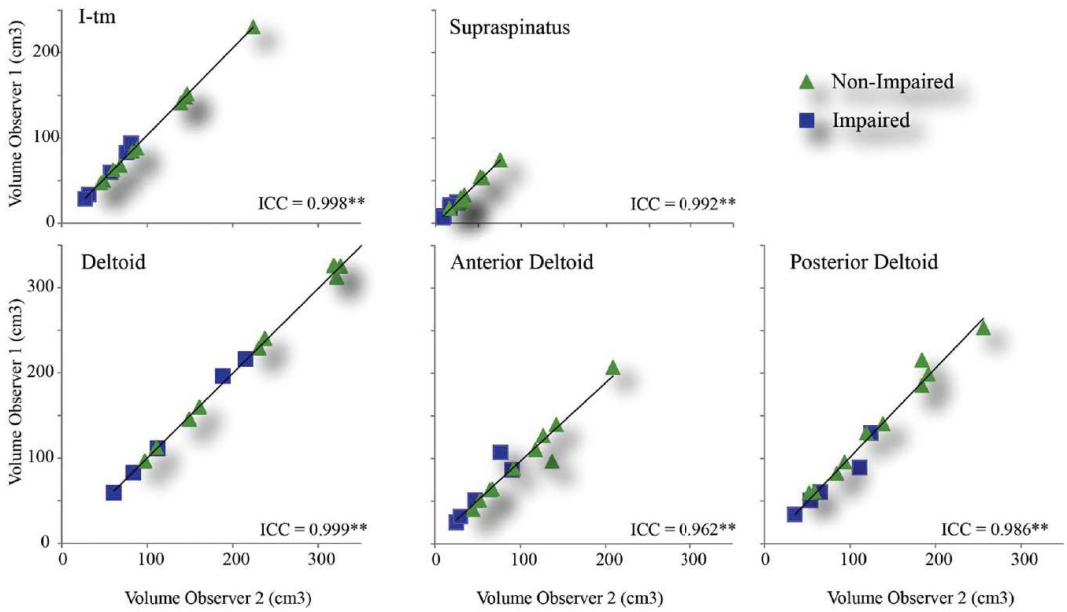

Fig. 2. Interobserver reliability of muscle volume measurement. All Intraclass Correlation Coefficients (ICC) all had *P*-values < 0.001, as indicated by the double star. Abbreviations: I-tm – infraspinatus-teres minor.

$\beta = 0.9$) assuming 50% atrophy in the subscapularis volume, as previously reported (Van Gelein Vitringa et al., 2009). A signed rank Wilcoxon paired-test was used for between-side comparisons and a signed Mann-Whitney test was used for sub-group comparisons. Using a linear regression analysis, the adjusted coefficient of determination between groups (R^2) was calculated between each muscle and the strength in the related direction. All statistical analyses were run in SPSS (IBM, version 22). To quantify inter-rater reliability, the intraclass correlation coefficients (ICCs), using a two-way mixed effects model, were computed. A *P*-value < 0.05 was considered significant.

3. Results

The inter-rater reliability for quantifying muscle volumes was excellent (ICC = 0.962–0.999, Fig. 2). Removing the data from the involved shoulder created minimal changes in the reliability. The percent error between raters ranged from −2.0% to 3.5%. The larger percent errors were due to the small volumes of the muscle.

For all subjects every muscle on the involved side was smaller relative to the uninvolved side (Fig. 3, top graph), with one exception for one muscle for one subject (3.8% hypertrophy in the PM). The TM, supraspinatus, and subscapularis muscle volumes were the most affected. In contrast, the PM and posterior deltoid volumes were the least affected. The children with previous surgeries tended to have more severe functional limitations (a trend towards lower Mallet scores) and significantly greater atrophy in all muscles, excluding the deltoid (Fig. 3, bottom graph). The loss of muscle volume was approximately 20 percentage points higher in the post-surgical group, except for the TM, which was 51 percentage points higher and the deltoid that demonstrated little difference between groups.

The muscle volume distribution was significantly different between shoulders (Fig. 4, top graph). For the involved side, the PM had a larger proportional volume ($P = 0.002$), relative to the uninvolved shoulder. In contrast, the TM, subscapularis, and supraspinatus made up a significantly lower proportional volume ($P = 0.024$, 0.003 and 0.010), as compared with the uninvolved shoulder. The muscle volume distribution on the involved side was not significantly different between the surgical and non-surgical groups for all muscles, with the exception of the deltoid and I-tm (Fig. 4, bottom graph).

The varying degrees of muscle atrophy led to significant changes in antagonist/agonist volume ratios (Fig. 5). This was true for extension/flexion (sagittal plane imbalance, $P = 0.002$), external/internal rotation (transverse plane imbalance, $P = 0.016$), and ab/adduction (frontal plane imbalance, $P = 0.025$).

For the uninvolved shoulder, 72% to 91% of the maximal voluntary isometric torques could be predicted using the muscle volumes (Table 1). For the involved side, 24% to 90% of the strength could be predicted, but external rotation strength could not be predicted (Table 1).

4. Discussion

This study advances our understanding of the complexity of shoulder muscle atrophy in OBPP by providing the first comprehensive evaluation of muscle volume loss across all the main shoulder muscles of the glenohumeral joint in children/adolescents with unilateral OBPP. In the impaired shoulder, all the muscles are atrophied, the TM, supraspinatus, and subscapularis muscle volumes are the most affected and the PM the least affected, inducing different distribution of shoulder muscle volume and three-dimensional imbalance around the palsied shoulder. Quantifying this variable pattern and severity of muscle atrophy fosters understanding of the impairments and functional limitations associated with OBPP, as well as, promotes improved subject-specific treatment planning. Substantiating the volume-strength relationship allows for deeper insights into how atrophy across various muscles relates to weakness at the shoulder. Identifying differential atrophy in the post-operative subgroup provides novel data which enhances our understanding of the long term musculoskeletal sequela associated with OBPP.

The inclusion of all "main" muscles of the shoulder provides a more detailed picture of the variability of atrophy across the shoulder in patients with OBPP. The greater atrophy in the current participants, relative to past studies(Pöyhiä et al., 2005; Talbert et al., 2011; Van Gelein Vitringa et al., 2009; Van Gelein Vitringa et al., 2011; Waters et al., 2009), is likely due to the older age of the current participants. Specifically, Talbert and colleagues (Talbert et al., 2011) demonstrated a correlation between age and I-tm atrophy in a group of patients with OBPP (age 1.1 to 13.2 years). Of note is the 23% loss of volume in the

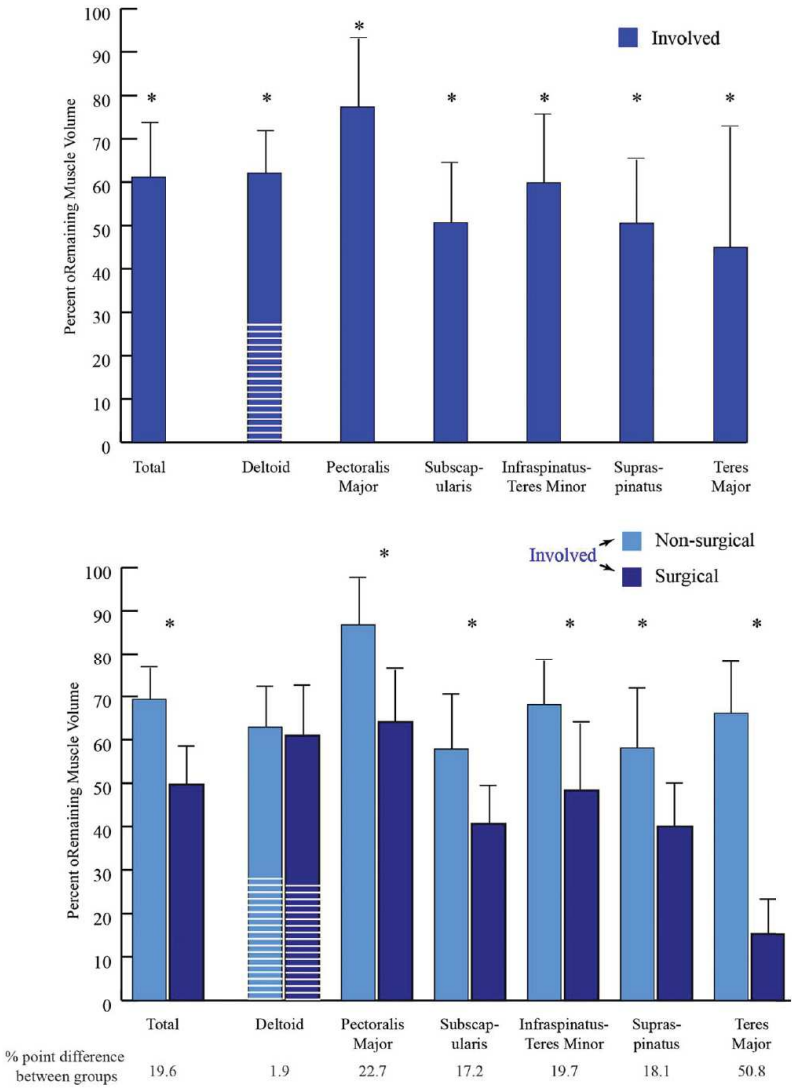

Fig. 3. Percentage of remaining muscle: $\%\text{remaining muscle} = \frac{\text{volume of the muscle from the involved side}}{\text{volume of the muscle from the uninvolved side}}$ One standard deviation is represented by the black bar and line. The white lines on the bar representing the deltoid demonstrate the percentage of the entire deltoid assigned to the anterior deltoid. "Total" represents the total remaining muscle volume of all muscles evaluated. Top: percent remaining muscle for the entire cohort ($n = 12$). Bottom: percent remaining muscle for the separated into the non-surgical group (light blue, $n = 7$) and the surgical group (dark blue, $n = 5$). The numbers at the bottom of the graph represent the differences between the two groups. Significant differences between sides (top) and between surgical/non-surgical group (bottom) are represented by: $^*P < 0.05$. (For interpretation of the references to colour in this figure legend, the reader is referred to the web version of this article.)

PM, which contrasts past reports (Waters et al., 2009) that assumed the PM was "unaffected". One possible explanation of this difference might be atrophy induced by a lack of use of the arm. The 3D muscle models take into account the entire volume and geometrical complexity of the shoulder muscles, which previous techniques did not, with the exception of one study evaluating the I-tm (Talbert et al., 2011). This volumetric information is particularly important in atrophic muscle where the relationship between the entire muscle volume and the area within a single slice may be quite different than in uninvolved muscles (Fig. 1). The length of the affected muscles may also be altered. These factors combined with the knowledge that muscle volume has been found to correlate more with age than cross sectional area (Pitcher et al., 2012; Vidt et al., 2012) support the concept that a 3D, volume-based, method is needed for accurately measuring muscle atrophy in individuals with OBPP.

The shifts in the muscle volume distribution between affected and unaffected shoulders likely relate to muscle innervation and the site and severity of the injury, as well as the extent of re-innervation. The lower percent contribution to the total muscle volume for the subscapularis, supraspinatus, and TM muscles highlights their potential key role in OBPP. Similarly, the PM's increase in percent muscle volume is likely due to the relative preservation of this muscle, which has dual innervation from multiple trunks and both the medial and lateral cords. The alterations in muscle volume balance in all three anatomical planes, with a greater volume imbalance in the sagittal plane, clearly demonstrates that treatment focused solely on the axial plane is too restrictive. The ratio of muscle volumes producing external rotation (I-tm) to muscle volume producing internal rotation (subscapularis and PM) matched previous results (Waters et al., 2009). If the PM is removed from the internal rotation group, then the previously reported decreased ratio is seen (Waters et al., 2009). These comparisons highlight the fact that subscapularis atrophy was compensated for by the fairly well preserved PM for both internal rotation and adduction, leading to the transverse and coronal plane imbalances. This makes the PM the major player in generating muscle volume imbalance. Since imbalance, more than muscle atrophy, is likely the cause of the glenohumeral deformities(Bahm et al., 2007; Gharbaoui et al., 2015; Sibinski et al., 2010; Van Der Sluijs et al., 2002), evaluating and targeting the imbalances in all three planes may improve global shoulder muscle balance, posture, motion, and joint integrity.

The markedly greater atrophy seen in the surgical, relative to the non-surgical, sub-group is noted in one previous study (Pöyhiä et al., 2005). Unique to the current study, the shoulder muscles do not show a consistent difference between groups. The deltoid shows no difference

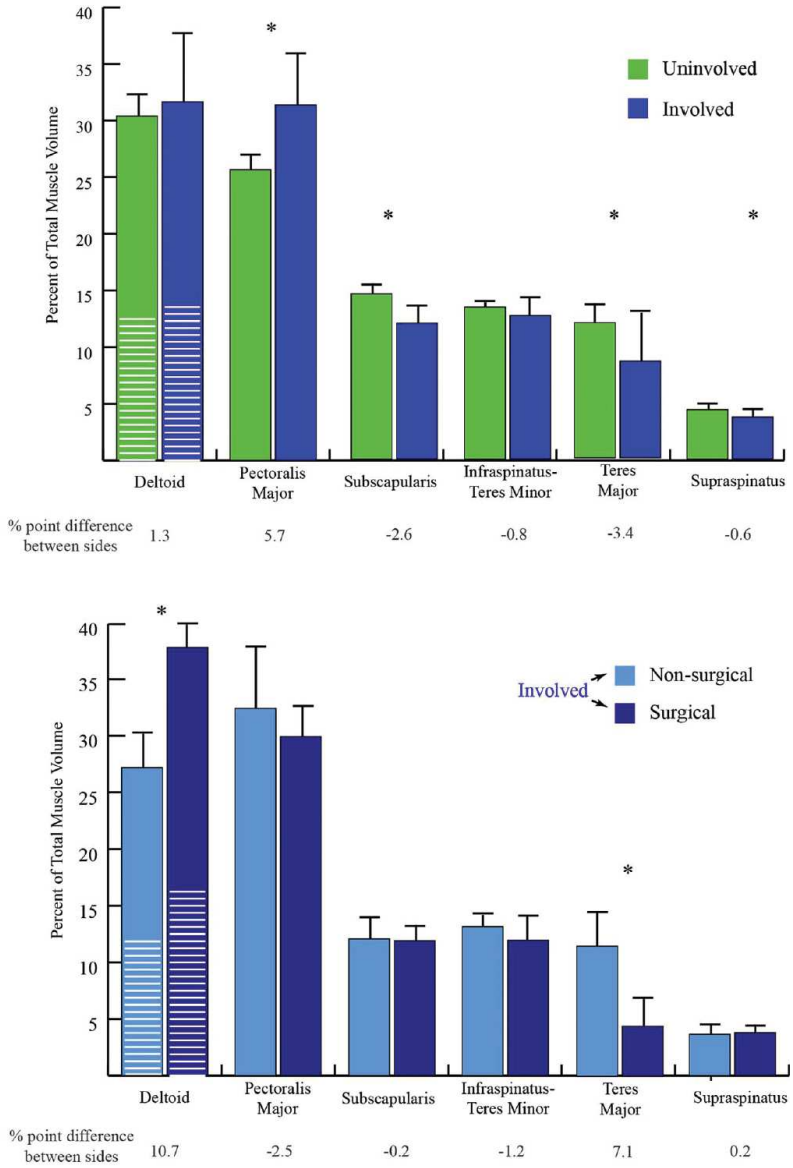

Fig. 4. Muscle volume distribution changes. Uninvolved (left columns) and involved (right columns) muscle volume distributions and standard deviations (error bars) are displayed. The distribution was calculated as a percentage that an individual muscle's volume contributes to the total volume of all six muscles. The white lines in the deltoid column represent the anterior deltoid. The between side differences expressed as a percentage of the control is provided below the graph. A significant difference is denoted with a * if $P < 0.05$. The anterior and posterior deltoids between side volume distributions were not significantly different.

in atrophy across groups and the difference in TM atrophy between groups (66% and 15% remaining for the non-surgical and surgical groups) is more than double all other muscle evaluated. As all children in this subgroup had a TM transfer, from a functional perspective, these results call into question the efficacy of the TM transfer and its potential long term benefits in the surgery subgroup. This is true regardless of whether the TM atrophy occurred preoperatively or post operatively. Longitudinal and controlled studies involving more children undergoing reconstructive/transfer surgeries are thus needed to evaluate accurately the biomechanical impacts of these interventions.

Accurately assessing muscle strength is of critical importance when considering reconstructive surgery in patients with OBPP (Aydın et al., 2011). It has long been recognized that the multiple muscles contributing to a given movement inhibit the direct assessment of an individual muscle's contribution to an overall joint torque. Further, overall joint torque cannot be assessed in individuals who cannot follow directions. Thus, establishing that muscle volume does predict strength in this population with unilateral OBPP provides the most direct insights into the remaining strength for individual muscles and will help advance the decision making process for reconstructive procedures (Jeng et al., 2012). However, the weaker R^2 values on the involved side coupled with a non-significant relationship between muscle volume and external rotation torque suggests that additional variables such as rheological changes in non-contractile muscle elements, fatty infiltration (Hogendoorn et al., 2010), changes in muscle architecture and/or osseous deformation(Eismann et al., 2016; Van Der Sluijs et al., 2002; Voigt et al., 2011) may also contribute to the loss of strength.

A limitation of this study is the use of the contralateral side as a control, as the uninvolved side may be altered relative to that of a typically developing child. Yet, an evaluation of nine typically developing children (Im et al., 2014), age and sex matched to nine children in the current study, demonstrated no significant differences in the dominant arm muscle volumes (deltoid, pectoralis major, supraspinatus, infraspinatus, teres major, subscapularis) or in the average height and weight in typically developing children relative to the children with unilateral OBPP. Using the dominant arm as a control provides the best anthropometric match, which is a main methodological issue in pediatric research. In order to avoid the use of anesthesia in this research

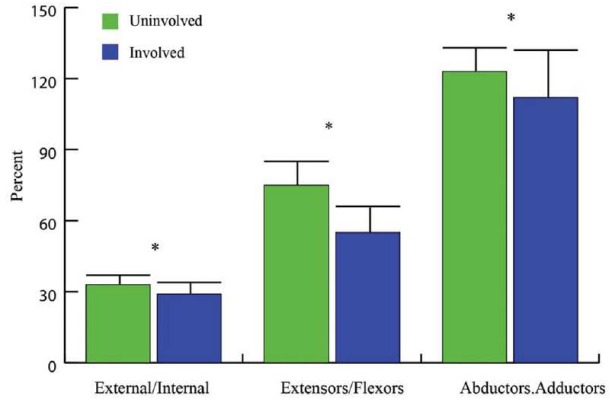

Fig. 5. Shoulder muscle group ratio (balance). The volume for each group was calculated based on the categorization provided in Table 1. For example, extensors/flexors ratio = (volume of anterior deltoid + volume of supraspinatus + volume of pectoralis major) / (volume of posterior deltoid + volume of teres major). Mean and standard deviations (error bars) are displayed. A significant between side difference is denoted with a * if $P < 0.05$.
Abbreviations: external = external rotators, and internal = internal rotators.

study and to accurately assess strength, the subjects were older than those in previous studies (Hogendoorn et al., 2010; Pöyhiä et al., 2005; Talbert et al., 2011; Van Gelein Vitringa et al., 2009; Van Gelein Vitringa et al., 2011; Waters et al., 2009). Further, the current segmentation and reconstruction methods are, at present, time-consuming. This limits their use in routine clinical practice, but for decisions involving invasive procedures, the time could easily be justified. Future work on developing/validating a more efficient, reliable technique is warranted (Blazevich et al., 2009; Lund et al., 2002).

This study clearly demonstrates muscle atrophy across all the main shoulder muscles of the glenohumeral joint. This atrophy varied across the muscle groups, leading to significant 3D muscle volume imbalances. As the PM is relatively preserved, compared to other muscles, this muscle is a key factor in generating 3D volumetric and strength imbalances. Based on the regression analysis, this study also emphasizes that other variables in addition to atrophy (*e.g.*, joint deformity and/or muscle inefficiency) may contribute to the loss of strength, especially in external rotation. An individualized, comprehensive, 3D musculoskeletal evaluation, including a muscle volume specific evaluation should be considered a prerequisite for interventions in OBPP children with complex clinical presentation.

Supplementary data to this article can be found online at http://dx.doi.org/10.1016/j.clinbiomech.2017.07.010.

Funding sources

This work was funded by grants awarded to Dr. Brochard from the University Hospital of Brest, the French Society of Physical Medicine and Rehabilitation (SOFMER), the French Society of Research in Children with Disabilities (SFERHE) and by the Intramural Research Program of the National Institutes of Health Clinical Center, Bethesda, MD, USA.

Acknowledgements

We thank Diane Damiano, PhD, Christopher Hollingsworth, Lindsey Curatalo, Christopher Stanley, and Lori Ohlrich for their help and support in the work. In addition, we would like to thank the Radiology Department, headed by Dr. David Bluemke, at the Clinical Center of the National Institutes of Health for their support of this work.

Conflicts of interests

None.

References

Aydın, A., Biçer, A., Özkan, T., Mersa, B., Özkan, S., Yıldırım, Z., 2011. Does primary brachial plexus surgery alter palliative tendon transfer surgery outcomes in children with obstetric paralysis? BMC Musculoskelet. Disord. 12 (1), 1.
Bahm, J., Wein, B., Alhares, G., Dogan, C., Radermacher, K., Schuind, F., 2007. Assessment and treatment of glenohumeral joint deformities in children suffering from upper obstetric brachial plexus palsy. J. Pediatr. Orthop. B 16 (4), 243–251.
Blazevich, A.J., Coleman, D.R., Horne, S., Cannavan, D., 2009. Anatomical predictors of maximum isometric and concentric knee extensor moment. Eur. J. Appl. Physiol. 105 (6), 869–878.
Brochard, S., Alter, K., Damiano, D., 2014. Shoulder strength profiles in children with and without brachial plexus palsy. Muscle Nerve 50 (1), 60–66.
Brochard, S., Mozingo, J.D., Alter, K.E., Sheehan, F.T., 2016. Three dimensionality of gleno-humeral deformities in obstetrical brachial plexus palsy. J. Orthop. Res. 34 (4), 675–682.
Brown, J., Wickham, J., McAndrew, D., Huang, X.-F., 2007. Muscles within muscles: coordination of 19 muscle segments within three shoulder muscles during isometric motor tasks. J. Electromyogr. Kinesiol. 17 (1), 57–73.
Chauhan, S.P., Blackwell, S.B., Ananth, C.V., 2014. Neonatal brachial plexus palsy: incidence, prevalence, and temporal trends. Semin. Perinatol. 38, 210–218.
Eismann, E.A., Little, K.J., Laor, T., Cornwall, R., 2015. Glenohumeral abduction contracture in children with unresolved neonatal brachial plexus palsy. J. Bone Joint Surg. Am. 97 (2), 112–118.
Eismann, E.A., Laor, T., Cornwall, R., 2016. Three-dimensional magnetic resonance imaging of glenohumeral dysplasia in neonatal brachial plexus palsy. J. Bone Joint Surg. Am. 98 (2), 142–151.
Ezaki, M., Malungpaishrope, K., Harrison, R.J., Mills, J.K., Oishi, S.N., Delgado, M., et al., 2010. Onabotulinumtoxin A injection as an adjunct in the treatment of posterior shoulder subluxation in neonatal brachial plexus palsy. J. Bone Joint Surg. Am. 92 (12), 2171–2177.
Gharbaoui, I.S., Gogola, G.R., Aaron, D.H., Kozin, S.H., 2015. Perspectives on glenohumeral joint contractures and shoulder dysfunction in children with perinatal brachial plexus palsy. J. Hand Ther. 28 (2), 176–184.
Hoeksma, A.F., Steeg, T., Marie, A., Nelissen, R.G., Van Ouwerkerk, W.J., Lankhorst, G.J., et al., 2004. Neurological recovery in obstetric brachial plexus injuries: an historical cohort study. Dev. Med. Child Neurol. 46 (2), 76–83.
Hogendoorn, S., van Overvest, K.L.J., Watt, I., Duijsens, A.H.B., Nelissen, R.G.H.H., 2010. Structural changes in muscle and glenohumeral joint deformity in neonatal brachial plexus palsy. J. Bone Joint Surg. Am. 92 (4), 935–942.
Im, H.S., Alter, K.E., Brochard, S., Pons, C., Sheehan, F.T., 2014. In vivo pediatric shoulder muscle volumes and their relationship to 3D strength. J. Biomech. 47 (11), 2730–2737.
Jeng, C.L., Thawait, G.K., Kwon, J.Y., Machado, A., Boyle, J.W., Campbell, J., Carrino, J.A., 2012. Relative strengths of the calf muscles based on MRI volume measurements. Foot Ankle Int. 33 (5), 394–399.
Kamath, S., Venkatanarasimha, N., Walsh, M., Hughes, P., 2008. MRI appearance of muscle denervation. Skelet. Radiol. 37 (5), 397–404.
Kirkos, J., Kyrkos, M., Kapetanos, G., Haritidis, J., 2005. Brachial plexus palsy secondary to birth injuries long-term results of anterior release and tendon transfers around the shoulder. J. Bone Joint Surg. Br. 87 (2), 231–235.
Kozin, S.H., Boardman, M.J., Chafetz, R.S., Williams, G.R., Hanlon, A., 2010. Arthroscopic treatment of internal rotation contracture and glenohumeral dysplasia in children with brachial plexus birth palsy. J. Shoulder Elb. Surg. 19 (1), 102–110.
Kuechle, D.K., Newman, S.R., Itoi, E., Morrey, B.F., An, K.-N., 1997. Shoulder muscle moment arms during horizontal flexion and elevation. J. Shoulder Elb. Surg. 6 (5), 429–439.
Kuechle, D.K., Newman, S.R., Itoi, E., Niebur, G.L., Morrey, B.F., An, K.-N., 2000. The relevance of the moment arm of shoulder muscles with respect to axial rotation of the glenohumeral joint in four positions. Clin. Biomech. 15 (5), 322–329.
Lagerkvist, A.L., Johansson, U., Johansson, A., Bager, B., Uvebrant, P., 2010. Obstetric brachial plexus palsy: a prospective, population-based study of incidence, recovery, and residual impairment at 18 months of age. Dev. Med. Child Neurol. 52 (6), 529–534.
Lund, H., Christensen, L., Savnik, A., Boesen, J., Danneskiold-Samsøe, B., Bliddal, H., 2002. Volume estimation of extensor muscles of the lower leg based on MR imaging. Eur. Radiol. 12 (12), 2982–2987.
Menashe, S.J., Tse, R., Nixon, J.N., Ishak, G.E., Thapa, M.M., McBroom, J.A., Iyer, R.S., 2015. Brachial plexus birth palsy: multimodality imaging of spine and shoulder abnormalities in children. AJR Am. J. Roentgenol. 204 (2), W199–W206.
Michaud, L.J., Louden, E.J., Lippert, W.C., Allgier, A.J., Foad, S.L., Mehlman, C.T., 2014. Use of botulinum toxin type A in the management of neonatal brachial plexus palsy. PM R 6 (12), 1107–1119.
Odeh, R., Odeh, M., 2015. A modified Sever-L'Episcopo procedure for restoration of shoulder joint function in Erb's palsy. Int. Orthop. 39 (2), 309–317.
Ozben, H., Atalar, A.C., Bilsel, K., Demirhan, M., 2011. Transfer of latissmus dorsi and teres major tendons without subscapularis release for the treatment of obstetrical brachial plexus palsy sequela. J. Shoulder Elb. Surg. 20 (8), 1265–1274.
Ozturk, K., Bulbul, M., Demir, B.B., Buyukkurt, C.D., Ayanoglu, S., Esenyel, C.Z., 2010. Reconstruction of shoulder abduction and external rotation with latissimus dorsi and

teres major transfer in obstetric brachial plexus palsy. Acta Orthop. Traumatol. Turc. 44 (3), 186–193.
Pitcher, C.A., Elliott, C.M., Williams, S.A., Licari, M.K., Kuenzel, A., Shipman, P.J., Valentine, J.P., Reid, S.L., 2012. Childhood muscle morphology and strength: alterations over six months of growth. Muscle Nerve 46 (3), 360–366.
Pöyhiä, T.H., Nietosvaara, Y.A., Remes, V.M., Kirjavainen, M.O., Peltonen, J.I., Lamminen, A.E., 2005. MRI of rotator cuff muscle atrophy in relation to glenohumeral joint incongruence in brachial plexus birth injury. Pediatr. Radiol. 35 (4), 402–409.
Ruoff, J.M., van der Sluijs, J.A., Van Ouwerkerk, W.J., Jaspers, R.T., 2012. Musculoskeletal growth in the upper arm in infants after obstetric brachial plexus lesions and its relation with residual muscle function. Dev. Med. Child Neurol. 54 (11), 1050–1056.
Sheehan, F.T., Brochard, S., Behnam, A.J., Alter, K.E., 2014. Three-dimensional humeral morphologic alterations and atrophy associated with obstetrical brachial plexus palsy. J. Shoulder Elb. Surg. 23 (5), 708–719.
Sibinski, M., Woźniakowski, B., Drobniewski, M., Synder, M., 2010. Secondary glenohumeral joint dysplasia in children with persistent obstetric brachial plexus palsy. Int. Orthop. 34 (6), 863–867.
Talbert, R.J., Michaud, L.J., Mehlman, C.T., Kinnett, D.G., Laor, T., Foad, S.L., et al., 2011. EMG and MRI are independently related to shoulder external rotation function in neonatal brachial plexus palsy. J. Pediatr. Orthop. 31 (2), 194–204.
Van Der Sluijs, J., Van Ouwerkerk, W., De Gast, A., Wuisman, P., Nollet, F., Manoliu, R., 2002. Retroversion of the humeral head in children with an obstetric brachial plexus lesion. J. Bone Joint Surg. Br. 84 (4), 583–587.
Van Gelein Vitringa, V.M., van Kooten, E.O., Mullender, M.G., van Doorn-Loogman, M.H., van der Sluijs, J.A., 2009. An MRI study on the relations between muscle atrophy, shoulder function and glenohumeral deformity in shoulders of children with obstetric brachial plexus injury. J. Brachial Plexus Peripheral Nerve Inj. 4 (1), 5.
Van Gelein Vitringa, V.M., Jaspers, R., Mullender, M., Ouwerkerk, W.J., van der Sluijs, J.A., 2011. Early effects of muscle atrophy on shoulder joint development in infants with unilateral birth brachial plexus injury. Dev. Med. Child Neurol. 53 (2), 173–178.
Vidt, M.E., Daly, M., Miller, M.E., Davis, C.C., Marsh, A.P., Saul, K.R., 2012. Characterizing upper limb muscle volume and strength in older adults: a comparison with young adults. J. Biomech. 45 (2), 334–341.
Voigt, C., Kreienborg, S., Megatli, O., Schulz, A.-P., Lill, H., Hurschler, C., 2011. How does a varus deformity of the humeral head affect elevation forces and shoulder function? A biomechanical study with human shoulder specimens. J. Orthop. Trauma 25 (7), 399–405.
Waters, P.M., Monica, J.T., Earp, B.E., Zurakowski, D., Bae, D.S., 2009. Correlation of radiographic muscle cross-sectional area with glenohumeral deformity in children with brachial plexus birth palsy. J. Bone Joint Surg. Am. 91 (10), 2367–2375.

Cette étude est la première à proposer une évaluation précise des muscles mobilisateurs principaux de l'articulation gléno-humérale chez l'enfant avec POPB et à établir un lien avec la fonction musculaire en établissant des corrélations avec la force.

Les difficultés méthodologiques étaient similaires à celles explicitées pour l'étude chez l'enfant à développement typique. Nous reviendrons simplement sur le choix réalisé concernant la formation des **groupes fonctionnels**. Seuls les muscles avec un bras de levier d'au moins 6 mm pouvaient être inclus dans un groupe fonctionnel. Cette simplification était nécessaire du fait de la migration postérieure, inférieure et médiale de la tête humérale par rapport à la glène, modifiant les lignes d'action et bras de levier des muscles gléno-huméraux (Kuechle et al. 1997, 2000). En conservant le seuil de 3 mm utilisé pour l'enfant à développement typique dans l'étude précédente, nous craignions d'attribuer une action mécaniquement impossible à un des muscles étudiés du fait de la déformation. Comme dans l'étude précédente, cette méthode représente une limite et un biais dans le raisonnement pour l'étude de la relation volume-force.

Cette étude évalue six muscles mobilisateurs principaux de l'articulation gléno-humérale, et **permet une vision plus globale des atteintes musculaires et déséquilibres** au niveau de l'épaule que les études précédentes. Cependant, **l'ensemble des muscles potentiellement impliqués dans la pathologie de l'épaule** chez l'enfant avec POPB, du fait de leur **innervation ou de leur potentielle participation dans la déformation** de l'épaule (Crouch et al. 2014), **n'a pas pu être étudié**. Les chefs long du biceps et long du triceps et le muscle grand dorsal, transféré dans certaines chirurgies (Michael L. Pearl et al. 2006; Kozin et al. 2006), mériteraient d'être également étudiés dans les études futures concernant les muscles dans cette population. Ils ne pouvaient pas être considérés ici du fait de l'impossibilité de segmentation, même manuelle, pour le grand dorsal et des limites de champ de vue pour les deux autres muscles.

Les **coefficients de corrélation entre le volume et la force étaient présents mais plus faibles** pour les muscles **du côté de la POPB** que du côté non affecté ou que ceux retrouvés chez les enfants à développement typique. En plus de l'atrophie, **d'autres facteurs limitent les muscles**

dans leur production de force, telles que l'infiltration graisseuse, les modifications de l'architecture musculaire.

Le muscle pectoral était à la fois le moins atrophique et le muscle dont les coefficients de corrélation volume-force étaient les plus élevés, suggérant la trophicité comme un bon reflet de l'importance de l'atteinte d'un muscle chez les enfants avec POPB. L'existence des corrélations volume-force dans tous les degrés de liberté de l'épaule sauf un est un argument en faveur de l'utilisation des volumes musculaires dans l'étude de la genèse de la déformation gléno-humérale.

Aucune relation entre l'infraépineux et la force en rotation externe n'était retrouvée. On peut dans ce cas faire l'hypothèse que la subluxation de la tête humérale en arrière, en diminuant l'espace entre l'insertion du muscle infraépineux sur la scapula et sa terminaison sur l'humérus, modifie son bras de levier et rende le muscle « trop long » empêchant la contraction efficace du muscle. Une **étude EMG** associée à l'étude morphologique des éléments présentés ci-dessus, **contribuerait à améliorer notre compréhension** de cette absence de relation et évaluer la contraction du muscle infraépineux lors des tentatives de mouvement en rotation externe (J. M. M. Brown et al. 2007; Hurov 2009; Talbert et al. 2011; Gross et al. 2015) .

III Analyse du mouvement du membre supérieur

L'atteinte musculo-squelettique de l'épaule a pour conséquence la **limitation des mouvements de l'épaule** chez les enfants avec POPB, avec un retentissement sur **l'ensemble des mouvements des membres supérieurs et les activités et la participation** de ces enfants.
L'évaluation clinique ne permet pas une analyse précise et compréhensive biomécaniquement du mouvement chez les enfants avec POPB. Bialocerkowski et al. ont comparé, sur 30 enfants avec POPB, la cotation de l'AMS avec le seul examen clinique et avec un système d'analyse 2D du mouvement le V Scope (A. E. Bialocerkowski, Wrigley et Galea 2006). Ils retrouvaient des erreurs systématiques dans la cotation de l'AMS lors de l'évaluation clinique visuelle et montraient ainsi l'intérêt d'une analyse quantifiée instrumentale du mouvement pour améliorer la précision de la mesure (A. E. Bialocerkowski et Galea 2006). Le système V scope était toutefois limité pour l'analyse compréhensive du mouvement du membre supérieur par son caractère bidimensionnel, ne permettant pas l'analyse complète du tronc ou de l'épaule, possédant 3 degrés de liberté articulaire.
Les **systèmes optoélectroniques d'analyse quantifiée du mouvement** utilisent des marqueurs externes positionnés sur des repères anatomiques (G. Wu et al. 2005). Pour pouvoir déterminer le mouvement des structures en mouvement dans les trois dimensions de l'espace et avec une fréquence d'acquisition élevée, les systèmes optiques mesurent les coordonnées 3D de ces marqueurs (Jaspers et al. 2011; Desroches et al. 2010; Alt Murphy, Willén et Sunnerhagen 2013). Lors d'un mouvement, ces systèmes permettent d'obtenir les **données cinématiques de chaque articulation en 3D**, et permettent donc au niveau du membre supérieur l'exploration dynamique du mouvement et sa quantification dans chaque articulation, notamment au niveau de l'épaule. Chez l'enfant avec POPB, la faisabilité et l'intérêt de l'utilisation de ce système au niveau du membre supérieur pour quantifier le mouvement tridimensionnel et évaluer l'impact d'un traitement ont été montrés dans deux études (Fitoussi et al. 2009; Mosqueda et al. 2004).

Ces systèmes ont aussi permis de montrer les limitations importantes du mouvement actif au niveau de **l'articulation gléno-humérale** et les **compensations au niveau de l'articulation scapulo-thoracique** (Duff, Dayanidhi et Kozin 2007; Russo et al. 2014). Une **atteinte au niveau du coude** a été objectivée, avec une tendance à l'augmentation de la flexion (Herisson et al. 2017; Mosqueda et al. 2004; Fitoussi et al. 2009) (paragraphe 2.3).

Etant donné la possibilité de compensations au niveau de l'ensemble des articulations du membre supérieur atteint mais également le possible impact sur la motricité du membre supérieur sain dont la dextérité peut être affectée (Aktaş et al. 2018; Immerman et al. 2012; Matthews 2018), **une analyse du mouvement des deux membres supérieurs dans un groupe d'enfants POPB par rapport à des enfants TD permettrait de caractériser les spécificités** du mouvement chez les **enfants avec POPB**.

Dans le travail ci-dessous, ayant pour objectif de caractériser le mouvement des deux membres supérieurs dans un groupe d'enfants avec POPB par rapport à des enfants avec dévelopement typique, des tâches testant spécifiquement **l'amplitude des mouvements de l'épaule étaient évaluées** étant donné l'atteinte importante connue à ce niveau. Afin de connaître les stratégies de mouvement utilisées lors de tâches quotidiennes et l'efficacité de celles-ci, **trois tâches fonctionnelles étaient évaluées**. Lors de ces tâches fonctionnelles, les paramètres spatio-temporels étaient mesurés afin d'évaluer la performance du mouvement.

Cet article est en préparation pour une soumission dans Gait and Posture. La relecture de l'Anglais n'a pas encore été réalisée. Les appendices seront trouvés en annexe 4.

Three-dimensional upper limb movement characteristics in children with brachial plexus birth palsy

Christelle Pons[1, 2], Mathieu Lempereur[2,3,4], Katharine Alter[5], Diane Damiano[5], Sylvain Brochard[1,2,3,4¶]

[1]Pediatric rehabilitation department, Fondation ILDYS, Brest, France

[2]Laboratoire de Traitement de l'Information Médicale, INSERM U1101, Brest, France

[3]Université de Bretagne Occidentale, Brest, France

[4]PMR department, CHRU de Brest, Hopital Morvan, Brest, France

[5]Functional and Applied Biomechanics Section, Rehabilitation Medicine Department, National Institutes of Health, USA

Abstract (N= 271/ 275 words max)

Objective : To investigate which kinematic and spatiotemporal parameters differentiate upper limbs movements in children with obstetrical brachial plexus palsy (OBPP) from typically developing children (TDC).

Design: Case control study

Setting: Functional Applied Biomechanics laboratory, NIH, USA

Participants: 12 children with unilateral OBPP (mean age = 11.7 years (SD 4.2) years) and 11 TDC (age=10.9 (SD 2.5))

Interventions: not applicable

Main outcome measures: Three-dimensional motions of both upper limbs of children with OBPP and of the non-dominant limb of TD children were collected during the execution of 5 shoulder amplitude tasks and 3 functional tasks. Total active range of motion (ROM) start and stop angles were calculated. Kinematics between groups were compared using the Arm Profile Score. Spatio-temporal parameters were computed for the functional tasks.

Results:

Spatio-temporal parameters did not differ between groups for most of the tasks. Significant changes were found during all the tasks at the gleno-humeral joint, especially in the rotation plane, but also on all the other segment/joints (trunk, scapulo-thoracic, elbow, wrist). For all the tasks, children with OBPP had significantly higher APS-scores compared to TDC. In the unimpaired side of children with OBPP, significant kinematic differences compared to TDC were found, especially in the shoulder rotation plane.

Conclusions: Effective movements with good motor control but with atypical patterns of movements were highlighted on the impaired upper limb of children with OBPP. The major Involvement of the gleno-humeral joint was confirmed and compensatory movements were found at the other levels. Management of gléno-humeral mobility appears as a key point. Compensations were also found on the unimpaired limb, in favor of an overall evaluation of children with OBPP.

Key words: brachial plexus palsy, upper limb, kinematics, spatio-temporal, rehabilitation

Introduction

Obstetrical Brachial Plexus Palsy (OBPP) refers to injury to one or more cervical nerve roots (C5-C8) and/or the first thoracic nerve root (T1), usually caused by excessive traction during birth. The incidence is around 1.5 per 1000 births. In one third of cases, nerve recovery is incomplete or absent (1,2), resulting in permanent impairment (1). The upper part of the brachial plexus is most commonly affected, resulting in paresis of shoulder movements and elbow flexion (3,4). On the impaired side, active and passive range of motions (ROM) are known to be limited (4–6). On the unimpaired side also, performances are reported to be worse compared to typically developing children (TDC). One of the main goals of the care and rehabilitative management is to improve these movements in order to improve function and participation (7,8).

The use of three-dimensional movement analysis have been reported in children with OBPP to quantify differences with typically developing children (TDC) in upper limb position during movements (9,10). It adds to our insights in the upper limb movement pathology in children with OBPP and provide valuable information for intervention evaluations (10,11). Compared to TD children differences were highlighted at the gleno-humeral, scapulo-thoracic and elbow levels with decreased gleno-humeral contribution, increased scapulathoracic contributions and a more flexed elbow position (9–13). However, a more global analysis of both upper-limbs movements is still lacking. To our knowledge, spatiotemporal parameters, which can provide relevant information about upper limb motor "performance" (14–16) has not been studied yet in children with OBPP. Better characterizing the impaired and unimpaired upper limb movement of children with OBPP will help as well in understanding, and thus adapt rehabilitation strategies.

The aim of this study was to investigate which spatiotemporal, and kinematic parameters obtained from 3D motion analysis differentiate upper limbs movements in children with OBPP

from TDC, during the execution of 5 full shoulder tasks and 3 tasks which simulated activities of daily living.

Our hypotheses were that upper limb spatiotemporal and kinematic parameters would be different between groups on the impaired and unimpaired sides with most significant changes at the shoulder level.

Methods

Participants

Data from an ongoing IRB (National Institute of Child Health and Human Development, intramural, MD, USA) approved study (17–19) formed the basis of this case-controlled study. Inclusion criteria were: age 5–18 years, unilateral OBPP, and ability to flex and abduct the impaired arm at least 30°. Exclusions were any other significant neurological or orthopedic impairment, orthopedic surgery with secondary interventions (4), botulinum toxin injections to upper limbs within 6 months, inability to follow verbal directions. Medical histories were reviewed to confirm eligibility (figure 1). Functional evaluation using Mallet scale (20) was performed for all the children with OBPP. For comparison purposes, TDC with no history of neuro-musculo-skeletal disorders were also recruited.

The protocol was approved by the institutional review board at the National Institutes of Health, Bethesda, MD. Parents and children if possible provided informed consent.

Data collection

Three-dimensional motion of the markers was captured using a 10 camera Vicon MX system (Vicon Motion Systems, Oxford, UK) at a rate of 100 Hz. Markers were placed on the trunk, in the arm, on medial and lateral epicondyles, on forearm and on the hand (21). An acromion

marker cluster (AMC) with three markers was positioned on the flat surface of the acromion. A scapula locator, placed over the angulus acromius, angulus inferius and trigonum spinae, was used to calibrate the scapula position in the AMC frame.

The movement protocol consisted first in static calibration in rest position to identify the anatomical landmarks (21). Next children were asked to perform 5 full shoulder movements (flexion, extension, abduction, adduction and external rotation) named hereafter amplitude tasks and 3 tasks which simulated activities of daily living (reach to grasp, hand to top of the head, hand to contralateral shoulder) named functional tasks. All movements were performed three times at self-selected speed with the non-dominant arm for TD children and with both arms for children with OBPP. Movements were systematically carried out in the same order. Children with OBPP performed the set of tasks in the impaired side and then with the other side. Oral instructions were given to help the children to perform the movements in a standardized way

Participants seated in an armless chair with their feet on the ground with ankle in neutral position and the hips and knees flexed 90°. Horizontal adduction was performed from maximal horizontal abduction. External rotation was performed with the arm supported by an examiner at 90° of abduction from maximal internal rotation. Functional tasks began with the arm hanging freely at the participant's side. For the reach to grasp task, a cylindrical rod was placed on a table at elbow height and at a distance near but less than maximum reach for each individual.

Data processing

The gleno-humeral center of rotation was estimated using the functional method of Gamage & Lasenby (22,23). Upper limb kinematics of the trunk, shoulder, scapula, elbow and wrist were

computed following the ISB recommendations (21), using visual 3D (C-Motion, Inc., Germantown, MD). Double calibration was used (24,25) to better estimate scapular rotations during flexion and abduction movements. Discrete kinematic parameters included total active range of motion (ROM, calculated as the difference between minimum and maximum angles) start angles and point of task achievement (PTA) angles. Kinematics were compared using the Arm Profile Score (APS), a summary index to grade the severity of upper limb movement pathology, decomposed of 13 Arm Variable Scores (AVS) which are calculated as the RMSE between the point by point comparison of the joint angle of the involved upper limb and the same joint angle of the reference database (26). For the functional tasks, spatio-temporal parameters including movement duration(s), peak velocity of the wrist marker (m/s), timing of maximum velocity (%) and the index of curvature (27) were calculated.

Statistical analysis

Kinematic, spatiotemporal and APS data were analyzed using R (version 3.4.3). Statistical analyses were made on the available data. Means and standard deviations between the trials for a same movement were calculated for each parameter. Comparisons between impaired side of children with OBPP and non-dominant side of TDC, and between the unimpaired side of children with OBPP and non-dominant side of TDC (kinematic, spatio temporal and APS data) were carried out using a Mann Whitney U test. The level of significant was set at 0.05.

Results

Participants

Twelve children with OBPP (7 boys, 5 girls, age = 11.7 (SD 4.2) years) and 11 TDC (7 boys, 4 girls, age=10.9 (SD 2.5)) were included. No statistical difference between ages in the two groups was found.

In the group of children with OBPP, the impaired side was the right side in 8 children and the left side in 4 children. Mean Mallet scale was 15.5, Narakas evaluation was 1 for 3 children, 2 for 5 children and 3 for 4 children. TD children were all right handed.

Comparison between impaired side of children with OBPP (I OBPP) and non-dominant side of TD children (ND TD)

Spatio-temporal parameters (table 1)

Movement time, timing of maximum velocity and index of curvature did not differ between groups for all the functional tasks. During hand to shoulder movement, children with OBPP had a significantly lower velocity (13% slower).

Kinematic parameters (Table 2)

Children with OBPP had significantly higher APS-scores compared to the TDC. Mean APS were respectively of 24.4 and 10.8 for OBPP and TDC. Regarding individual joint angles, significant task-dependent differences in AVS were highlighted.

At the level of the trunk, children with OBPP had altered rest and starting positions with a significantly increased trunk rotation with the impaired side frontward (difference 6-10°) and less lateral tilt (difference ≅3°). While performing flexion, abduction, and the three functional tasks, children with OBPP used more ROM in flexion/extension (difference 3-13°). At PTA, they had less lateral tilt on the impaired side for flexion, abduction and external rotation tasks (difference ≅6°), and increased tilt for reach to grasp task (difference ≅4°). Trunk rotation AVS was increased in all the tasks.

At the level of the scapula, children with OBPP started external rotation task with less anterior tilt and more lateral rotation. They started hand to shoulder and hand to head tasks with more medial rotation. For the amplitude tasks except abduction, lower ROM were found in all planes.

As a result, at PTA, they had less posterior tilt for flexion (difference ≅13°), less anterior tilt for extension and adduction tasks (difference ≅11°). They also had less lateral rotation for flexion, extension and adduction tasks (difference ≅15°). Regarding functional tasks, children with OBPP used greater ROM with more tilt for reach to grasp and hand to head movements (difference 7-11°), more rotation for reach to grasp task (difference ≅7°) and more pro/retraction for hand to head movement (difference ≅11°).

At the gleno-humeral level, children with OBPP had altered rest and starting positions with more internal rotation for all the tasks (difference 27-53°) but extension, more elevation for all the tasks (difference ≅ 10°). They finished their movement with more internal rotation for all the tasks (difference 25-61°) but hand to shoulder. Shoulder rotation AVS was increased in all the tasks. Lower ROM in the two other planes were found for the amplitude tasks (plane of elevation, difference: 7-52.6°; elevation: difference 10-35°). For reach to grasp and hand to shoulder tasks, children finished their movement with a less anterior position and more elevation. Shoulder elevation AVS was increased in 7/8 tasks.

At the elbow level, children with OBPP had a more flexed position for the amplitude tasks (difference 22-33°). They used less ROM for reach to grasp and hand to head movements (difference ≅20°). They finished hand to shoulder task with less supination (difference ≅30°). and reach to grasp task with less pronation (difference ≅25°). ROM were decreased for prono/supination in all the tasks (difference 18-38°) but three (adduction, external rotation, reach to grasp).

At the wrist level, for the hand to head task, greater extension was used (difference ≅12°). Mobility was greater in the two planes of mobility for abduction task and in inclination for adduction. Wrist deviation AVS was increased in 7/8 tasks.

Comparison between unimpaired side of children with OBPP (UI OBPP) and non-dominant side of TD children (ND TD)(Table 1, appendix 1 and 2)

Spatio-temporal parameters (table 1) did not differ between groups for the functional tasks. APS were significantly greater except for flexion task. Mean APS were respectively of 14,6 and 10.8 for OBPP and TD children. At the trunk level, lateral tilts and rotations were reversed and AVS were significantly higher. At the gleno-humeral level, children with OBPP had more internal rotation at the start of the movement for flexion and abduction (difference 10-17°), leading to greater internal rotation at the shoulder level (flexion, abduction, extension). At PTA, they had less external rotation for external rotation task.

Discussion

The brachial plexus is a peripheral neurological lesion. However it occurs before motor programs have been developed fully and thus central developmental consequences are expected in children with OBPP, like changes in brain organization (28–30). Specific consequences on the development of central motor programs are suspected in the literature (31–33). In populations with central brain lesions like children with cerebral palsy (14,34), adults with multiple sclerosis (35) or stroke (36), movements exhibits less straight trajectories in the impaired upper limb with discontinuous spatial and temporal movement trajectories. In this study however, no consequence was found on timing of maximum velocity and index of curvature in functional tasks in the involved upper limb of children with OBPP. This first result is in favor of at least a relatively preserved motor control in children with OBPP, who can produce smooth trajectories, similar to controls, despite the earliness of the lesions. These new data on spatio-temporal parameters which showed good upper limb motor performance, are in

favor of the acquisition of compensatory mechanisms allowing children with OBPP to have effective movements.

Children with OBPP showed discernable differences in joint kinematics on their impaired side compared to the TDC for all the joints and tasks. Depending of the amplitude or functional tasks, movements at individual joints could differ.

APS scores were quite high compared to children with cerebral palsy (14). Greater AVS were found at the shoulder level but also at the other levels, including levels whose motricity is preserved.

As previously shown, major changes were confirmed at the gleno-humeral level with decrease ROM in all the planes (9,11,13). The humerus was more internally rotated at rest and for all the tasks (11). These changes can be explained by the involvement of all the shoulder muscles (18,37,38) and the bone deformity (17,39). Regarding axial rotation, the impaired growth with internal rotation contractures of the subscapularis (40) and the internal and external rotators imbalance are involved in the external rotation limitation (6,41–43). For reach to grasp and hand to shoulder tasks, children finished their movement with a less anterior position and more elevation of the arm (13), suggesting that less anterior elevation might be easier for these children. At the scapula level, for the amplitude tasks, decrease ROM were found, which can be related to the decrease in amplitudes at the gleno-humeral level. For the functional tasks, greater scapula ROM without greater gleno-humeral ROM were found in some cases, in favor of the scapulo-humeral rhythm disturbance and a greater contribution of the scapulo-thoracic joint for these movements (9–12).

At the trunk level, an increased trunk rotation with the impaired side frontward was highlighted at the start but not at the end of the movement, in favor of an impaired position with possibilities of correction and compensations to avoid impaired upper limb to be even more internally rotated. The decrease of the lateral tilt highlighted for the amplitude tasks could be linked with

the reduced gleno-humeral ROM. The increase of trunk flexion for flexion, abduction, and functional tasks could aim to increase the mobility of the impaired upper limb and compensate the gleno-humeral involvment.

At the elbow level, as previously shown, a more flexed elbow position was found with reduced ROM (10,12,13). ROM decrease for prono/supination was expected because of the frequent involvement of the supinator muscles in these children. Some compensations were highlighted for the reach to grasp task, during which children finished with less pronation possibly to well orientate the internal rotated upper limb to achieve the task.

Lastly, regarding wrist joint, greater mobility in the sagittal plane was found for abduction and adduction tasks, that can be interpreted as an attempt to increase the mobility of the upper limb.

In this article, we confirmed the predominant impairment of the gleno-humeral joint in the impaired side of children with OBPP. A specific organization of the movement involving all the upper limb joints was also highlighted with an interdependence of the functioning of the joints. Consequences such as a decrease in amplitude of the movements or compensatory movements were highlighted showing the interest of considering the whole upper limb when evaluating children with OBPP. More compensations were found for functional tasks.

On the unimpaired limb of children with OBPP, less external rotation at the beginning of the tasks and during movement were found for some of the tasks compared to TDC. As no change for unimpaired trunk rotation was obvious, except the inverse rotations and tilt because of the comparisons of unimpaired side with the non-dominant side, we did not interpret this as a compensation. As central motor reorganization was shown to involve both hemispheres (31), central reorganization of the position and movements can be questioned in this case, with a mirroring of the involved and uninvolved sides. We thus believe that TDC should serve as controls for future upper extremity motion analysis studies in children with OBPP (44).

Clinical implications can be drawn from the results of this study. The management of the gleno-humeral internal rotation contracture, which, associated with increased trunk rotation and limitation of prono-supination largely disturbed the rest position and movement during all the tasks in this study is a key point. As external rotation is necessary during humeral elevation, internal rotation contracture may further limit shoulder movement (45). Thus, a careful monitoring of active and passive range of motions in shoulder rotations is necessary. More data on the treatment strategy of internal rotation contracture, using early passive and active mobilization in physiotherapy (46), botulinum toxin injections (7) and secondary surgeries (4) are warranted.

The presence of effective movements in both sides with good motor control but with atypical pattern of movements questions the type of rehabilitative therapies to set up in this pathology. Use of techniques like constraint induced movement therapies (47) can be questioned, because of the good performances of both upper limbs. The risk of preventing compensations from being used and thus limiting the effectiveness of the movement can also question therapies aiming to restore a typical pattern of movement (48). An involvement of the unimpaired upper limb was suspected, further evaluations of both upper limbs are warranted (49). Bimanual therapies (50) could be interesting if the organization of the movement between upper limbs is affected.

The large number of statistical comparisons carried out in this pilot study induce a high risk of type 1 error (some significant differences may have occurred due to chance). However, the conclusions were determined by overall comparisons and was not based on specific comparisons. Further oriented studies in a larger population have to be carried out. Important variability in spatio temporal and kinematic parameters remain in the impaired side of children with OBPP compared to TD children which can be in favor of variations in motion strategies among children with OBPP. Further studies are warranted to identify motion specificities and propose more individualized managements in subgroups of children with OBPP (9).

In this study, effective movements with good motor control but with atypical pattern of joint mobility were highlighted on the impaired upper limb of children with OBPP. Changes were also highlighted on the unimpaired limb. Involvement of the gleno-humeral joint was confirmed on the impaired limb, especially in the rotation plane, with impacts the mobility of other joints. Management of internal rotation contracture appears thus as a key point in the management of children with OBPP to improve all upper-limb movements.

References

1. Chauhan SP, Blackwell SB, Ananth CV. Neonatal brachial plexus palsy: incidence, prevalence, and temporal trends. Semin Perinatol. 2014 Jun;38(4):210–8.

2. Hoeksma AF, ter Steeg AM, Nelissen RGHH, van Ouwerkerk WJR, Lankhorst GJ, de Jong BA. Neurological recovery in obstetric brachial plexus injuries: an historical cohort study. Dev Med Child Neurol. 2004 Feb;46(2):76–83.

3. van Dijk JG, Pondaag W, Malessy MJ. Obstetric lesions of the brachial plexus. Muscle Nerve. 2001 Nov;24(11):1451–61.

4. Pearl ML. Shoulder problems in children with brachial plexus birth palsy: evaluation and management. J Am Acad Orthop Surg. 2009 Apr;17(4):242–54.

5. Julka A, Vander Have KL. Shoulder sequelae of neonatal brachial plexus injuries: orthopedic assessment and management. J Pediatr Rehabil Med. 2011;4(2):131–40.

6. Van Gelein Vitringa VM, Jaspers R, Mullender M, Ouwerkerk WJ, Van Der Sluijs JA. Early effects of muscle atrophy on shoulder joint development in infants with unilateral birth brachial plexus injury. Dev Med Child Neurol. 2011 Feb;53(2):173–8.

7. Gobets D, Beckerman H, de Groot V, Van Doorn-Loogman MH, Becher JG. Indications and effects of botulinum toxin A for obstetric brachial plexus injury: a systematic literature review. Dev Med Child Neurol. 2010 Jun;52(6):517–28.

8. Louden EJ, Broering CA, Mehlman CT, Lippert WC, Pratt J, King EC. Meta-analysis of function after secondary shoulder surgery in neonatal brachial plexus palsy. J Pediatr Orthop. 2013 Sep;33(6):656–63.

9. Russo SA, Kozin SH, Zlotolow DA, Thomas KF, Hulbert RL, Mattson JM, et al. Scapulothoracic and glenohumeral contributions to motion in children with brachial plexus birth palsy. J Shoulder Elbow Surg. 2014 Mar;23(3):327–38.

10. Fitoussi F, Maurel N, Diop A, Laassel EM, Ilharreborde B, Presedo A, et al. Upper extremity kinematics analysis in obstetrical brachial plexus palsy. Orthopaedics & Traumatology: Surgery & Research. 2009 Sep 1;95(5):336–42.

11. Duff SV, Dayanidhi S, Kozin SH. Asymmetrical shoulder kinematics in children with brachial plexus birth palsy. Clinical Biomechanics. 2007 Jul 1;22(6):630–8.

12. Herisson O, Maurel N, Diop A, Le Chatelier M, Cambon-Binder A, Fitoussi F. Shoulder and elbow kinematics during the Mallet score in obstetrical brachial plexus palsy. Clinical Biomechanics. 2017 Mar 1;43:1–7.

13. Mosqueda T, James MA, Petuskey K, Bagley A, Abdala E, Rab G. Kinematic Assessment of the Upper Extremity in Brachial Plexus Birth Palsy. Journal of Pediatric Orthopaedics. 2004 Dec;24(6):695.

14. Jaspers E, Desloovere K, Bruyninckx H, Klingels K, Molenaers G, Aertbeliën E, et al. Three-dimensional upper limb movement characteristics in children with hemiplegic cerebral palsy and typically developing children. Research in Developmental Disabilities. 2011 Nov 1;32(6):2283–94.

15. Alt Murphy M, Willén C, Sunnerhagen KS. Responsiveness of Upper Extremity Kinematic Measures and Clinical Improvement During the First Three Months After Stroke. Neurorehabil Neural Repair. 2013 Nov 1;27(9):844–53.

16. Mateo S, Roby-Brami A, Reilly KT, Rossetti Y, Collet C, Rode G. Upper limb kinematics after cervical spinal cord injury: a review. Journal of NeuroEngineering and Rehabilitation. 2015 Jan 30;12(1):9.

17. Brochard S, Mozingo JD, Alter KE, Sheehan FT. Three dimensionality of gleno-humeral deformities in obstetrical brachial plexus palsy. J Orthop Res. 2016 Apr;34(4):675–82.

18. Pons C, Sheehan FT, Im HS, Brochard S, Alter KE. Shoulder muscle atrophy and its relation to strength loss in obstetrical brachial plexus palsy. Clin Biomech (Bristol, Avon). 2017 Oct;48:80–7.

19. Mayfield CH, Kukke SN, Brochard S, Stanley CJ, Alter KE, Damiano DL. Inter-joint coordination analysis of reach-to-grasp kinematics in children and adolescents with obstetrical brachial plexus palsy. Clinical Biomechanics. 2017 Jul 1;46:15–22.

20. Mallet J. [Obstetrical paralysis of the brachial plexus. II. Therapeutics. Treatment of sequelae. Priority for the treatment of the shoulder. Method for the expression of results]. Rev Chir Orthop Reparatrice Appar Mot. 1972;58:Suppl 1:166-168.

21. Wu G, van der Helm FCT, (DirkJan) Veeger HEJ, Makhsous M, Van Roy P, Anglin C, et al. ISB recommendation on definitions of joint coordinate systems of various joints for the reporting of human joint motion—Part II: shoulder, elbow, wrist and hand. Journal of Biomechanics. 2005 May 1;38(5):981–92.

22. Gamage SSHU, Lasenby J. New least squares solutions for estimating the average centre of rotation and the axis of rotation. Journal of Biomechanics. 2002 Jan 1;35(1):87–93.

23. Lempereur M, Leboeuf F, Brochard S, Rousset J, Burdin V, Rémy-Néris O. In vivo estimation of the glenohumeral joint centre by functional methods: Accuracy and repeatability assessment. Journal of Biomechanics. 2010 Jan 19;43(2):370–4.

24. Brochard S, Lempereur M, Mao L, Rémy-Néris O. The role of the scapulo-thoracic and gleno-humeral joints in upper-limb motion in children with hemiplegic cerebral palsy. Clinical Biomechanics. 2012 Aug 1;27(7):652–60.

25. Lempereur M, Brochard S, Leboeuf F, Rémy-Néris O. Validity and reliability of 3D marker based scapular motion analysis: a systematic review. J Biomech. 2014 Jul 18;47(10):2219–30.

26. Jaspers E, Feys H, Bruyninckx H, Klingels K, Molenaers G, Desloovere K. The Arm Profile Score: A new summary index to assess upper limb movement pathology. Gait & Posture. 2011 Jun 1;34(2):227–33.

27. Heide JC van der, Fock JM, Otten B, Stremmelaar E, Hadders-Algra M. Kinematic Characteristics of Reaching Movements in Preterm Children with Cerebral Palsy. Pediatric Research. 2005 Jun;57(6):883–9.

28. Auer T, Pinter S, Kovacs N, Kalmar Z, Nagy F, Horvath RA, et al. Does obstetric brachial plexus injury influence speech dominance? Ann Neurol. 2009 Jan;65(1):57–66.

29. Buitenhuis S, van Wijlen-Hempel RS, Pondaag W, Malessy MJA. Obstetric brachial plexus lesions and central developmental disability. Early Hum Dev. 2012 Sep;88(9):731–4.

30. Yang LJ-S, Anand P, Birch R. Limb Preference in Children with Obstetric Brachial Plexus Palsy. Pediatric Neurology. 2005 Jul 1;33(1):46–9.

31. Anguelova GV, de Vlugt E, Vardy AN, van Zwet EW, van Dijk JG, Malessy MJA, et al. Cocontraction measured with short-range stiffness was higher in obstetric brachial plexus lesions patients compared to healthy subjects. Journal of Biomechanics. 2017 Oct 3;63:192–6.

32. Colon AJ, Vredeveld JW, Blaauw G. Motor Evoked Potentials After Transcranial Magnetic Stimulation Support Hypothesis of Coexisting Central Mechanism in Obstetric Brachial Palsy. Journal of Clinical Neurophysiology. 2007 Feb;24(1):48.

33. Boylan LS, Fouladvand M. Developmental apraxia arising from neonatal brachial plexus palsy. Neurology. 2001 Feb 27;56(4):576–7.

34. Chang J-J, Wu T-I, Wu W-L, Su F-C. Kinematical measure for spastic reaching in children with cerebral palsy. Clin Biomech (Bristol, Avon). 2005 May;20(4):381–8.

35. Corona F, Gervasoni E, Coghe G, Cocco E, Ferrarin M, Pau M, et al. Validation of the Arm Profile Score in assessing upper limb functional impairments in people with multiple sclerosis. Clinical Biomechanics. 2018 Jan 1;51:45–50.

36. Thrane G, Sunnerhagen K, Persson H c, Opheim A, Alt Murphy M. Kinematic upper extremity performance in people with near or fully recovered sensorimotor function after stroke. Physiotherapy Theory and Practice. 2018 Apr 16;

37. Brochard S, Alter K, Damiano D. Shoulder strength profiles in children with and without brachial PLEXUS PALSY. Muscle Nerve. 2014 Jul;50(1):60–6.

38. Cheng W, Cornwall R, Crouch DL, Li Z, Saul KR. Contributions of Muscle Imbalance and Impaired Growth to Postural and Osseous Shoulder Deformity Following Brachial Plexus Birth Palsy: A Computational Simulation Analysis. The Journal of Hand Surgery. 2015 Jun 1;40(6):1170–6.

39. Frich LH, Schmidt PH, Torfing T. Glenoid morphology in obstetrical brachial plexus lesion: a three-dimensional computed tomography study. Journal of Shoulder and Elbow Surgery. 2017 Aug 1;26(8):1374–82.

40. Nikolaou S, Peterson E, Kim A, Wylie C, Cornwall R. Impaired Growth of Denervated Muscle Contributes to Contracture Formation Following Neonatal Brachial Plexus Injury. JBJS. 2011 Mar 2;93(5):461.

41. Waters PM, Monica JT, Earp BE, Zurakowski D, Bae DS. Correlation of radiographic muscle cross-sectional area with glenohumeral deformity in children with brachial plexus birth palsy. J Bone Joint Surg Am. 2009 Oct;91(10):2367–75.

42. Hogendoorn S, van Overvest KLJ, Watt I, Duijsens AHB, Nelissen RGHH. Structural changes in muscle and glenohumeral joint deformity in neonatal brachial plexus palsy. J Bone Joint Surg Am. 2010 Apr;92(4):935–42.

43. Pöyhiä TH, Nietosvaara YA, Remes VM, Kirjavainen MO, Peltonen JI, Lamminen AE. MRI of rotator cuff muscle atrophy in relation to glenohumeral joint incongruence in brachial plexus birth injury. Pediatr Radiol. 2005 Apr;35(4):402–9.

44. Wang JS, Petuskey K, Bagley AM, James MA, Rab G. The Contralateral Unimpaired Arm as a Control for Upper Extremity Kinematic Analysis in Children With Brachial Plexus Birth Palsy. Journal of Pediatric Orthopaedics. 2007 Sep;27(6):709.

45. Ludewig PM, Reynolds JF. The association of scapular kinematics and glenohumeral joint pathologies. J Orthop Sports Phys Ther. 2009 Feb;39(2):90–104.

46. Bialocerkowski A, Kurlowicz K, Vladusic S, Grimmer K. Effectiveness of primary conservative management for infants with obstetric brachial plexus palsy. Int J Evid Based Healthc. 2005 Mar;3(2):27–44.

47. Santamato A, Panza F, Ranieri M, Fiore P. Effect of botulinum toxin type A and modified constraint-induced movement therapy on motor function of upper limb in children with obstetrical brachial plexus palsy. Childs Nerv Syst. 2011 Dec;27(12):2187–92.

48. Russo SA, Zlotolow DA, Chafetz RS, Rodriguez LM, Kelly D, Linamen H, et al. Efficacy of 3 therapeutic taping configurations for children with brachial plexus birth palsy. J Hand Ther. 2018 Sep;31(3):357–70.

49. Gaillard F, Cretual A, Cordillet S, Le Cornec C, Gonthier C, Bouvier B, et al. Kinematic motion abnormalities and bimanual performance in children with unilateral cerebral palsy. Dev Med Child Neurol. 2018;60(8):839–45.

50. Tervahauta M, Girolami G, Øberg G. Efficacy of constraint-induced movement therapy compared with bimanual intensive training in children with unilateral cerebral palsy: a systematic review. Clin Rehabil. 2017 Nov 1;31(11):1445–56.

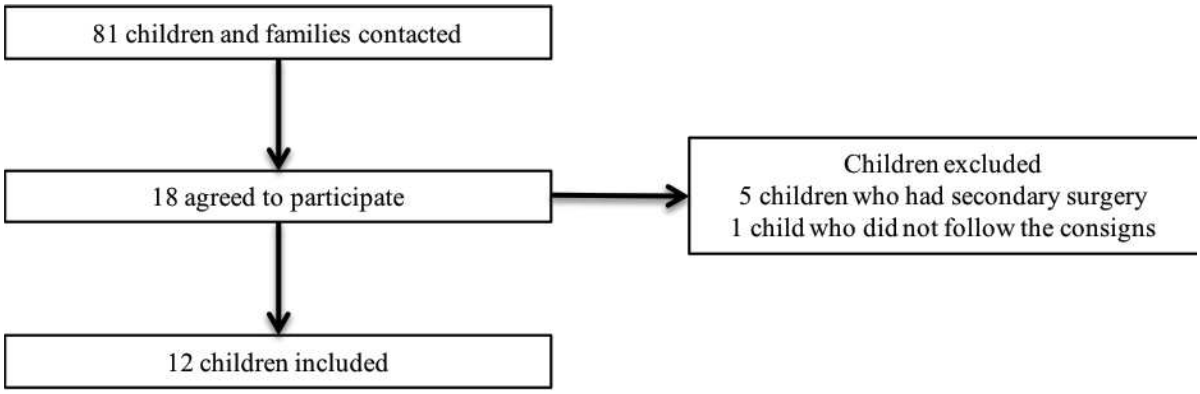

Figure 1 : flow chart

Figure 2 : Arm Profile Score, impaired side of children with OBPP (I OBPP), non-dominant side of TD children (ND TDC)
*: $p<0.05$

	reach to grasp					hand to head					hand to shoulder				
	ND TDC (N=11)		UI OBPP (N=10)		p	ND TDC (N=11)		UI OBPP (N=11)		p	ND TDC (N=11)		UI OBPP (N=10)		p
	mean	SD	mean	SD		mean	SD	mean	SD		mean	SD	mean	SD	
movement time	1,17	0,15	1,18	0,17	0,61	1,38	0,43	1,44	0,33	0,80	1,20	0,32	1,24	0,26	0,35
maximum velocity	1,00	0,10	0,94	0,15	0,24	1,27	0,19	1,22	0,17	0,48	1,15	0,14	1,12	0,19	0,35
timing of maximum velocity	0,35	0,04	0,35	0,08	0,53	0,39	0,06	0,41	0,65	0,37	0,49	0,05	0,45	0,10	0,15
index of curvature	0,82	0,06	0,83	0,08	0,41	0,68	0,07	0,68	0,56	0,85	0,64	0,11	0,68	0,07	0,25
	ND TDC (N=11)		I OBPP (N=10)		p	ND TDC (N=11)		NI OBPP (N=11)		p	ND TDC (N=11)		I OBPP (N=10)		p
	mean	SD	mean	SD		mean	SD	mean	SD		mean	SD	mean	SD	
movement time	1,17	0,15	1,19	0,25	0,83	1,38	0,43	1,72	0,71	0,33	1,20	0,32	1,41	0,42	0,20
maximum velocity	1,00	0,10	0,87	0,18	0,09	1,27	0,19	1,10	0,30	0,12	1,15	0,14	1,00	0,17	**0,01**
timing of maximum velocity	0,35	0,04	0,34	0,10	0,83	0,39	0,06	0,44	0,12	0,27	0,49	0,05	0,47	0,10	0,86
index of curvature	0,82	0,06	0,83	0,08	0,49	0,68	0,07	0,70	0,08	0,52	0,64	0,11	0,71	0,05	0,13

Table 1 : spatio-temporal parameters of the non dominant side of typically developping children, impaired and unimpaired sides of children with OBPP

ND TDC : non dominant side of typically developping children
UI OBPP : unimpaired side of children with OBPP
I OBPP : impaired side of children with OBPP
N : number of children

		arm down (rest)			flexion			abduction			extension			adduction		
		ND (N=11)	I (N=12)	p	ND (N=11)	I (N=12)	p	ND (N=11)	I (N=12)	p	ND (N=11)	I (N=12)	p	ND (N=11)	I (N=11)	p
start angle																
wrist	fl-ext	-2,6	-3,2		0,3	-10,1		-15,6	-22,0		1,5	-4,8		-26,5	-22,8	
	rad-ulnar inclination	-7,3	-2,3		-1,4	-0,2		-4,1	-0,4		-2,9	0,8		-5,9	6,3	*
elbow	fl ext	21,1	36,1		10,8	33,3	***	7,3	34,7	****	10,6	36,4	***	0,9	33,8	****
	pro-supination	106,2	93,1		85,6	75,7		28,3	72,3	***	86,6	82,0		58,3	79,1	
gleno humeral	plane of elevation	6,6	6,4		8,2	5,4		8,6	6,3		8,3	9,3		-16,3	13,0	****
	elevation	-13,8	-28,4	**	-9,5	-24,5	**	-7,4	-19,8	**	-12,6	-28,1	***	-36,3	-51,9	*
	axial Rotation	-31,3	2,1	**	-23,0	6,1	*	-53,3	0,0	***	-25,8	-5,6		-67,0	-13,5	****
shoulder (thoraco humeral)	plane of elevation	-1,5	8,4	*	-2,3	4,8	*	-3,0	5,5	*	-3,0	8,5	*	-23,9	19,2	****
	elevation	-11,5	-22,1	*	-10,7	-18,3	*	-8,0	-16,5	*	-12,0	-17,7		30 et 25 vs 40)	-64,7	
	axial Rotation	2,0	46,7	***	-0,8	33,7	***	-19,5	30,4	***	3,3	34,1	**	-59,8	-1,7	****
scapula	ant-post tilt	-14,8	-15,4		-16,5	-13,7		-16,1	-14,5		-16,9	-14,5		-10,8	-8,3	
	med-lat rotation	4,4	5,8		1,5	4,5		1,5	2,5		2,7	7,7		-14,9	-15,6	
	pro-retraction	30,4	39,9		26,9	32,0		19,0	28,7		25,9	34,5		3,3	12,4	*
trunk	fl-ext	5,4	8,5		3,4	7,4		-0,4	4,3		3,2	7,5		1,2	-7,2	*
	lat tilt	-0,8	2,1		0,7	3,6	*	0,9	4,4	*	-0,2	2,2		-13,3	-3,1	***
	rotation	1,7	-4,7	*	3,3	-3,4	**	-0,7	-9,7	**	2,3	-7,6	***	-14,1	-23,1	
PTA angle																

wrist	fl-ext		-13,4	-20,5		-15,5	-22,4		18,0	4,8		-23,6	-17,8	
	rad-ulnar inclination		-5,6	-3,0		0,6	5,7		1,8	7,3		-4,0	-3,4	
elbow	fl ext		15,8	45,3	**	11,7	43,2	**	1,5	35,2	****	31,1	60,9	*
	pro-supination		48,7	62,5		81,6	75,6		112,3	88,1		58,9	83,0	
gleno humeral	plane of elevation		11,9	16,3		10,7	16,7		-27,0	4,7	****	59,1	34,4	***
	elevation		-99,6	-76,2	**	-105,6	-70,8	***	-11,8	-21,2	*	-48,6	-58,4	
	axial Rotation		-62,3	-15,5	***	-50,9	-13,1	**	-30,8	-4,6	*	-48,4	-4,0	***
shoulder (thoraco humeral)	plane of elevation		21,3	42,2	**	27,8	35,1		-50,8	-4,8	****	57,1	62,8	*
	elevation		-144,8	-107,4	**	-148,4	-101,7	****	-35,6	-19,8	**	50,9	23,4	
	axial Rotation		-93,6	-34,3	****	-89,8	-27,8	****	1,0	27,9	**	97,5	75,2	
scapula	ant-post tilt		15,9	2,9	**	7,2	1,3		-29,7	-19,1	**	-21,5	-9,8	*
	med-lat rotation		-46,1	-31,7	*	-41,5	-31,7		1,3	5,8		-33,0	-16,8	**
	pro-retraction		21,0	32,3		31,8	25,7		14,0	26,1		68,0	61,2	
trunk	fl-ext		-13,8	-14,9		-10,4	-11,4		15,3	9,5		-6,6	-5,2	
	lat tilt		-9,4	-1,9	*	-14,7	-9,2	**	-7,0	0,3	**	-3,9	0,5	
	rotation		2,27	1,2		-3,4	-14,0		-17,8	-22,4		35,4	25,6	*
ROM angle														
wrist	fl-ext		18,4	26,1		11,3	25,9	*	21,0	13,8		15,7	13,9	
	rad-ulnar inclination		8,7	29,9		7,1	15,9	**	10,3	28,8		6,3	34,6	*
elbow	fl ext		16,2	15,1		13,6	16,0		13,9	5,8	**	34,1	30,2	

	pro-supination		39,0	21,4	***	57,7	20,0	****	34,4	12,2	***	23,6	19,9	
gleno humeral	plane of elevation		25,2	18,3	*	30,8	16,1	***	36,1	8,1	****	75,8	23,2	****
	elevation		90,9	53,0	***	98,4	54,2	****	12,1	9,6		32,5	17,1	**
	axial Rotation		45,1	24,7	**	27,6	21,0		14,1	5,9	****	27,6	17,4	*
shoulder (thoraco humeral)	plane of elevation		64,0	47,3	**	34,5	31,7		47,8	15,8	****	99,9	50,4	****
	elevation		136,2	90,5	****	140,4	85,5	****	27,7	6,2	****	125,7	98,3	
	axial Rotation		100,2	72,4	*	71,1	58,9		19,0	9,3	***	164,3	125,0	
scapula	ant-post tilt		34,2	20,5	***	25,8	18,8		14,1	6,0	***	15,7	10,2	
	med-lat rotation		48,1	36,5	*	44,0	34,7		8,6	5,5	*	21,1	10,3	***
	pro-retraction		22,8	15,3	*	17,3	16,6		14,5	9,1	*	65,7	49,6	**
trunk	fl-ext		17,8	22,8	*	10,6	16,9	**	13,0	4,6	****	11,4	6,4	*
	lat tilt		11,3	9,4		16,5	15,6		8,5	2,8	***	12,8	9,6	
	rotation		11,2	9,5		7,3	10,7		21,1	15,2		56,3	49,2	

		external rotation			RTG			HTS			HTH		
		ND (N=11)	I (N=12)	p	ND (N=11)	I (N=12)	p	ND (N=11)	I (N=10)	p	ND (N=11)	I (N=11)	p
start angle													
wrist	fl-ext	19,7	14,7		-6,7	-15,4		-8,1	-9,3		-3,7	-7,8	
	rad-ulnar inclination	-9,4	-4,3		-6,0	-1,2		-6,9	-1,8		-6,7	0,3	
elbow	fl ext	90,2	85,9		21,2	43,8		22,0	33,1		22,7	35,5	
	pro-supination	110,5	92,3		103,4	94,0		103,7	91,9		104,8	84,2	
gleno humeral	plane of elevation	-24,1	1,1	****	6,9	8,3		6,5	7,1		8,1	5,5	
	elevation	-44,1	-56,0	**	-12,3	-27,9	**	-11,1	-27,9	***	-11,6	-26,9	***
	axial Rotation	-18,2	11,3	*	-30,7	-4,3	*	-28,7	-3,7	*	-28,2	-4,5	**
shoulder (thoraco humeral)	plane of elevation	-7,4	24,5	****	-3,0	9,5	*	-3,3	3,9	*	-2,9	3,8	*
	elevation	-72,3	-72,1		-10,6	-18,8	**	-11,3	-17,2		-11,2	-16,9	
	axial Rotation	16,8	31,1		1,9	35,5	**	1,7	33,8	**	2,2	32,5	*
scapula	ant-post tilt	-24,0	-12,8	**	-15,6	-13,1		-16,1	-15,0		-16,6	-13,2	
	med-lat rotation	-10,1	-16,8	*	4,4	6,8		2,1	10,5	*	2,7	9,8	*
	pro-retraction	34,4	31,9		29,8	35,2		28,0	31,8		27,4	32,5	
trunk	fl-ext	6,7	2,3		5,5	6,3		4,8	5,7		4,6	4,2	
	lat tilt	-9,1	-3,3	*	-0,3	-2,9	*	-0,4	2,1	*	-0,5	2,5	*
	rotation	0,3	-18,0	****	0,8	5,0		2,3	-7,1	***	2,0	-5,9	**
PTA angle													
wrist	fl-ext	-47,6	-39,0		-22,2	-30,5		-10,6	-12,2		-2,2	-32,0	**

	rad-ulnar inclination	-13,1	-2,8		-19,1	-6,0	*	-9,7	-16,4		-13,3	-11,0	
elbow	fl ext	103,9	74,0	**	55,5	57,4		118,3	123,4		118,7	115,9	
	pro-supination	91,7	73,7		94,2	69,3	*	45,6	75,3	**	36,1	48,2	
gleno humeral	plane of elevation	1,2	16,8	*	30,4	18,7	*	50,4	28,3	**	21,2	18,2	
	elevation	-39,1	-62,7	****	-36,7	-48,7	*	-25,9	-58,4	***	-70,9	-66,8	
	axial Rotation	-79,3	-18,1	****	-42,5	-8,0	****	-15,8	-9,0		-73,7	-30,7	****
shoulder (thoraco humeral)	plane of elevation	10,0	34,2	***	38,6	44,2		52,2	60,0		44,0	35,7	
	elevation	-67,6	-89,3	*	-15,3	-35,6	***	16,2	0,0		-113,9	-103,1	
	axial Rotation	-80,2	-18,7	****	10,2	32,5	*	70,0	44,0		-80,8	-38,0	****
scapula	ant-post tilt	4,9	1,5		-14,5	-7,0		-15,8	-6,5	*	-3,2	9,3	*
	med-lat rotation	-27,9	-26,4		-4,5	-7,9		-23,4	-6,8	**	-38,2	-28,6	
	pro-retraction	5,6	17,8	*	42,8	42,0		53,2	54,7		25,6	17,8	
trunk	fl-ext	-7,4	-13,2		5,3	2,8		2,9	1,8		-1,5	-14,3	**
	lat tilt	-8,4	0,6	**	0,1	-4,2	*	0,2	2,2		-3,8	-0,1	
	rotation	-6,3	-23,0	****	11,7	0,9		8,0	1,6		1,6	-5,8	*
ROM angle													
wrist	fl-ext	71,4	67,3		32,0	31,6		28,1	29,2		28,2	40,2	*
	rad-ulnar inclination	11,7	31,1		16,7	31,8		10,6	40,1		13,6	43,5	*
elbow	fl ext	25,8	24,7		61,8	38,8	***	100,4	91,2		99,2	81,6	**
	pro-supination	40,6	27,0		28,3	34,1		60,5	30,5	***	72,4	46,0	**

gleno humeral	plane of elevation	26,3	16,9	*	26,6	14,7	**	44,7	23,5	***	17,4	17,5	
	elevation	11,4	12,4		26,3	22,3		24,3	35,6	*	59,6	43,4	*
	axial Rotation	61,8	30,0	***	14,8	11,0		22,5	16,3		46,5	29,0	**
shoulder (thoraco humeral)	plane of elevation	19,4	12,7	*	45,0	36,3		58,0	60,6		49,3	41,8	
	elevation	10,6	20,4	**	14,1	26,6	*	38,3	50,7		103,6	90,8	
	axial Rotation	97,1	49,9	****	20,6	17,5		74,9	69,2		84,6	78,0	
scapula	ant-post tilt	29,4	15,0	***	4,2	11,3	****	7,7	12,7		15,0	26,5	**
	med-lat rotation	20,1	11,3	**	10,8	17,2	*	26,2	20,0	*	41,9	40,4	
	pro-retraction	29,3	15,3	**	15,1	12,2		27,0	24,4		11,0	22,2	*
trunk	fl-ext	14,8	15,8		2,5	5,4	**	3,0	5,6	*	6,4	19,4	****
	lat tilt	4,4	5,6		2,1	3,7		2,4	4,2	*	4,3	6,7	
	rotation	7,7	6,0		11,4	13,4		7,8	10,2		4,0	8,7	**

Table 2 : Mean of the discrete joint angles of the non dominant side of typically developping children and impaired side of children with OBPP

ND : non dominant, N : number of children, I : impaired

Fl-ext : flexion extension, pro-supination : pronation-supination, ant-post tilt : anterio-posterior tilt, med-lat rotation : medial-materal rotation, pro-retraction : protraction-retraction, lat tilt : lateral tilt

RTG : reach to grasp, HTS : hand to shoulder, HTH : hand to head

Les résultats de cette étude montrent l'intérêt de considérer le membre supérieur dans son ensemble pour quantifier les conséquences de l'atteinte nerveuse au niveau des articulations dont les mobilisateurs principaux sont affectés mais également pour comprendre les stratégies d'adaptation mises en place au niveau des autres articulations dans un groupe d'enfants avec POPB.

Une **stratégie de mouvement différente mais avec une bonne performance** chez ces enfants **était montrée**. L'hypothèse d'un mouvement efficace et fonctionnel sous réserve de la possibilité de mettre en place des compensations avec les articulations dont les muscles sont moins ou non affectés par la dénervation peut être formulée. L'association des limitations d'amplitudes articulaires actives et passives et du dépassement des capacités de compensation pourrait être un facteur explicatif des limitations d'activité (Bae, Waters, et Zurakowski 2008). **Lors de l'évaluation des enfants avec POPB, un élément clé à considérer pourrait donc être les possibilités de compensation et leurs limites**.

Dans cette étude, les angles de départ, de fin et les amplitudes articulaires étaient comparés dans les analyses statistiques. Cette **discrétisation des données** d'analyse du mouvement permet une simplification de leur traitement mais peut également être à l'origine d'informations manquantes. L'utilisation de l'APS autorisait une comparaison globale des courbes de cinématique mais sans permettre de visualiser les moments où les mouvements différaient.

IV Perspectives dans l'exploration de l'épaule et du membre supérieur de l'enfant avec POPB

1 Exploration IRM

L'étude des volumes des muscles gléno-huméraux apparaissait particulièrement intéressante dans l'exploration du fonctionnement de l'épaule chez les enfants avec développement typique et avec POPB étant donné le lien volume-force objectivé dans les deux populations (articles 2 et 3). Le **temps nécessaire pour la technique de segmentation manuelle** sur un grand nombre de coupes utilisée dans les articles 2 et 3 **ne permettait cependant pas de l'utiliser sur des populations larges ou en pratique clinique**. Les techniques de segmentation automatiques sont prometteuses du fait du potentiel gain de temps qu'elles permettent (article 1).

Afin d'avoir accès plus facilement aux volumes musculaires lors de l'évaluation des enfants avec POPB, une technique de segmentation utilisant des **réseaux de neurones** a été développée et testée au sein de notre équipe de recherche (annexe 2). Les segmentations réalisées sur les IRM d'épaule des enfants avec développement typique et avec POPB pour les articles 2 et 3 étaient utilisés et servaient de référence pour l'apprentissage et pour l'évaluation de la segmentation automatique développée. Des résultats particulièrement intéressants ont été obtenus pour l'ensemble des muscles testés (deltoide, supra-épineux, infra-épineux et subscapulaire) (annexe 2). Les images provenaient cependant toutes de la même machine et de la même séquence, des tests restent à réaliser afin de savoir si la segmentation automatique d'images réalisées sur une autre machine et une autre séquence est possible. En effet, les résultats de segmentation peuvent être dépendants des techniques d'obtention des images (paramètres IRM, prétraitement). Une plus grande base de données d'apprentissage contenant des images provenant de machines et séquences variées pourrait être nécessaire.

Au niveau morphologique, certains **autres éléments caractérisant les muscles** pourraient être accessibles et quantifiables en IRM et **seraient intéressants à explorer** spécifiquement chez **l'enfant avec POPB** dans un cadre de recherche initialement avec évaluation dans un second temps de l'intérêt de ces mesures pour la pratique clinique.

Chez ces enfants, les coefficients de corrélation entre le volume et la force étaient présents mais plus faibles pour les muscles du côté de la POPB que du côté non affecté ou que ceux retrouvés chez les enfants à développement typique. L'importance de **l'infiltration graisseuse** et son implication dans la diminution de genèse de force mériterait d'être évaluée et quantifiée au niveau de l'épaule, comme cela a déjà été fait au niveau du bras dans cette population (Duijnisveld et al. 2017; Kälin et al. 2018) en utilisant une séquence Dixon. De même, **les tissus conjonctifs** pourraient être quantifiés en utilisant une séquence « ultra short echo time » (Csapo et al. 2014). **L'architecture musculaire** pourrait être étudiée en utilisant la tractographie mais à notre connaissance, cela n'a pas encore été réalisé chez l'enfant avec POPB et la faisabilité nécessite d'être examinée (Heemskerk et al. 2005; Khalil et al. 2010).

La **longueur musculaire,** qui impacte la mobilité passive et active, et qui a un rôle suspecté dans la genèse de la déformation gléno-humérale (Cheng et al. 2015; Crouch et al. 2014) est elle aussi mesurable en IRM.

Enfin, la **connaissance des bras de levier** des muscles gléno-huméraux **apparaît un point clé chez les enfants avec POPB**. En effet, la déformation gléno-humérale les modifie probablement. Les muscles peuvent alors être dans une position plus ou moins favorable pour mobiliser l'articulation. Les groupes fonctionnels de muscles impliqués dans la mobilité de l'articulation gléno-humérale dans ses différents degrés de liberté pourraient être modifiés. L'utilisation des bras de levier détérminés chez des sujets adulte répresente une limite dans les articles 2 et 3. **L'obtention de ces bras de levier à partir des données d'imagerie (Maganaris 2004) mériterait d'être testée étant donné la non possibilité d'utilisation de la méthode « tendon excursion » dans cette population d'enfants** (An et al. 1984). Cela représente cependant un challenge scientifique au niveau de l'épaule étant donné sa structure complexe et sa mobilité dans les trois plans de l'espace ainsi que la nécessité de définir le centre de rotation de l'articulation. Cette difficulté est accrue par la présence de la déformation osseuse modifiant les rapports entre l'humérus et la glène chez les enfants avec POPB.

2 Exploration en analyse quantifiée du mouvement

L'analyse quantifiée du mouvement permettait de montrer des changements cinématiques au niveau de l'ensemble des articulations du membre supérieur du côté atteint chez les enfants avec POPB (article 4). Une organisation différente mais efficace du mouvement chez les enfants avec POPB était retrouvée.

Afin d'affiner la compréhension du mouvement chez l'enfant avec POPB, des techniques évaluant les modifications cinématiques et les différences d'organisation dans la coordination des mouvements des articulations sur l'ensemble du mouvement et non uniquement au début et à la fin pourraient être intéressantes. La technique de **« statistical parametric mapping »** (SPM) (Pataky 2010) pourrait être utilisée dans les études futures pour l'évaluation des données cinématiques. Cette technique permet de détecter des périodes durant le mouvement, durant lesquelles les groupes testés ont des différences cinématiques au niveau d'une articulation (Pataky 2010; Santos et al. 2018). Les patterns de coordination entre les articulations pourraient être évalués à l'aide du **« multi-joint coordination measure »** (MJCM) (Kukke et al. 2016). Cette méthode précise la manière dont les résultats cinématiques sont coordonnés selon les différents degrés de liberté. Ceci est réalisé à l'aide d'une analyse en composante principale mesurant les contributions des différents degrés de liberté pour un mouvement (Kukke et al. 2016; Mayfield et al. 2017).

Etant donné les modifications cinématiques trouvées dans l'article 4 au niveau des deux membres supérieurs et le questionnement sur le développement des programmes moteurs (Anguelova et al. 2017; Colon, Vredeveld, et Blaauw 2007), un autre facteur à l'origine de limitations d'activités chez ces enfants pourrait être leur difficulté à réaliser **un mouvement bimanuel**, qui, à notre connaissance, n'a pas encore été évalué dans cette population. Des protocoles existent en analyse quantifiée du mouvement (Gaillard et al. 2018) pour l'évaluer et seraient intéressants à tester dans cette population.

3 Modélisation biomécanique

Chez les enfants avec POPB, la connaissance et la compréhension précise de l'**ensemble des éléments intervenant dans le cercle vicieux de la pathologie de l'épaule, mais aussi leur organisation dans le temps** et la **pondération** de l'importance de chacun d'entre eux représente un enjeu pour l'amélioration de leur évaluation et du choix des cibles thérapeutiques. Il est en effet actuellement peu aisé de rattacher précisément ces éléments entre eux**. La connaissance de la physiopathologie du dysfonctionnement de l'épaule chez ces enfants reste donc imparfaite**.

L'utilisation de modèles biomécaniques représente une possibilité d'aide dans cette compréhension. A notre connaissance, **dans trois études chez l'enfant avec POPB, des modèles biomécaniques ont été utilisés** à cette fin (Kleiber et al. 2013; Crouch et al. 2014; Cheng et al. 2015).

Dans la première étude, un **modèle biomécanique obtenu à partir de données d'analyse du mouvement et d'une technique dynamique inverse** permettait de montrer qu'une rétraction en rotation interne au niveau de l'épaule était à l'origine d'une augmentation des forces appliquées sur l'articulation thoraco-humérale lors d'un mouvement de flexion extension (Kleiber et al. 2013). L'étude concluait à un potentiel impact de la perturbation du mouvement de l'épaule dans la genèse de la déformation osseuse. Ce modèle présentait certaines faiblesses. **Le raisonnement était limité aux forces s'appliquant sur l'articulation** empêchant la distinction des éléments à l'origine de la rétraction en rotation interne. **L'étude a été faite sur l'articulation humero-thoracique e**t non pas gléno-humérale.

Dans deux autres études, **des simulations sur un modèle informatique tridimensionnel du membre supérieur ont été réalisées** afin d'identifier les muscles et le type d'atteinte (déséquilibre musculaire, perturbation de la croissance) impliqués dans la genèse de la déformation osseuse (Crouch et al. 2014; Cheng et al. 2015). Sept muscles (infraépineux, subscapulaire, grand dorsal, chef long du biceps, deltoïde antérieur, grand pectoral, chef long

du triceps) étaient identifiés comme pouvant produire une force favorisant la déformation de l'articulation gléno-humérale (Crouch et al. 2014). L'association des déséquilibres musculaires et de la perturbation de la croissance de ces muscles avaient l'impact le plus fort, comparé au déséquilibre musculaire seul ou à la perturbation de la croissance isolée. Dans ce modèle, les données anatomiques des os, les degrés de liberté au niveau des articulations (scapulo-thoracique, gléno-humérale, coude, poignet et doigts), les données d'architecture et de capacité de génération de force des muscles étaient intégrés *(figure 16).* Cela permettait d'évaluer l'impact de plusieurs muscles et plusieurs types d'atteinte musculaires sur les contraintes mécaniques s'appliquant sur l'articulation gléno-humérale. **Les données intégrées provenaient d'études chez l'adulte** (Holzbaur, Murray, et Delp 2005; Holzbaur, Delp, et al. 2007; Holzbaur, Murray, et al. 2007) et **avaient simplement été mises à l'échelle pour les enfants**. L'utilisation de **données dans le modèle provenant d'adultes non pathologiques représente un biais** et limite la force des conclusions de ces études. Dans le contexte de l'enfant en croissance, des modèles musculo-squeletiques pédiatriques **par âge** seraient plus adaptés.

Chez l'enfant **l'absence de données cadavériques** empêche l'obtention directe de certains des éléments à intégrer au modèle. Les techniques d'analyse quantifiée du mouvement et d'IRM présentées ci-dessus, adjointes à l'EMG pour caractériser l'activation musculaire, pourraient être intéressantes à utiliser pour la collecte des données chez l'enfant et l'obtention de **modèles spécificiques à l'enfant avec POPB.** Un travail de thèse sur cette problématique est actuellement réalisé au sein du laboratoire par Asma Salhi.

Ce type de modélisation a été utilisé pour analyser les conséquences de certains traitements dans des pathologies de l'épaule chez l'adulte (Jastifer et al. 2012; Ling, Angeles, et Horodyski 2009). De la même manière, chez l'enfant avec POPB, ces modèles pourraient être utilisés en recherche pour **préciser les conséquences des thérapeutiques** de rééducation, des injections de toxines botuliniques ou des chirurgies secondaires.

Les atteintes du plexus brachial peuvent être diverses. De même la récupération suite à une atteinte du plexus brachial chez le bébé sera différente d'un enfant à l'autre (Yang 2014; Van Dijk et al. 2012). De ce fait, **l'exploration et la modélisation individuelle de l'enfant avec POPB est prometteuse**, lors des questionnements pour les choix thérapeutiques en pratique clinique courante par exemple. Au niveau de l'épaule, en fonction de l'atteinte musculaire et

de la déformation osseuse, des résultats variables pourraient être obtenus avec des conséquences en termes de mobilité active et passive différentes selon les choix réalisés. Cet objectif apparait comme un objectif à long terme, du fait des travaux nécessaires au préalable pour permettre **l'obtention rapide des données** permettant de spécifier le modèle (Charbonnier et al. 2017; Noble et al. 2018).

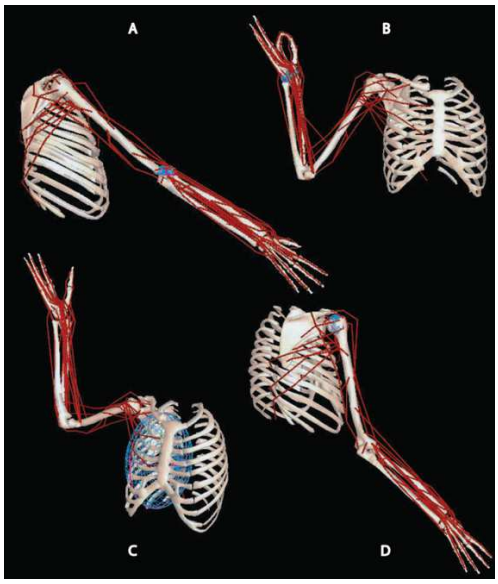

Figure 16 : Modèle du membre supérieur d'Holzbaur. A : vue latérale, B : vue antérieure, C : vue antéro-médiale, D : vue postéro-latérale.
(Tiré de l'article Holzbaur KRS 2005)

V Perspectives thérapeutiques

La récupération de la motricité initialement, la **lutte contre les rétractions musculaires et déformations articulaires pour l'obtention d'une bonne mobilité du membre supérieur** sont les objectifs thérapeutiques principaux chez les enfants avec POPB (Shenaq et al. 2005; Peter M. Waters 2005). L'association des travaux présentés ci-dessus, visant à mieux comprendre le fonctionnement de l'épaule et du mouvement du membre supérieur chez l'enfant avec POPB, et des éléments physiopathologiques déjà connus et présentés dans l'introduction, permettent de discuter plus précisément certains objectifs et cibles thérapeutiques.

Dans l'article 4, évaluant le mouvement des membres supérieurs d'un groupe d'enfants présentant des séquelles de POPB, une organisation différente mais efficace du mouvement était objectivée avec des compensations des degrés de liberté manquants au niveau des articulations les plus impactées par la POPB par une mobilité différente au niveau des articulations moins affectées. Dans un objectif de favoriser le mouvement et l'utilisation du membre supérieur atteint et éviter les limitations d'activité malgré la parésie et les limitations d'amplitudes articulaires passives, si ces résultats sont confirmés dans un échantillon d'enfants plus important, les thérapies par contrainte induite, visant à forcer l'utilisation du membre supérieur parésié semblent peu nécessaires étant donné l'efficacité du mouvement retrouvée. La lutte contre les compensations (Russo et al. 2014) au niveau des articulations préservées semble également peu appropriée car risquant de limiter les possibilités de mobilisation du membre supérieur atteint et impactant les activités de vie quotidienne. Au contraire, étant donné l'utilité des compensations pour l'obtention d'un mouvement fonctionnel, un axe de prise en charge pourrait être le travail spécifique de ces compensations (Cusack et al. 2014).

L'association d'une atteinte de l'ensemble des muscles de l'épaule, de déséquilibres musculaires dans les trois plans de l'espace (article 3) et d'une atteinte de l'ensemble des

mouvements au niveau de l'articulation gléno-humérale (article 4), est un argument en faveur d'une **stratégie de prise en charge globale pour cette articulation** et va avec l'objectif de rétablir les équilibres musculaires pour les rotateurs mais aussi pour les muscles intervenant dans les autres mouvements afin de permettre une meilleure mobilisation du membre supérieur (Bialocerkowski 2005, justice D 2015). **La limitation précoce de ces déséquilibres musculaires pourrait aussi être un enjeu pour la prévention de la déformation tri-dimensionnelle gléno-humérale**. Davantage d'études sont cependant nécessaires pour bien comprendre le lien entre l'atteinte musculaire dans tous les plans de l'espace et la déformation osseuse, de même que pour évaluer les thérapeutiques visant à améliorer cet équilibre musculaire.

Plus spécifiquement, concernant l'atteinte des rotateurs, l'atteinte des **muscles subscapulaire et infraépineux** et les conséquences de leur atteinte sur la déformation osseuse et le mouvement sont déjà bien connues et décrites (Pöyhiä et al. 2005; Peter M. Waters et al. 2009; Van Gelein Vitringa et al. 2011; van Gelein Vitringa et al. 2009; Hogendoorn et al. 2010). Le muscle subscapulaire est particulièrement ciblé dans les traitements chirurgicaux. Des chirurgies secondaires de libération du sous scapulaire chez les enfants présentant une rétraction en rotation interne d'épaule sont pratiquées couramment, afin de libérer cette rétraction, et corriger la déformation osseuse (Hultgren et al. 2014; Pedowitz et al. 2007; Mehlman et al. 2011).

Dans l'article 4, la **perturbation de la rotation** au niveau de l'articulation gléno-humérale était présente pour **toutes les tâches**. Des mouvements compensatoires étaient nécessaires dans les autres articulations. Cette perturbation des mouvements en rotation pourrait à son tour favoriser la déformation de l'articulation gléno-humérale (Kleiber et al. 2013), montrant l'intérêt de limiter (chez le bébé) puis libérer (chez l'enfant plus âgé) la rétraction en rotation interne dans le double objectif de 1/ favoriser la mobilité du membre supérieur et 2/ limiter la déformation osseuse.

Les résultats de l'article 3 dont l'objectif était de caractériser plus précisément l'atteinte des muscles et à faire le lien avec la fonction musculaire, montrent l'intérêt de considérer le couple subscapulaire-infarépineux mais aussi chacun des autres rotateurs internes dans le questionnement sur les stratégies thérapeutiques.

Un résultat notable était **l'absence de relation entre le volume musculaire du muscle infraépineux et la force générée en rotation externe**. Un élément pouvant expliquer cette absence de relation est la **modification des bras de levier induite par la déformation osseuse**. La lutte contre la genèse de la déformation osseuse avec le travail de conservation des amplitudes articulaires passives en rotation externe pour limiter la rétraction du subscapulaire lié à la diminution des sollicitations mécaniques ainsi que la récupération d'une contraction active du muscle infraépineux sont dans ce contexte des objectifs prioritaires dans la prise en charge initiale chez le bébé. Chez l'enfant plus âgé présentant une déformation installée, le travail actif en rotation externe réalisé en kinésithérapie peut être questionné étant donné l'absence de relation volume- force pour le muscle infraépineux.

Le **muscle grand pectoral apparaissait relativement préservé**. Cette relative préservation était à l'origine du déséquilibre entre les volumes des rotateurs internes et externes. Dans l'article de modélisation de Crouch et al . (2014), le muscle grand pectoral était identifié comme pouvant générer une force contribuant à la déformation de l'articulation gléno-humérale. Ces éléments montrent l'intérêt de considérer le muscle grand pectoral comme **potentielle cible thérapeutique** pour l'objectif d'amélioration des équilibres musculaires (Peter M. Waters et al. 2009; Ozben et al. 2011).

Enfin, le **muscle grand rond**, rotateur interne accessoire, est couramment utilisé dans les chirurgies de transfert pour obtenir une rotation externe active Kirkos 2005, Kozin 2006 HUltgren. Son volume était particulièrement diminué chez les 5 enfants avec POPB ayant eu des chirurgies secondaires (transferts de grand rond pour les 5 enfants, libération du sous scapulaire pour 4 d'entre eux) (article 3). D'un point de vue fonctionnel, du fait de son **atrophie majeure**, ce muscle semble peu susceptible d'avoir un impact fort sur les amplitudes articulaires actives. **L'efficacité et l'intérêt du transfert peuvent être questionnés** (Kirkos et al. 2005; Hultgren et al. 2013).

La **lutte contre le déséquilibre musculaire de l'ensemble des rotateurs internes par rapport aux rotateurs externes** apparaît donc comme une **priorité dans la prise en charge** des enfants avec POPB. **La précocité de la prise en charge est un point clé** étant donné la présence de la déformation osseuse à seulement quelques mois de vie (van der Sluijs et al. 2001; Van Gelein Vitringa et al. 2011).

Des études de faibles puissances ont montré le potentiel intérêt de la toxine botulinique au niveau des rotateurs internes d'épaule chez les enfants présentant une POPB pour lutter contre ce déséquilibre musculaire, améliorer les amplitudes articulaires et limiter la déformation gléno-humérale (Ezaki et al. 2010).

Nous proposons **d'évaluer l'intérêt d'injections de toxine botulinique précoces au niveau de l'ensemble des rotateurs internes dans le traitement des enfants avec POPB** présentant une déformation de l'épaule **pour prévenir l'évolution de cette déformation**, et conserver la mobilité active et passive de l'épaule avec une étude de forte puissance (article 5).

Article 5 : Efficacité et innocuité des injections intramusculaires précoces de toxine botulinique pour prévenir la déformation de l'épaule chez les bébés atteints de paralysie obstétricale du plexus brachial (POPB-TOX), un essai contrôlé randomisé : protocole de l'étude

Ce protocole a été soumis dans BMJ open et est financé par le PHRC National. L'étude a débuté en avril 2018. La dernière mise en place a été faite à Nîmes le 8 octobre 2018. Deux enfants ont été inclus.

Effectiveness and safety of early intramuscular botulinum toxin injections to prevent shoulder deformity in babies with obstetrical brachial plexus palsy (POPB-TOX), a randomized controlled trial: study protocol

Christelle Pons MD[1,2,3] ; Dauphou Eddi PhD[4] ; Grégoire le Gal MD, PhD[5] ; Marc Garetier MD[2,6] ; Douraied Ben Salem MD, PhD[2,7,8] ; Laetitia Houx MD[1,2,3] ; Franck Fitoussi MD, PhD[9] ; Nathaly Quintero MD[10] ; Sylvain Brochard MD, PhD[1,2,3,8] ; and the POPB-TOX Group (Marianne Alison, Madeleine Aslan, Jennifer Bastien, Gilles Dautel, Floriane Colin, Marion Delpont, Bruno Dohin, Marie Agnes Galloy, Vincent Gautheron Salem Hassan Al Khoury, Pascal Jehanno , Mélanie Kaas, Olivier Prodhomme, Mélanie Porte, Anne Gaelle Py, Helène Rauscent, Emilie Rumilly, Katherine Sanchez Barr , Catherine Tréguier, and Philippe Violas)

1 Pediatric rehabilitation, Fondation ILDYS, Brest, France
2 Laboratory of Medical Information Processing, INSERM 1101, Brest, France
3 PMR department, Brest CHRU, Brest, France
4 DRCI, Brest CHRU, Brest, France
5 Centre for Clinical Investigation INSERM CIC 1412, Brest CHRU, Brest, France
6 Radiology department, hôpital d'Instruction des Armées Clermont-Tonerre, Brest, France
7 Radiology department, Brest CHRU, Brest, France
8 Université de Bretagne Occidentale, Brest, France
9 CHU Paris Est - Hôpital d'Enfants Armand-Trousseau; Paris, France
10 Hôpitaux de St Maurice, St Maurice, France

Corresponding author
Christelle Pons
SSR pédiatrique brestois, Fondation ILDYS, rue Alain Colas, 29200 Brest
Tel : 0256310145
christelle.ponsbecmeur@ildys.org

Word count : 4792

ABSTRACT

Introduction

In children with Obstetrical Brachial Plexus Palsy (POPB), denervation of the shoulder muscles leads to bony deformity in the first months of life, reducing active and passive range of motion (ROM), and causing activity limitation. The aim of this multicentre randomised controlled trial is to evaluate the effectiveness of botulinum toxin injections (BTI) in the shoulder internal rotator muscles of 12 month-old babies in limiting the progression of posterior subluxation of the glenohumeral joint, compared with a sham procedure mimicking BTI. The secondary aims are to evaluate the effectiveness of BTI in (I) limiting the progression of glenoid retroversion and 3D deformity and (II) improving shoulder range of motion and upper limb function, as well as to confirm the tolerance of BTI.

Methods and analysis

Sixty-two babies with unilateral POPB and a risk of posterior humeral head subluxation will be included. Only those with at least 7% posterior subluxation of the humeral head compared with the contralateral shoulder on the MRI will be randomized to one of two groups: "BTI" and "Sham". The BTI group will receive BOTOX injections at the age of 12 months in the internal shoulder rotator muscles (8UI/kg). The sham group will undergo a sham BTI procedure. Both groups will undergo repeated shoulder MRI at 18 months of age to quantify changes in the percentage of posterior migration of the humeral head (primary outcome), glenoid version and 3D bone deformity. Clinical evaluations (passive shoulder range of motion, Active Movement Scale) will be carried out at baseline and 15 and 18 months of age. The mini Assisting Hand Assessment will be rated between 10 and 11 months, and at 18months of age. Adverse events will be recorded at least monthly for each child.

Ethics and dissemination

Full ethical approval for this study has been obtained.

Trial registration number

EudraCT: 2015-001402-34 in European Clinical Trial database; NCT03198702 in Clinical Trial database.

Keywords: Obstetrical Brachial Plexus Palsy, shoulder, botulinum toxin, bone deformity

Strengths and limitations of this study

We expect botulinum toxin injections to limit shoulder deformity and improve shoulder range of motion in children with obstetrical brachial plexus palsy.

This randomized controlled study will evaluate the safety and effectiveness of early botulinum toxin injections in the shoulder internal rotator muscles.

The effect on bony deformities (glenohumeral subluxation and glenoid version), active and passive range of motion and upper limb function will be evaluated.

INTRODUCTION

Obstetrical Brachial Plexus Palsy (POPB) refers to injury to one or more cervical nerve roots (C5-C8) and/or the first thoracic nerve root (T1), usually caused by excessive traction during a difficult birth. The incidence is around 1.5 per 1000 births(Chauhan, Blackwell, et Ananth 2014). In one third of cases, nerve recovery is incomplete or absent(Chauhan, Blackwell, et Ananth 2014; Hoeksma et al. 2004), resulting in permanent impairment which in turn may lead to activity limitation and participation as defined by the International Classification of Functioning(Julka et Vander Have 2011; Zafeiriou et Psychogiou 2008).

POPB greatly affects the musculoskeletal development of the shoulder complex(Julka et Vander Have 2011; Michael L. Pearl 2009; Van Gelein Vitringa et al. 2011). Deformities occur very early, within the months following birth(Van Gelein Vitringa et al. 2011; van der Sluijs et al. 2001, 2004), and gradually worsen with the child's growth(van der Sluijs et al. 2001; Peter M. Waters 2005). Bony and joint deformities are caused by the partial denervation of the shoulder muscles, which results in an imbalance of the forces acting on the glenohumeral joint (Van Gelein Vitringa et al. 2011; Pöyhiä et al. 2005). In particular, there is often a dominance of the internal rotator muscles (Crouch et al. 2014; Kleiber et al. 2013). Excess glenoid retroversion is typical, along with deformation of the glenoid fossa. This allows posterior migration of the humeral head to occur, eventually progressing to complete subluxation(Van Gelein Vitringa et al. 2011; van der Sluijs et al. 2001, 2004; Moukoko et al. 2004). These deformities increase the risk of early degenerative joint changes and pain during childhood and adulthood(Partridge et Edwards 2004; Kirkos et al. 2005). Active and passive shoulder range of motion (ROM) are also reduced, causing a vicious circle in which the muscles cannot contract effectively because of the bony deformities and altered lever arms (Peter M. Waters 2005). These changes reduce the functional capacity and quality of life of children with POPB(Hulleberg et al. 2014; Squitieri et al. 2013).

Botulinum toxin injections (BTI) are a common treatment to reduce muscle activity. This treatment is mostly used to treat spasticity in children, particularly in the case of cerebral palsy(Novak et al. 2013), however it is also becoming more widely used in children with POPB(Ruchelsman et al. 2009; Gobets et al. 2010), combined with other treatments such as physiotherapy, occupational therapy, orthoses and sometimes surgery. The dominant internal

shoulder rotators are often targeted in order reduce the strength imbalance between agonist and antagonist muscles (Brochard, Alter, et Damiano 2014). Studies have shown that BTI combined with immobilisation could reduce posterior subluxation or dislocation of the shoulder in babies with POPB(Ezaki et al. 2010), as well as improve passive and active shoulder ROM and functional capacity(Gobets et al. 2010; Michaud et al. 2014; Shin et al. 2014). BTI is a minimally invasive treatment that is well tolerated. When used prior to surgery, it can avert or reduce the complexity of surgical secondary orthopaedic procedures (e. g. subscapularis release, latissimus dorsi and teres major transfers) (Ezaki et al. 2010; Michaud et al. 2014). Although the results of studies of early BTI for POPB are encouraging, most studies are retrospective, include small samples and do not have a control group, limiting the conclusions that can be drawn regarding any effects on the musculoskeletal system. Randomized controlled trials to evaluate the efficacy of early BTI are therefore warranted. With regard to the control treatment, a sham procedure mimicking BTI without injection is ethically more appropriate than an invasive placebo procedure because of the young age of the children involved.

AIMS and HYPOTHESES

Aims

The main aim of this study is to evaluate the effectiveness of BTI in the internal shoulder rotator muscles of 12 month-old babies in limiting the progression of posterior subluxation of the glenohumeral joint.

The secondary aims are (I) to compare the effectiveness of BTI with a sham treatment in limiting the progression of glenoid retroversion and three-dimensional glenoid deformity; (II) to compare the effectiveness of BTI with a sham treatment in improving active and passive joint range of motion and upper limb function; (III) to assess the tolerance of BTI in babies with POPB; (IV) to evaluate the effects of BTI on muscle growth and fatty infiltration of the injected muscles, as well as muscle volume balance around the shoulder, and (V) to determine the long-term effect of BTI on frequency and type of surgical interventions.

Hypotheses

Our primary hypothesis is that BTI will limit posterior subluxation of the glenohumeral joint in the BTI group compared with the Sham group.

We further hypothesize that the progression of glenoid retroversion and three dimensional deformities will be reduced, that active and passive range of motion will be increased, and that number of secondary surgical interventions will be reduced in the BTI group

compared with the Sham group. The robust design of this study will confirm the results of previous un-controlled studies, providing a strong level of evidence for BTI treatment. We also hypothesize that BTI will be well tolerated by the babies. With regards to morphological changes following BTI, we expect slight atrophy to occur in the injected muscles, with some fatty infiltration (Williams et al. 2013) but no change in non-injected muscles, leading to an improvement in the volume balance of agonist and antagonist muscles REF +++.

MEDTHODS/DESIGN

Design

A randomised, multicentre, double-blind, controlled, parallel group, superiority trial will be performed (version 3, 17.01.2018). One group will receive BTI and the other will undergo a Sham procedure.

Ethics

Full ethical approval for this study has been obtained by the ethical committee Ouest 1 of Tours and Agence Nationale de Sécurité du Médicament et des produits de santé (ANSM). The trial has been registered in the European Clinical Trial database (EudraCT: 2015-001402-34) and Clinical Trial database (NCT03198702). All families will be given a written information letter detailing the study and parents or guardians will sign informed consent prior to the child's inclusion. Any modification or amendment to the protocol will be submitted to the ethical committees and ANSM for approval. After approval, investigators and trial participants will be informed of the changes by letter or email. All trial databases will also be updated.

Recruitment

The sponsor is CHRU Brest. Babies will be recruited from six French hospitals (CHRU Brest, Centre de Réadaptation pour enfant Flavigny-sur-Moselle, Hôpital National de Saint Maurice, CHU Saint-Etienne, CHU Nîmes, CHU Rennes), all of which are specialized in the management of children with brachial plexus palsy and have access to MRI. All doctors involved are skilled in BTI. Hospitals were selected by the study coordinator and sponsor based on their responses to a feasibility questionnaire. It is predicted that during the 29 months of inclusion, around 2590 children will be born with POPB in France (Chauhan, Blackwell, et Ananth 2014), of whom 466 will left with sequelae(Chauhan, Blackwell, et Ananth 2014). This study will recruit 13.5% of these babies (62 patients over 29 months). The investigator in each

of the specialist participating centres will inform clinicians in local maternity units about the study, and flyers and posters will be displayed in the reception areas of clinics and maternity units. Clinicians will be asked to refer babies with OBBP to their nearest participating specialist centre and they will be provided with information leaflets to give to the parents. External advertising will also include a webpage on the Brest CHRU website. If inclusion goals are not achieved, more centers will be asked to participate.

A rehabilitation physician and/or a surgeon in each participating specialist centre will identify potentially eligible babies for the study during routine consultations. The protocol will be explained and proposed to parents of babies between 10 and 11 months of age who have a high risk of bony deformity. An information letter will be given to the parents (supplementary file).If the parents agree to their baby's participation, and the baby fulfils the inclusion criteria, he or she will be enrolled in the study for 7 months.

The inclusion criteria are: male or female babies aged between 10 and 11 months with unilateral POPB; at least one of the following risk factors for posterior subluxation of the humeral head: 10° less passive external ROM of the affected shoulder compared with the contralateral shoulder and/ or a score below 6 on the Active Movement Scale (AMS) for shoulder external rotation and abduction, elbow flexion or supination; whose parents or guardians have signed the consent form. Babies with bilateral POPB, microsurgery or shoulder muscle surgery planned between 12 and 18 months of age, contraindications to the use of botulinum toxin (hypersensitivity to botulinum toxin or the excipients used, or myasthenia), contraindications to MRI (pace maker, metal implants, foreign metal body in the eye, etc.), MRI not possible in the Paediatric Day Hospital setting because of contraindications to the premedication protocol or organizational constraints, parents inapt to provide consent for the participation of their child, or parents under the age of 18 years, will be excluded.

Study procedure (Figure 1 and Table 1)

At visit 1 (between 10 and 11 months of age), the parents or guardians will sign the informed consent form and the baby will be included. The physician or surgeon will carry out a physical examination and will collect socio-demographic data including history of POPB in a brother or sister, overweight or obesity of the mother, any medical conditions during the pregnancy (e.g. gestational diabetes), the birth procedure (caesarean section, vaginal delivery with epidural, induction of labour, instrumental delivery, shoulder dystocia, term and duration), birth weight and length, and APGAR score.

Visit 2 (at 11 months of age) will involve MRI to confirm the diagnosis of bony deformity (at least 7% subluxation of the humeral head on the involved side compared with the

controlateral side). Once confirmed, randomisation will be carried out. This will ensure that only children with verified glenohumeral deformity are included, since clinical tests are not sufficiently sensitive to confirm this. Babies who do not fulfil this randomisation criterion will be withdrawn from the study and will pursue the usual medical follow-up. The parents will be informed of the results of the MRI within 10 days by means of a telephone call from the research investigators. The randomisation will allocate the babies to one of two treatment groups (each with the same number of babies): BTI group and sham group.

Visit 3 (12 months +/-15 days of age) will include treatment (BTI or sham procedure).

Both groups will then attend seven follow up visits: visit 4 will be carried out ten days after treatment administration, and visits 6-10 will be carried out each month until 18 months of age. Visits 1, 7 and 10 will involve a standardized clinical examination by occupational therapists or physiotherapists and visits 5, 6, 8 and 9 will involve a telephone call from a member of the study team.

Un-blinding will be performed at visit 10 (18-months of age). Following un-blinding, the baby will attend a follow-up visit at 24 months then yearly follow-up visits, as is usual practice. The aim of this is to determine the safety of the use of botulinum toxin before the age of two years (after which there is a marketing authorization for children with cerebral palsy), and to compare the frequency and complexity of surgical interventions between groups until the age of 10 years.

MRI

The babies included in this study will undergo MRI of both shoulders at visits 2 and 10 (at 11 and 18 months of age). A three-dimensional, T1-weighted gradient-echo sequence will be used. This anatomical sequence highlights bones and muscles, including denervated muscles(Kamath et al. 2008). The child will lie supine with his/her arms in neutral and hands pronated. The T1 protocol(Pons et al. 2017) will be adapted in each centre depending on the type of MRI scan they have. Acquisition time will be less than 5 minutes per shoulder. No contrast injection will be required. Images will have to include sternum and spine medially, the whole deltoid laterally and the spine of the scapula at the back down. Premedication (sedation or general anaesthetic) will be necessary for both MRI exams, at 11 and 18 months of age. The premedication will be adapted to the clinical status of each child and the customs of each centre. After premedication, the child will be monitored by a paediatrician in the day hospital of each centre using a validated protocol.

Randomisation process and blinding

Randomisation will be possible 24 hours per day using centralised computer randomisation by Internet, according to the usual procedures in effect at Brest Regional University Hospital. After MRI confirmation that the baby fulfils the randomisation criterion (visit 2), randomisation will be performed by the study investigator during visit 3 (12 months of age). Stratification will be carried out by centre and by microsurgery prior to inclusion, since early surgery could influence the progression of bony deformity. Neither the parents or guardians, nor the clinical and radiological evaluators will be aware of the treatment administered. The doctors carrying out the BTI will not take part in subsequent visits, to ensure the blinding of the examiner. A central analysis of MRI data will be carried out in order to ensure blinding of the evaluator to the primary outcome measure.

Study Treatments

BTI procedure

The botulinum toxin that will be used in the study is BOTOX (Allergan). Doses will be injected into the pectoralis major, subscapularis and teres major/latissimus dorsi muscles on one occasion (visit 3: 12months +/- 15 days of age). These muscles have been the target of BTI treatment to prevent the progression of humeral head subluxation and to improve active and passive shoulder ROM in previous studies of children with POPB(Ezaki et al. 2010). Following reconstitution, the toxin will be injected intramuscularly using a transcutaneous approach with ultrasound guidance. The chosen doses are based on data in the literature in children and babies with POPB(Gobets et al. 2010; Ezaki et al. 2010; Michaud et al. 2014): a total of 8U/kg will be injected (2U/kg in subscapularis, 3U/kg in pectoralis major and 3U/kg in teres major/latissimus dorsi). Because there is no marketing authorisation for the use of botulinum toxin in children under the age of two years, the chosen doses are smaller than the maximal doses authorized for the treatment of spasticity in older children with cerebral palsy. Moreover, the doses chosen correspond with doses used in previous studies. A standardized protocol for the prevention and treatment of induced pain and post-injection pain will be systematically used. This will involve the administration of topical anaesthesia (such as EMLA) and paracetamol (dose according to the baby's weight) one hour prior to the injection. Distraction techniques will be used during the injection. The parents will be instructed to bring reassuring, familiar objects belonging to the child (e.g. soft toy, pacifier, nursery rhyme, music). In order to standardize practices and to ensure maximum safety, staff from the different centres will all be trained in BTI of the shoulder muscles using ultrasound guidance in babies prior to participating in the study.

Sham procedure

The aim of the Sham procedure is to mimic the BTI and to maintain the blinding of the research team and the parents or guardians. The same anesthetic procedure will be carried out as for BTI. The physician performing the injection will prepare a syringe containing physiological saline solution 10 minutes prior to the Sham procedure. The procedure will be simulated with ultrasound and use of a blunt needle (that will not penetrate the skin) on the sites selected for injection. All sites will be covered with adhesive dressings and tincture of betadine, as for the BTI. With regard to the control treatment, a sham procedure mimicking BTI without injection is ethically more appropriate than an invasive placebo procedure because of the young age of the children involved.

Rehabilitation and medical follow up

To ensure comparability, the babies in both groups will receive 2 sessions of physiotherapy per week. A standardized medical prescription will be made. An information and advice letter will be given to the physiotherapists via the parents to standardize and optimise physiotherapy treatment. Advice will be given to parents regarding exercises to carry out at home. All other medical and rehabilitation will be carried out according to usual procedures.

Adverse events

Adverse events relating to the use of botulinum toxin

The secondary effects of BTI are mostly mild, temporary and related to the dose and the injection site. Local reactions such as contusions or pain at the injection site may occur, or excessive, localised muscle weakness. Systemic effects are rare and include generalised allergic reactions and effects related to product diffusion (rash, erythema, pruritus, anaphylactic reaction, flu-like syndrome, headaches, dizziness, fever, shivering, hypertension, and abdominal pain and dry mouth). Exceptionally, serious effects have been observed, a type of excessive muscle weakness, dysphagia and aspiration pneumonia, however these occurred principally when the recommended doses were not respected(Bourseul et al. 2017; Papavasiliou et al. 2013; Albavera-Hernández, Rodríguez, et Idrovo 2009; Dahan-Oliel et al. 2012). The safety of BTI in infants under two years of age was shown to be good in a recent systematic review(Bourseul et al. 2017) and the tolerance of this treatment also seems good in this population(Ezaki et al. 2010; Dahan-Oliel et al. 2012; Desiato et Risina 2001). The specific effects on muscle structure and the contractile properties of muscles are, however, poorly understood. Moderate muscle atrophy and fatty infiltration may occur following injections(Williams et al. 2013; Fortuna et al. 2011; Schroeder et al. 2009).

Families will be given a contact phone number to enable them to discuss any questions or doubts regarding the effects of the treatment, or to report any suspected adverse event. Parents will be questioned regarding adverse events at 10 days and each month between 12 and 18 months of age using standardized questionnaires that include all possible side effects.

Adverse events related to MRI premedication

The risks related to the premedication are the standard risks for the sedation or anaesthesia of children (gastritis, anticholinergic effects, oxygen desaturation, excessive sedation). The child will be examined for potential risks during a routine paediatric or anaesthetic consultation.

Independent Data Monitoring Committee and un-blinding procedure

An independent data safety monitoring Committee (DSMC) comprised of five independent members will be set up. The purpose of the DSMC will be to provide an independent evaluation of any adverse events that occur during the research, as well as to monitor the benefit / risk ratio.

Should an adverse event that requires different care than that planned in the study occur, unblinding will be carried out. Unblinding will not be carried out in any other condition.

Patient and Public involvement statement

Patients were not involved in the development of the research, and will not be involved in the recruitment and conduct of the study. Results of the study will be given to the parents after the study during a medical consultation in their participating center.

OUTCOME MEASURES

Primary Outcome (table 1)

The primary outcome measure is the change in the percentage of posterior migration of the humeral head measured on an axial MRI image between 11 months (before the BTI at 12 months) and 18 months of age (6 months post BTI) at visits 2 and 10. Posterior subluxation will be evaluated using the method described by Waters, on an axial MRI slice taken just below the coracoid process (H Kozin 2004; Lippert et al. 2012; P. M. Waters, Smith, et Jaramillo 1998). Percentage posterior subluxation will be calculated in the following manner: a line will be traced from the medial border of the scapula to the middle of the glenoid fossa. A segment will then be drawn perpendicularly to the line, from the widest part of the humeral head (AC). The

length of the anterior part of this segment (AB) divided by the (AC) segment will be multiplied by 100 to obtain the percentage migration of the humeral head. A percentage below 50% indicates posterior migration of the humeral head. This measurement is quick to carry out and is used in both research and routine clinical practice in children and babies with POPB to help preoperative decision making for the type of intervention and post-operative follow up(Van Gelein Vitringa et al. 2011; van der Sluijs et al. 2004; P. M. Waters, Smith, et Jaramillo 1998). Intra- and inter-rater reliability have been shown to be excellent, with a 7% estimated measurement error (Lippert et al. 2012). MRI data will be analysed centrally (at Brest CHRU) by two trained investigators using the same guidelines in order to minimise inter-rater variability and to ensure the blinding of the evaluator.

Secondary Outcome Measures (table 1)

Glenoid retroversion and three-dimensional deformity

The following MRI measurements will be compared at visits 2 and 10 (11 and 18 months of age) to determine the effectiveness of BTI relative to the sham treatment in limiting the progression of glenoid retroversion and three-dimensional deformity:

1) 2D glenoid version will be measured on an axial image using Friedman's technique(Friedman, Hawthorne, et Genez 1992). This measurement has been validated and is used in clinical practice and research(Pöyhiä et al. 2005; Lippert et al. 2012).
2) 3D glenoid version and 3D migration of the humeral will be measured on MRIs following 3D reconstruction. These original measurements were recently used for the first time(Brochard et al. 2016) and will provide an evaluation of 3D shoulder deformity and the effect of BTI on the deformity.

Passive and active movement and upper limb function

Three standardized evaluations will be carried out by occupational therapists or physiotherapists to compare the effect of BTI and the sham treatment on active and passive joint range of motion and upper limb function. All therapists will undergo training prior to their involvement in the study in order to ensure the reliability of measures.

1) Passive shoulder ROM will be measured at the baseline (before the MRI at visit 1, between 10 and 11 months of age), at visits 7 and 10 (15-months and 18-months of age visits).
2) The AMS (Active Movement Scale) will be rated at baseline (before the MRI at visit 1, between 10 and 11 months of age), and at visits 7 and 10 (15-months and 18-

months of age visits). This test evaluates upper limb strength in babies with POPB during active movements. Each movement is rated on an 8-point scale from 0 (no movement) to 7 (complete movement against gravity). It has satisfactory psychometric properties(Curtis et al. 2002; A. Bialocerkowski, O'shea, et Pin 2013).

3) The Mini-AHA (Mini-assistive Hand Assessment) will be rated at visit 1 and 10 (baseline and the 18-months of age visits). This functional evaluation measures bimanual performance during games and tasks. It was designed for children aged from 8 to 18 months(Greaves et al. 2013).

Tolerance

The parents of the babies in both groups will be questioned at 10 days and each month between 12 and 18 months of age using a standardized questionnaire that includes a list of all possible side effects of BTI.

Changes in muscle structure (BTI group only)

3D MRI reconstruction(Pons et al. 2017) and the validated technique described by Hogendoorn et al.(Hogendoorn et al. 2010) will be used to respectively evaluate the direct effects of BTI injections on muscle volume and fatty infiltration of the shoulder muscles. This evaluation will only be carried out in the BTI group.

Future surgical interventions

To determine if BTI reduces the frequency and complexity of surgical interventions in the long term, surgical procedures undergone by the children in both groups (recorded during routine medical follow-up) will be compared up to the age of 10 years.

Locations and data management

Each centre will manage their own recruitment of babies and organization of MRIs, clinical evaluations and treatment. Electronic data will be secured and analyzed in a central database managed by the Brest CHRU. Data will be the property of CHRU Brest.

In accordance with Good Clinical Practice (GCP) guidelines, the sponsor is in charge of obtaining agreement from all centers involved in the clinical research, in order to guarantee direct access to all the clinical research sites, to all the source data, source documents and all the reports for the purpose of Quality Control and audit by the sponsor.

All information required for the study will be entered in the paper case report forms during evaluations, then transferred to the electronic case report form (Clinsigth). Items of

missing data will be coded. Each centre will be responsible for completing the CRFs for the babies enrolled in their centre. Each investigator will receive an instruction document regarding the use of this tool. The investigator will be responsible for the accuracy, quality and relevance of all the data entered. In addition, the data will be immediately verified as they are entered, using consistency checks. The investigator must validate any changes to the values in the CRF. These modifications will be subject to an audit trail. A justification can be added when applicable, as a comment. Data management and query processing will be carried out by a data manager.

A Clinical Research Assistant (CRA) appointed by the sponsor will ensure the good running of the study, data collection on the paper CRF, data recording in the electronic CRF, data saving and reporting in accordance with the sponsor's Standardized Operating Procedures as well as the GCP guidelines and current legislation and laws in force.
The investigator and the members of his/her team will agree to be available during all the routine and planned Quality Control visits by the CRA. During these visits, the following will be audited: signed informed consent, compliance with the study protocol and procedures, data recorded in the CRF: accuracy, missing data, consistency between these data and their "source" (medical files, original laboratory results, etc.), product management and investigator file. The investigators agree to accept the quality assurance audits carried out by the sponsor as well as the inspections carried out by the competent authorities. All data, documents and reports may be subject to regulatory audits and inspections. Medical confidentiality cannot be invoked in opposition to these audits and inspections.
Any data sent to the sponsor by the investigators (or any other specialised parties) during or after the biomedical research will be anonymised. These data should not reveal any visibly accurate names and addresses of enrolled (involved) individuals. Only the first letter of the subject's name and first name will be saved along with a coded number indicating the order of inclusion of the subjects. The sponsor will ensure that the parent of each research subject has given permission in writing for access to personal information about the baby which is strictly necessary for the quality control of the research.

Sample size and statistical analysis

No longitudinal data regarding the progression of bony deformities in children with POPB are available in the literature. Only transversal studies have been carried out, indicating that posterior subluxation is significantly greater on the affected side compared with the healthy side at the age of 4.8 months (affected side: 32.1% - SD=19.7% vs. healthy side: 49.8% -

SD=7.3%)(Van Gelein Vitringa et al. 2011). The calculation of the number of subjects necessary for this study was based on a difference of one standard deviation at 12 months, for a standard deviation of 5%.

In order to guarantee a power of 90%, a sample of 22 babies per group is required, thus a total of 44. In order to account for babies lost to follow-up (10%) and babies who will not be treated because of a lack of true subluxation on MRI, 62 babies will be recruited.

The characteristics of the babies in both groups will be described using means, standard deviations, medians, quartiles or frequencies. Mean changes in 2D percentage humeral subluxation, 3D humeral subluxation, 2D and 3D glenoid version, the AMS score and passive shoulder ROM will be compared using analysis of covariance (ANCOVA) adjusted on the initial values. If the hypotheses underlying the analysis of covariance model are not respected, a non-parametric Wilcoxon test will be used. Shoulder muscle volumes and the mini-AHA scores will be compared between the groups using a Student test or a non-parametric Mann-Whitney test, depending on the distribution of the variable of interest. Lastly, the number of serious and non-serious adverse events, and the degree of fibrosis and fatty infiltration will be compared between the two groups using a Chi2 test or Fisher's exact test, so as the number of secondary surgeries. $p<0.05$ will be considered as statistically significant.

Data analysis will be carried out on an intention to treat basis by a biostatistician after blind review and database freezing at the end of the study. No intermediate analysis is planned during this trial.

DISCUSSION

This paper presents the background and design for a multicentre double-blind randomised controlled trial to evaluate the effectiveness of BTI in the shoulder internal rotator muscles of 12 month old babies in limiting the progression of posterior subluxation of the glenohumeral joint, compared with a sham procedure. To our knowledge, this is the first study with a sufficiently robust methodology to allow conclusions to be based on a high level of evidence. The primary end-point, change in the percentage posterior migration of the humeral head measured on an axial MRI image between 11 months (before BTI) and 18 months of age (6 months post BTI), has been chosen for its clinical relevance and its strong psychometric properties compared with clinical or functional assessment in this population. Clinical evaluations carried out before and after BTI will determine the effects of the treatment on shoulder ROM and functional capacity. Evaluations will be carried out monthly, with alternate phone contacts and direct consultations in order to limit traveling, promote adherence and limit losses to follow-up. Because there is currently no marketing authorisation for BTI in infants

under the age of two years, special attention was paid to the safety assessment. The use of a systematic and detailed questionnaire will yield detailed and specific data, confirming or not the safety of BTI before the age of two years. The results of the study could lead to a request for an evaluation by the French National Agency for Medicines and Health Products Safety (ANSM) for Temporary Recommendation for Use (TRUs) of botulinum toxin in children with POPB. It is expected that the results of this trial will be published in peer-reviewed scholarly journals and international academic conferences.

Table 1 : Visits and study procedure

Action	***Visit 1 :*** *10 months of age (Inclusion, medical and therapists)*	***Visit 2:*** *11 months of age (MRI)*	***Visit 3:*** *12 months of age (injection, medical follow-up l)*	***Visit 4:*** *D10 post-injection (medical follow-up)*	***Visit 5:*** *13 months of age (Phone call)*	***Visit 6:*** *14 months of age (Phone call)*	***Visit 7 :*** *15 months of age (medical and therapists)*	***Visit 8 :*** *16 months of age (Phone call)*	***Visit 9 :*** *17 months of age (Phone call)*	***Visit 10:*** *18 months of age (MRI, therapists medical)*
Informed consent	*X*									
Incl./excl. criteria	*X*									
Medical history	X									
Notification of existing and planned POPB care	X* →									
Active and passive shoulder range of motion (ROM)	X* →						X			X
Active Movement Scale (AMS)	X* →						X			X
MRI of both shoulders		X								X
mini-AHA Scale	X* →									X
Ramdomisation criterion		X								
Randomisation			X							
BTI Injections or Sham procedure			X							
Notification of care (surgery or other)			X							
Establishment of standardized			X							

physiotherapy follw-up										
Follow-up of physiotherapy				X	X	X	X	X	X	X
Adverse Events		X	X	X	X	X	X	X	X	X
Unblinding										X

X* ⟶ : *Will be carried out before MRI*

Figure 1 : Flow chart

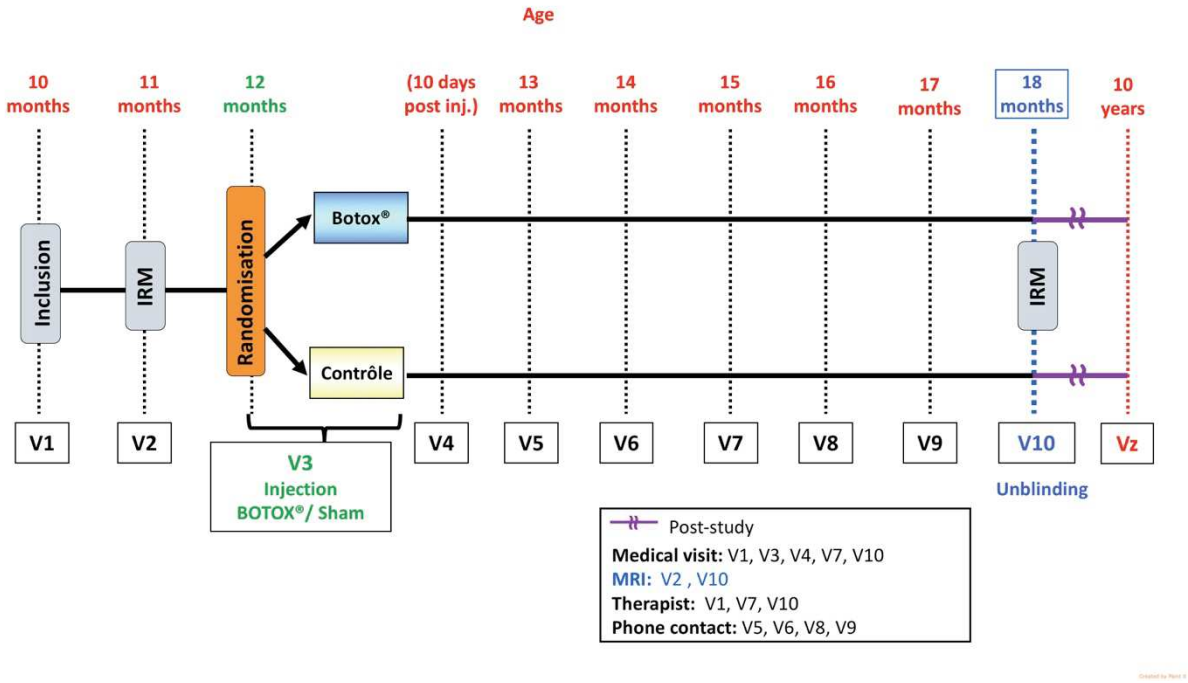

Acknowledgements

The authors acknowledge Chloe Bureau, Bhushan Borotikar, Céline Dolou, Valentine Guiton, Mélanie Pelouin, Emmanuel Novak for their help in building this project and Johanna Robertson for her help in revising English.

Author statement

CP and SB conceived the study and defined the original study protocol. NQP, FF, CP and SB developed the intervention parameters. MG and DBS defined the radiological parameters and developed radiological protocols. ED is responsible for the ethics applications and the ethical reporting of the study. FF, NQP, CP, LH, are responsible for recruitment, data collection and implementation of the study. GG is responsible for the study methodology. POPBtox group involves physicians who are only implicated for recruitment and data collection.

All authors have read and approved the final manuscript. CP, ED and SB drafted the final version of this manuscript

Funding

This work was supported by a French national PHRC 15 -282

Disclaimer

The funding body is not involved in the study design, data collection, management, analysis, and interpretation of data. The authors have the ultimate authority over these activities.

Competing interests None.

Sponsor

Brest CHRU, 2 avenue Foch, 29200 Brest, France

Ethics approval

The Ouest 1 Research Ethics Committee (n° 2015-R22) and ANSM (151357A-31)approved the protocol.

Data sharing statement

In accordance with the protocol, the study data will be published.

VI Conclusions de la thèse

Chez les enfants présentant une paralysie obstétricale du plexus brachial (POPB) sans récupération complète, des séquelles secondaires à l'atteinte nerveuse du membre supérieur persistent. Ces séquelles sont à l'origine de déficiences, limitations des activités, restrictions de participation au sens de la CIF (Classification Internationale du Fonctionnement) et d'une réduction de la qualité de vie.

L'atteinte de l'épaule et plus particulièrement de l'articulation gléno-humérale, est la principale cause de morbidité dans cette population. Les conséquences musculo-squelettiques sont majeures au niveau de cette articulation. Elles sont présentes très précocement et persistent à l'âge adulte. Au niveau musculaire, la dénervation est à l'origine d'une altération de leur fonction. Les muscles gléno-huméraux sont ainsi limités dans leur capacité à générer de la force et à mobiliser l'articulation gléno-humérale. Une perturbation de la croissance musculaire est également présente, à l'origine d'une perte d'amplitudes articulaires passives, plus particulièrement dans certains degrés de liberté, comme la rotation externe. L'atteinte musculaire et la limitation des mouvements au niveau de l'articulation gléno-humérale sont à l'origine d'une modification des contraintes mécaniques exercées sur cette articulation conduisant à sa déformation. Le maintien de la congruence gléno-humérale et la mobilité de l'épaule sont des objectifs de prise en charge majeurs chez l'enfant avec POPB sans récupération complète.

Chez ces enfants, l'atteinte du couple agoniste-antagoniste subscapulaire-infraépineux ainsi que ses conséquences ont été spécifiquement étudiées. Cependant, la connaissance de l'atteinte de l'ensemble des muscles impliqués dans la mobilisation de l'articulation gléno-humérale reste incomplète. De même, la perturbation de la motricité de l'épaule a été bien décrite mais les spécificités de mouvement des membres supérieurs et les modifications de cinématique au niveau des autres articulations sont moins connues.

Afin d'obtenir une évaluation précise, objective et quantitative de de la dysfonction du membre supérieur et plus particulièrement de l'articulation complexe qu'est l'épaule, l'évaluation clinique doit être complétée par des explorations complémentaires.

Etant donné le lien entre la morphologie des muscles et leur fonction, l'utilisation de techniques d'imagerie paraît la meilleure évaluation pour explorer l'atteinte des muscles de l'épaule. Les volumes musculaires en particulier, bien corrélés avec la force musculaire, peuvent être obtenus en IRM par des techniques de segmentation manuelles ou automatiques après acquisition. Les propriétés métrologiques de ces techniques variant en fonction des techniques mais aussi des muscles à segmenter, le choix de la technique doit se faire en fonction du type de muscles à explorer et de la précision recherchée. Chez l'enfant avec POPB, nous souhaitions une importante précision et avons choisi une technique de segmentation manuelle d'un grand nombre de coupes. Nous avons montré une atrophie variable des muscles mobilisateurs de l'articulation gléno-humérale évalués (subscapulaire, infraépineux et petit rond, grand rond, supraépineux, deltoïde, grand pectoral) à l'origine de déséquilibres dans tous les couples agonistes-antagonistes. Le muscle grand pectoral apparaissait relativement préservé, contribuant ainsi au déséquilibre en faveur des rotateurs internes. Le muscle grand rond au contraire était particulèrement affecté. Des corrélations entre les volumes musculaires et la force étaient présentes mais plus faibles que chez l'enfant avec un développement typique.

Pour explorer le mouvement des membres supérieurs chez ces enfants, nous l'avons enregistré lors de huit tâches standardisées avec un système optoélectronique d'analyse quantifiée du mouvement. La performance du mouvement était satisfaisante mais la cinématique de l'ensemble des articulations était changée. Au niveau de l'articulation gléno-humérale, des amplitudes articulaires réduites étaient retrouvées dans les trois plans de l'espace avec une limitation particulièrement importante en rotation externe. Des compensations et adaptations cinématiques étaient notées au niveau de l'ensemble du membre supérieur.

L'utilisation d'outils tels que IRM et l'analyse quantifiée du mouvement permettent l'obtention de données quantitatives caractérisant les muscles individuellement et les amplitudes articulaires autorisées pour chaque degré de liberté, mais aussi les os et les déformations osseuses. Ces données pourraient être intégrées dans un modèle biomécanique

générique tridimensionnel du membre supérieur pour obtenir un modèle spécifique à l'enfant avec POPB. En permettant une meilleure compréhension des relations entre les différentes atteintes, musculaires, osseuses et du mouvement, ce type de modèle pourrait contribuer à améliorer la connaissance de la physiopathologie de l'atteinte de leur épaule et ainsi améliorer et spécifier les prises en charge proposées.

A partir des résultats obtenus dans les articles explorant le fonctionnement de l'épaule et du membre supérieur chez les enfants avec POPB, différents objectifs et cibles thérapeutiques sont discutés. La lutte contre le déséquilibre musculaire de l'ensemble des rotateurs internes par rapport aux rotateurs externes apparaît comme une priorité dans la prise en charge des enfants avec POPB. Nous proposons d'évaluer l'intérêt d'injections de toxine botulinique précoces dans les rotateurs internes pour rétablir l'équilibre du couple agoniste-antagoniste et ainsi limiter l'évolution de la déformation gléno-humérale, et améliorer la mobilité de l'épaule dans un essai contrôle randomisé multicentrique.
Etant donné l'efficacité du mouvement des membres supérieurs, le respect des compensations mises en place et non la lutte contre celles-ci apparaît nécessaire chez les enfants plus âgés

L'IRM de l'épaule et l'analyse du mouvement du membre supérieur, en plus d'être des outils de recherche comme dans cette thèse pourraient devenir des outils d'exploration clinique guidant le suivi et des décisions thérapeutiques rééducatives et chirurgicale individualisées. .

VII Bibliographie de la thèse

1-Abid, A. 2016. « Brachial Plexus Birth Palsy: Management during the First Year of Life ». *Orthopaedics & Traumatology, Surgery & Research: OTSR* 102 (1 Suppl): S125-132. https://doi.org/10.1016/j.otsr.2015.05.008.

2- Ackland, D. C., F. Keynejad, et M. G. Pandy. 2011. « Future Trends in the Use of X-Ray Fluoroscopy for the Measurement and Modelling of Joint Motion ». *Proceedings of the Institution of Mechanical Engineers Part H-Journal of Engineering in Medicine* 225 (H12): 1136-48. https://doi.org/10.1177/0954411911422840.

3- Akagi, Ryota, Yohei Takai, Megumi Ohta, Hiroaki Kanehisa, Yasuo Kawakami, et Tetsuo Fukunaga. 2009. « Muscle Volume Compared to Cross-Sectional Area Is More Appropriate for Evaluating Muscle Strength in Young and Elderly Individuals ». *Age and Ageing* 38 (5): 564-69. https://doi.org/10.1093/ageing/afp122.

4- Aktaş, Dilek, Beyhan Eren, Özge Keniş-Coşkun, et Evrim Karadag-Saygi. 2018. « Function in unaffected arms of children with obstetric brachial plexus palsy ». *European Journal of Paediatric Neurology* 22 (4): 610-14. https://doi.org/10.1016/j.ejpn.2018.03.005.

5- Al Qattan, M.M., A.A.F.El-Sayed, A.Y.Al-Zahrani, S.A. Al-Mutairi, M.S Al-Harbi, A.M.Al-Mutairi, et F;S. Al-Kahtani. 2009. « Narakas Classification of Obstetric Brachial Plexus Palsy Revisited ». *Journal of Hand Surgery (European Volume)* 34 (6): 788-91. https://doi.org/10.1177/1753193409348185.

6-Alt Murphy, Margit, Carin Willén, et Katharina S. Sunnerhagen. 2013. « Responsiveness of Upper Extremity Kinematic Measures and Clinical Improvement During the First Three Months After Stroke ». *Neurorehabilitation and Neural Repair* 27 (9): 844-53. https://doi.org/10.1177/1545968313491008.

7-An, K.N., Takahashi K., Harrigan T.P., Chao E.Y. 1981. « Determination of muscle orientations and moment arms». *Journal of Biomechanical Engineering* 106 (3): 280-282.

8- Anguelova, Galia V., Erwin de Vlugt, Alistair N. Vardy, Erik W. van Zwet, J. Gert van Dijk, Martijn J. A. Malessy, et Jurriaan H. de Groot. 2017. « Cocontraction measured with short-range stiffness was higher in obstetric brachial plexus lesions patients compared to healthy subjects ». *Journal of Biomechanics* 63 (octobre): 192-96. https://doi.org/10.1016/j.jbiomech.2017.08.015.

9-Bae, Donald S., Peter M. Waters, et David Zurakowski. 2008. « Correlation of Pediatric Outcomes Data Collection Instrument with Measures of Active Movement in Children with Brachial Plexus Birth Palsy ». *Journal of Pediatric Orthopedics* 28 (5): 584-92. https://doi.org/10.1097/BPO.0b013e31817bb88b.

10- Bahm, Jörg, Bertold Wein, Gaith Alhares, Can Dogan, Klaus Radermacher, et Frédéric Schuind. 2007. « Assessment and Treatment of Glenohumeral Joint Deformities in Children Suffering from Upper Obstetric Brachial Plexus Palsy ». *Journal of Pediatric Orthopedics. Part B* 16 (4): 243-51. https://doi.org/10.1097/BPB.0b013e3280925681.

11- Bayot, Marlon L., et Eman Elzeftawy. 2018. « Anatomy, Upper Limb, Brachial Plexus ». In *StatPearls*. Treasure Island (FL): StatPearls Publishing. http://www.ncbi.nlm.nih.gov/books/NBK500016/.

12- Beaton, D. E., C. Bombardier, J. N. Katz, et J. G. Wright. 2001. « A Taxonomy for Responsiveness ». *Journal of Clinical Epidemiology* 54 (12): 1204-17.

13- Bhardwaj, Praveen, Tanya Burgess, S. Raja Sabapathy, Hari Venkataramani, et Venkatachalam Ilayaraja. 2013. « Correlation between Clinical Findings and CT Scan Parameters for Shoulder Deformities in Birth Brachial Plexus Palsy ». *The Journal of Hand Surgery* 38 (8): 1557-66. https://doi.org/10.1016/j.jhsa.2013.04.025.

14- Bialocerkowski, Andrea E., et Mary Galea. 2006. « Comparison of visual and objective quantification of elbow and shoulder movement in children with obstetric brachial plexus palsy ». *Journal of Brachial Plexus and Peripheral Nerve Injury* 1 (1): 5. https://doi.org/10.1186/1749-7221-1-5.

15- Bialocerkowski, Andrea E., Tim Wrigley, et Mary Galea. 2006. « Reliability of the V-Scope System in the Measurement of Arm Movement in Children with Obstetric Brachial Plexus Palsy ». *Developmental Medicine and Child Neurology* 48 (11): 913-17. https://doi.org/10.1017/S001216220600199X.

16- Bialocerkowski, Andrea, Kate O'shea, et Tamis W. Pin. 2013. « Psychometric Properties of Outcome Measures for Children and Adolescents with Brachial Plexus Birth Palsy: A Systematic Review ». *Developmental Medicine and Child Neurology* 55 (12): 1075-88. https://doi.org/10.1111/dmcn.12194.

17- Blazevich, Anthony J., David R. Coleman, Sara Horne, et Dale Cannavan. 2009. « Anatomical Predictors of Maximum Isometric and Concentric Knee Extensor Moment ». *European Journal of Applied Physiology* 105 (6): 869-78. https://doi.org/10.1007/s00421-008-0972-7.

18- Bottomley, P. A., T. H. Foster, R. E. Argersinger, et L. M. Pfeifer. 1984. « A Review of Normal Tissue Hydrogen NMR Relaxation Times and Relaxation Mechanisms from 1-100 MHz: Dependence on Tissue Type, NMR Frequency, Temperature, Species, Excision, and Age ». *Medical Physics* 11 (4): 425-48. https://doi.org/10.1118/1.595535.

19- Boylan, L. S., et M. Fouladvand. 2001. « Developmental Apraxia Arising from Neonatal Brachial Plexus Palsy ». *Neurology* 56 (4): 576-77.

20- Brink, Yolandi, et Quinette A. Louw. 2012. « Clinical Instruments: Reliability and Validity Critical Appraisal ». *Journal of Evaluation in Clinical Practice* 18 (6): 1126-32. https://doi.org/10.1111/j.1365-2753.2011.01707.x.

21- Brochard, Sylvain, Katharine Alter, et Diane Damiano. 2014. « Shoulder Strength Profiles in Children with and without Brachial PLEXUS PALSY ». *Muscle & Nerve* 50 (1): 60-66. https://doi.org/10.1002/mus.24099.

22- Brochard, Sylvain, Joseph D. Mozingo, Katharine E. Alter, et Frances T. Sheehan. 2016. « Three Dimensionality of Gleno-Humeral Deformities in Obstetrical Brachial Plexus Palsy ». *Journal of Orthopaedic Research* 34 (4): 675-82. https://doi.org/10.1002/jor.23049.

23- Brown, J. M. M., J. B. Wickham, D. J. McAndrew, et X.-F. Huang. 2007. « Muscles within Muscles: Coordination of 19 Muscle Segments within Three Shoulder Muscles during Isometric Motor Tasks ». *Journal of Electromyography and Kinesiology: Official Journal of the International Society of Electrophysiological Kinesiology* 17 (1): 57-73. https://doi.org/10.1016/j.jelekin.2005.10.007.

24- Brown, Susan H., Rachel Napier, Virginia S. Nelson, et Lynda J.-S. Yang. 2015. « Home-Based Movement Therapy in Neonatal Brachial Plexus Palsy: A Case Study ». *Journal of Hand Therapy: Official Journal of the American Society of Hand Therapists* 28 (3): 307-12; quiz 313. https://doi.org/10.1016/j.jht.2014.10.004.

25- Buesch, Francisca Eugster, Barbara Schlaepfer, Eling D. de Bruin, Gabriela Wohlrab, Corinne Ammann-Reiffer, et Andreas Meyer-Heim. 2010. « Constraint-Induced Movement Therapy for Children with Obstetric Brachial Plexus Palsy: Two Single-Case Series ». *International Journal of Rehabilitation Research. Internationale Zeitschrift Fur Rehabilitationsforschung. Revue Internationale De Recherches De Readaptation* 33 (2): 187-92. https://doi.org/10.1097/MRR.0b013e3283310d6e.

26- Butler, Lesley, Janith Mills, Heather M. Richard, Russell Riddle, Marybeth Ezaki, et Scott Oishi. 2017. « Long-Term Follow-up of Neonatal Brachial Plexopathy: Psychological and Physical Function in Adolescents and Young Adults ». *Journal of Pediatric Orthopedics* 37 (6): e364-68. https://doi.org/10.1097/BPO.0000000000001054.

27- Charbonnier, Caecilia, Alexandre Lädermann, Bart Kevelham, Sylvain Chagué, Pierre Hoffmeyer, et Nicolas Holzer. 2017. « Shoulder Strengthening Exercises Adapted to Specific Shoulder Pathologies Can Be Selected Using New Simulation Techniques: A Pilot Study ». *International Journal of Computer Assisted Radiology and Surgery*, septembre. https://doi.org/10.1007/s11548-017-1668-4.

28- Chauhan, Suneet P., Sean B. Blackwell, et Cande V. Ananth. 2014. « Neonatal Brachial Plexus Palsy: Incidence, Prevalence, and Temporal Trends ». *Seminars in Perinatology* 38 (4): 210-18. https://doi.org/10.1053/j.semperi.2014.04.007.
Cheng, Wei, Roger Cornwall, Dustin L. Crouch, Zhongyu Li, et Katherine R. Saul. 2015. « Contributions of Muscle Imbalance and Impaired Growth to Postural and Osseous Shoulder Deformity Following Brachial Plexus Birth Palsy: A Computational Simulation Analysis ». *The Journal of Hand Surgery* 40 (6): 1170-76. https://doi.org/10.1016/j.jhsa.2015.02.025.

29- Clark, Brian C., Summer B. Cook, et Lori L. Ploutz-Snyder. 2007. « Reliability of Techniques to Assess Human Neuromuscular Function in Vivo ». *Journal of Electromyography and Kinesiology: Official Journal of the International Society of Electrophysiological Kinesiology* 17 (1): 90-101. https://doi.org/10.1016/j.jelekin.2005.11.008.

30- Clarke, H. M., et C. G. Curtis. 1995. « An Approach to Obstetrical Brachial Plexus Injuries ». *Hand Clinics* 11 (4): 563-80; discussion 580-581.

31- Cohen, G., V. Rampal, F. Aubart-Cohen, R. Seringe, et P. Wicart. 2010. « Brachial Plexus Birth Palsy Shoulder Deformity Treatment Using Subscapularis Release Combined to Tendons Transfer ». *Orthopaedics & Traumatology, Surgery & Research: OTSR* 96 (4): 334-39. https://doi.org/10.1016/j.otsr.2010.02.004.

32- Colon, A. J., J. W. Vredeveld, et G. Blaauw. 2007. « Motor Evoked Potentials After Transcranial Magnetic Stimulation Support Hypothesis of Coexisting Central Mechanism in Obstetric Brachial Palsy ». *Journal of Clinical Neurophysiology* 24

(1): 48. https://doi.org/10.1097/01.wnp.0000237075.85689.33.

33- Cormie, Prue, Michael R. McGuigan, et Robert U. Newton. 2011. « Developing Maximal Neuromuscular Power: Part 1--Biological Basis of Maximal Power Production ». *Sports Medicine (Auckland, N.Z.)* 41 (1): 17-38. https://doi.org/10.2165/11537690-000000000-00000.

34- Costil, Vanessa, Claudia Romana, et Frank Fitoussi. 2018. « Pectoralis Minor Transfer for Elbow Flexion Restoration in Late Obstetric Brachial Plexus Palsy ». *International Orthopaedics* 42 (5): 1137-41. https://doi.org/10.1007/s00264-017-3725-6.

35- Crouch, Dustin L., Johannes F. Plate, Zhongyu Li, et Katherine R. Saul. 2014. « Computational Sensitivity Analysis to Identify Muscles That Can Mechanically Contribute to Shoulder Deformity Following Brachial Plexus Birth Palsy ». *The Journal of Hand Surgery* 39 (2): 303-11. https://doi.org/10.1016/j.jhsa.2013.10.027.

36- Csapo, Robert, Vadim Malis, Usha Sinha, Jiang Du, et Shantanu Sinha. 2014. « Age-Associated Differences in Triceps Surae Muscle Composition and Strength - an MRI-Based Cross-Sectional Comparison of Contractile, Adipose and Connective Tissue ». *BMC Musculoskeletal Disorders* 15 (juin): 209. https://doi.org/10.1186/1471-2474-15-209.

37- Curtis, Christine, Derek Stephens, Howard M. Clarke, et David Andrews. 2002. « The Active Movement Scale: An Evaluative Tool for Infants with Obstetrical Brachial Plexus Palsy ». *The Journal of Hand Surgery* 27 (3): 470-78.

38- Cusack, William F., Rebecca Patterson, Scott Thach, Robert S. Kistenberg, et Lewis A. Wheaton. 2014. « Motor Performance Benefits of Matched Limb Imitation in Prosthesis Users ». *Experimental Brain Research* 232 (7): 2143-54. https://doi.org/10.1007/s00221-014-3904-2.

39- Das, Rosalina, Jason Rich, H. Mike Kim, Audrey McAlinden, et Stavros Thomopoulos. 2011. « Effects of Botulinum Toxin-Induced Paralysis on Postnatal Development of the Supraspinatus Muscle ». *Journal of Orthopaedic Research* 29 (2): 281-88. https://doi.org/10.1002/jor.21234.

40- Deighan, M., M. De Ste Croix, C. Grant, et N. Armstrong. 2006. « Measurement of Maximal Muscle Cross-Sectional Area of the Elbow Extensors and Flexors in Children, Teenagers and Adults ». *Journal of Sports Sciences* 24 (5): 543-46. https://doi.org/10.1080/02640410500357184.

41- Desroches, Guillaume, Raphaël Dumas, Didier Pradon, Philippe Vaslin, François-Xavier Lepoutre, et Laurence Chèze. 2010. « Upper Limb Joint Dynamics during Manual Wheelchair Propulsion ». *Clinical Biomechanics (Bristol, Avon)* 25 (4): 299-306. https://doi.org/10.1016/j.clinbiomech.2009.12.011.

42- Dodwell, Emily, Jamie O'Callaghan, Alison Anthony, Paul Jellicoe, Maulin Shah, Christine Curtis, Howard Clarke, et Sevan Hopyan. 2012. « Combined Glenoid Anteversion Osteotomy and Tendon Transfers for Brachial Plexus Birth Palsy: Early Outcomes ». *The Journal of Bone and Joint Surgery. American Volume* 94 (23): 2145-52. https://doi.org/10.2106/JBJS.K.01256.

43- Duff, Susan V., Sudarshan Dayanidhi, et Scott H. Kozin. 2007. « Asymmetrical shoulder kinematics in children with brachial plexus birth palsy ». *Clinical Biomechanics* 22 (6): 630-38. https://doi.org/10.1016/j.clinbiomech.2007.02.002.

44- Duijnisveld, Bouke J., Jan Ferdinand Henseler, Monique Reijnierse, Marta Fiocco, Hermien E. Kan, et Rob G. H. H. Nelissen. 2017. « Quantitative Dixon MRI Sequences to Relate Muscle Atrophy and Fatty Degeneration with Range of Motion and Muscle Force in Brachial Plexus Injury ». *Magnetic Resonance Imaging* 36 (février): 98-104. https://doi.org/10.1016/j.mri.2016.10.020.

45- Dysart, P. S., E. M. Harkness, et G. P. Herbison. 1989. « Growth of the Humerus after Denervation. An Experimental Study in the Rat ». *Journal of Anatomy* 167 (décembre): 147-59.

46- Einarsson, F., T. Hultgren, B. -O. Ljung, E. Runeeson, et J Friden. « Subscapularis Muscle Mechanics in Children with Obstetric Brachial Plexus Palsy ». *Journal of Hand Surgery (European Volume)* 33 (4): 507-12. https://doi.org/10.1177/1753193408090764.

47- Eismann, Emily A., Kevin J. Little, Tal Laor, et Roger Cornwall. 2015. « Glenohumeral Abduction Contracture in Children with Unresolved Neonatal Brachial Plexus Palsy ». *The Journal of Bone and Joint Surgery. American Volume* 97 (2): 112-18. https://doi.org/10.2106/JBJS.N.00203.

48- Engstrom, Craig M., Jurgen Fripp, Valer Jurcak, Duncan G. Walker, Olivier Salvado, et Stuart Crozier. 2011. « Segmentation of the Quadratus Lumborum Muscle Using Statistical Shape Modeling ». *Journal of Magnetic Resonance Imaging: JMRI* 33 (6): 1422-29. https://doi.org/10.1002/jmri.22188.

49- Engstrom, Craig M., Duncan G. Walker, Vaughan Kippers, et Andrew J. H. Mehnert. 2007. « Quadratus Lumborum Asymmetry and L4 Pars Injury in Fast Bowlers: A Prospective MR Study ». *Medicine and Science in Sports and Exercise* 39 (6): 910-17. https://doi.org/10.1249/mss.0b013e3180408e25.

50- Ezaki, Marybeth, Kanchai Malungpaishrope, Richard J. Harrison, Janith K. Mills, Scott N. Oishi, Mauricio Delgado, Patricia A. Bush, et Richard H. Browne. 2010. « Onabotulinum ToxinA Injection as an Adjunct in the Treatment of Posterior Shoulder Subluxation in Neonatal Brachial Plexus Palsy ». *The Journal of Bone and Joint Surgery. American Volume* 92 (12): 2171-77. https://doi.org/10.2106/JBJS.I.00499.

51- Fitoussi, F., N. Maurel, A. Diop, E. M. Laassel, B. Ilharreborde, A. Presedo, K. Mazda, et G. -F. Penneçot. 2009. « Upper extremity kinematics analysis in obstetrical brachial plexus palsy ». *Orthopaedics & Traumatology: Surgery & Research* 95 (5): 336-42. https://doi.org/10.1016/j.otsr.2009.04.012.

52- Fleckenstein, J. L., P. T. Weatherall, L. A. Bertocci, M. Ezaki, R. G. Haller, R. Greenlee, W. W. Bryan, et R. M. Peshock. 1991. « Locomotor System Assessment by Muscle Magnetic Resonance Imaging ». *Magnetic Resonance Quarterly* 7 (2): 79-103.

53- Forro, Stephen D., et Jason B. Lowe. 2018. « Anatomy, Upper Limb ». In *StatPearls*. Treasure Island (FL): StatPearls Publishing. http://www.ncbi.nlm.nih.gov/books/NBK507841/.

54- Frich, Lars H., Pernille H. Schmidt, et Trine Torfing. 2017. « Glenoid morphology in obstetrical brachial plexus lesion: a three-dimensional computed tomography study ». *Journal of Shoulder and Elbow Surgery* 26 (8): 1374-82. https://doi.org/10.1016/j.jse.2017.02.020.

55- Fukunaga, T., M. Miyatani, M. Tachi, M. Kouzaki, Y. Kawakami, et H. Kanehisa. 2001. « Muscle Volume Is a Major Determinant of Joint Torque in Humans ». *Acta Physiologica Scandinavica* 172 (4): 249-55. https://doi.org/10.1046/j.1365-201x.2001.00867.x.

56- Gaillard, Florence, Armel Cretual, Sebastien Cordillet, Caroline Le Cornec, Corentin Gonthier, Brice Bouvier, Rachel Heyman, Sylvette Marleix, Isabelle Bonan, et Hélène Rauscent. 2018. « Kinematic Motion Abnormalities and Bimanual Performance in Children with Unilateral Cerebral Palsy ». *Developmental Medicine and Child Neurology* 60 (8): 839-45. https://doi.org/10.1111/dmcn.13774.

57- Gelein Vitringa, Valerie M. van, Ed O. van Kooten, Margriet G. Mullender, Mirjam H. van Doorn-Loogman, et Johannes A. van der Sluijs. 2009. « An MRI Study on the Relations between Muscle Atrophy, Shoulder Function and Glenohumeral Deformity in Shoulders of Children with Obstetric Brachial Plexus Injury ». *Journal of Brachial Plexus and Peripheral Nerve Injury* 4 (mai): 5. https://doi.org/10.1186/1749-7221-4-5.

58- Giroux-Metges, Marie-Agnès, Jean-Pierre Pennec, Julien Petit, Julie Morel, Hélène Talarmin, Mickaël Droguet, Germaine Doange, et Maxime Gioux. 2005. « Effects of Immobilizing a Single Muscle on the Morphology and the Activation of Its Muscle Fibers ». *Experimental Neurology* 194 (2): 495-505. https://doi.org/10.1016/j.expneurol.2005.03.008.

59- Godi, Claudia, Alessandro Ambrosi, Francesca Nicastro, Stefano C. Previtali, Corrado Santarosa, Sara Napolitano, Antonella Iadanza, et al. 2016. « Longitudinal MRI Quantification of Muscle Degeneration in Duchenne Muscular Dystrophy ». *Annals of Clinical and Translational Neurology* 3 (8): 607-22. https://doi.org/10.1002/acn3.319.

60- Greenhill, Dustin A., Kevin Wissinger, Arianna Trionfo, Mark Solarz, Scott H. Kozin, et Dan A. Zlotolow. 2018. « External Rotation Predicts Outcomes After Closed Glenohumeral Joint Reduction With Botulinum Toxin Type A in Brachial Plexus Birth Palsy ». Text. janvier 2018. https://doi.org/info:doi/10.1097/BPO.0000000000000735.

61- Gross, Raphaël, Fabien Leboeuf, Jean Benoit Hardouin, Brigitte Perrouin-Verbe, Sylvain Brochard, et Olivier Rémy-Néris. 2015. « Does Muscle Coactivation Influence Joint Excursions during Gait in Children with and without Hemiplegic Cerebral Palsy? Relationship between Muscle Coactivation and Joint Kinematics ». *Clinical Biomechanics (Bristol, Avon)* 30 (10): 1088-93. https://doi.org/10.1016/j.clinbiomech.2015.09.001.

62- Heemskerk, A. M., G. J. Strijkers, A. Vilanova, M. R. Drost, et K. Nicolay. 2005. « Determination of Mouse Skeletal Muscle Architecture Using Three-Dimensional Diffusion Tensor Imaging ». *Magnetic Resonance in Medicine* 53 (6): 1333-40. https://doi.org/10.1002/mrm.20476.

63- Herisson, Olivier, Nathalie Maurel, Amadou Diop, Morgane Le Chatelier, Adeline Cambon-Binder, et Franck Fitoussi. 2017. « Shoulder and elbow kinematics during the Mallet score in obstetrical brachial plexus palsy ». *Clinical Biomechanics* 43 (mars): 1-7. https://doi.org/10.1016/j.clinbiomech.2017.01.006.

64- Hoffer, M. M., R. Wickenden, et B. Roper. 1978. « Brachial Plexus Birth Palsies. Results of Tendon Transfers to the Rotator Cuff ». *The Journal of Bone and Joint Surgery. American Volume* 60 (5): 691-95.

65- Hogendoorn, Simone, Karlijn L. J. van Overvest, Iain Watt, AnneWil H. B. Duijsens, et Rob G. H. H. Nelissen. 2010. « Structural Changes in Muscle and Glenohumeral Joint Deformity in Neonatal Brachial Plexus Palsy ». *The Journal of Bone and Joint Surgery. American Volume* 92 (4): 935-42. https://doi.org/10.2106/JBJS.I.00193.

66- Holst, Menno van der, Jeroen Groot, Duco Steenbeek, Willem Pondaag, Rob Ghh Nelissen, et Thea Pm Vliet Vlieland. 2017. « Participation Restrictions among Adolescents and Adults with Neonatal Brachial Plexus Palsy: The Patient Perspective ». *Disability and Rehabilitation*, septembre, 1-9. https://doi.org/10.1080/09638288.2017.1380717.

67- Holst, Menno van der, Thea P. M. Vliet Vlieland, Jorit J. L. Meesters, W. Peter Bekkering, Jochem Nagels, et Rob G. H. H. Nelissen. 2015. « Evaluation of Shoulder Function after Secondary Surgery in Children with Neonatal Brachial Plexus Palsy ». *Journal of Pediatric Rehabilitation Medicine* 8 (3): 187-96. https://doi.org/10.3233/PRM-150332.

68- Holzbaur, Katherine R. S., Scott L. Delp, Garry E. Gold, et Wendy M. Murray. 2007. « Moment-Generating Capacity of Upper Limb Muscles in Healthy Adults ». *Journal of Biomechanics* 40 (11): 2442-49. https://doi.org/10.1016/j.jbiomech.2006.11.013.

69- Holzbaur, Katherine R. S., Wendy M. Murray, et Scott L. Delp. 2005. « A Model of the Upper Extremity for Simulating Musculoskeletal Surgery and Analyzing Neuromuscular Control ». *Annals of Biomedical Engineering* 33 (6): 829-40. https://doi.org/10.1007/s10439-005-3320-7.

70- Holzbaur, Katherine R. S., Wendy M. Murray, Garry E. Gold, et Scott L. Delp. 2007. « Upper Limb Muscle Volumes in Adult Subjects ». *Journal of Biomechanics* 40 (4): 742-49. https://doi.org/10.1016/j.jbiomech.2006.11.011.

71- Hulleberg, Gunn, Ann-Kristin G. Elvrum, Merethe Brandal, et Torstein Vik. 2014. « Outcome in Adolescence of Brachial Plexus Birth Palsy. 69 Individuals Re-Examined after 10–20 Years ». *Acta Orthopaedica* 85 (6): 633-40. https://doi.org/10.3109/17453674.2014.964614.

72- Hultgren, T., K. Jönsson, H. Pettersson, et H. Hammarberg. 2013. « Surgical Correction of a Rotational Deformity of the Shoulder in Patients with Obstetric Brachial Plexus Palsy: Short-Term Results in 270 Patients ». *The Bone & Joint Journal* 95-B (10): 1432-38. https://doi.org/10.1302/0301-620X.95B10.32049.

73- Hultgren, T., K. Jönsson, F. Roos, H. Järnbert-Pettersson, et H. Hammarberg. 2014. « Surgical Correction of Shoulder Rotation Deformity in Brachial Plexus Birth Palsy: Long-Term Results in 118 Patients ». *The Bone & Joint Journal* 96-B (10): 1411-18. https://doi.org/10.1302/0301-620X.96B10.33813.

74- Hurov, Jack. 2009. « Anatomy and Mechanics of the Shoulder: Review of Current Concepts ». *Journal of Hand Therapy: Official Journal of the American Society of Hand Therapists* 22 (4): 328-42; quiz 343. https://doi.org/10.1016/j.jht.2009.05.002.

75- Immerman, Igor, Daniel T. Alfonso, Lorna E. Ramos, Leslie A. Grossman, Israel Alfonso, Patricia Ditaranto, et John a. I. Grossman. 2012. « Hand Function in Children with an Upper Brachial Plexus Birth Injury: Results of the Nine-Hole Peg Test ». *Developmental Medicine & Child Neurology* 54 (2): 166-69. https://doi.org/10.1111/j.1469-8749.2011.04120.x.

76- Iorio, Matthew L., Sarah J. Menashe, Ramesh S. Iyer, Sarah P. Lewis, Suzanne Steinman, Kathryn B. Whitlock, et Raymond W. Tse. 2015. « Glenohumeral Dysplasia Following Neonatal Brachial Plexus Palsy: Presentation and Predictive Features During Infancy ». *The Journal of Hand Surgery* 40 (12): 2345-2351.e1. https://doi.org/10.1016/j.jhsa.2015.08.029.

77- Jaspers, Ellen, Kaat Desloovere, Herman Bruyninckx, Katrijn Klingels, Guy Molenaers, Erwin Aertbeliën, Leen Van Gestel, et Hilde Feys. 2011. « Three-dimensional upper limb movement characteristics in children with hemiplegic cerebral palsy and typically developing children ». *Research in Developmental Disabilities* 32 (6): 2283-94. https://doi.org/10.1016/j.ridd.2011.07.038.

78- Jastifer, James, Peter Gustafson, Bipin Patel, et Christopher Uggen. 2012. « Pectoralis Major Transfer for Subscapularis Deficiency: A Computational Study ». *Shoulder & Elbow* 4 (1): 25-29. https://doi.org/10.1111/j.1758-5740.2011.00161.x.

79- Jenkins, Thomas M., Christine Burness, Daniel J. Connolly, D. Ganesh Rao, Nigel Hoggard, Susan Mawson, Christopher J. McDermott, Iain D. Wilkinson, et Pamela J. Shaw. 2013. « A Prospective Pilot Study Measuring Muscle Volumetric Change in Amyotrophic Lateral Sclerosis ». *Amyotrophic Lateral Sclerosis & Frontotemporal Degeneration* 14 (5-6): 414-23. https://doi.org/10.3109/21678421.2013.795597.

80- Julka, Abhishek, et Kelly L. Vander Have. 2011. « Shoulder Sequelae of Neonatal Brachial Plexus Injuries: Orthopedic Assessment and Management ». *Journal of Pediatric Rehabilitation Medicine* 4 (2): 131-40. https://doi.org/10.3233/PRM-2011-0165.

81- Kaick, Oliver van, Ghassan Hamarneh, Aaron D. Ward, Mark Schweitzer, et Hao Zhang. 2010. « Learning Fourier Descriptors for Computer-Aided Diagnosis of the Supraspinatus ». *Academic Radiology* 17 (8): 1040-49. https://doi.org/10.1016/j.acra.2010.04.006.

82- Kälin, Pascal S., Rebecca J. Crawford, Magda Marcon, Andrei Manoliu, Samy Bouaicha, Michael A. Fischer, et Erika J. Ulbrich. 2018. « Shoulder Muscle Volume and Fat Content in Healthy Adult Volunteers: Quantification with DIXON MRI to Determine the Influence of Demographics and Handedness ». *Skeletal Radiology* 47 (10): 1393-1402. https://doi.org/10.1007/s00256-018-2945-1.

83- Kamina, Pierre, et André Gouazé. 2009. *Anatomie clinique : Tome 1, Anatomie générale, membres*. 4e édition. Paris: Maloine.

84- Kanehisa, H., S. Ikegawa, N. Tsunoda, et T. Fukunaga. 1994. « Strength and Cross-Sectional Area of Knee Extensor

Muscles in Children ». *European Journal of Applied Physiology and Occupational Physiology* 68 (5): 402-5.

85- Kanehisa, H., S. Ikegawa, et T. Fukunaga. 1994 1995. « Strength and Cross-Sectional Areas of Reciprocal Muscle Groups in the Upper Arm and Thigh during Adolescence ». *International Journal of Sports Medicine* 16 (1): 54-60. https://doi.org/10.1055/s-2007-972964.

86- Kapandji, Adalbert-I., et Raoul Tubiana. 2005. *Anatomie fonctionnelle 1 : Membres supérieurs. Physiologie de l'appareil locomoteur*. 6e édition. Paris: Maloine.

87- Kattan, Abdullah E., et Gregory H. Borschel. 2011. « Anatomy of the Brachial Plexus ». *Journal of Pediatric Rehabilitation Medicine* 4 (2): 107-11. https://doi.org/10.3233/PRM-2011-0163.

88- Khalil, C., J. F. Budzik, E. Kermarrec, V. Balbi, V. Le Thuc, et A. Cotten. 2010. « Tractography of Peripheral Nerves and Skeletal Muscles ». *European Journal of Radiology* 76 (3): 391-97. https://doi.org/10.1016/j.ejrad.2010.03.012.

89- Khanna, Paritosh C., et Mahesh M. Thapa. 2009. « The Growing Skeleton: MR Imaging Appearances of Developing Cartilage ». *Magnetic Resonance Imaging Clinics of North America* 17 (3): 411-21, v. https://doi.org/10.1016/j.mric.2009.03.012.

90- Kim, H. Mike, Leesa M. Galatz, Rosalina Das, Nikunj Patel, et Stavros Thomopoulos. 2010. « Musculoskeletal Deformities Secondary to Neurotomy of the Superior Trunk of the Brachial Plexus in Neonatal Mice ». *Journal of Orthopaedic Research* 28 (10): 1391-98. https://doi.org/10.1002/jor.21128.

91- Kirkos, J. M., M. J. Kyrkos, G. A. Kapetanos, et J. H. Haritidis. 2005. « Brachial Plexus Palsy Secondary to Birth Injuries ». *The Journal of Bone and Joint Surgery. British Volume* 87 (2): 231-35.

92- Kleiber, Tim, Nikica Popovic, Jörg Bahm, et Catherine Disselhorst-Klug. 2013. « A modeling approach to compute modification of net joint forces caused by coping movements in obstetric brachial plexus palsy ». *Journal of Brachial Plexus and Peripheral Nerve Injury* 8 (octobre): 10. https://doi.org/10.1186/1749-7221-8-10.

93- Kozin, Scott H., Matthew J. Boardman, Ross S. Chafetz, Gerald R. Williams, et Alexandra Hanlon. 2010. « Arthroscopic Treatment of Internal Rotation Contracture and Glenohumeral Dysplasia in Children with Brachial Plexus Birth Palsy ». *Journal of Shoulder and Elbow Surgery* 19 (1): 102-10. https://doi.org/10.1016/j.jse.2009.05.011.

94- Kozin, Scott H., Ross S. Chafetz, Diane Barus, et Linda Filipone. 2006. « Magnetic Resonance Imaging and Clinical Findings before and after Tendon Transfers about the Shoulder in Children with Residual Brachial Plexus Birth Palsy ». *Journal of Shoulder and Elbow Surgery* 15 (5): 554-61. https://doi.org/10.1016/j.jse.2005.11.004.

95- Kubo, Keitaro, Hiroaki Kanehisa, Kasumi Azuma, Masao Ishizu, Shin-Ya Kuno, Morihiro Okada, et Tetsuo Fukunaga. 2003. « Muscle Architectural Characteristics in Women Aged 20-79 Years ». *Medicine and Science in Sports and Exercise* 35 (1): 39-44. https://doi.org/10.1249/01.MSS.0000043385.66520.09.

96- Kuechle, D. K., S. R. Newman, E. Itoi, B. F. Morrey, et K. N. An. 1997. « Shoulder Muscle Moment Arms during Horizontal Flexion and Elevation ». *Journal of Shoulder and Elbow Surgery* 6 (5): 429-39.

97- Kuechle, D. K., S. R. Newman, E. Itoi, G. L. Niebur, B. F. Morrey, et K. N. An. 2000. « The Relevance of the Moment Arm of Shoulder Muscles with Respect to Axial Rotation of the Glenohumeral Joint in Four Positions ». *Clinical Biomechanics (Bristol, Avon)* 15 (5): 322-29.

98- Kukke, Sahana N., Lindsey A. Curatalo, Ana Carolina de Campos, Mark Hallett, Katharine E. Alter, et Diane L. Damiano. 2016. « Coordination of Reach-to-Grasp Kinematics in Individuals With Childhood-Onset Dystonia Due to Hemiplegic Cerebral Palsy ». *IEEE Transactions on Neural Systems and Rehabilitation Engineering: A Publication of the IEEE Engineering in Medicine and Biology Society* 24 (5): 582-90. https://doi.org/10.1109/TNSRE.2015.2458293.

99- Le Troter, Arnaud, Alexandre Fouré, Maxime Guye, Sylviane Confort-Gouny, Jean-Pierre Mattei, Julien Gondin, Emmanuelle Salort-Campana, et David Bendahan. 2016. « Volume Measurements of Individual Muscles in Human Quadriceps Femoris Using Atlas-Based Segmentation Approaches ». *Magma (New York, N.Y.)* 29 (2): 245-57. https://doi.org/10.1007/s10334-016-0535-6.

100- Lehtinen, Janne T., Markus J. Tingart, Maria Apreleva, David Zurakowski, William Palmer, et Jon J. P. Warner. 2003. « Practical Assessment of Rotator Cuff Muscle Volumes Using Shoulder MRI ». *Acta Orthopaedica Scandinavica* 74 (6): 722-29. https://doi.org/10.1080/00016470310018270.

101- Lieber, Richard L., et Jan Fridén. 2000. « Functional and Clinical Significance of Skeletal Muscle Architecture ». *Muscle & Nerve* 23 (11): 1647-66. https://doi.org/10.1002/1097-4598(200011)23:11<1647::AID-MUS1>3.0.CO;2-M.

102- Ling, H. Y., J. G. Angeles, et M. B. Horodyski. 2009. « Biomechanics of Latissimus Dorsi Transfer for Irreparable Posterosuperior Rotator Cuff Tears ». *Clinical Biomechanics (Bristol, Avon)* 24 (3): 261-66. https://doi.org/10.1016/j.clinbiomech.2008.12.002.

103- Louden, Emily J., Chad A. Broering, Charles T. Mehlman, William C. Lippert, Jesse Pratt, et Eileen C. King. 2013. « Meta-Analysis of Function after Secondary Shoulder Surgery in Neonatal Brachial Plexus Palsy ». *Journal of Pediatric Orthopedics* 33 (6): 656-63. https://doi.org/10.1097/BPO.0b013e3182a11f0f.

104- Maganaris, Constantinos N. 2004. « Imaging-Based Estimates of Moment Arm Length in Intact Human Muscle-Tendons ». *European Journal of Applied Physiology* 91 (2-3): 130-39. https://doi.org/10.1007/s00421-003-1033-x.

105- Mathur, Sunita, Karen Pr Takai, Donna L. Macintyre, et Darlene Reid. 2008. « Estimation of Thigh Muscle Mass with Magnetic Resonance Imaging in Older Adults and People with Chronic Obstructive Pulmonary Disease ». *Physical Therapy* 88 (2): 219-30. https://doi.org/10.2522/ptj.20070052.

106- Matthews, Dennis J. 2018. « Function of the Unaffected Arms of Children with Neonatal Brachial Plexus Injuries ». *European Journal of Paediatric Neurology* 22 (4): 581. https://doi.org/10.1016/j.ejpn.2018.05.014.

107- Mayfield, Christian H., Sahana N. Kukke, Sylvain Brochard, Christopher J. Stanley, Katharine E. Alter, et Diane L. Damiano. 2017. « Inter-joint coordination analysis of reach-to-grasp kinematics in children and adolescents with obstetrical brachial plexus palsy ». *Clinical Biomechanics* 46 (juillet): 15-22. https://doi.org/10.1016/j.clinbiomech.2017.04.010.

108- Mehlman, Charles T., William B. DeVoe, William C. Lippert, Linda J. Michaud, Allison J. Allgier, et Susan L. Foad. 2011. « Arthroscopically Assisted Sever-L'Episcopo Procedure Improves Clinical and Radiographic Outcomes in Neonatal Brachial Plexus Palsy Patients ». *Journal of Pediatric Orthopedics* 31 (3): 341-51. https://doi.org/10.1097/BPO.0b013e31820cada8.

109- Midrio, Menotti. 2006. « The Denervated Muscle: Facts and Hypotheses. A Historical Review ». *European Journal of Applied Physiology* 98 (1): 1-21. https://doi.org/10.1007/s00421-006-0256-z.

110- Mokkink, Lidwine B., Caroline B. Terwee, Donald L. Patrick, Jordi Alonso, Paul W. Stratford, Dirk L. Knol, Lex M. Bouter, et Henrica C. W. de Vet. 2010. « The COSMIN Study Reached International Consensus on Taxonomy, Terminology, and Definitions of Measurement Properties for Health-Related Patient-Reported Outcomes ». *Journal of Clinical Epidemiology* 63 (7): 737-45. https://doi.org/10.1016/j.jclinepi.2010.02.006.

111- Mollberg, Margareta, Henrik Hagberg, Börje Bager, Håkan Lilja, et Lars Ladfors. 2005. « Risk Factors for Obstetric Brachial Plexus Palsy among Neonates Delivered by Vacuum Extraction ». *Obstetrics and Gynecology* 106 (5 Pt 1): 913-18. https://doi.org/10.1097/01.AOG.0000183595.32077.83.
109- Morse, C. I., J. M. Thom, K. M. Birch, et M. V. Narici. 2005. « Changes in Triceps Surae Muscle Architecture with Sarcopenia ». *Acta Physiologica Scandinavica* 183 (3): 291-98. https://doi.org/10.1111/j.1365-201X.2004.01404.x.

112- Mosqueda, Teresa, Michelle A. James, Kyria Petuskey, Anita Bagley, Estelle Abdala, et George Rab. 2004. « Kinematic Assessment of the Upper Extremity in Brachial Plexus Birth Palsy ». *Journal of Pediatric Orthopaedics* 24 (6): 695.

113- Moukoko, Didier, Marybeth Ezaki, David Wilkes, et Peter Carter. 2004. « Posterior Shoulder Dislocation in Infants with Neonatal Brachial Plexus Palsy ». *The Journal of Bone and Joint Surgery. American Volume* 86-A (4): 787-93.

114- Narakas, AO. 1987. « Obstetrical brachial plexus injuries ». In *The Paralyzed Hand*, 116-35. Edinburgh: Churchill Livingstone: Lamb DW.

115- Nath, Rahul K., et Melia Paizi. 2007. « Scapular deformity in obstetric brachial plexus palsy: a new finding ». *Surgical and Radiologic Anatomy* 29 (2): 133-40. https://doi.org/10.1007/s00276-006-0173-1.

116- Netter, Frank. 2015. *Atlas d'anatomie humaine*. 6e édition. Elsevier Masson.

117- Noble, Jonathan J., Nicola Rd Fry, Carly R. Bingham, Rebecca H. East, et Adam P. Shortland. 2018. « A Practical Clinical Kinematic Model for the Upper Limbs ». *Proceedings of the Institution of Mechanical Engineers. Part H, Journal of Engineering in Medicine* 232 (2): 207-12. https://doi.org/10.1177/0954411917749617.

118- Ohl, Xavier, Fabien Billuart, Pierre-Yves Lagacé, Olivier Gagey, Nicola Hagemeister, et Wafa Skalli. 2012. « 3D Morphometric Analysis of 43 Scapulae ». *Surgical and Radiologic Anatomy: SRA* 34 (5): 447-53. https://doi.org/10.1007/s00276-012-0933-z.

119- Okby, Rania, et Eyal Sheiner. 2012. « Risk Factors for Neonatal Brachial Plexus Paralysis ». *Archives of Gynecology and Obstetrics* 286 (2): 333-36. https://doi.org/10.1007/s00404-012-2272-z.

120- Ozben, Hakan, Ata Can Atalar, Kerem Bilsel, et Mehmet Demirhan. 2011. « Transfer of Latissmus Dorsi and Teres Major Tendons without Subscapularis Release for the Treatment of Obstetrical Brachial Plexus Palsy Sequela ». *Journal of Shoulder and Elbow Surgery* 20 (8): 1265-74. https://doi.org/10.1016/j.jse.2011.01.004.

121- Partridge, Cecily, et Susan Edwards. 2004. « Obstetric Brachial Plexus Palsy: Increasing Disability and Exacerbation of Symptoms with Age ». *Physiotherapy Research International: The Journal for Researchers and Clinicians in Physical Therapy*

9 (4): 157-63.

122- Pataky, Todd C. 2010. « Generalized N-Dimensional Biomechanical Field Analysis Using Statistical Parametric Mapping ». *Journal of Biomechanics* 43 (10): 1976-82. https://doi.org/10.1016/j.jbiomech.2010.03.008.

123- Pearl, M. L., et B. W. Edgerton. 1998. « Glenoid Deformity Secondary to Brachial Plexus Birth Palsy ». *The Journal of Bone and Joint Surgery. American Volume* 80 (5): 659-67.

124- Pearl, Michael L. 2009. « Shoulder Problems in Children with Brachial Plexus Birth Palsy: Evaluation and Management ». *The Journal of the American Academy of Orthopaedic Surgeons* 17 (4): 242-54.

125- Pearl, Michael L., Bradford W. Edgerton, Paul A. Kazimiroff, Raoul J. Burchette, et Karyn Wong. 2006. « Arthroscopic Release and Latissimus Dorsi Transfer for Shoulder Internal Rotation Contractures and Glenohumeral Deformity Secondary to Brachial Plexus Birth Palsy ». *The Journal of Bone and Joint Surgery. American Volume* 88 (3): 564-74. https://doi.org/10.2106/JBJS.D.02872.

126- Pedowitz, David I., Brett Gibson, Gerald R. Williams, et Scott H. Kozin. 2007. « Arthroscopic Treatment of Posterior Glenohumeral Joint Subluxation Resulting from Brachial Plexus Birth Palsy ». *Journal of Shoulder and Elbow Surgery* 16 (1): 6-13. https://doi.org/10.1016/j.jse.2006.04.008.

127- Pitcher, Christian A., Catherine M. Elliott, Sian A. Williams, Melissa K. Licari, Alex Kuenzel, Peter J. Shipman, Jane P. Valentine, et Siobhan L. Reid. 2012. « Childhood Muscle Morphology and Strength: Alterations over Six Months of Growth ». *Muscle & Nerve* 46 (3): 360-66. https://doi.org/10.1002/mus.23326.

128- Pondaag, Willem, et Martijn J. A. Malessy. 2014. « The Evidence for Nerve Repair in Obstetric Brachial Plexus Palsy Revisited ». Research article. BioMed Research International. 2014. https://doi.org/10.1155/2014/434619.

129- Pöyhiä, Tiina H., Mika P. Koivikko, Jari I. Peltonen, Mikko O. Kirjavainen, Antti E. Lamminen, et A. Yrjänä Nietosvaara. 2007. « Muscle Changes in Brachial Plexus Birth Injury with Elbow Flexion Contracture: An MRI Study ». *Pediatric Radiology* 37 (2): 173-79. https://doi.org/10.1007/s00247-006-0374-0.

130- Pöyhiä, Tiina H., Yrjänä A. Nietosvaara, Ville M. Remes, Mikko O. Kirjavainen, Jari I. Peltonen, et Antti E. Lamminen. 2005. « MRI of Rotator Cuff Muscle Atrophy in Relation to Glenohumeral Joint Incongruence in Brachial Plexus Birth Injury ». *Pediatric Radiology* 35 (4): 402-9. https://doi.org/10.1007/s00247-004-1377-3.

131- Raducha, Jeremy E., Brian Cohen, Travis Blood, et Julia Katarincic. 2017. « A Review of Brachial Plexus Birth Palsy: Injury and Rehabilitation ». *Rhode Island Medical Journal (2013)* 100 (11): 17-21.

132- Rasmussen, Lynnette, Denise Justice, Kate W.-C. Chang, Virginia S. Nelson, et Lynda J.-S. Yang. 2013. « Home Exercise DVD Promotes Exercise Accuracy by Caregivers of Children and Adolescents with Brachial Plexus Palsy ». *PM & R: The Journal of Injury, Function, and Rehabilitation* 5 (11): 924-30. https://doi.org/10.1016/j.pmrj.2013.06.003.

133- Rodary, C., V. Pezet-Langevin, et C. Kalifa. 2001. « [Quality of life in children: what is a good evaluation tool?] ». *Archives De Pediatrie: Organe Officiel De La Societe Francaise De Pediatrie* 8 (7): 744-50.

134- Ruchelsman, David E., John A. I. Grossman, et Andrew E. Price. 2011. « Glenohumeral Deformity in Children with Brachial Plexus Birth Injuries ». *Bulletin of the NYU Hospital for Joint Diseases* 69 (1): 36-43.

135- Ruchelsman, David E., Sarah Pettrone, Andrew E. Price, et John A. I. Grossman. 2009. « Brachial Plexus Birth Palsy: An Overview of Early Treatment Considerations ». *Bulletin of the NYU Hospital for Joint Diseases* 67 (1): 83-89.

136- Russo, Stephanie A., Scott H. Kozin, Dan A. Zlotolow, Kristen F. Thomas, Robert L. Hulbert, Jeffrey M. Mattson, K. Michael Rowley, et James G. Richards. 2014. « Scapulothoracic and Glenohumeral Contributions to Motion in Children with Brachial Plexus Birth Palsy ». *Journal of Shoulder and Elbow Surgery* 23 (3): 327-38. https://doi.org/10.1016/j.jse.2013.06.023.

137- Safoury, Yasser A., Mohamed T. Eldesoky, Enas E. Abutaleb, Mohamed R. Atteya, et Ahmed M. Gabr. 2017. « Postoperative Physical Therapy Program for Latissimus Dorsi and Teres Major Tendons Transfer to Rotator Cuff in Children with Obstetrical Brachial Plexus Injury ». *European Journal of Physical and Rehabilitation Medicine* 53 (2): 277-85. https://doi.org/10.23736/S1973-9087.16.03910-1.

138- Santos, Gabriela Lopes, Thiago Luiz Russo, Angela Nieuwenhuys, Davide Monari, et Kaat Desloovere. 2018. « Kinematic Analysis of a Drinking Task in Chronic Hemiparetic Patients Using Features Analysis and Statistical Parametric Mapping ». *Archives of Physical Medicine and Rehabilitation* 99 (3): 501-511.e4. https://doi.org/10.1016/j.apmr.2017.08.479.

139- Sarac, Cigdem, Evelien Bastiaansen, Menno Van der Holst, Martijn J. A. Malessy, Rob G. H. H. Nelissen, et Thea P. M. Vliet Vlieland. 2013. « Concepts of Functioning and Health Important to Children with an Obstetric Brachial Plexus Injury: A Qualitative Study Using Focus Groups ». *Developmental Medicine and Child Neurology* 55 (12): 1136-42. https://doi.org/10.1111/dmcn.12270.

140- Sarac, Cigdem, Bouke J. Duijnisveld, Amber van der Weide, Jan W. Schoones, Martijn J. A. Malessy, Rob G. H. H. Nelissen, et Thea P. M. Vliet Vlieland. 2015. « Outcome Measures Used in Clinical Studies on Neonatal Brachial Plexus Palsy: A Systematic Literature Review Using the International Classification of Functioning, Disability and Health ». *Journal of Pediatric Rehabilitation Medicine* 8 (3): 167-86. https://doi.org/10.3233/PRM-150335.

141- Shenaq, Saleh M., Jamal M. Bullocks, Gupreet Dhillon, Rita T. Lee, et John P. Laurent. 2005. « Management of Infant Brachial Plexus Injuries ». *Clinics in Plastic Surgery* 32 (1): 79-98. https://doi.org/10.1016/j.cps.2004.09.001.

142- Sibinski, Marcin, Bartłomiej Woźniakowski, Marek Drobniewski, et Marek Synder. 2010. « Secondary Gleno-Humeral Joint Dysplasia in Children with Persistent Obstetric Brachial Plexus Palsy ». *International Orthopaedics* 34 (6): 863-67. https://doi.org/10.1007/s00264-010-0965-0.

143- Skorupska, Elżbieta, Przemysław Keczmer, Rafał M. Łochowski, Paulina Tomal, Michał Rychlik, et Włodzimierz Samborski. 2016. « Reliability of MR-Based Volumetric 3-D Analysis of Pelvic Muscles among Subjects with Low Back with Leg Pain and Healthy Volunteers ». *PloS One* 11 (7): e0159587. https://doi.org/10.1371/journal.pone.0159587.

144- Sluijs, J. A. van der, W. J. R. van Ouwerkerk, R. A. Manoliu, et P. I. J. M. Wuisman. 2004. « Secondary Deformities of the Shoulder in Infants with an Obstetrical Brachial Plexus Lesions Considered for Neurosurgical Treatment ». *Neurosurgical Focus* 16 (5): E9.

145- Sluijs, J. A. van der, W. J. van Ouwerkerk, A. de Gast, P. I. Wuisman, F. Nollet, et R. A. Manoliu. 2001. « Deformities of the Shoulder in Infants Younger than 12 Months with an Obstetric Lesion of the Brachial Plexus ». *The Journal of Bone and Joint Surgery. British Volume* 83 (4): 551-55.

146- Smith, Brandon W., Alecia K. Daunter, Lynda J.-S. Yang, et Thomas J. Wilson. 2018. « An Update on the Management of Neonatal Brachial Plexus Palsy-Replacing Old Paradigms: A Review ». *JAMA Pediatrics* 172 (6): 585-91. https://doi.org/10.1001/jamapediatrics.2018.0124.

147- Soldado, Francisco, David Benito-Castillo, Cesar G. Fontecha, Ignasi Barber, Mario Marotta, Sleiman Haddad, Mariano E. Menendez, Vasco V. Mascarenhas, et Scott H. Kozin. 2012. « Muscular and glenohumeral changes in the shoulder after brachial plexus birth palsy: an MRI study in a rat model ». *Journal of Brachial Plexus and Peripheral Nerve Injury* 7 (1): 9. https://doi.org/10.1186/1749-7221-7-9.

148- Soldado, Francisco, Cesar G. Fontecha, Mario Marotta, David Benito, Marcelo Casaccia, Vasco V. Mascarenhas, Dan Zlotolow, et Scott H. Kozin. 2014. « The role of muscle imbalance in the pathogenesis of shoulder contracture after neonatal brachial plexus palsy: a study in a rat model ». *Journal of Shoulder and Elbow Surgery* 23 (7): 1003-9. https://doi.org/10.1016/j.jse.2013.09.031.

149- Spaargaren, Els, Jasmyn Ahmed, Willem J. R. van Ouwerkerk, Vincent de Groot, et Heleen Beckerman. 2011. « Aspects of Activities and Participation of 7-8 Year-Old Children with an Obstetric Brachial Plexus Injury ». *European Journal of Paediatric Neurology: EJPN: Official Journal of the European Paediatric Neurology Society* 15 (4): 345-52. https://doi.org/10.1016/j.ejpn.2011.03.008.

150- Springer, I., M. Müller, B. Hamm, et M. Dewey. 2012. « Intra- and Interobserver Variability of Magnetic Resonance Imaging for Quantitative Assessment of Abductor and External Rotator Muscle Changes after Total Hip Arthroplasty ». *European Journal of Radiology* 81 (5): 928-33. https://doi.org/10.1016/j.ejrad.2011.01.113.

151- Squitieri, Lee, Bradley P. Larson, Kate W. C. Chang, Lynda J. S. Yang, et Kevin C. Chung. 2013. « Understanding Quality of Life and Patient Expectations among Adolescents with Neonatal Brachial Plexus Palsy: A Qualitative and Quantitative Pilot Study ». *The Journal of Hand Surgery* 38 (12): 2387-2397.e2.

152- Sundholm, L. K., A. C. Eliasson, et H. Forssberg. 1998. « Obstetric Brachial Plexus Injuries: Assessment Protocol and Functional Outcome at Age 5 Years ». *Developmental Medicine and Child Neurology* 40 (1): 4-11.

153- Talbert, Robert J., Linda J. Michaud, Charles T. Mehlman, Douglas G. Kinnett, Tal Laor, Susan L. Foad, Beverly Schnell, et Shelia Salisbury. 2011. « EMG and MRI Are Independently Related to Shoulder External Rotation Function in Neonatal Brachial Plexus Palsy ». *Journal of Pediatric Orthopedics* 31 (2): 194-204. https://doi.org/10.1097/BPO.0b013e3182092892.

154- Tatara, Alexander M., Justin H. Lipner, Rosalina Das, H. Mike Kim, Nikunj Patel, Eleni Ntouvali, Matthew J. Silva, et Stavros Thomopoulos. 2014. « The Role of Muscle Loading on Bone (Re)Modeling at the Developing Enthesis ». *PLOS ONE* 9 (5): e97375. https://doi.org/10.1371/journal.pone.0097375.

155- Tate, Christine Marie, Glenn N. Williams, Peter J. Barrance, et Thomas S. Buchanan. 2006. « Lower Extremity Muscle Morphology in Young Athletes: An MRI-Based Analysis ». *Medicine and Science in Sports and Exercise* 38 (1): 122-28.

156- Theodorou, D. J., S. J. Theodorou, et Y. Kakitsubata. 2012. « Skeletal Muscle Disease: Patterns of MRI Appearances ». *The British Journal of Radiology* 85 (1020): e1298-1308. https://doi.org/10.1259/bjr/14063641.

157- Tingart, Markus J., Maria Apreleva, Janne T. Lehtinen, Brian Capell, William E. Palmer, et Jon J. P. Warner. 2003. « Magnetic Resonance Imaging in Quantitative Analysis of Rotator Cuff Muscle Volume ». *Clinical Orthopaedics and Related Research*, nº 415 (octobre): 104-10. https://doi.org/10.1097/01.blo.0000092969.12414.e1.

158- Tonson, Anne, Sébastien Ratel, Yann Le Fur, Patrick Cozzone, et David Bendahan. 2008. « Effect of Maturation on the Relationship between Muscle Size and Force Production ». *Medicine and Science in Sports and Exercise* 40 (5): 918-25. https://doi.org/10.1249/MSS.0b013e3181641bed.

159- Valentin, Stephanie, Tobey DeMott Yeates, Theresia Licka, et James Elliott. 2015. « Inter-Rater Reliability of Trunk Muscle Morphometric Analysis ». *Journal of Back and Musculoskeletal Rehabilitation* 28 (1): 181-90. https://doi.org/10.3233/BMR-140552.

160- Van Dijk, J. Gert, Willem Pondaag, Sonja M. Buitenhuis, Erik W. Van Zwet, et Martijn J. A. Malessy. 2012. « Needle Electromyography at 1 Month Predicts Paralysis of Elbow Flexion at 3 Months in Obstetric Brachial Plexus Lesions ». *Developmental Medicine and Child Neurology* 54 (8): 753-58. https://doi.org/10.1111/j.1469-8749.2012.04310.x.

161- Van Gelein Vitringa, Valerie M., Richard Jaspers, Margriet Mullender, Willem J. Ouwerkerk, et Johannes A. Van Der Sluijs. 2011. « Early Effects of Muscle Atrophy on Shoulder Joint Development in Infants with Unilateral Birth Brachial Plexus Injury ». *Developmental Medicine and Child Neurology* 53 (2): 173-78. https://doi.org/10.1111/j.1469-8749.2010.03783.x.

162- Vanmechelen, Inti M., Adam P. Shortland, et Jonathan J. Noble. 2017. « Lower Limb Muscle Volume Estimation from Maximum Cross-Sectional Area and Muscle Length in Cerebral Palsy and Typically Developing Individuals ». *Clinical Biomechanics (Bristol, Avon)* 51 (novembre): 40-44. https://doi.org/10.1016/j.clinbiomech.2017.11.004.

163- Vaz, Daniela Virgínia, Marisa Cotta Mancini, Maíra Ferreira do Amaral, Marina de Brito Brandão, Adriana de França Drummond, et Sérgio Teixeira da Fonseca. 2010. « Clinical Changes during an Intervention Based on Constraint-Induced Movement Therapy Principles on Use of the Affected Arm of a Child with Obstetric Brachial Plexus Injury: A Case Report ». *Occupational Therapy International* 17 (4): 159-67. https://doi.org/10.1002/oti.295.

164- Veeger, H. E. J., et F. C. T. van der Helm. 2007. « Shoulder Function: The Perfect Compromise between Mobility and Stability ». *Journal of Biomechanics* 40 (10): 2119-29. https://doi.org/10.1016/j.jbiomech.2006.10.016.

165- Vidt, Meghan E., Melissa Daly, Michael E. Miller, Cralen C. Davis, Anthony P. Marsh, et Katherine R. Saul. 2012. « Characterizing Upper Limb Muscle Volume and Strength in Older Adults: A Comparison with Young Adults ». *Journal of Biomechanics* 45 (2): 334-41. https://doi.org/10.1016/j.jbiomech.2011.10.007.

166- Vidt, Meghan E., Anthony C. Santago, Christopher J. Tuohy, Gary G. Poehling, Michael T. Freehill, Robert A. Kraft, Anthony P. Marsh, Eric J. Hegedus, Michael E. Miller, et Katherine R. Saul. 2016. « Assessments of Fatty Infiltration and Muscle Atrophy From a Single Magnetic Resonance Image Slice Are Not Predictive of 3-Dimensional Measurements ». *Arthroscopy: The Journal of Arthroscopic & Related Surgery: Official Publication of the Arthroscopy Association of North America and the International Arthroscopy Association* 32 (1): 128-39. https://doi.org/10.1016/j.arthro.2015.06.035.

167- Waters, P. M., G. R. Smith, et D. Jaramillo. 1998. « Glenohumeral Deformity Secondary to Brachial Plexus Birth Palsy ». *The Journal of Bone and Joint Surgery. American Volume* 80 (5): 668-77.
166- Waters, Peter M. 2005. « Update on Management of Pediatric Brachial Plexus Palsy ». *Journal of Pediatric Orthopedics. Part B* 14 (4): 233-44.

168- Waters, Peter M., James T. Monica, Brandon E. Earp, David Zurakowski, et Donald S. Bae. 2009. « Correlation of Radiographic Muscle Cross-Sectional Area with Glenohumeral Deformity in Children with Brachial Plexus Birth Pasy ». *The Journal of Bone and Joint Surgery. American Volume* 91 (10): 2367-75. https://doi.org/10.2106/JBJS.H.00417.

169- Weizsaecker, K., J. E. Deaver, et W. R. Cohen. 2007. « Labour Characteristics and Neonatal Erb's Palsy ». *BJOG: An International Journal of Obstetrics and Gynaecology* 114 (8): 1003-9. https://doi.org/10.1111/j.1471-0528.2007.01392.x.

170- Wickham, J. B., et J. M. Brown. 1998. « Muscles within Muscles: The Neuromotor Control of Intra-Muscular Segments ». *European Journal of Applied Physiology and Occupational Physiology* 78 (3): 219-25. https://doi.org/10.1007/s004210050410.

171- Wood, L. E., S. Dixon, C. Grant, et N. Armstrong. 2004. « Elbow Flexion and Extension Strength Relative to Body or Muscle Size in Children ». *Medicine and Science in Sports and Exercise* 36 (11): 1977-84. https://doi.org/10.1249/01.MSS.0000145453.02598.7E.

172- Wu, Ed X., Haiying Tang, Christopher Tong, Steve B. Heymsfield, et Joseph R. Vasselli. 2008. « In Vivo MRI Quantification of Individual Muscle and Organ Volumes for Assessment of Anabolic Steroid Growth Effects ». *Steroids* 73 (4): 430-40. https://doi.org/10.1016/j.steroids.2007.12.011.

173- Wu, Ge, Frans C. T. van der Helm, H. E. J. (DirkJan) Veeger, Mohsen Makhsous, Peter Van Roy, Carolyn Anglin, Jochem Nagels, et al. 2005. « ISB recommendation on definitions of joint coordinate systems of various joints for the reporting of human joint motion—Part II: shoulder, elbow, wrist and hand ». *Journal of Biomechanics* 38 (5): 981-92.

https://doi.org/10.1016/j.jbiomech.2004.05.042.

174- Yang, Lynda J.-S. 2014. « Neonatal Brachial Plexus Palsy--Management and Prognostic Factors ». *Seminars in Perinatology* 38 (4): 222-34. https://doi.org/10.1053/j.semperi.2014.04.009.

175- Yilmaz, Volkan, Ebru Umay, Nihal Tezel, et Ibrahim Gundogdu. 2018. « Timing of Rehabilitation in Children with Obstetric Upper Trunk Brachial Plexus Palsy ». *Child's Nervous System: ChNS: Official Journal of the International Society for Pediatric Neurosurgery* 34 (6): 1153-60. https://doi.org/10.1007/s00381-018-3790-1.

176- Zafeiriou, Dimitrios I., et Katerina Psychogiou. 2008. « Obstetrical Brachial Plexus Palsy ». *Pediatric Neurology* 38 (4): 235-42. https://doi.org/10.1016/j.pediatrneurol.2007.09.013.

VIII Annexes

Annexe 1: muscles du membre supérieur, innervation, mobilisation(s) principale(s)

Les éléments contenus dans ce tableau proviennent des articles Raducha J 2017 et Kattan AE 2011.

muscle	nerf	racine	mobilisation(s) principale(s)
Trapeze	-accessoire (faisceau supérieur) -nerf du trapèze	11e paire crânienne, C3C4	adducteur (rétraction) et fixateur de la scapula contre le thorax
Grand dorsal	thoraco dorsal	C6C8 (faisceau postérieur)	adducteur et rotateur médial du bras/ adducteur (rétraction) et abaisseur de la scapula
Elevateurs de la scapula	scapulaire dorsal	C5 (racine C5)	élévateur de la scapula
Rhomboides	scapulaire dorsal	C5 (racine C5)	adducteur (rétraction) de la scapula
Grand pectoral	pectoral latéral	C5C6 (faisceau latéral)	adducteur, fléchisseur et rotateur interne du bras
Petit pectoral	pectoral médial	C8T1 (faisceau médial)	adducteur du bras
Subclavier	subclavier	C5C6 (tronc supérieur)	limitée
Dentelé antérieur	thoracique long	C5C7 (racines C5C6C7)	abducteur (protraction) de la scapula
Deltoide	axillaire	C5C6	abducteur du bras, fléchisseur/extenseur du bras selon les chefs

Supraépineux	supra-scapulaire	C5C6 (tronc supérieur)	abducteur et fléchisseur du bras
Infraépineux	supra-scapulaire	C5C6 (tronc supérieur)	rotateur externe du bras
Petit rond	axillaire	C5C6	rotateur externe du bras
Grand rond	subscapulaire inférieur	C5C6 (faisceau postérieur)	extenseur du bras
Subscapulaire	subscapulaire supérieur et inférieur	C5C6 (faisceau postérieur)	rotateur interne du bras
Biceps brachial	musculocutané	C5C7	fléchisseur de l'avant-bras, supinateur
Coracobrachial	musculocutané	C5C7 (faisceau latéral)	fléchisseur et adducteur du bras
Brachial	musculocutané	C5C7	fléchisseur de l'avant-bras
Brachio-radial	radial	C5C7	fléchisseur de l'avant-bras
Triceps brachial	radial	C6C8	extenseur de l'avant-bras
Rond pronateur	médian	C8T1	pronateur de l'avant-bras
Fléchisseur radial du carpe	médian	C6C7	fléchisseur du poignet
Long palmaire	médian	C6C7	tenseur de l'aponévrose palmaire et fléchisseur de la main
Fléchisseur ulnaire du carpe	ulnaire	C8T1	fléchisseur et adducteur de la main
Supinateur	radial	C5C6	supinateur de l'avant-bras
Carré pronateur	médian	C8T1	pronateur de l'avant-bras
Long extenseur radial du carpe	radial	C7C8	extenseur et abducteur de la main
Extenseur ulnaire du carpe	radial	C5T1	extenseur et adducteur de la main

Annexe 2: supporting information article 1

S1 Table : Prisma checklist

S2 Table : Quality assessment of the articles included in the review

S3 Table: Description of the population and MRI technique in the articles included

F: female, M: male, SD: standard deviation, NR: not reported

RF: rectus femoris, VI: vastus intermedius, VL: vastus lateralis, VM : vatsus medialis, Qua : quadriceps, Pir : Piriformis, GlMi : Gluteus Minimus, GlMe : Gluteus Medius, GlMa : Gluteus Maximus, FCU: flexor carpi ulnaris, ECU: extensor carpi ulnaris, Sspi: Supraspinatus, Ssca: Subscapularis, Ispi+Tmin: Infraspinatus and Teres minor, ES: Erector Spinae, M: multifidus, RA: rectus abdominis, Ps: Psoas, Sar: Sartorius, Gra: Gracilis, AddM: Adductor Magnus, Add L: Adductor longus, BFL: Biceps Femoris Long head, BFS: Biceps Femoris Short head, ST: Semi Tendinosus, SM: Semi Membranosus, GL: Gastrocnemius Lateralis, GM: Gastrocnemius Medialis, So+FHL: Soleus and flexor hallucis longus, TP: Tibialis Posterior, FDL: flexor digitorum longus, Per LBT: Peroneus (Longus, Brevis, Tertius), TA+EDL+EHL: tibialis anterior and extensor digitorum longus and extensor hallucis longus, So: Soleus, TS: triceps surae, TB: triceps brachii, TA: Tibialis Anterior, VLMI: Vastus Lateralis and Medius and Intermedius, TFL: tensor Fascia Lata, Add BLM: adductor (brevis, longus, magnus), Il: Iliacus , Obl: Obliquus (transversus abdominis, internus and externus obliquus), QL: Quadratus Lumborum, VLI: Vastus Lateralis and Intermedius together, VLMI: Vastus Lateralis and Medialis and Intermedius, BF: Biceps Femoris, SMT: Semi Membranosus and Tendinosis, ESM : erector spinae and multifidus, PT: pronator teres, ECRB : Extensor Carpi Radialis Brevis, EPL : Extensor Pollicis Longus, Br : Brachioradialis

FOV: Field of View, NEX: Number of Excitations, TR: Repetition Time, TE: Time to echo

S4 Table: metrological properties of techniques

ICC: intraclass correlation coefficient, mean diff: mean difference, SD: standard deviation, CV: coefficient of variation, SDD: smallest detectable difference, RMSE: root mean square error, SEE: standard error of the estimate, DSI: Dice similarity index, mean surf D: mean surface distance, max surf D: maximal surface distance, TC: Tannimoto coefficient, FNVF: false negative volume fraction, FPVF: false positive volume fraction, MVSF: muscle volume similarity fraction

RF: rectus femoris, VI: vastus intermedius, VL: vastus lateralis, VM : vatsus medialis, Qua : quadriceps, Pir : Piriformis, GlMi : Gluteus Minimus, GlMe : Gluteus Medius, GlMa : Gluteus Maximus, FCU: flexor carpi ulnaris, ECU: extensor carpi ulnaris, Sspi: Supraspinatus, Ssca: Subscapularis, Ispi+Tmin: Infraspinatus and Teres minor, ES: Erector Spinae, M: multifidus, RA: rectus abdominis, Ps: Psoas, Sar: Sartorius, Gra: Gracilis, AddM: Adductor Magnus, Add L: Adductor longus, BFL: Biceps Femoris Long head, BFS: Biceps Femoris Short head, ST: Semi Tendinosus, SM: Semi Membranosus, GL: Gastrocnemius Lateralis, GM: Gastrocnemius Medialis, So+FHL: Soleus and flexor hallucis longus, TP: Tibialis Posterior, FDL: flexor digitorum longus, Per LBT: Peroneus (Longus, Brevis, Tertius), TA+EDL+EHL: tibialis anterior and extensor digitorum longus and extensor hallucis longus, So: Soleus, TS: triceps surae, TB: triceps brachii, TA: Tibialis Anterior, VLMI: Vastus Lateralis and Medius and Intermedius, TFL: tensor Fascia Lata, Add BLM: adductor (brevis, longus, magnus), Il: Iliacus , Obl: Obliquus (transversus abdominis, internus and externus obliquus), QL: Quadratus Lumborum, VLI: Vastus Lateralis and Intermedius together, VLMI: Vastus Lateralis and Medialis and Intermedius, BF: Biceps Femoris, SMT: Semi Membranosus and Tendinosis, ESM : erector spinae and multifidus, PT: pronator teres, ECRB : Extensor Carpi Radialis Brevis, EPL : Extensor Pollicis Longus, Br : Brachioradialis

S5 Table: metrological properties of techniques

S1 Text: Search String

Supporting information

S1 Table : Prisma checklist

Section/topic	#	Checklist item	Reported on page #
TITLE			
Title	1	Identify the report as a systematic review, meta-analysis, or both.	1
ABSTRACT			
Structured summary	2	Provide a structured summary including, as applicable: background; objectives; data sources; study eligibility criteria, participants, and interventions; study appraisal and synthesis methods; results; limitations; conclusions and implications of key findings; systematic review registration number.	2
INTRODUCTION			
Rationale	3	Describe the rationale for the review in the context of what is already known.	3
Objectives	4	Provide an explicit statement of questions being addressed with reference to participants, interventions, comparisons, outcomes, and study design (PICOS).	4
METHODS			
Protocol and registration	5	Indicate if a review protocol exists, if and where it can be accessed (e.g., Web address), and, if available, provide registration information including registration number.	5
Eligibility criteria	6	Specify study characteristics (e.g., PICOS, length of follow-up) and report characteristics (e.g., years considered, language, publication status) used as criteria for eligibility, giving rationale.	5
Information sources	7	Describe all information sources (e.g., databases with dates of coverage, contact with study authors to identify additional studies) in the search and date last searched.	5
Search	8	Present full electronic search strategy for at least one database, including any limits used, such that it could be repeated.	5, appendix 2
Study selection	9	State the process for selecting studies (i.e., screening, eligibility, included in systematic review, and, if applicable, included in the meta-analysis).	5-6
Data collection process	10	Describe method of data extraction from reports (e.g., piloted forms, independently, in duplicate) and any processes for obtaining and confirming data from investigators.	6-7
Data items	11	List and define all variables for which data were sought (e.g., PICOS, funding sources) and any assumptions and simplifications made.	6-7

Risk of bias in individual studies	12	Describe methods used for assessing risk of bias of individual studies (including specification of whether this was done at the study or outcome level), and how this information is to be used in any data synthesis.	6
Summary measures	13	State the principal summary measures (e.g., risk ratio, difference in means).	NA (no meta analysis)
Synthesis of results	14	Describe the methods of handling data and combining results of studies, if done, including measures of consistency (e.g., I^2) for each meta-analysis.	NA (no meta analysis)

Section/topic	#	Checklist item	Reported on page #
Risk of bias across studies	15	Specify any assessment of risk of bias that may affect the cumulative evidence (e.g., publication bias, selective reporting within studies).	NA (no meta analysis)
Additional analyses	16	Describe methods of additional analyses (e.g., sensitivity or subgroup analyses, meta-regression), if done, indicating which were pre-specified.	NA (no meta analysis)
RESULTS			
Study selection	17	Give numbers of studies screened, assessed for eligibility, and included in the review, with reasons for exclusions at each stage, ideally with a flow diagram.	17, fig 1
Study characteristics	18	For each study, present characteristics for which data were extracted (e.g., study size, PICOS, follow-up period) and provide the citations.	17, 18, table 1 and appendix 4
Risk of bias within studies	19	Present data on risk of bias of each study and, if available, any outcome level assessment (see item 12).	17, appendix 3
Results of individual studies	20	For all outcomes considered (benefits or harms), present, for each study: (a) simple summary data for each intervention group (b) effect estimates and confidence intervals, ideally with a forest plot.	18, 33-35, 40-42, tables 1, 2 and appendix 5

Synthesis of results	21	Present results of each meta-analysis done, including confidence intervals and measures of consistency.	NA (no meta analysis)
Risk of bias across studies	22	Present results of any assessment of risk of bias across studies (see Item 15).	NA (no meta analysis)
Additional analysis	23	Give results of additional analyses, if done (e.g., sensitivity or subgroup analyses, meta-regression [see Item 16]).	NA (no meta analysis)
DISCUSSION			
Summary of evidence	24	Summarize the main findings including the strength of evidence for each main outcome; consider their relevance to key groups (e.g., healthcare providers, users, and policy makers).	36
Limitations	25	Discuss limitations at study and outcome level (e.g., risk of bias), and at review-level (e.g., incomplete retrieval of identified research, reporting bias).	42
Conclusions	26	Provide a general interpretation of the results in the context of other evidence, and implications for future research.	36-40
FUNDING			
Funding	27	Describe sources of funding for the systematic review and other support (e.g., supply of data); role of funders for the systematic review.	Declaration of interest

S2 Table: Quality assessment of the articles included in the review

Questions	1	2	3	4	5	6	7	8	9	10	11	12	13	14	15	subtotal, score/30	16	17	18	19	20	21	subtotal score /11	total score= Q score/100
Albracht 2008	2	0	1	2	2	**2**	2	2	0	2	0	2	2	0	1	20	1	2	2	0	0	0	5	61
Amabile 2016	2	2	2	2	1	1	2	2	0	1	0	2	2	2	2	23	0	2	1	0	0	0	3	63
Andrew 2015	2	0	0	1	1	1	2	2	2	0	0	1	2	2	2	18	0	2	1	0	0	0	3	51
Barnouin 2014	2	2	1	2	2	2	2	2	0	2	0	2	2	2	2	25	2	0	0	2	0	1	5	73
Barnouin 2015	2	2	2	2	2	2	2	1	0	2	0	2	2	0	2	23	2	2	2	0	0	0	6	71
Belavy 2011	1	2	2	0.5	2	2	2	2	0	2	0	1	2	2	2	22	2	2	1	0	0	0	5	66
Elliott 1997	1	0	0	1	0	1	2	2	1	0	0	1	2	1	1	13	0	0	0	1	0	0	1	34
Eng 2007	1	NA	1	0.5	2	2	2	2	0	1	0	1	2	1	2	17	2	2	2	1	0	0	7	62
Engstrom 2011	2	0	0	1.5	2	2	1	2	1	2	0	1	2	0	2	17	0	2	1	0	0	0	3	49
Jolivet 2014	1	0	0	1.5	2	2	1	2	0	1	0	1	2	2	1	15	0	2	2	0	0	0	4	46
Kim 2017	2	0	0	0	2	1	0	2	1	2	0	1	2	2	2	17	0	2	1	0	0	0	3	49
Lehtinen 2003	2	NA	0	1,5	2	2	2	1	1	2	0	2	1	1	2	19,5	2	2	1	1	1	0	7	68
Le troter 2016	2	2	0	2	2	1	2	2	1	1	0	1	2	2	2	22	2	2	2	0	2	0	8	73
Lund 2002	2	2	2	1.5	2	2	1	1	0	2	0	2	2	0	2	20	2	2	2	2	2	0	10	73
Marcon 2015	1	2	2	1,5	2	2	2	1	1	2	0	2	2	2	2	24,5	1	1	1	0	2	0	5	72
Mersmann 2015	2	2	1	2	2	2	2	2	0	2	0	2	2	0	2	23	1	2	2	0	0	0	5	68
Mersmann 2014	2	2	0	1.5	2	2	2	2	0	2	0	2	2	0	2	20	2	2	2	0	0	0	6	63
Moal 2014	1	0	1	2	2	1	2	2	1	2	0	2	1	0	2	19	0	2	1	2	2	0	7	63
Morse 2007	1	2	1	2	1	2	2	1	0	2	0	1	1	2	1	19	2	2	2	0	0	0	6	61
Nordez 2009	1	2	1	2	2	1	1	1	0	2	0	2	2	0	2	19	2	2	2	2	2	0	10	71
Popadic 2011	2	2	1	2	1	1	2	2	0	2	2	2	2	2	1	24	2	2	2	0	0	0	6	73
Skorupska 2016	2	2	2	1.5	2	2	2	2	2	2	0	2	2	1	1	24	0	0	0	1	0	1	2	63

Smeulders 2010	1	2	1	1.5	2	1	2	2	0	2	0	2	2	2	2	21	2	0	0	2	2	0	6	66
Springer 2012	1	2	1	2	2	1	2	1	0	2	0	1	2	0	2	19	2	0	0	2	2	0	6	61
Sudhoff 2009	2	2	2	1	2	1	2	1	0	1	0	2	2	2	2	22	0	2	2	2	0	0	6	68
Tingart 2003	1	NA	1	1	2	1	2	2	0	2	0	1	1	0	2	16	2	2	2	2	2	0	10	63
Tracy 2003	1	2	0	2	2	2	2	2	0	2	0	2	2	1	2	22	1	2	2	0	0	1	6	68
Valentin 2015	1	2	2	2	2	1	1	2	2	2	0	2	2	2	1	24	2	0	0	2	0	1	5	71
Vanmecheln 2017	1	2	2	1,5	2	2	2	2	0	1	0	2	2	2	2	23,5	2	2	2	0	0	0	6	72
Yamauchi 2017	2	2	2	2	1	2	2	2	1	2	2	2	2	0	2	26	2	2	2	0	0	0	6	78

S3 Table: Description of the population and MRI technique in the articles included

	Sample			Muscles evaluated	MRI			
	N of subjects (F, M)	**type**	**ages (years)**		**session**	**Strength and scanner, coil**	**sequence type**	**sequence parameters**
Albracht 2008 [52]	13 (13M)	healthy	29 (SD: 6)	GM, GL, SO	1 MRI	0.2T Esaote coil : NR	3D T1 weighted gradient echo	**TR**: 38 ms **TE**: 16 ms **FOV**: 159*159 mm **flip angle**: NR **NEX**: NR **slice orientation**: axial **slice thickness**: 2mm **slice gap**: 0 mm **resolution**: pixel spacing 0.625*0.625mm
Amabile 2016 [53]	23 (12F, 11M)	healthy	19.3 (SD: 0.8)	QL, ES, GlMa, GlMe, GlMi, AddOP, VLI, VM, TFL, RF, Gra, Sar, BFS, BLF, SM, ST, grouped in spine extensors/flexors, hip extensors/flexors, knee extensors/flexors, both sides	1 MRI	1.5T GE, coil ; NR	T1, turbo spin echo	**TR**: 427ms **TE**: 11.3ms **FOV**: 16 x 16 x 19.6cm **flip angle**: 160° **NEX**: NR **slice orientation**: axial **slice thickness**: 5mm **slice gap**: 0 mm **resolution**: pixel : 0.82*0.82 mm

Andrews 2015 [65]	-	patients with moderate to severe chronic obstructive pulmonary disease	> 50	Gra, Sar, BFL, RF, ST, BFS, SM, VI, VM, Add, VL, left side	1 MRI	1.5T GE, coil : NR	T1 weighted, fast spin echo	**TR**: 650ms **TE**: 8ms **FOV**: 40cm^3 **flip angle**: NR **NEX**: NR **slice orientation**: axial **slice thickness**: 5mm **slice gap**: 0 mm **resolution**: pixel : 0.78*0.78 mm
Barnouin 2014 [46]	20 (11F, 9M)	healthy	49.7	RF, VI, VL, VM, Qua, both sides	1 MRI	3T Siemens, quadrature birdcage body coil, sets of phased-array receiver coils	3D 3-point Dixon gradient echo	**TR**: 10msec **TE**: 2.75/3.95/5.15 msec **FOV**: 448*224*320 mm **flip angle**: 3° **NEX**: 1 **slice orientation:** axial **slice thickness:** 5mm **slice gap**: 3D **resolution:** matrix 448*224 *64

Barnouin 2015 [47]	20 (9F, 11M)	healthy	49,7	RF, VI, VL, VM, both sides	1 MRI	3T Siemens, coil : NR	T1 weighted, 3D 3-point dixon sequence	**TR**: 10 ms **TE**: 2.75/3.95 then 2.75/5.15 ms **FOV**: 448×224×320 mm **flip angle**: NR **NEX**: 1 **slice orientation**: axial **slice thickness**: 5mm **slice gap**: 0mm **resolution:** matrix: 448×224×64

Belavy 2011 [55]	20 (20M)	NR	NR	RF, VM, VL, VI, Sar, Gra,Add M, Add L, BFL, BFS,ST, SM, GL, GM, So+FHL, TP, FDL, Per LBT, TA +EDL + EHL, left side	1st MRI the day of bed rest, then at 2 week intervals (day 14, day 28, day 42 and day 56) through to the end of the bed-rest period	1.5T Siemens, coil : NR	Proton density turbo spin echo	*thigh, 35 images* **TR**: 6000msec **TE**: 15msec **FOV**: 480*480mm **flip angle**: 180° **NEX**: NR **slice orientation**: axial **slice thickness**: 10mm **slice gap**: 5mm **resolution**: matrix : 512*512 *lower leg, 30 images* **TR**: 4800msec **TE**: 15msec **FOV**: 340*340mm **flip angle**: 180° **NEX**: NR **slice orientation**: axial **slice thickness**: 10mm **slice gap**: 5mm **resolution**: matrix : 512*512

Elliot 1997 [66]	3 (NR)	NR	19-50	GM, GL, So	1 MRI	1.5T GE, birdcage extremity coil	T1 weighted, 3D fast gradient echo	**TR**: 100ms **TE**: 10ms **FOV**: 16 x 16 x 19.6cm **flip angle**: 30° **NEX**: NR **slice orientation**: 3D **slice thickness**: 3D **slice gap**: 3D **resolution**: voxel size: 2.73 mm
Eng 2007 [54]	17 (NR)	cadavers	82 (SD: 8)	PT (10times), ECRB (10 times), EPL (10 times), FCU (7 times), BR (6 times)	1 MRI	3T GE, coil : NR	T1 weighted, 3D fast spoiled gradient recalled echo pulse sequence	**TR**: 9.2msec **TE**: 3.9msec **FOV**:35 × 35 cm **flip angle**: 30° **NEX**: 1 **slice orientation**: sagittal **slice thickness**: 1.0mm **slice gap**: NR **resolution**: voxel dimension: 1 mm^3

Engstrom 2011 [67]	20 (20M)	healthy (cricket fast bowlers, athletic control subjects)	18–35 y	QL, Ps, ESM, both sides	1 MRI	1.5T Siemens, phased-array spinal coil	T1, turbo spin echo	**TR**: 650ms **TE**: 15ms **FOV**: 250 mm **flip angle**: NR **NEX**: 2 **slice orientation**: axial **slice thickness**: 7mm **slice gap**: 0 mm **resolution**: pixel : 0.98*0.98 mm
Jolivet 2014 [68]	4 (NR)	NR	28 (SD: 2.7)	RF, VLMI, Sar, TFL, BFS, BFL, ST, ST, Gra	1 MRI	1.5T Philips, Q body coil	T1 spin echo	**TR**: 680ms **TE**: 50ms **FOV**: NR **flip angle**: NR **NEX**: NR **slice orientation**: axial **slice thickness**: 10 mm **slice gap**: NR **resolution**: 0.78*0.78 mm

Kim 2017 [29]	5 (-'-)	NR	NR	Sspi	1 MRI	3T, coil : NR	3D	**TR**: NR **TE**: NR **FOV**: NR **flip angle**: NR **NEX**: NR **slice orientation**: sagittal **slice thickness**: 0.7mm **slice gap**: 3D **resolution**: pixel : 0.63*0.63mm
Lehtinen 2003 [56]	10 (6F, 4M)	cadavers	76 (67-82)	Sspi,Ssca, Ispi+Tmin	1 MRI	1.5T GE, shoulder coil	T1 weighted gradient echo	**TR**: 100 ms **TE**: minimum **FOV**: 260*260 mm **flip angle**: NR **NEX**: 1 **slice orientation**: coronal **slice thickness**: 5mm **slice gap**: 5mm **resolution:** matrix: 256*128

Le Troter 2016 [48]	7 (7M)	healthy	32 (SD: 7)	RF, VI, VM, VL, Qua, right side	2 MRI sessions repeated twice	1.5T Siemens, flexible surface 6-channel body coil	T1-weighted, gradient echo	**TR**: 549 ms **TE**: 13 ms **FOV**: 220*220 mm2 **flip angle**: NR, **NEX**: NR, **slice orientation**: axial, **slice thickness**: 6mm, **slice gap**: 6mm, **resolution**: matrix 576 × 576
Lund 2002 [49]	11 (4F, 7 M)	healthy	24–40	TA+EDL+EHL, left side	1 MRI	1.5T Philips, knee coil	T2 weighted fast-field echo fat-saturated (spectral inversion recovery, SPIR)	**TR**: 56 ms **TE**: 14 ms **FOV**:180 *180 mm **flip angle**:15° **NEX**: NR **slice orientation**: axial **slice thickness**: 1.5 mm **slice gap:** 0mm **resolution:** matrix: 256*256

Marcon 2015 [9]	34 (12F, 22M)	persons with ACL reconstructions	F: 31.3 (SD: 8.8) M: 30.9 (SD: 6.5)	Qua	1 MRI	1.5T GE, coil : NR	T1 weighted, 3D spoiled dual gradient-echo water signal only	**TR**: 6.14 ms **TE**: 2.1/4.2 ms **FOV**: NR **flip angle**: 5° **NEX**: 2 **slice orientation**: axial **slice thickness**: 6mm **slice gap**: 3D **resolution:** matrix: 320*224
Mersmann 2014 [57]	21 (NR)	healthy	25 (SD: 8)	GM, GL, SO, TS, right side	1 MRI	1.5 T Siemens, coil : NR	T1, gradient echo	**TR**: 3.11 ms **TE**: 1.18 ms **FOV**: 244*449 mm **flip angle**: NR **NEX**: NR **slice orientation**: axial **slice thickness**: 1.8mm **slice gap**: 0mm **resolution**: NR

Mersmann 2015 [58]	37 (20F, 17M)	healthy	W: 31 (SD: 17) M: 32 (SD: 16)	VL, VM, VI, one side	1 MRI	1.5T Siemens, coil : NR	T1 weighted, turbo spin echo	**TR**: 641 ms **TE**: 11 ms **FOV**: 230*420 mm **flip angle**: NR **NEX**: NR **slice orientation**: axial **slice thickness**: 4mm **slice gap**: 0.8mm **resolution**: NR

Moal 2014 [59]	2 (2F)	healthy	35, 38	Add BLM, BF, ES, GlMa, GlMe, GlMi, Gra, Il, Obl, Ps, QL, RA, RF, Sar, SMT, TFL, VLI, VM	1 MRI, 2 sequences	3T Siemens, 24-channel spine matrix coil and three 4-channel flex coils	T1weighted turbo spin echo, T1 weighted turbo spin echo for the 3 point Dixon method	*T1weighted TSE* **TR**: 1220 ms **TE**: 11 ms **FOV**: NR **flip angle**: 150° **NEX**: NR **slice orientation**: axial **slice thickness**: 5mm **slice gap**: 5mm **resolution**: 0.98*0.98mm, *T1 weighted TSE for the 3 point Dixon method* **TR**: 829 ms **TE**: 15.7 ms **FOV**: NR **flip angle**: 150° **NEX**: NR **slice orientation**: axial **slice thickness**: 5mm **slice gap**: 5mm **resolution**: pixel : 0.98*0.98mm

Morse 2007 [60]	18 (18M)	healthy	23.9 (SD: 3.4)	Qua, VL, VM, VI, RF, right side	1 MRI	0.2T Esaote coil : NR	T1 weighted, gradient echo	**TR**: 100 ms **TE**: 16 ms **FOV**: 330*254 mm **flip angle**: NR **NEX**: NR **slice orientation**:11 axial planes **slice thickness**: 5mm **slice gap**: NR **resolution**: matrix 256 * 256 11 slices along the femur
Nordez 2009 [27]	10 (10M)	healthy	29 (SD: 4)	Qua (VL+VI+VM+RF)	1 MRI	1.5T Siemens, angiography radiofrequency coil	volume interpolated GRE T1	**TR**: 4.47 ms **TE**: 2.10 ms **FOV**: 400*400 mm flip angle: NR **NEX**: NR **slice orientation**: axial **slice thickness**: 4mm **slice gap**: 0mm **resolution**: voxel: 0.78 *0.78*4 mm

Popadic 2011 [50]	35 (35M)	healthy	21.6 (SD: 2.5)	TB, both sides	2 MRIs 1 before/ 1 after training	1.5T Siemens extremity coil	T1 weighted, gradient echo	**TR**: 232msec **TE**: 4.76msec **FOV**: 162*288 mm **flip angle**: NR **NEX**: NR **slice orientation**: axial **slice thickness**: 10mm **slice gap**: 3mm **resolution**: matrix 288*512
Skorupska 2016 [61]	100 (63F, 37M)	71 low back pain, 29 healthy	low back pain 47.7 (SD: 8.4); healthy 47.6 (SD: 9.9)	Pir, GlMi, GlMe, GlMa, both sides	1 MRI	1.5T GE, coil : NR	T2 weighted	**TR**: 3500 ms **TE**: 110 ms **FOV**: 320*324 mm **flip angle**: NR **NEX**: NR **slice orientation**: sagittal **slice thickness**: 4mm **slice gap**: 0mm **resolution**: matrix 320*224

Smeulders 2010 [62]	10 (5F, 5M)	healthy	30 (20-35)	FCU, ECU, right side	2 MRIs, 1 week between sessions	3T Philips, flexibles surface coils with two elliptical elements	T1 weighted axial spin echo	**TR:** 500 ms **TE**: 12 ms **FOV**: 160*160 mm **flip angle**: NR **NEX**: NR **slice orientation**: axial **slice thickness**: 6mm **slice gap**: NR **resolution**: matrix : 300*300

Springer 2012 [63]	10 (6F, 4M)	with unilateral total hip arthroplasty	61.8 (SD: 12.2; 35–76)	GlMe, GlMi, OE, both sides	1 MRI, 12 months after hip arthroplasty	1.5T Siemens, flexible wraparound phased-aray surface coil	T1 weighted turbo spin echo	*OE* **TR**: 667 ms **TE**: 12 ms **FOV**: 400*400 mm **flip angle**: 150° **NEX**: NR **slice orientation**: coronal **slice thickness**: 5mm **slice gap**: NR **resolution**: matrix 512*256 *Glutei muscles* **TR**: 667 ms **TE**: 12 ms **FOV**: 420*275.52 mm **flip angle**: NR **NEX**: NR **slice orientation**: axial **slice thickness**: 6mm **slice gap**: NR **resolution**: matrix 512*168

Sudhoff 2009 [64]	10 (10M)	healthy	29 (SD: 4)	SM, ST, BFS, BFL, Sar, TFL, Gra, VLI, VM, RF, GM, GL	1 MRI	1.5T Siemens, , angiography radiofrequency coil	volume interpolated GRE T1	**TR**: NR **TE**: NR **FOV**: NR **flip angle**: NR **NEX**: NR **slice orientation**: axial **slice thickness**: 4 mm **slice gap**: 0 mm **resolution**: pixel : 0.78*0.78 mm
Tingart 2003 [25]	10 (6F, 4M)	cadavers	76 (67-82)	Sspi,Ssca, Ispi+Tmin	1 MRI	1.5T GE, linear shoulder array coil	T1 weighted fast spin echo	**TR**: 650msec **TE**: 10msec **FOV**: 180*180 mm **flip angle**: NR **NEX**: NR **slice orientation**: oblique sagittal **slice thickness**: 3mm **slice gap**: 0mm **resolution**: matrix 512*224

Tracy 2003 [26]	47 (21F, 26 M)	healthy	young: 26 (SD: 3) (N= 23); older: 69 (SD: 3) (N= 24)	Qua, trained side	2 MRIs 1 before/ 1 after training	1.5T Picker Edge, coil : NR	T1 weighted	**TR**: 700 ms **TE**: 14 ms **FOV**: 50cm **flip angle**: NR **NEX**: NR **slice orientation**: axial **slice thickness**: 9mm **slice gap**: 1mm **resolution**: matrix 256*256
Valentin 2015 [45]	10 (10M)	healthy	5 young (18-25) 5 mature (45-60)	ES, M, RA, Ps both sides	1 MRI	1.5T Siemens, **coil** : NR	T1 weighted gradient echo	**TR**: 9.3 ms **TE**: 4.6 ms **FOV**: rectangular, 78% **flip angle**: NR **NEX**: NR **slice orientation**: axial **slice thickness**: 10mm **slice gap**: NR **resolution**: NR

Vanmechelen 2017 [51]	44 (11F, 33M)	21 bilateral cerebral palsy, 23 healthy	cerebral palsy: 14.7 (SD: 3) helathy: 16.8 (SD: 3.3)	GM, SOL, TA, RF, SM, ST, left side	1 MRI	1.5T Philips (22 subjects) 3T Philips (22 subjects) , quadrature body coil	T2 weighted, 3 point Dixon	*For 1,5T scanner* **TR:** 4.6ms **TE:** 13ms **FOV:** NR **flip angle:** 20° **slice orientation:** axial **slice thickness:** 5mm **slice gap:** NR **resolution:** voxel size 0.9*0.9*0.5mm *For 3T scanner* **TR:** 2.11ms **TE:** 5.2ms **FOV:** NR **flip angle:** 10° **slice orientation:** axial **slice thickness:** 5mm **slice gap:** NR **resolution:** voxel size 0.9*0.9mm

Yamauchi 2017 [28]	24 (12F, 12M)	12 with knee osteoarthritis grade 1 and 12 with knee osteoarthritis grade >=2	74.3 (SD: 4.4)	VL, VM, VI, RF, SM, ST, BFS, BFL, painful side	1 MRI	1.5T Toshiba	T1 weighted, turbo spin-echo coil: NR	**TR**: 625ms **TE**: 15ms **FOV**: 250mm **flip angle**: NR **NEX**: NR **slice orientation**: axial **slice thickness**: 10mm **slice gap**: 0mm **resolution**: matrix: 512*512

F: female, M: male, SD: standard deviation, NR: not reported
RF: rectus femoris, VI: vastus intermedius, VL: vastus lateralis, VM : vatsus medialis, Qua : quadriceps, Pir : Piriformis, GlMi : Gluteus Minimus, GlMe : Gluteus Medius, GlMa : Gluteus Maximus, FCU: flexor carpi ulnaris, ECU: extensor carpi ulnaris, Sspi: Supraspinatus, Ssca: Subscapularis, Ispi+Tmin: Infraspinatus and Teres minor, ES: Erector Spinae, M: multifidus, RA: rectus abdominis, Ps: Psoas, Sar: Sartorius, Gra: Gracilis, AddM: Adductor Magnus, Add L: Adductor longus, BFL: Biceps Femoris Long head, BFS: Biceps Femoris Short head, ST: Semi Tendinosus, SM: Semi Membranosus, GL: Gastrocnemius Lateralis, GM: Gastrocnemius Medialis, So+FHL: Soleus and flexor hallucis longus, TP: Tibialis Posterior, FDL: flexor digitorum longus, Per LBT: Peroneus (Longus, Brevis, Tertius), TA+EDL+EHL: tibialis anterior and extensor digitorum longus and extensor hallucis longus, So: Soleus, TS: triceps surae, TB: triceps brachii, TA: Tibialis Anterior, VLMI: Vastus Lateralis and Medius and Intermedius, TFL: tensor Fascia Lata, Add BLM: adductor (brevis, longus, magnus), Il: Iliacus , Obl: Obliquus (transversus abdominis, internus and externus obliquus), QL: Quadratus Lumborum, VLI: Vastus Lateralis and Intermedius together, VLMI: Vastus Lateralis and Medialis and Intermedius, BF: Biceps Femoris, SMT: Semi Membranosus and Tendinosis, ESM : erector spinae and multifidus, PT: pronator teres, ECRB : Extensor Carpi Radialis Brevis, EPL : Extensor Pollicis Longus, Br : Brachioradialis
FOV: Field of View, NEX: Number of Excitations, TR: Repetition Time, TE: Time to echo

S4 Table: metrological properties of techniques

	Measure	Muscle	Concurrent validity	Intra rater reliability	Inter rater reliability	Other	Duration
Albracht 2008 [52]	single slice manual segmentation (CSAmax), muscle length (ML) and shape factor (p), volume: p* CSAmax* ML	GM	RMSE: 7%	-	-	-	
		GL	RMSE: 10%	-	-	-	
		SO	RMSE: 5%	-	-	-	
Amabile 2016 [53]	use of ACSAmax and muscle length (ML) obtained using full muscle reconstruction and shape factor (p), volume: p* ACSAmax* ML	QL	volume RMSE: 17.7%	-	-	-	-
		ES	volume RMSE: 5.2%	-	-	-	-
		GlMa	volume RMSE: 5.9%	-	-	-	-
		GlMe	volume RMSE: 6.6%	-	-	-	-
		GlMi	volume RMSE: 11.9%	-	-	-	-
		Add OP	volume RMSE: 7.1%	-	-	-	-
		VLI	volume RMSE: 4.8%	-	-	-	-
		VM	volume RMSE: 5.2%	-	-	-	-
		TFL	volume RMSE: 9.0%	-	-	-	-
		RF	volume RMSE: 4.6%	-	-	-	-
		Gra	volume RMSE: 5.0%	-	-	-	-
		Sar	volume RMSE: 4.7%	-	-	-	-
		BFS	volume RMSE: 8.8%	-	-	-	-
		BFL	volume RMSE: 7.1%	-	-	-	-
		SM	volume RMSE: 6.7%	-	-	-	-

		ST	volume RMSE: 7.4%		-	-	-	-
	reduced MRI set method: model using the DPSO method, with 5 segmented slices, volume predicted from a multilinear regression	Spine flexors (iliacus, psoas)	volume RMSE: 5.7%		-	-	-	-
		spine extensors (ES+QL)	volume RMSE: 10.7%		-	-	-	-
		hip flexors (Add+Gra+Il+Ps+RF+Sar+TFL)	volume RMSE: 9.7%		-	-	-	-
		hip extensors (BFL+ BFS+GlMa+SM+ST	volume RMSE: 8.7%		-	-	-	-
		knee flexors (BFS + BFL+ Gra+Sar+SM+ST)	volume RMSE: 6%		-	-	-	-
		knee extensors (RF+ VLI+ VM)	volume RMSE: 6%		-	-	-	-
Andrews 2015 [65]	interactive segmentation using shape priors + statistical shape model	Gra	mean Surf D: 1.54; SD:0.67mm	DSI: 0.72; SD:0.24	-	-	-	50+/- 4.3minutes per image to run
		Sar		DSI: 0.71; SD:0.27	-	-	-	
		BFL		DSI: 0.70; SD:0.16	-	-	-	
		RF		DSI: 0.75; SD: 0.20	-	-	-	
		ST		DSI: 0.80; SD:0.16	-	-	-	
		BFS		DSI:0.89; SD:0.08	-	-	-	
		SM		DSI: 0.85; SD:0.11	-	-	-	
		VI		DSI: 0.79; SD:0.06	-	-	-	
		VM		DSI: 0.93; SD:0.06	-	-	-	
		Add		DSI: 0.81; SD:0.11	-	-	-	
		VL		DSI: 0.86; SD:0.03	-	-	-	
Barnouin 2014 [46]	slice-by-slice manual segmentation, volume: muscle tissue area * interslice distance	RF	-		-	ICC: 0.995 significant inter rater difference mean diff: -3.8%; SD: 2.9%	contribution of individual muscles within QF significant interoperator differences for VI	5 hours/subject (whole segmentation procedure)

		VI	-	-	ICC:0.997 no significant inter rater difference mean diff: -1.4%; SD: 3.3%	and VL, mean diff: 1.8% for VI; 1.3% for VL ICC 0.836-0.995	
		VL	-	-	ICC: 0.988 significant inter rater difference mean diff: -4.5%; SD: 2.9%		
		VM	-	-	ICC: 0.992 significant inter rater difference mean diff: -3.1%; SD: 1.9%		
		Qua	-	-	ICC: 0.995 significant inter rater difference mean diff: -3.1%; SD: 1.8%		
Barnouin 2015 [47]	slice-by-slice manual segmentation, volume: cylinder/ cone method/ 3d-order polynomial regression/ 4th-order polynomial regression	RF, VI, VL, VM	effect of the method statistically significant for all the muscles. mean diff < 1% (all individuals and muscles)	-	-	mean CV between methods= 0.41% (SD=0.45%, range: 0.03–2.75%)	-

	manual segmentation of a reduced number of slices, volume: cylinder/ cone method/ 3d-order polynomial regression/ 4th-order polynomial regression		inter-slice distances >5 cm: none of the methods correctly estimate the muscle volume (error> 5%). increasing the distance between slices: greater inter-individual variability	-	-	effect of inter-slice distance very significant for the TC method and the VM muscle. most stable method: cylinder method	-

Belavy 2011 [55]	manual segmentation of a reduced number of slices, selection of the segmented slices with 5 algorithms including subalgorithms with various number of slices (1-largest CSA and the sum of the 3,6,9 … largest CSA measurement/ 2-largest CSA with immediately adjacent CSAs/ 3-same as 2 except every second images taken/ 4-method using CSA at 30, 40, 50, 80%/ 5- most psoximal CSA with every 2d, 3d, 4th... CSA measurements), volume: linear interpolation	RF, VM, VL, VI, Sar, Gra,Add M, Add L, BFL, BFS,ST, SM, GL, GM, SO+FHL, TP, FDL, PER LBT, TA +EDL + EHL, left side	As the number of slices included in the measure of muscle size increased, the correlation with muscle volume tended to approach 1. All the correlations were statistically significant. 366 individual CSA measurements for a typical data set (measurements from all of the muscles on one lower limb) Algorithms 1, 2 or 3, required 193, 191 or 232 individual CSA measurements to accurately estimate the volumes of all lower-limb muscles considered. Depending on the muscles, algorithms and subalgorithms differed.	-	-	-	-

Elliott, 1997 [66]	image based segmentation + manual segmentation correction algorithm for partial volume effect, volume: addition of the number of voxels	GM, GL, So	-	-	for 9 muscles (3 GM, 3GL, 3So) correlation coefficient: 0.99 max diff: 4.3%	-	average time to segment an individual muscle: 45 minutes.
Eng 2007 [54]	manual segmentation in the 3 planes, volume: addition of the number of voxels	PT	ICC: 0.97 mean diff: 8.4%	-	ICC: 0.97 mean diff: 8.8%	-	-
		ECRB	ICC: 0.93 mean diff: 7.7%	-		-	-
		EPL	ICC: 0.68 mean diff: 21.6%	-		-	-
		FCU	ICC: 0.91 mean diff: 9.8%	-		-	-
		BR	ICC: 0.93 mean diff: 17.2%	-		-	-
Engstrom 2011 [67]	atlas based + statistical shape based segmentation	QL	DSI: 0.86; SD:0.06 TC: 0.75; SD: 0.08 mean Surf D: 1.32mm; SD:0.60mm	-	-	results errors obtained from non rigid registration and 3D SSM segmentation methods alone were greater than atlas based + statistical shape based segmentation method	-
		Ps	DSI: 0.91; SD:0.03 TC: 0.84; SD:0.05 mean Surf D: 1.42mm; SD:0.51mm	-	-		-
		ESM	DSI: 0.92; SD:0.03 TC: 0.85; SD:0.06 mean Surf D: 1.81mm; SD:0.81mm	-	-		-

Jolivet 2014 [68]	improved DPSO	RF, VLMI, Sar, TFL, BFS, BFL, ST, SM, Gra	volume 6 manual contours required for ST muscle, 5 for BFS, RF and SAR and 4 for BFL,GRA, SM, TFL and VLMI, instead of 7 for RF and SAR, 6 for BFL, 5 for BFS, GRA, SM, TFL and ST, 4 for VLMI with the non-optimised method. point to surface distance 5 manual contours required for RF, SM, ST and VLMI muscles; 4 for BFS, BFL, SAR and TFL; 3 for GRA instead of 7 for Sar; 6 for BFL, RF, Gra, SM, ST, VLMI, 5 for BFS; 4 for TFL	-	-	-	-
Kim 2017 [29]	thresholding and manual post-processing	Sspi	-	-	DSI: 0.95 (SD: 0.012) kappa: 0.948 (SD:0.012)	-	-
	image based and shape based segmentation		DSI: 0.95 accuracy: 0.99 mean Surf D: 0.44mm max Surf D: 3.04mm	-	-	-	-
Lehtinen 2003 [56]	single slice manual segmentation (at the Y-shaped position), volume: calculated by the software	Sspi	mean volume: 27cm^3 (ref volume: 36cm^3); 2SD: 18cm^3	CV: 4.2%	CV: 1.6%	-	average time to complete the tracing of the 3 muscles: 70sec (30min for slice-by-slice segmentation)
		Ssca	mean volume: 80cm^3 (ref volume: 99cm3); 2SD: 50cm^3	CV: 4.5%	CV: 4.4%	-	
		Ispi+Tmin	mean volume: 87cm^3 (ref volume: 96cm^3); 2SD: 72cm^3	CV: 3.0%	CV: 2.7%	-	
	manual segmentation of 2 slices (at the Y-shaped position and at a defined more medial position), volume: calculated by the software	Sspi	mean volume: 32cm^3 (ref volume: 36cm^3); 2SD: 20cm^3	CV: 3.3%	CV: 1.6%	-	average time to complete the tracing of the 3 muscles: 115sec (30min for slice-by-slice segmentation)
		Ssca	mean volume: 91cm^3 (ref volume: 99cm3); 2SD: 61cm^3	CV: 3.5%	CV: 2.6%	-	
		Ispi+Tmin	mean volume: 89cm^3 (ref volume: 96cm^3); 2SD: 79cm^3	CV: 2.5%	CV: 1.0%	-	

Le Troter 2016 [48]	slice-by-slice manual segmentation, volume: cone method	RF	-	-	-	Interscan reliabilityy: ICC>= 0.98 for all the muscles	volume CV: 4.5%	-
		VI	-	-	-		volume CV: 2.1%	-
		VL	-	-	-		volume CV: 5.5%	-
		VM	-	-	-		volume CV: 1.7%	-
		Qua	-	-	-		volume CV: 2%	-
	atlas based segmentation (semi automated)	RF	volume ICC: 0.99; CV: 3.6% DSI: 0.89; SD:0.07 FNVF: 0.10; SD:0.06 FPVF: 0.10; SD:0.09 MVSF: 0.05; SD:0.09	-	-	-		-
		VI	volume ICC: 0.98; CV: 1.1% DSI: 00.94; SD:0.01 FNVF: 0.05; SD:0.02 FPVF: 0.05; SD:0.02 MVSF: 0.02; SD:0.02	-	-	-		-
		VL	volume ICC: 0.99; CV: 2.1% DSI: 0.93; SD: 0.03 FNVF: 0.07; SD: 0.03; FPVF: 0.07; SD: 0.05 MVSF: 0.03; SD: 0.04	-	-	-		-
		VM	volume ICC: 0.98; CV: 1.8% DSI: 0.95; SD: 0.04 FNVF: 0.06; SD:0.05 FPVF: 0.04; SD:0.04 MVSF: 0.02; SD:0.03	-	-	-		-
	atlas based segmentation (fully automated)	RF	volume ICC: 0.78; CV: 17.3% DSI: 0.84; SD:0.12 FNVF: 0.20; SD:0.24 FPVF: 0.33; SD:0.13 MVSF: 0.23; SD:0.24	-	-	best results obtained with the combination of 2 deformation fields resulting from the		-

		VI	volume ICC: 0.70; CV: 10.5% DSI: 0.87; SD:0.07 FNVF: 0.12; SD:0.11 FPVF: 0.13; SD:0.05 MVSF: 0.10; SD:0.07	-	-	non-parametric symmetric diffeomorphic normalization and the STEPS fusion algorythm,	-
		VL	volume ICC: 0.90; CV: 17.3% DSI: 0.88; SD:0.08 FNVF: 0.05; SD:0.05 FPVF: 0.23; SD:0.16 MVSF: 0.23; SD:0.23	-	-		-
		VM	volume ICC: 0.96; CV: 3.9% DSI: 0.91; SD:0.05 FNVF: 0.10; SD:0.06 FPVF: 0.08; SD:0.06 MVSF: 0.04; SD:0.04	-	-		-
Lund 2002 [49]	manual segmentation of a reduced number of slices (13 slices)	TA+EDL+EHL, left side	-	ICC: 0.99 significant difference mean diff: 0.07%	ICC: 0.96 significant difference mean diff: 4.7%	- no difference between cone and cylinder method using 50 slices - mean difference: 0.31% between cone and cylinder method using 8 slices	-
	slice-by-slice manual segmentation, volume: cylinder/ cone method		mean diff: 0.31ml, 2SD: 0.66ml	-	-		-
	manual segmentation of a reduced number of slices (8 slices), volume: cylinder method		mean diff: 0.3ml (0.004%); 2SD: -0.66ml	-	-		-

	manual segmentation of a reduced number of slices (8 slices), volume: cone method		-	-	-		-
Marcon 2015 [9]	manual segmentation of a reduced number of slices (every third slice), volume: NR	Qua	-	ICC: 0.90	-	-	-
	single slice manual segmentation (at 25cm above the knee joint), volume: NR	Qua	SEE: 8.1%	-	-	-	-
Mersmann 2014 [57]	single slice manual segmentation (CSA max), muscle length (ML) and shape factor (p), volume: p* ACSAmax* ML	SO	r^2: 0.864 no significant difference volume RMSE: 7.9%	-	-	-	-
		GM	r^2: 0.953 no significant difference volume RMSE: 4.8%	-	-	-	-
		GL	r^2: 0.849 no significant difference volume RMSE: 8.3%	-	-	-	-
Mersmann 2015 [58]	single slice manual segmentation (CSA max), muscle length (ML), and shape factor (p), volume: p* ACSAmax* ML	VI	r^2: 0.955 no significant difference volume RMSE: 5.2%	-	-	-	-
		VL	r^2: 0.972 no significant difference volume RMSE: 4.6%	-	-	-	-
		VM	r^2: 0.943 no significant difference volume RMSE: 5.7%	-	-	-	-

Moal 2014 [59]	DPSO method T1 images	Add BLM, BF, ES, GlMa, GlMe, GlMi, Gra, Il, Obl, Ps, QL, RA, RF, Sar, SMT, TFL, VLI, VM	on all the muscles, mean diff: 1.10%; SD: 2.50%; mean point to surface distance 2RMSE< 3mm, (0.88mm-11.30mm)	on all the muscles, mean CV: 2.16%; SD: 0.86%; range: 0.95 - 3.75% GlMi: CV> 5%	on all the muscles, mean CV: 2.55%; SD: 1.07%; range: 0.95- 5.78% GlMi, GlMe, RA: CV> 5%	no significant differences between sequences for intra and inter rater reliability	time to obtain a reconstruction reference method: 14-15 hours time to obtain a reconstruction DPSO method: 7 hours
	DPSO method Fat images		on all the muscles, mean diff: 2.19%; SD: 2.85%; mean point to surface distance 2RMSE< 3mm, (1.15mm-16.41mm)	on all the muscles, mean CV: 2.05%; SD: 1.01%; range: 0.90 - 5.62% GlMi: CV> 5%	on all the muscles, mean CV: 2.61%; SD: 1.82%; range: 0.93 - 11.80% GlMi, GlMe, RA: CV> 5%		
Morse 2007 [60]	single slice manual segmentation (CSAmax), volume: equation using length and CSA max	VL	r^2: 0.726	-	-	-	-
		VI	r^2: 0.810	-	-	-	-
		VM	r^2: 0.798	-	-	-	-
		RF	r^2: 0.694	-	-	-	-
		Qua	r^2: 0.945 SEE: 4.5%; SD: 2.7%, mean diff: 25.6 cm^3; 1.96SD: 250 cm^3	-	-	-	-
	single slice manual segmentation (CSA at 40% from the distal end of the femur), regression equation to estimate the maximum muscle cross-sectional area, volume: equation using length and CSA max	Qua	$r^{2:}$: 0.84 SEE: 26.8%; SD: 5.2% mean diff: 551 cm^3; 1.96SD: 141 cm^3	-	-	-	-

	single slice manual segmentation (CSA at 50% from the distal end of the femur), regression equation to estimate the maximum muscle cross-sectional area, volume: equation using length and ACSA max	Qua	r^2: 0.93 SEE : 12.5%; SD: 5.4% mean diff: 254cm^3; 1.96SD: 107 cm^3	-	-	-	-
	single slice manual segmentation (CSA at 60% from the distal end of the femur), regression equation to estimate the maximum muscle cross-sectional area, volume: equation using length and ACSA max	Qua	r^2: 0.90 SEE: 9.9%; SD: 5.7% mean diff: –190 cm^3; 1.96SD: 135 cm^3	-	-	-	-
Nordez 2009 [27]	slice-by-slice manual segmentation,volume using 3D shape	Qua (VL+VI+VM+RF)		ICC: 0.999 CV: 0.5%	ICC: 0.997 CV: 0.8%	global reliability: 1.1%	-

	manual segmentation of a reduced number of slices, volume: cone method		volume error decreased when the number of available slices increased for VL+VI, VM, RF, quadriceps	with 12 slices, mean diff: 0.7%; 1.96SD: 0.7%	-	-	cone method error higher than that of the Cavalieri and DPSO methods from 3 to 11 slices. Cavalieri method error higher than that of the DPSO method from 3 to 7 slices. Number of slices required to reach a given volume error different for the different methods.	-
	manual segmentation of a reduced number of slices, volume: Cavalieri formula			with 9 slices mean diff: 0.7%; 1.96SD: 0.9%	-	-		-
	manual segmentation of a reduced number of slices, cubic spline interpolation to estimate missing CSAs			with 5 slices mean diff: 1.0%; 1.96SD: 2.3%	-	-		-
	manual segmentation of a reduced number of slices, volume: DPSO			with 7 slices mean diff: 0.9%; 1.96SD: 1.1%	-	-		-
Popadic 2011 [50]	single slice manual segmentation (CSA max), humerus length (HL) volume: equation using CSA max, humerus length (HL), BMI	TB	mean volume change before/after training using multi slice calculation: +7.8% / using model A: +6.3% / using model CSAmax:	volume r^2: 0.830 RSE: 8.0%	-	-	-	-

	single slice manual segmentation (CSA max), humerus length (HL) volume: equation using CSA max, HL		+6.4% / using model CSA50%: +3.3% / using model CSA60%: +7%	volume r^2: 0.805 RSE: 8.55%	-	-	-	-
	single slice manual segmentation (CSA 50%), humerus length (HL) volume: equation using CSA50%, HL			volume r^2: 0.842 RSE=7.7%	-	-	-	-
	single slice manual segmentation (CSA 60%), humerus length (HL) volume: equation using CSA60%, HL			volume $r^{2:}$ 0.836 RSE:7.8%	-	-	-	-
Skorupska 2016 [61]	slice-by-slice manual segmentation, volume: addition of the voxels and multiplication by the voxel dimension	Pir	-		-	healthy: ICC: 0.94 low back pain: ICC: 0.97	-	-
		GlMi	-			healthy: ICC: 0.99 low back pain: ICC: 0.98	-	-
		GlMe	-		-	healthy: ICC: 0.984 low back pain: ICC: 0.848	-	-
		GlMa	-		-	healthy: ICC: 0.942 low back pain: ICC: 0.969	-	-

Smeulders 2010 [62]	slice-by-slice manual segmentation, volume: muscle tissue area * interslice distance	FCU	-	ICC:1.0 no significant difference mean diff: 0.21ml; SD: 0.26ml; CV: 0.8%	ICC: 0.99 no significant difference mean diff: 0.45ml; SD: 1.02ml; CV: 3.3%	Interscan reliability: ICC: 0.99 no significant difference mean diff: 0.27ml; SD: 1.11ml; CV: 3.6% SDD: 2.2 mL	-
		ECU	-	ICC:1.0 no significant difference mean diff: -0.08ml; SD: 0.30ml; CV: 1.8%	ICC: 0.99 significant difference mean diff: -0.87ml; SD: 0.94ml; CV: 5.7%	Interscan reliability: ICC: 0.99 no significant difference mean diff: -0.34ml; SD: 0.50 ml; CV: 3.0% SDD: 1.0 mL	-
Springer 2012 [63]	slice-by-slice manual segmentation, volume: NR	GlMe	-	no significant difference non operated side mean diff: 0.1%; 1.96SD: 5.4%; CV: 2.0% operated side mean diff: -0.7%; 1.96SD: 5.6%; CV: 2.4%	significant difference on both sides non operated side mean diff: 6.4%; 1.96SD: 13.7%; CV: 5.2% operated side mean diff: 10.2%; 1.96SD: 10.2%; CV: 4.6%	-	-

		GlMi	-	no significant difference non operated side mean diff: 1.0%; 1.96SD: 4.3%; CV: 5.2% operated side: mean diff: -2.5%; 1.96SD : 12.2%; CV: 18.8%	significant difference on both sides non operated side mean diff: 5.9%; 1.96SD: 5.8%; CV: 5.2% operated side mean diff: 5.2%; 1.96SD: 8.0%; CV:13.9%	-	-
		OE	-	no significant difference non operated side mean diff: -0.1%; 1.96SD: 2.6%; CV: 5.7% operated side: mean diff: -0.4%; 1.96SD: 3.2%; CV: 8.4%	no significant difference non operated side mean diff: 1.7%; 1.96SD: 6.1%; CV: 14% operated side mean diff: 0.8%; 1.96SD: 5.4%; CV:15%	-	-

Sudhoff 2009 [64]	slice-by-slice manual segmentation (T1 images), volume: using 3D shape	SM, ST, BFS, BFL, Sar, TFL, Gra, VLI, VM, RF, GM, GL	-	-	For one subject: mean diff<6%, except for the BFS, Sar, Gra (10%) point to surface distance 1RMSE<1mm, 2RMSE<3mm.	-	reconstruction of 12 muscles: 1h (12h when using manual slice-by-slice segmentation)
	DPSO	SM, 6 slices	for 2 subjects mean diff: 2.18%, point to surface distance error: 2.57mm	ICC: 0.99 mean diff: 5.8%; 2SD: 5.4% point to surface distance 2RMSE: 2.8mm	-	-	
		ST, 6 slices	for 2 subjects mean diff: 3.55% point to surface distance error: 3.06mm	ICC: 0.96 mean diff: 7.5%; 2SD: 6.5% point to surface distance 2RMSE: 2.7mm	-	-	
		BFL, 6 slices	for 2 subjects mean diff: 1.28% point to surface distance error: 1.60mm	ICC: 0.99 mean diff: 5.9%; 2SD: 5,6% point to surface distance 2RMSE: 3.3mm	-	-	

		BFS, 8 slices	for 2 subjects mean diff: 4.17% point to surface distance error: 2.40mm	ICC: 0.96 mean diff: 10.8%; 2SD: 10.6% point to surface distance 2RMSE: 2.7mm	-	-	
		SAR, 7 slices	for 2 subjects mean diff: 2.87% point to surface distance error: 3.49mm	ICC: 0.93 mean diff: 8.4%; 2SD: 10.9% point to surface distance 2RMSE: 3.6mm	-	-	
		TFL, 6 slices	for 2 subjects mean diff: 2.73% point to surface distance error: 1.29mm	ICC: 0.98 mean diff: 4.3%; 2SD: 6.0% point to surface distance 2RMSE: 3.1mm	-	-	
		GRA, 7 slices	for 2 subjects mean diff: 3.27% point to surface distance error: 2.51mm	ICC: 0.99 mean diff: 8.6%; 2SD: 5,2% point to surface distance 2RMSE: 3.1mm	-	-	

		VLI, 7 slices	for 2 subjects mean diff: 3.12% point to surface distance error: 4.89mm	ICC: 0.99 mean diff: 1.9%; 2SD: 2.7% point to surface distance 2RMSE: 5.6mm	-	-	
		VM, 7 slices	for 2 subjects mean diff: 3.35% point to surface distance error: 3.92mm	ICC: 0.99 mean diff: 3.2%; 2SD: 3.4% point to surface distance 2RMSE: 3.7mm	-	-	
		RF, 6 slices	for 2 subjects mean diff: 0.60% point to surface distance error: 3.60mm	ICC: 0.98 mean diff: 4.9%; 2SD: 4.3% point to surface distance 2RMSE: 3.4mm	-	-	
		GM, 8 slices	for 2 subjects mean diff: 3.28% point to surface distance error: 3.31mm	ICC: 0.96 mean diff: 5.6%; 2SD: 8.9% point to surface distance 2RMSE: 6.3mm	-	-	

		GL, 6 slices	for 2 subjects mean diff: 2.01% point to surface distance error: 2.40mm		ICC: 0.86 mean diff:: 7.1%; 2SD: 13.9% point to surface distance 2RMSE: 6.1mm	-	-	
Tingart 2003 [25]	slice-by-slice manual segmentation, volume: muscle tissue area * interslice distance	Sspi	r^2: 0.99 mean diff: 4%; SD 3%		r^2: 0.98 CV: 2.56%	r^2: 0.97 CV: 3.63%	-	7 minutes
		Ssca	r^2: 0.99 mean diff : 3%; SD 2%		r^2: 0.98 CV: 2.05%	r^2: 0.98 CV: 1.76%	-	13 minutes
		Ispi+Tmin	r^2: 0.996 mean diff: 2%; SD 2%		r^2: 0.98 CV: 1.94%	r^2: 0.98 CV: 1.83%	-	12 minutes
Tracy 2003 [26]	manual segmentation of a reduced number of slices, muscle volume: cone method	Qua	significant underestimation of MV for each of the alternative measures, least for MV2 and greatest for MV10. significant underestimation of change of MV by method using every 8th/ 10th section	for every 4th slices (3.1cm gap) baseline MV mean diff: 23cm^3, 2SD: 1.7% MV change mean diff: 0.25cm3, 2SD: 16.4%	-	-	-	3/4 of time gained with every 4 slices segmentation

	single slice manual segmentation (CSAmax), volume: univariate regression		baseline MV r^2: 0.96 2SEE: 14.1% MV change r^2: 0.74 2SEE: 59.7%	-	-	-	-
Valentin 2015 [45]	slice-by-slice manual segmentation, volume: muscle tissue area * interslice distance	RA	-	-	ICC: 0.77 mean diff: 2%; 2SD: 3%	-	-
		Ps	-	-	ICC: 0.92 mean diff: 0.5%; 2SD: 3%	-	-
		M	-	-	ICC: 0.59 mean diff: -4%; 2SD: 5%	-	-
		ES	-	-	ICC: 0.93 mean diff: 1%; 2SD: 2%	-	-
		MES	-	-	ICC: 0.904	-	-
Vanmechelen 2017 [51]	single slice manual segmentation (CSAmax) muscle length (ML) obtained using full muscle reconstruction and form factor (FF), volume: ((CSAmax* ML)-Offset)*FF	GM	r^2: 0.998 SEE: 5.3%	-	-	-	-
		SOL	r^2: 0.993 SEE: 8.9%	-	-	-	-
		TA	r^2: 0.994 SEE: 8.7%	-	-	-	-
		RF	r^2: 0.988 SEE: 4.8%	-	-	-	-
		SM	r^2: 0.996 SEE: 6.5%	-	-	-	-

		ST	r^2: 0.994 SEE: 9.0%		-	-	-	-
Yamauchi 2017 [28]	single slice manual segmentation (CSAs at 60% of the femoral length),femoral length (FL), volume: regression equations which varied for each muscle	RF	No significant difference between measured and estimated MVs	SEE: 12.5%	-	-	-	-
		VL		SEE: 7.1%	-	-	-	-
		VI		SEE: 7.5%	-	-	-	-
		VM		SEE: 8.1%	-	-	-	-
		BFS		SEE: 14.4%	-	-	-	-
		BFL		SEE: 7.2%	-	-	-	-
		ST		SEE: 10.9%	-	-	-	-
		SM		SEE: 13.9%	-	-	-	-
	use of muscle thickness at 50% of the femur and femoral length (FL), volume: regression equations which varied for each muscle	RF	No significant difference between measured and estimated MVs	SEE: 21.8%	-	-	-	-
		VL		SEE: 13.0%	-	-	-	-
		VI		SEE: 15.5%	-	-	-	-
		VM		SEE: 18.6%	-	-	-	-

ICC: intraclass correlation coefficient, mean diff: mean difference, SD: standard deviation, CV: coefficient of variation, SDD: smallest detectable difference, RMSE: root mean square error, SEE: standard error of the estimate, DSI: Dice similarity index, mean surf D: mean surface distance, max surf D: maximal surface distance, TC: Tannimoto coefficient, FNVF: false negative volume fraction, FPVF: false positive volume fraction, MVSF: muscle volume similarity fraction
RF: rectus femoris, VI: vastus intermedius, VL: vastus lateralis, VM : vatsus medialis, Qua : quadriceps, Pir : Piriformis, GlMi : Gluteus Minimus, GlMe : Gluteus Medius, GlMa : Gluteus Maximus, FCU: flexor carpi ulnaris, ECU: extensor carpi ulnaris, Sspi: Supraspinatus, Ssca: Subscapularis, Ispi+Tmin: Infraspinatus and Teres minor, ES: Erector Spinae, M: multifidus, RA: rectus abdominis, Ps: Psoas, Sar: Sartorius, Gra: Gracilis, AddM: Adductor Magnus, Add L: Adductor longus, BFL: Biceps Femoris Long head, BFS: Biceps Femoris Short head, ST: Semi

Tendinosus, SM: Semi Membranosus, GL: Gastrocnemius Lateralis, GM: Gastrocnemius Medialis, So+FHL: Soleus and flexor hallucis longus, TP: Tibialis Posterior, FDL: flexor digitorum longus, Per LBT: Peroneus (Longus, Brevis, Tertius), TA+EDL+EHL: tibialis anterior and extensor digitorum longus and extensor hallucis longus, So: Soleus, TS: triceps surae, TB: triceps brachii, TA: Tibialis Anterior, VLMI: Vastus Lateralis and Medius and Intermedius, TFL: tensor Fascia Lata, Add BLM: adductor (brevis, longus, magnus), Il: Iliacus , Obl: Obliquus (transversus abdominis, internus and externus obliquus), QL: Quadratus Lumborum, VLI: Vastus Lateralis and Intermedius together, VLMI: Vastus Lateralis and Medialis and Intermedius, BF: Biceps Femoris, SMT: Semi Membranosus and Tendinosis, ESM : erector spinae and multifidus, PT: pronator teres, ECRB : Extensor Carpi Radialis Brevis, EPL : Extensor Pollicis Longus, Br : Brachioradialis

S5 Table: validity and reliability of the articles included

	validity	intra rater reliability	intra rater reliability	comparison between methods
slice-by-slice CSA segmentation	Tingart 2003 [25],	Tingart 2003 [25], Smeulders 2010 [62], Springer 2012 [63], Nordez 2009 [27]	Tingart 2003[25], Smeulders 2010 [62], Springer 2012 [63], Barnouin 2014 [46], Valentin 2015 [45], Skorupska 2016 [61], Sudhoff 2009 [64], Nordez 2009 [27]	Lund 2002 [49]
segmentation of CSA in a reduced number of slice[s]	Nordez 2009 [27], Tracy 2003 [26], Barnouin 2015 [47], Lund 2002 [49], Belavy 2011 [55]	Marcon 2015 [9], Lund 2002 [49]	Lund 2002 [49]	
using CSA segmentation on a single slice and muscle length	Albracht 2008 [52], Amabile 2016 [53], Mersmann 2014 [57], Mersmann 2015 [58], Vanmechelen 2017 [51], Popadic 2011 [50], Morse 2007 [60], Yamauchi 2017 [28]	-	-	
segmentation on a single slice	Marcon 2015 [9], Tracy 2003 [26], Lehtinen 2003 [56]	Lehtinen 2003 [56]	Lehtinen 2003 [56]	
DPSO method	Sudhoff 2009 [64], Nordez 2009 [27], Amabile 2016 [53], Moal 2014 [59], Jolivet 2014 [68]	Sudhoff 2009 [64], Moal 2014 [59]	Moal 2014 [59]	
Automatic segmentation methods	Engstrom 2011 [67], Andrews 2015 [65], Le Troter 2016 [48], Kim 2017 [29]			

Pubmed – Medline Search String, December 26, 2017:

((((((((((MRI*[Text Word]) OR magnetic resonance imaging[MeSH Terms])) AND ((((("muscles"[MeSH Terms]) OR "muscle, skeletal"[MeSH Terms])) OR ((muscle*[Text Word]) OR muscul*[Text Word])))) AND ((((("models, anatomic"[MeSH Terms]) OR "organ size"[MeSH Terms])) OR ((((((volum*[Text Word]) OR cross sectional area[Text Word]) OR three-dimension*[Text Word]) OR 3D[Text Word]) OR shape[Text Word]) OR segmentation[Text Word])))) AND (((((("reproducibility of results"[MeSH Terms]) OR "data accuracy"[MeSH Terms])) OR (((((((reliability[Text Word]) OR reproducibility[Text Word]) OR validity[Text Word]) OR repeatability[Text Word]) OR accuracy[Text Word]) OR measur*[Text Word]) OR metrologic*[Text Word])) OR "validation studies"[Publication Type])))) NOT myocard*[Text Word]) NOT cardia*[Text Word]) NOT cardiol*[Text Word]

Cochrane Library search string, December 30, 2017

(("MRI" OR "magnetic resonance imaging") AND ("muscle" OR "skeletal muscle" OR "muscul*") AND ("volum*" OR "cross sectional area" OR "three dimension*" OR "3D" OR "shape" OR "segmentation" OR "organ size") AND ("reliability" OR "reproducibility" OR "repeatability" OR "validity" OR "accuracy" OR "measur*" OR "metrologic*" OR "validation stud*")) in all Studies

Web of Science Search string, December 29, 2017

(TS = (((“MRI” or “magnetic resonance imaging”) AND (“muscle” OR “skeletal muscle” OR “muscul*”) AND (“volum*” OR “cross sectional area” OR “three-dimension*” OR “3D” OR “shape” OR “segmentation” OR “organ size”) AND ("reliability" OR "reproducibility" OR "repeatability" OR "validity" OR "accuracy" OR "measur*" OR "metrologic*" OR "validation stud*")) NOT (“cardiol*” or “cardia*”)) *AND* **DOCUMENT TYPES:** (Article)

Scopus search string, January 2, 2018

(TITLE-ABS-KEY (("MRI" OR “magnetic resonance imaging”) AND ("muscle" OR "skeletal muscle" OR "muscul*") AND (“volum*” OR “cross sectional area” OR “three-dimension*” OR “3D” OR “shape” OR “segmentation” OR “organ size”) AND ("reliability" OR "reproducibility" OR "repeatability" OR "validity" OR “accuracy” OR “measur*” OR “metrologic*” OR “validation stud*))) AND NOT TITLE-ABS-KEY ("cardiol*" OR “cardia*”)) AND (LIMIT-TO (SRCTYPE , *"j"*))

Annexe 3 : Healthy versus pathological learning transferability on shoulder muscle MRI segmentation using Deep convolutional encoder-decoders

Cet article est en préparation pour une soumission dans la revue IEEE TBME

Healthy versus Pathological Learning Transferability on Shoulder Muscle MRI Segmentation using Deep Convolutional Encoder-Decoders

Pierre-Henri Conze*, Sylvain Brochard, Valérie Burdin, Frances T. Sheehan-Gavelli and Christelle Pons

***Abstract*—Automatic segmentation of pathological shoulder muscles in magnetic resonance images is a challenging task for patients with obstetrical brachial plexus palsy due to the huge variability in muscle shape, size, location, texture and injury. A reliable fully-automated segmentation method can greatly help clinicians to plan therapeutic interventions and predict interventional outcomes while eliminating time consuming manual segmentation tasks. The purpose of this work is three-fold. First, we investigate the feasibility of pathological shoulder muscle segmentation using deep learning techniques, given the very limited amount of available annotated data. Second, we address the learning transferability from healthy to pathological data by comparing different learning schemes in terms of model generalizability. Third, extended versions of deep convolutional encoder-decoder architectures using encoders pre-trained on non-medical data are proposed to improve the segmentation accuracy. Methodological aspects are evaluated in a leave-one-out fashion on a dataset of 24 shoulder examinations and focus on 4 different muscles including deltoid as well as infraspinatus, supraspinatus and subscapularis from the rotator cuff. The most relevant segmentation model is partially pre-trained on ImageNet and jointly exploits inter-patient healthy and pathological annotated data. Its performance reaches Dice scores of 82.4%, 82.0%, 71.0% and 82.8% for deltoid, infraspinatus, supraspinatus and subscapularis muscles with absolute surface estimation errors of 134.6mm^2 for supraspinatus and all below 83mm^2 for other muscles. These contributions offer new insights for force inference in the context of musculo-skeletal disorder management.**

***Index Terms*—Obstetrical brachial plexus palsy, shoulder muscle MRI segmentation, deep convolutional encoder-decoder, healthy versus pathological transferability, pre-trained encoders**

I. Introduction

Pixel-wise segmentation is a crucial task in medical image analysis with many applications such as computer-assisted diagnosis, surgery planning, visual augmentation, image-guided interventions or extraction of quantitative indices from images. The rapid development of non-invasive imaging technologies over the last decades has opened new horizons in studying both healthy and pathological anatomy. However, the analysis of complex Magnetic Resonance (MR) imaging datasets could be tedious and time-consuming for clinicians. It justifies the development of computerized assistance methods including robust image segmentation techniques to guide and improve their clinical practice.

The need for accurate muscle delineations arises for the management of musculo-skelatal disorders including obstetrical brachial plexus palsy (OBPP), one of the most common birth injury [1]. Characterized by the disorder of the peripheral nervous system conducting signals from the spinal cord to shoulders, arms and hands, OBPP occurs most often during the delivery phase when lateral tractions are applied to the head to permit shoulder clearance [2]. Its incidence is estimated around 1.4 every 1000 live births [3]. While full recovery is possible, prognosis is variable and up to 35% of children may have from weak to severe life-long functional impairments [2]. Shoulder involvment is the main cause of morbidity. At this level, nerve injuries lead to variable muscle denervations and induce muscle degeneration with fatty and fibrosis infiltration, disruption of growth, muscle atrophy and force imbalances between agonist and antagonist muscle pairs [4]. It is involved in gleno-humeral deformity and can greatly impact upper limb mobilization and the functional use of arms and hands for activities of daily living and specific tasks [5].

Treatment and prevention of shoulder muscle strength imbalances are main therapeutic goals for children with OBPP who do not fully recover [6]. Therapeutic interventions mainly aim at restoring a physiological balance between muscles length and strength to prevent or treat joint deformity and facilitate movement of the upper limb through muscle stretching/strengthening, botulinum toxin injection, muscle transfer/lengthening [7]. Patient-specific information related to the degree of muscle atrophy across shoulder muscles is therefore needed to plan interventions and predict interventional outcomes [8]. However, clinical examinations do not allow the distinction and precise evaluation of each shoulder muscle. Conversely, recent works report a clear relationship between muscle atrophy and strength loss for children with OBPP [1], showing the interest of such morphological evaluation to better understand and treat shoulder problems. In this direction, shoulder muscle segmentation on MR images is useful to both quantify individual muscle involvement and analyze shoulder strength balance profiles of non-dominant and dominant shoulders for children with OBPP.

Considering the large variability in shoulder muscle shape, size, location, texture and injury, muscle segmentation from MR images has been commonly noticed as challenging [9].

P.-H. Conze is with IMT Atlantique, Inserm UMR 1101, UBL, Brest, France. E-mail: pierre-henri.conze@imt-atlantique.fr. S. Brochard is with Rehabilitation Medicine Department, University Hospital of Brest, Brest, France. E-mail : sylvain.brochard@chu-brest.fr. V. Burdin is with IMT Atlantique, Inserm UMR 1101, UBL, Brest, France. E-mail: valerie.burdin@imt-atlantique.fr. Frances T. Sheehan-Gavelli is with Rehabilitation Medicine, National Institutes of Health, Bethesda, USA. E-mail : gavellif@cc.nih.gov. C. Pons is with SSR pdiatrique, Fondation ILDYS, Brest, France. E-mail : christelle.ponsbecmeur@ildys.org. *Asterisk indicates corresponding author.*
Manuscript received —– XX, 2017; revised —– XX, 2017.

Both healthy and pathological muscles are prone to subtle or more severe changes regarding their visual properties and could be difficult to delineate near their insertion areas due to the vicinity with other structures (Fig.1). In the case of pathological muscles, changes in muscle shape and signal occur because of muscle degeneration which can render identification of muscle boundaries even more difficult. To circumvent these difficulties, muscle segmentation is traditionally performed manually in a slice-by-slice fashion [10]. However, manual segmentation is a time-consuming task, prone to errors due to intra and inter-expert variability. There has been a recent and growing interest in developing fully-automated techniques for muscle segmentation. This question is all the more significant as many efforts have been recently devoted to pixel-wise segmentation based on deep learning techniques using convolutional encoder-decoders [11].

In this direction, the purpose of our study is three-fold. First, we aim at studying the feasibility of automatic pathological shoulder muscle segmentation using deep convolutional encoder-decoder networks, given the small amount of available annotated data in children with OBPP. To our knowledge, shoulder muscle delineations have never been achieved automatically through deep learning techniques. Second, our work addresses the learning transferability from healthy to pathologic data and focuses in particular on how data available on both healthy and pathological shoulder muscles can be jointly exploited for pathological shoulder muscle delineation. Third, extended versions of deep convolutional encoder-decoder architectures using encoders pre-trained on non-medical data are investigated to improve the segmentation accuracy. These contributions reach all together a robust and fully-automated muscle segmentation pipeline which provides new insights for force inference in the context of OBPP management.

II. Related works

To obtain quantitative measures from muscles such as forces, muscle segmentation is traditionally performed manually in a slice-by-slice fashion [10] from 3D MR images. This task is extremely time-consuming and requires tens of minutes to get accurate delineations for one single muscle. It is not usable for a great amount of data in research and clinical practice. Moreover, manual segmentation is prone to intra and inter-expert variability given the high variability of muscle shapes and the lack of clearly visible boundaries between muscles and surrounding anatomy. To facilitate the process, a semi-automatic processing based on transversal propagations of manually-drawn masks can be considered [12]. It consists of several ascending and descending non-linear registrations applied to manual masks to finally get volumetric results with a small amount of time devoted to manual segmentation.

A model-based approach for muscle segmentation consists in considering a prior statistical shape model which is matched to target slices. A patient-spectific 3D geometry can thus be reached based on the deformation of a parametric ellipse which tends to fit muscle contours starting from a reduced set of initial slices [13], [14]. Segmentation models can be further improved by exploiting shape information relying on

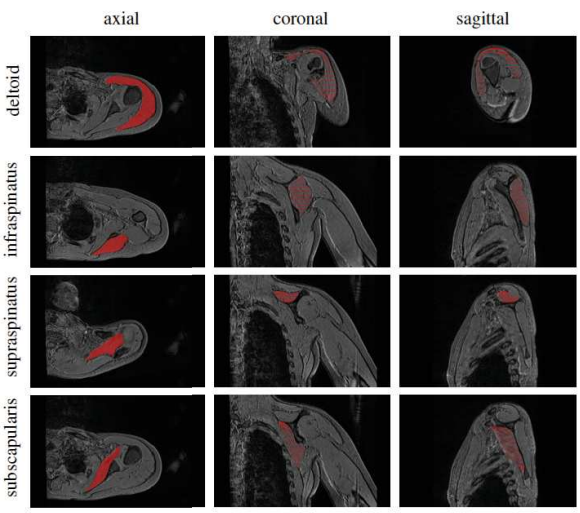

Fig. 1: Groundtruth segmentations of pathological shoulder muscles including deltoid as well as infraspinatus, supraspinatus and subscapularis from the rotator cuff. Axial, coronal and sagittal slices are extracted from a 3D MR examination acquired for a child with obstetrical brachial plexus palsy.

internal shape fitting and auto-correction to guide muscle delineation [15]. Baudin et al. associated in [16] a statistical shape atlas with a random walks graph-based algorithm to automatically segment individual muscles through iterative linear optimization. Andrews et al. [17] used a probabilistic shape representation called generalized log-ratio representation that included adjacency information along with a rotationally invariant boundary detector to segment thigh muscles.

Aligning and merging manually segmented images into specific atlas coordinate spaces can be a reliable alternative. In this direction, single and multi-atlas methods have been proposed for quadriceps muscle segmentation [18], [19] relying on non-linear registration. Engstrom et al. [20] used a statistical shape model constrained using probabilistic MR atlases to automatically segment quadratus lumborum. Segmentation of muscle versus fatty tissues has been also performed through possibilistic clustering [21], histogram-based thresholding followed by region growing [22] and active contours [23] techniques. However, all the previously described methods (except [17]) are not perfectly suited for high inter-subject shape variability and significant differences of tissue appearance due to injury. The use of pathological pediatric shoulder data reinforces this finding. In addition, many of the previously described methods are semi-automatic and therefore require a-priori knowledge, usually associated with high computational costs.

Developing an accurate and robust muscle segmentation method is therefore challenging and still remains an open issue. Huge progress has been recently made for automatic image segmentation using deep Convolutional Neural Networks (CNN). Introduced in [24], deep CNNs are entirely data-driven supervised learning models formed by multi-layer neural networks. In contrast to conventional machine learning which requires hand-crafted features and therefore specialized

knowledge, deep CNNs automatically learn complex hierarchical features directly from data. CNNs obtained outstanding performance for many medical image segmentation tasks [11] which suggests that robust fully automated segmentation of shoulder muscles may be achieved by this way based on MR images. To our knowledge, no other study has been conducted on shoulder muscle segmentation using deep learning methods.

III. Method

A. Deep convolutional encoder-decoders

The simplest way to perform segmentation using deep CNNs consists in classifying each pixel individually by working on patches extracted around them [25]. Since input patches from neighboring pixels have large overlaps, the same convolutions are computed many time. By replacing fully connected layers with convolutional layers, a Fully Convolutional Network (FCN) is able to take entire images as inputs and to produce likelihood maps instead of single pixel outputs. It removes the need to select representative patches and eliminates redundant calculations due to patch overlaps. To avoid outputs with far lower resolution than input shapes, FCNs can be applied to shifted versions of the input images [26]. In this case, the multiple resulting outputs are stitched together to obtain results at full resolution.

Further improvements can be reached with architectures comprising a regular FCN to extract features and capture context, followed by an up-sampling part that enables to recover the input resolution using up-convolutions [11]. Compared to patch-based or *shift-and-stitch* methods, it allows a precise localization in one single pass while taking into account the full image context. Such architecture consisting of paired networks is called Convolutional Encoder-Decoder (CED).

U-Net [27] is the most well-known CED in the medical image analysis community. U-Net has a symmetrical architecture with equal amount of down-samping and up-samping layers between contracting and expanding paths (Fig.3*a*). The encoder gradually reduces the spatial dimension with pooling layers whereas the decoder gradually recovers object details and spatial dimension. One key aspect of U-Net is the use of *skip connections* which concatenate features from the encoder to the decoder to help in recovering object details better while improving localization accuracy. By allowing information to flow directly from low-level to high-level feature maps, it also leads to a faster convergence. This architecture can be exploited for 3D volume segmentation [28] by replacing all 2D operations with their 3D counterparts but it may suffer from high computational costs and GPU memory consumption. Processing 2D slices independently before reconstructing 3D medical volumes remains a simpler alternative. In addition, instead of cross-entropy measures used as loss function, the extension of U-Net proposed in [29] directly minimizes a segmentation error measure to deal with possible strong class imbalance between foreground and background.

B. Healthy versus pathological learning transferability

In this work, we investigate the feasibility of automatic pathological shoulder muscle segmentation using deep CEDs (Sect.III-A), given a small amount of available annotated data. In this context of OBPP, the availability of both healthy and pathological data for image segmentation brings new queries related to the learning transferability from healthy to pathological structures. This aspect is particulary suitable to musculo-skeletal pathologies for two main reasons. First, despite different shapes and sizes due to growth and atrophy, healthy and pathological muscles may share common characteristics such as anatomic locations and overall global aspects. Second, such medical applications suffer from a limited amount of available annotated data, usable for segmentation purposes. Combining healthy and pathological data for deep learning-based segmentation could thus act as a smart data augmentation strategy.

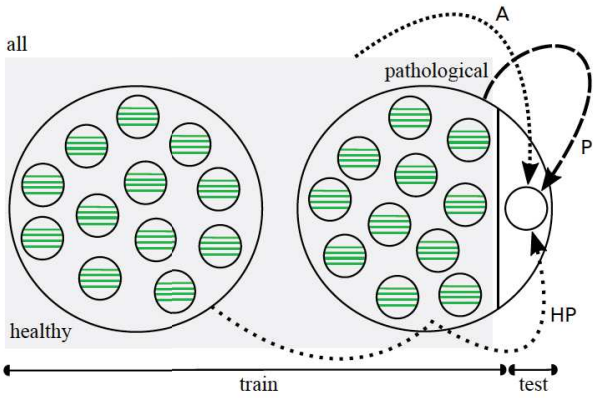

Fig. 2: Three different learning schemes (`P`, `HP`, `A`) involved in a leave-one-out setting for deep learning-based pathological shoulder muscle segmentation.

In this direction, we aim at exploring the joint use of healthy and pathological muscle data for pathological shoulder muscle segmentation. Finding the optimal learning scheme to be followed is key. Three different learning schemes (Fig.2) employed with deep CEDs can be thus considered:

- the most common configuration consists in exploiting annotations made on pathological shoulder muscles only, assuming that CED features extracted from healthy examinations are not suited enough for pathological anatomies.
- another strategy deals with transfer learning and fine tuning from healthy to pathological shoulder muscles. In this context, a first CED is trained using healthy data only. The weights of the resulting model are then used as initialization for a second CED network which is trained using pathological inputs only.
- the last configuration consists in training a CED with a groundtruth dataset comprising annotations made on both healthy and pathological shoulder muscles, which allows to benefit from a more consequent dataset.

By comparing these different training strategies, we can evaluate the benefits brought by combining healthy and pathological data together in terms of model generalizability. The balance between data augmentation and healthy versus pathological muscle variability is a crucial question which has never been investigated for muscle segmentation. These

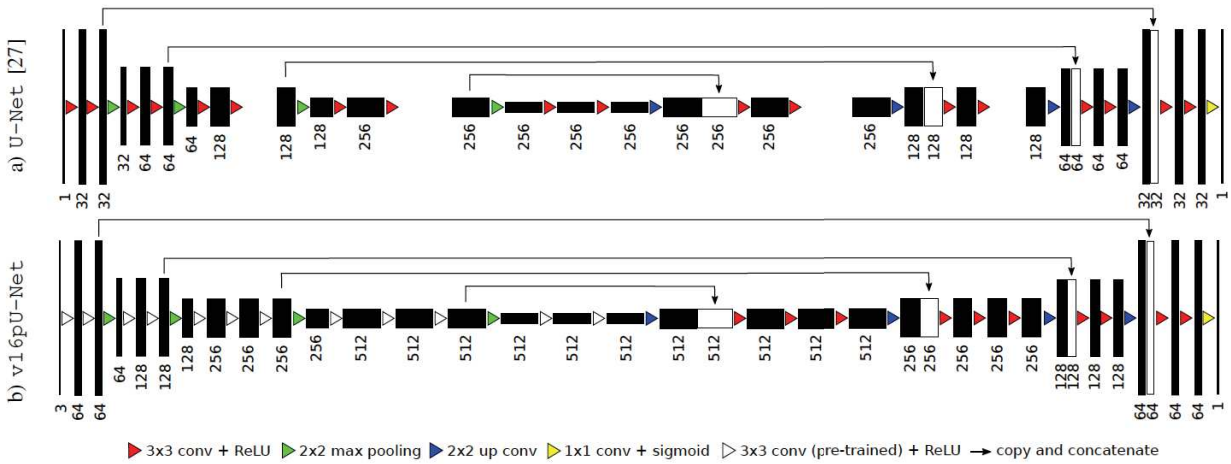

Fig. 3: Extension of the standard U-Net architecture (a) by exploiting as encoder a slightly modified VGG-16 network [30] whose weights are pre-trained on ImageNet [31], following [32], [33]. The decoder of the resulting architecture (b) has been modified to get an exactly symmetrical construction while keeping *skip connections* still possible.

three different schemes, referred as `P` (pathological only), `HP` (transfer learning and fine tuning) and `A` (healthy and pathological data simultaneously), are illustrated Fig.2 in a leave-one-out setting. The overall shoulder dataset is divided into healthy and pathological MR examinations. One pathological examination is extracted from the pathological MR dataset and considered as test examination for shoulder muscle segmentation. It will therefore not be used for training contrary to remaining pathological images.

C. Extended architectures with pre-trained encoders

Contrary to deep classification networks which are usually pre-trained on a very large image dataset, CED architectures used for segmentation are in most cases trained from scratch, relying on randomly initialized weights. Reaching a generic model without over-fitting is therefore difficult, especially when only a small amount of images is available as for musculo-skeletal datasets. As suggested by [32], the encoder part of a deep CED network can be easily replaced by a well-known classification network whose weights have been pre-trained on an initial classification task. It allows to exploit transfer learning and fine tuning from large datasets such as ImageNet [31] in the context of deep learning-based segmentation. In the literature, the encoder part of a deep CED has been already replaced by pre-trained VGG-11 [32] and ABN WideResnet-38 [33] networks with impressive improvements compared to their randomly weighted counterparts.

Following this idea, we propose to extend the standard U-Net architecture described in Sect.III-A by exploiting another simple network from the VGG family [30] as encoder, namely the VGG-16 architecture. To improve the segmentation task, this encoder branch is previously trained on ImageNet [31]. This database has been designed for object recognition purposes and contains more than 1 million natural images from 1000 classes. Pre-training our deep CED dedicated to muscle image segmentation using non-medical data is a clever way to reduce the data scarcity issue while improving model generalizability [34]. Pre-trained models can not only improve predictive performance but also require less training time to reach convergence for the target task. In particular, low-level features captured by first convolutional layers are usually shared between different image types which can explain the success of transfer learning from one task to another.

As shown in Fig.3*b*, the VGG-16 encoder consists of sequential layers including 3×3 convolutional layers followed by Rectified Linear Unit (ReLU) activation functions. Reducing the spatial size of the representation is handled by 2×2 max pooling layers. Compared to standard U-Net (Fig.3*a*), the first convolutional layer generates 64 channels instead of 32. As the network deepens, the number of channels doubles after each max pooling until it reaches 512 (256 for classical U-Net). After the second max pooling operation, the number of convolutional layers differ from U-Net with patterns of 3 consecutive convolutional layers instead of 2, following the original VGG-16 architecture. In addition, input images are extended from one single greyscale channel to 3 channels by repeating the same content in order to respect the dimensions of the RGB ImageNet images used for encoder pre-training. The only differences with VGG-16 rely in the fact that the last convolutional layer as well as top layers including fully-connected layers and softmax have been omitted. The two last convolutional layers taken from VGG-16 serve as central part of the CED and separate both contracting and expanding paths.

The extension of the U-Net encoder has been also transferred to the decoder branch by adding 2 convolutional layers as well as more features channels to get an exactly symmetrical construction while keeping *skip connections* still possible. Contrary to weights of the encoder which are initialized thanks to the pre-training performed on ImageNet, weights of the decoder are set randomly before fine tuning. As for U-Net, a final 1×1 convolutional layer followed by a sigmoid activation function reaches a pixel-wise segmentation mask whose resolution is the same as input slices.

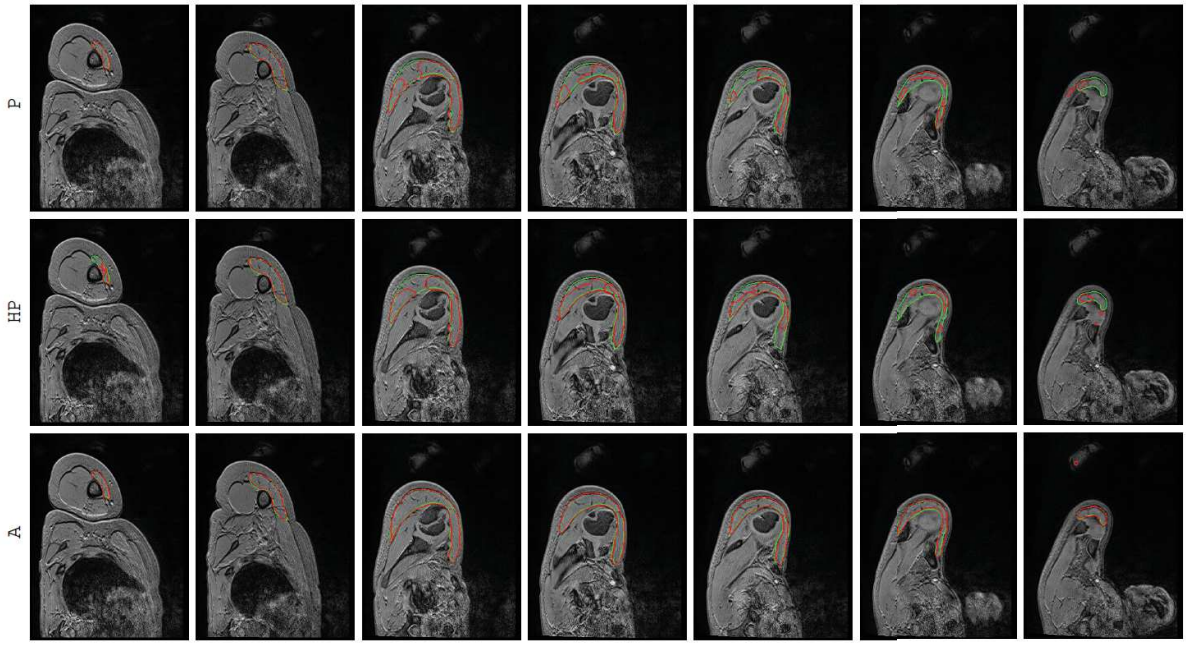

Fig. 4: Pathological deltoid segmentation using U-Net [27] embedded with learning schemes P, HP and A. Groundtruth and estimated delineations are in green and red. Displayed results cover the whole muscle spatial extent for L−P−0103 examination.

IV. Data and experimental results

A. Imaging dataset

Experiments focus on data collected from 12 children with unilateral OPBB and whose averaged age is 12.1 ± 3.3. For each patient, two T1-weighted gradient-echo MR images have been acquired with a 3T MR scanner: one for the healthy shoulder and another for the pathological one. For each healthy or pathological MR image, spatially equally distributed 2D axial slices have been selected for four different shoulder muscles including deltoid as well as infraspinatus, supraspinatus and subscapularis from the rotator cuff. These axial slices were annotated by an expert in pediatric physical medicine and rehabilitation to reach pixel-wise groundtruth delineations.

Image size for axial slices are constant for each subject with 416×312 pixels. The number of axial slices varies from 192 to 224 whereas slice thickness remains unchanged with 1.2mm. Overall, we have 374 (resp. 395) annotated axial slices for deltoid, 306 (367) for infraspinatus, 238 (208) for supraspinatus and 388 (401) for subscapularis across 2400 (2448) axial slices arising from 12 pathological (healthy) examinations. Among these 24 MR images, pairings are known between healthy and pathological shoulders. Due to sparse annotations (Fig.1), deep CEDs exploit as inputs 2D axial slices and produce 2D segmentation masks which can be then easily stacked to recover a full 3D volume for clinical purposes. Among pathological examinations, 8 correspond to right shoulders (R−P−0134, 0684, 0382, 0447, 0660, 0737, 0667, 0277) whereas 4 are left shoulders (L−P−0103, 0351, 0922, 0773). Training images displaying a right (resp. left) shoulder are flipped when a left (right) shoulder is considered for test.

B. Segmentation assessment

To assess both healthy versus pathological learning transferability (Sect.IV-C) and extended pre-trained deep convolutional architectures (Sect.IV-D), the accuracy of automatic pathological shoulder muscle segmentation is quantified based on Dice ($\frac{2TP}{2TP+FP+FN}$), sensitivity ($\frac{TP}{TP+FN}$), specificity ($\frac{TN}{TN+FP}$) and Jaccard ($\frac{TP}{TP+FP+FN}$) similarity scores where TP, FP, TN and FN are the number of true or false positive and negative pixels. We also exploit an absolute surface estimation error (ASE) which compares groundtruth and estimated muscle surfaces defined in mm^2 from segmentation masks. These scores tend to provide a complete assessment of the ability of CED models to provide contours identical to those manually performed. Results provided are averaged among all annotated slices arising from the 12 pathological shoulder examinations.

C. Healthy versus pathological learning transferability

The learning transferability from healthy to pathological data discussed in Sect.III-B is addressed by comparing the three learning schemes P (pathological only), HP (transfer learning and fine tuning) and A (healthy and pathological data simultaneously) in a leave-one-out fashion (Fig.2). To avoid any biais for HP and A, annotated data from the healthy shoulder of the patient whose pathological shoulder is considered for test is not taken into account during training.

Whatever the configuration, deep CED networks are trained using data augmentation since the amount of available training data is limited. To teach the network the desired invariance and robustness properties [27], training 2D axial slices undergo random scaling, rotation, shearing and shifting on both

metric	scheme	P	HP	A		
	network	U-Net [27]			v16U-Net	v16pU-Net
dice	deltoid	68.94±29.9	71.05±29.5	*78.32*±24.4	80.05±23.1	**82.42**±20.4
	infraspinatus	71.38±24.7	77.00±22.5	*81.58*±18.3	81.91±19.0	**81.98**±18.6
	supraspinatus	64.94±28.0	*65.69*±29.6	65.68±30.7	67.30±29.4	**70.98**±28.7
	subscapularis	78.10±18.1	74.55±25.2	*81.41*±15.0	81.58±15.2	**82.80**±14.4
sens	deltoid	70.85±30.5	70.74±29.5	*78.92*±25.4	81.45±23.7	**83.80**±21.3
	infraspinatus	72.12±26.4	79.45±23.1	***84.61***±18.2	83.74±18.6	83.48±19.0
	supraspinatus	64.02±31.8	63.16±33.2	*65.55*±34.5	67.21±33.0	**68.60**±32.3
	subscapularis	78.89±19.7	74.75±27.3	*82.53*±18.1	81.75±18.8	**84.36**±16.5
spec	deltoid	99.61±0.80	99.56±1.07	***99.85***±0.19	99.82±0.22	99.84±0.22
	infraspinatus	99.82±0.23	99.82±0.22	*99.84*±0.18	**99.86**±0.17	**99.86**±0.18
	supraspinatus	99.86±0.18	*99.90*±0.13	99.88±0.15	99.86±0.17	**99.91**±0.12
	subscapularis	99.86±0.13	99.83±0.28	*99.87*±0.13	**99.88**±0.12	99.86±0.15
jacc	deltoid	59.27±29.7	61.68±29.3	*69.48*±26.0	71.46±24.9	**74.00**±22.8
	infraspinatus	60.32±25.6	66.91±24.0	*72.00*±20.4	72.63±20.6	**72.71**±21.0
	supraspinatus	53.61±27.1	55.27±29.3	*55.70*±30.1	56.98±28.7	**61.31**±28.7
	subscapularis	66.93±19.6	64.31±24.7	*70.83*±17.6	71.13±17.7	**72.72**±17.16
ASE	deltoid	252.0±421.6	268.0±507.8	*105.5*±178.9	94.23±139.2	**80.38**±127.5
	infraspinatus	156.8±228.7	92.37±105.9	***74.47***±92.8	80.11±96.2	79.17±96.9
	supraspinatus	174.8±164.0	159.9±153.5	*153.9*±146.0	147.5±129.4	**134.6**±135.5
	subscapularis	*94.56*±95.5	102.0±110.7	95.19±109.0	94.06±111.3	**82.95**±86.88

TABLE I: Quantitative assessment of deep CEDs (U-Net [27], v16U-Net, v16pU-Net) embedded with learning schemes P, HP and A over the pathological dataset in terms of Dice, sensivity, specificity, Jaccard scores and absolute surface error (ASE). Best results are in bold. Italic underlined scores highlight best results among learning schemes employed with U-Net.

directions. 100 augmented images are thus produced for one single training axial slice. Comparisons between P, HP and A schemes are performed using standard U-Net [27] with 10 epochs, a batch size of 10 images, an *Adam* optimizer with 10^{-4} as learning rate for stochastic optimization, a fuzzy Dice score as loss function and randomly initialized weights for convolutional filters. Models were implemented using Keras and trained on a recent desktop PC with a single Nvidia GeForce GTX 1080 Ti GPU with 11Gb/s. Once training is performed, predictions for one single axial slice take around 28ms only which is suitable for routine clinical practice.

We present Tab.I a comparative assessment of P, HP and A averaged over the whole pathological dataset. Reported results correspond to the best results among those obtained after each of the 10 training epochs. Italic underlined scores highlight best results achieved among the three configurations.

Dice results show higher performance when both healthy and pathological data are simultaneously used for training (A) with scores of 78.32% for deltoid, 81.58% for infraspinatus and 81.41% for subscapularis. Scheme A outperforms transfer learning and fine tuning (HP) from 4 to 7% in terms of Dice since HP only obtains 71.05% for deltoid, 77% for infraspinatus and 74.55% for subscapularis. However, this conclusion does not apply to supraspinatus for which A and HP schemes get the same performance in Dice ($\approx$65.7%). In particular, A increases the sensitivity (65.55% instead of 63.16%) but provides a slightly smaller specificity compared to HP. Comparing ASE from HP to A reveals improvements for all shoulder muscles including deltoid whose surface estimation error decreases from 268 to 105.5mm^2. The same finding arise when studying Jaccard scores whose gains are 7.8% and 6.5% for deltoid and subscapularis. Directly combining healthy and pathological data therefore appears as a better strategy than dividing training into two parts focusing on first healthy and then pathological data via transfer learning. Another finding brought by Tab.I is that exploiting annotations made on pathological shoulder muscles only (P) is the worst training strategy, especially for deltoid (Dice loss of 10% from A to P). It proves that CED features extracted from healthy examinations are suited enough for pathological anatomies while acting as an efficient data augmentation strategy. Results for subscapularis deviate from this rule with higher similarity scores compared to HP combined with the best ASE (94.56mm^2).

Accuracy scores for supraspinatus are globally worse than for other shoulder muscles. This finding is mainly due to the presence of a severely injured supraspinatus muscle (L-P-0922) among the set of pathological examinations. Dice results for this single muscle is 42.99% for P against 38.59% and 32.33% for HP and A. It suggests that muscles undergoing very strong degrees of injury must be processed separately, relying on pathological data only or manual delineations. Nevetheless, A appears globally better suited from weak to moderately severe muscle impairments.

Dedicated to the deltoid muscle, a comparison between P, HP and A is provided Fig.5 for each annotated slices of the whole pathological dataset. The top raw displays Dice scores with respect to normalized axial slice number obtained by linearly scaling slice number from $[z_{min}, z_{max}]$ to $[0, 1]$ where $\{z_{min}, z_{max}\}$ are the minimal and maximal axial slice number displaying the deltoid. Overall, the bell-shape curves indicate that segmentation results are more accurate for mid-muscle regions than for both base and apex where muscles appear smaller with strong appearance similarities with surrounding tissues. Above conclusions (A>HP>P) are confirmed with much more individual Dice results grouped on the interval $[75, 95\%]$ for A. By studying the concordance between predicted and groundtruth deltoid surfaces (bottom row), we observe a stronger correlation for A than for P and

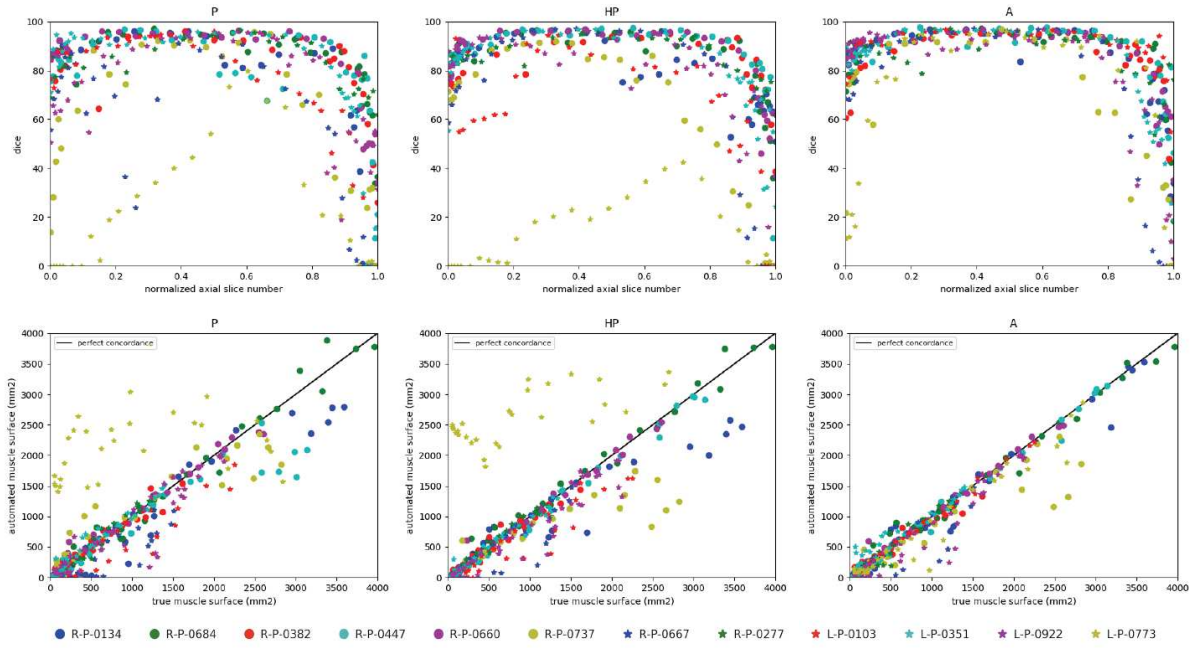

Fig. 5: Deltoid segmentation accuracy using U-Net [27] with learning schemes `P`, `HP` and `A` for each annotated slices of the whole pathological dataset. Top raw show Dice scores with respect to normalized axial slice number. Bottom row displays concordance between groundtruth and predicted muscle surfaces in mm^2. Black line indicates perfect concordance.

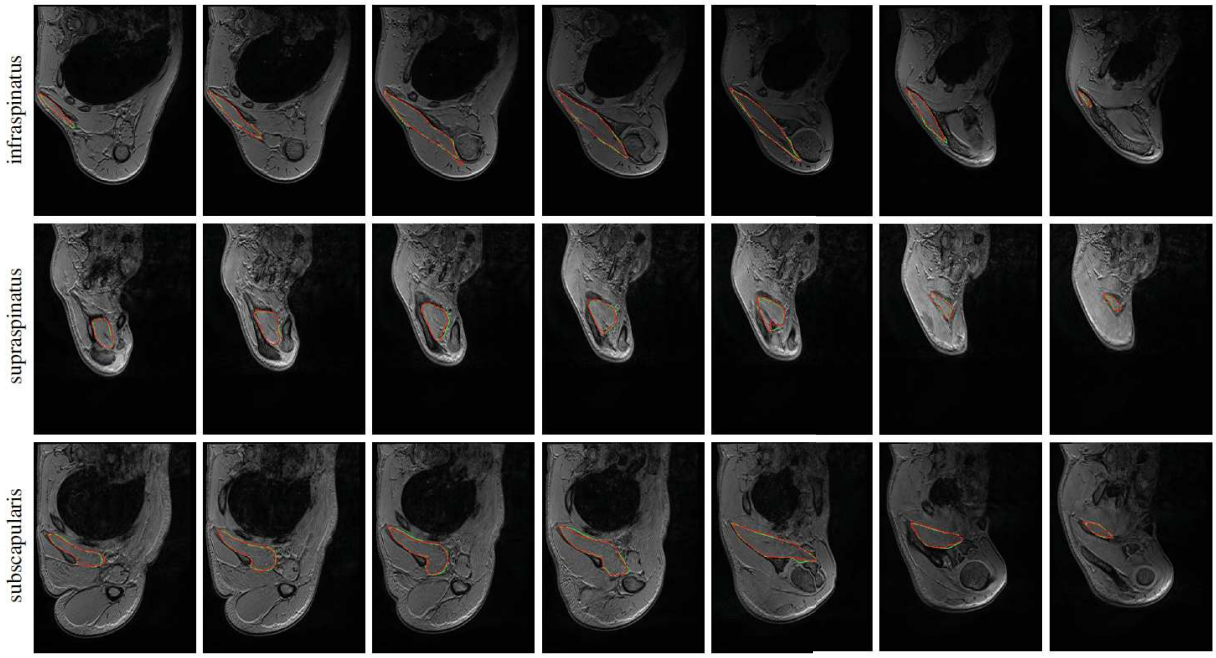

Fig. 6: Automatic pathological segmentation of infraspinatus, supraspinatus and subscapularis using U-Net [27] with training on both healthy and pathological data simultaneously (`A`). Groundtruth and estimated delineations are resp. in green and red. Displayed results cover whole muscle spatial extents resp. for `R-P-0447`, `R-P-0660` and `R-P-0134` examinations.

HP with individual estimations closer to the line of perfect concordance (L-P-0773 is the most telling example).

Evaluation is supplemented by qualitative results given Fig.4 for deltoid (P, HP and A) and Fig.6 for rotator cuff muscles (A only). Displayed results cover the whole muscle spatial extents. We notice Fig.4 a very accurate deltoid delineation for A whereas P and HP tend to under-segment the muscle area. Complex muscle shapes and subtle contours illustrated Fig.6 are relatively well captured. In addition, we can notice outstanding performance near muscle insertion regions whose contours are usually hard to extract due to the vicinity with other structures. These results confirm that using simultaneously healthy and pathological data for training helps in providing good model generalizability despite the data scarcity issue combined with large appearance variabilities.

D. Extended deep convolutional architectures

The standard U-Net architecture [27] is extended Sect.III-C by exploiting VGG-16 as encoder, without (v16U-Net) or with (v16pU-Net) pre-trained weights based on ImageNet. Let us compare these three deep CEDs for pathological shoulder muscle segmentation through leave-one-out experiments. We rely on the best obtained training scheme (Sect.IV-C) combining healthy and pathological data (A). As previously, networks are trained with data augmentation, 10 epochs, a batch size of 10 images, *Adam* optimizer and a fuzzy Dice score as loss function. Learning rates change from U-Net and v16pU-Net (10^{-4}) to v16U-Net (5×10^{-5}) to avoid divergence for deep networks trained with random weights.

Tab.I indicate the performance reached by U-Net, v16U-Net and v16pU-Net over the whole pathological dataset with best scores in bold. It clearly shows that v16pU-Net globally outperforms U-Net and v16U-Net with Dice scores of 82.42% for deltoid, 81.98% for infraspinatus, 70.98% for supraspinatus and 82.80% for subscapularis. On the contrary, v16U-Net (resp. U-Net) obtains 80.05% (78.32%) for deltoid, 81.91% (81.58%) for infraspinatus, 67.30% (65.68%) for supraspinatus and 81.58% (81.41%) for subscapularis. In one hand, despite slightly worse scores compared with U-Net for infraspinatus in terms of sensitivity (83.74 against 84.61) and ASE (80.11 against 74.47mm^2), v16U-Net is most likely to provide good predictive performance and model generalizability thanks to its deeper architecture. On the other hand, comparisons between v16U-Net and v16pU-Net reveals that pre-training the encoder using ImageNet brings non-negligible improvements. For instance, v16pU-Net provides significant gains for deltoid (resp. supraspinatus) whose Jaccard score goes from 71.46 (56.98) to 74% (61.31%). Surface estimation errors are among the lowest obtained with only 80.38mm^2 for deltoid and 82.95mm^2 for subscapularis. Despite their non-medical nature, the large amount of ImageNet images used for pre-training makes the network converge towards a better solution. v16pU-Net is therefore the most able to efficiently discriminate individual muscles from surrounding anatomical structures, compared to U-Net and v16U-Net. In average among the four shoulder muscles, gains for Dice, sensivity and Jaccard reaches 2.8, 2.7 and 3.2% from U-Net to v16pU-Net.

Fig.7 focuses on the deltoid muscle to compare U-Net, v16U-Net and v16pU-Net for each annotated slices of the whole pathological dataset. As previously, comparisons are performed according to Dice scores (top row) and predicted versus groundtruth surface concordance (bottom row). From U-Net to v16pU-Net, we can notice that individual Dice results are slightly pushed towards the upper limit (100%) with less variability and an increased overall consistency along axial slices, as for R-P-0737 and L-P-0773. Extreme axial slices are much better handled in the case v16pU-Net, especially when normalized slice numbers approach zero. In addition, compared to U-Net and v16U-Net, a slightly stronger correlation between predicted and groundtruth deltoid surface can be seen for v16pU-Net. Great improvements for R-P-0737 and L-P-0773 can be also highlighted.

Automatic pathological segmentation results given Fig.8 for deltoid, infraspinatus, supraspinatus and subscapularis using U-Net, v16U-Net and v16pU-Net allows to visually confirm the conclusions (v16pU-Net>v16U-Net>U-Net) given above. 8 pathological examinations among the 12 available are involved to give a complete overview. Globally, better contour adherence and shape consistency are reached by v16pU-Net whose ability to mimmic expert annotations is notable. The great diversity in terms of textures (smooth in R-P-0684 versus granular in R-P-0737) is accurately captured despite high similar visual properties with surrounding structures. Visual results also reveal that v16pU-Net has a good behavior for complex muscle insertion regions (R-P-0447). Despite a satisfactory overall quality, U-Net and v16U-Net are frequently prone to under- (R-P-0134, R-P-0277) or over-segmentation (R-P-0684). Some examples report inconsistent shapes (R-P-0667, R-P-0737), sometimes combined with false positive areas located far away from the groundtruth muscle location (R-P-0447, L-P-0773). Using a pre-trained and complex architecture such as v16pU-Net to process simultaneously healthy and pathological data definitely seems to be the right strategy to automatically provide accurate delineations of pathological shoulder muscles for patients with OPBB.

V. Conclusion

In this work, we addressed automatic pathological shoulder muscle segmentation in magnetic resonance images for patients with obstetrical brachial plexus palsy. Despite the small amount of available data, shoulder muscle segmentation were successfully explored by means of deep convolutional encoder-decoders. In particular, we studied healthy to pathological learning transferability by comparing different learning schemes in terms of model generalizability against large muscle shape, size, location, texture and injury variability. In addition, extended versions of deep convolutional encoder-decoder networks using VGG-16 encoders pre-trained on ImageNet were explored to improve the accuracy reached by standard U-Net architectures. Our contributions were evaluated through leave-one-out experiments performed for four different shoulder muscles including deltoid as well as infraspinatus, supraspinatus and subscapularis from the rotator cuff. First,

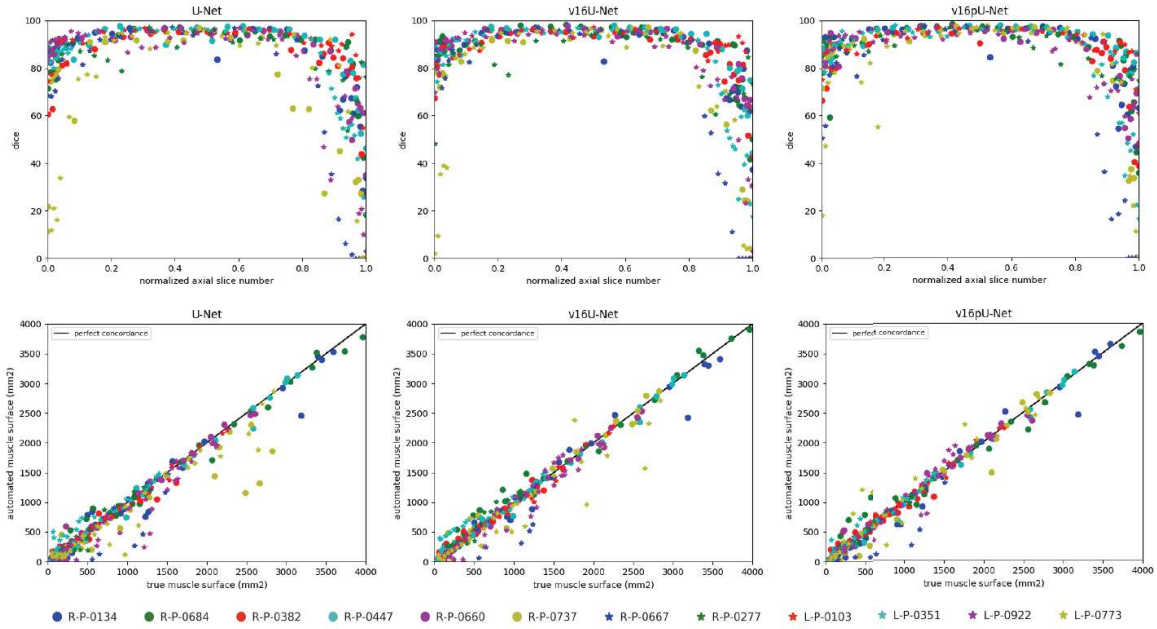

Fig. 7: Deltoid segmentation accuracy using U-Net [27], `v16U-Net` and `v16pU-Net` with learning scheme `A` for each annotated slices of the whole pathological dataset. Top raw show Dice scores with respect to normalized axial slice number. Bottom row displays concordance between groundtruth and predicted muscle surfaces. Black line indicates perfect concordance.

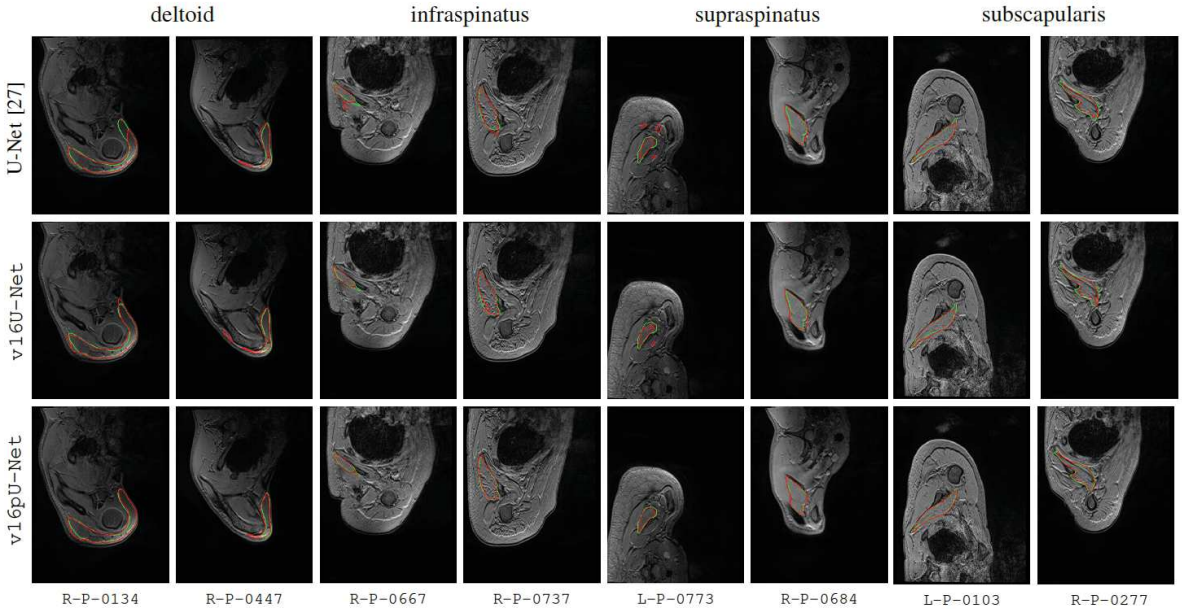

Fig. 8: Automatic pathological segmentation of deltoid, infraspinatus, supraspinatus and subscapularis using U-Net [27], `v16U-Net` and `v16pU-Net` with training on both healthy and pathological data simultaneously (`A`). Groundtruth and estimated delineations are resp. in green and red.

results clearly show that features extracted from healthy examinations are suited enough for pathological anatomies while acting as an efficient data augmentation strategy. Compared to transfer learning, directly combining healthy and pathological data for training provides the best segmentation accuracy together with outstanding delineation performance for muscle boundaries including muscle insertion areas. Second, experiments reveal that convolutional encoder-decoders built around a pre-trained VGG-16 encoder strongly outperforms classical U-Net. Despite the non-medical nature of pre-training data, such deeper networks are able to efficiently discriminate individual muscles from surrounding anatomical structures. These conclusions offer new perspectives for the management of musculo-skeletal diseases since it paves the way for automatic inference of muscle strength imbalances which could greatly help clinicians for intervention planning. Moreover, the proposed approach can be easily extended to other muscle types and imaging modalities with various applications including neuro-muscular diseases, sports related injuries or any other disorder affecting the balance between muscle forces.

REFERENCES

[1] C. Pons, F. T. Sheehan, H. S. Im, S. Brochard, and K. E. Alter, "Shoulder muscle atrophy and its relation to strength loss in obstetrical brachial plexus palsy," *Clinical Biomechanics*, vol. 48, pp. 80–87, 2017.

[2] P. OBerry, M. Brown, L. Phillips, and S. H. Evans, "Obstetrical brachial plexus palsy," *Current problems in pediatric and adolescent health care*, vol. 47, no. 7, pp. 151–155, 2017.

[3] S. P. Chauhan, S. B. Blackwell, and C. V. Ananth, "Neonatal brachial plexus palsy: incidence, prevalence, and temporal trends," in *Seminars in Perinatology*, vol. 38, no. 4, 2014, pp. 210–218.

[4] S. Brochard, K. Alter, and D. Damiano, "Shoulder strength profiles in children with and without brachial plexus palsy," *Muscle & Nerve*, vol. 50, no. 1, pp. 60–66, 2014.

[5] E. Spaargaren, J. Ahmed, W. J. van Ouwerkerk, V. de Groot, and H. Beckerman, "Aspects of activities and participation of 7–8 year-old children with an obstetric brachial plexus injury," *European Journal of Paediatric Neurology*, vol. 15, no. 4, pp. 345–352, 2011.

[6] P. M. Waters, J. T. Monica, B. E. Earp, D. Zurakowski, and D. S. Bae, "Correlation of radiographic muscle cross-sectional area with glenohumeral deformity in children with brachial plexus birth palsy," *The Journal of Bone and Joint Surgery*, vol. 91, no. 10, p. 2367, 2009.

[7] S. H. Kozin, "The evaluation and treatment of children with brachial plexus birth palsy," *The Journal of Hand Surgery*, vol. 36, no. 8, pp. 1360–1369, 2011.

[8] A. Aydin, A. Biçer, T. Özkan, B. Mersa, S. Özkan, and Z. H. Yildirim, "Does primary brachial plexus surgery alter palliative tendon transfer surgery outcomes in children with obstetric paralysis?" *BMC Musculoskeletal Disorders*, vol. 12, no. 1, p. 74, 2011.

[9] Y. Barnouin, G. Butler-Browne, T. Voit, D. Reversat, N. Azzabou, G. Leroux, A. Behin, J. S. McPhee, P. G. Carlier, and J.-Y. Hogrel, "Manual segmentation of individual muscles of the quadriceps femoris using MRI: a reappraisal," *Journal of Magnetic Resonance Imaging*, vol. 40, no. 1, pp. 239–247, 2014.

[10] M. J. Tingart, M. Apreleva, J. T. Lehtinen, B. Capell, W. E. Palmer, and J. J. Warner, "Magnetic resonance imaging in quantitative analysis of rotator cuff muscle volume," *Clinical Orthopaedics and Related Research*, vol. 415, pp. 104–110, 2003.

[11] G. Litjens, T. Kooi, B. E. Bejnordi, A. A. A. Setio, F. Ciompi, M. Ghafoorian, J. A. van der Laak, B. Van Ginneken, and C. I. Sánchez, "A survey on deep learning in medical image analysis," *Medical image analysis*, vol. 42, pp. 60–88, 2017.

[12] A. Ogier, M. Sdika, A. Foure, A. Le Troter, and D. Bendahan, "Individual muscle segmentation in MR images: A 3D propagation through 2D non-linear registration approaches," in *International Conference of the IEEE Engineering in Medicine and Biology Society*, 2017, pp. 317–320.

[13] I. Südhoff, J. A. de Guise, A. Nordez, E. Jolivet, D. Bonneau, V. Khoury, and W. Skalli, "3D-patient-specific geometry of the muscles involved in knee motion from selected MRI images," *Medical & biological engineering & computing*, vol. 47, no. 6, pp. 579–587, 2009.

[14] E. Jolivet, E. Dion, P. Rouch, G. Dubois, R. Charrier, C. Payan, and W. Skalli, "Skeletal muscle segmentation from MRI dataset using a model-based approach," *Computer Methods in Biomechanics and Biomedical Engineering: Imaging & Visualization*, vol. 2, no. 3, pp. 138–145, 2014.

[15] S. Kim, D. Lee, S. Park, K.-S. Oh, S. W. Chung, and Y. Kim, "Automatic segmentation of supraspinatus from MRI by internal shape fitting and autocorrection," *Computer methods and programs in biomedicine*, vol. 140, pp. 165–174, 2017.

[16] P.-Y. Baudin, N. Azzabou, P. G. Carlier, and N. Paragios, "Prior knowledge, random walks and human skeletal muscle segmentation," in *International Conference on Medical Image Computing and Computer-Assisted Intervention*, 2012, pp. 569–576.

[17] S. Andrews and G. Hamarneh, "The generalized log-ratio transformation: learning shape and adjacency priors for simultaneous thigh muscle segmentation," *IEEE Transactions on Medical Imaging*, vol. 34, no. 9, pp. 1773–1787, 2015.

[18] E. Ahmad, M. H. Yap, H. Degens, and J. S. McPhee, "Atlas-registration based image segmentation of MRI human thigh muscles in 3D space," in *Medical Imaging: Image Perception, Observer Performance, and Technology Assessment*, vol. 9037, 2014.

[19] A. Le Troter, A. Fouré, M. Guye, S. Confort-Gouny, J.-P. Mattei, J. Gondin, E. Salort-Campana, and D. Bendahan, "Volume measurements of individual muscles in human quadriceps femoris using atlas-based segmentation approaches," *Magnetic Resonance Materials in Physics, Biology and Medicine*, vol. 29, no. 2, pp. 245–257, 2016.

[20] C. M. Engstrom, J. Fripp, V. Jurcak, D. G. Walker, O. Salvado, and S. Crozier, "Segmentation of the quadratus lumborum muscle using statistical shape modeling," *Journal of Magnetic Resonance Imaging*, vol. 33, no. 6, pp. 1422–1429, 2011.

[21] V. Barra and J.-Y. Boire, "Segmentation of fat and muscle from MR images of the thigh by a possibilistic clustering algorithm," *Computer methods and programs in biomedicine*, vol. 68, no. 3, pp. 185–193, 2002.

[22] S. Purushwalkam, B. Li, Q. Meng, and J. McPhee, "Automatic segmentation of adipose tissue from thigh magnetic resonance images," in *International Conference Image Analysis and Recognition*. Springer, 2013, pp. 451–458.

[23] S. Orgiu, C. L. Lafortuna, F. Rastelli, M. Cadioli, A. Falini, and G. Rizzo, "Automatic muscle and fat segmentation in the thigh from T1-Weighted MRI," *Journal of Magnetic Resonance Imaging*, vol. 43, no. 3, pp. 601–610, 2016.

[24] Y. LeCun, L. Bottou, Y. Bengio, and P. Haffner, "Gradient-based learning applied to document recognition," *Proceedings of the IEEE*, vol. 86, no. 11, pp. 2278–2324, 1998.

[25] D. Ciresan, A. Giusti, L. M. Gambardella, and J. Schmidhuber, "Deep neural networks segment neuronal membranes in electron microscopy images," in *Advances in neural information processing systems*, 2012, pp. 2843–2851.

[26] J. Long, E. Shelhamer, and T. Darrell, "Fully convolutional networks for semantic segmentation," in *IEEE Conference on Computer Vision and Pattern Recognition*, 2015, pp. 3431–3440.

[27] O. Ronneberger, P. Fischer, and T. Brox, "U-Net: Convolutional networks for biomedical image segmentation," in *International Conference on Medical Image Computing and Computer-Assisted Intervention*, 2015, pp. 234–241.

[28] Ö. Çiçek, A. Abdulkadir, S. S. Lienkamp, T. Brox, and O. Ronneberger, "3D U-Net: learning dense volumetric segmentation from sparse annotation," in *International Conference on Medical Image Computing and Computer-Assisted Intervention*, 2016, pp. 424–432.

[29] F. Milletari, N. Navab, and S.-A. Ahmadi, "V-Net: Fully convolutional neural networks for volumetric medical image segmentation," in *International Conference on 3D Vision (3DV)*, 2016, pp. 565–571.

[30] K. Simonyan and A. Zisserman, "Very deep convolutional networks for large-scale image recognition," *arXiv preprint arXiv:1409.1556*, 2014.

[31] O. Russakovsky, J. Deng, H. Su, J. Krause, S. Satheesh, S. Ma, Z. Huang, A. Karpathy, A. Khosla, M. Bernstein *et al.*, "ImageNet large scale visual recognition challenge," *International Journal of Computer Vision*, vol. 115, no. 3, pp. 211–252, 2015.

[32] V. Iglovikov and A. Shvets, "TernausNet: U-Net with VGG11 encoder pre-trained on imagenet for image segmentation," *arXiv preprint arXiv:1801.05746*, 2018.

[33] V. Iglovikov, S. Seferbekov, A. Buslaev, and A. Shvets, "TernausNetV2: Fully convolutional network for instance segmentation," *arXiv preprint arXiv:1806.00844*, 2018.

[34] J. Yosinski, J. Clune, Y. Bengio, and H. Lipson, "How transferable are features in deep neural networks?" in *Advances in neural information processing systems*, 2014, pp. 3320–3328.

Annexe 4: supporting information article 4

		arm down			flexion			abduction			extensi			adduction		
		ND (N=11)	UI (N=11)	p	ND (N=11)	UI (N=12)	p	ND (N=11)	UI (N=12)	p	ND (N=11)	I (N=12)	p	ND (N=11)	UI (N=11)	p
start angle																
wrist	fl-ext	-2,6	-8,9		0,3	1,5		-15,6	-19,5		1,5	-2,7		-26,5	-18,5	
	rad-ulnar inclination	-7,3	-8,4		-1,4	-6,2		-4,1	-8,9		-2,9	-9,1	*	-5,9	-5,5	
elbow	fl ext	21,1	17,9		10,8	13,3		7,3	17,1	*	10,6	14,4		0,9	7,2	
	pro-supination	106,2	94,5		85,6	88,0		28,3	17,2		86,6	81,1		58,3	71,6	
gleno humeral	plane of elevation	6,6	8,5		8,2	7,6		8,6	11,1		8,3	10,2		-16,3	-21,1	
	elevation	-13,8	-12,4		-9,5	-10,9		-7,4	-8,8		-12,6	-15,8		-36,3	-41,5	
	axial Rotation	-31,3	-21,2	*	-23,0	-12,5	*	-53,3	-30,0	*	-25,8	-20,3		-67,0	-60,9	
shoulder (thoraco humeral)	plane of elevation	-1,5	1,4		-2,3	-0,1		-3,0	2,6		-3,0	3,7		-23,9	-21,6	
	elevation	-11,5	-9,6		-10,7	-8,6		-8,0	-5,1		-12,0	-9,9		-53,8	-59,2	
	axial Rotation	2,0	15,9	*	-0,8	9,0	*	-19,5	-6,1	*	3,3	15,4	*	-59,8	-59,1	
scapula	ant-post tilt	-14,8	-13,4		-16,5	-12,9		-16,1	-14,5	*	-16,9	-13,4		-10,8	-1,9	*
	med-lat rotation	4,4	3,4		1,5	3,0		1,5	2,5		2,7	4,6		-14,9	-17,3	

	pro-retraction	30,4	34,5		26,9	28,1		19,0	28,7		25,9	32,5		3,3	1,7	
trunk	fl-ext	5,4	7,8		3,4	6,4		-0,4	5,0		3,2	9,5		1,2	3,1	
	lat tilt	-0,8	-2,0		0,7	1,0		0,9	1,2		-0,2	1,3		-13,3	12,3	****
	rotation	1,7	4,5		3,3	-2,9	**	-0,7	0,8		2,3	-1,1		-14,1	11,8	**
PTA angle																
wrist	fl-ext				-13,4	-11,6		-15,5	-14,1		18,0	13,9		-23,6	-22,4	
	rad-ulnar inclination				-5,6	-7,7		0,6	-7,1		1,8	-4,9		-4,0	-6,5	
elbow	fl ext				15,8	21,0		11,7	21,1		1,5	5,5		31,1	39,3	
	pro-supination				48,7	63,1		81,6	73,8		112,3	108,7		58,9	61,3	
gleno humeral	plane of elevation				11,9	12,4		10,7	4,1		-27,0	-32,9		59,1	52,9	
	elevation				-99,6	-105,6		-105,6	-97,1		-11,8	-12,3		-48,6	-43,6	
	axial Rotation				-62,3	-71,7		-50,9	-64,7		-30,8	-23,7		-48,4	-35,8	
shoulder (thoraco humeral)	plane of elevation				21,3	20,0		27,8	22,0		-50,8	-49,8		57,1	60,7	
	elevation				-144,8	-143,2		-148,4	-145,8		-35,6	-29,0		50,9	38,6	
	axial Rotation				-93,6	-93,3		-89,8	-86,0		1,0	2,5		97,5	90,3	
scapula	ant-post tilt				15,9	15,6		7,2	1,3		-29,7	-22,2	*	-21,5	-12,5	
	med-lat rotation				-46,1	-38,2		-41,5	-31,7		1,3	3,9		-33,0	-30,4	
	pro-retraction				21,0	11,7	*	31,8	25,7	**	14,0	12,1		68,0	63,4	
trunk	fl-ext				-13,8	-8,9		-10,4	-5,0		15,3	16,1		-6,6	-4,8	
	lat tilt				-9,4	9,5	****	-14,7	12,8	****	-7,0	4,7	***	-3,9	4,9	***

	rotation		2,27	-2,6		-3,4	3,2	**	-17,8	13,2	****	35,4	-19,7	****
ROM angle														
wrist	fl-ext		18,4	16,0		11,3	11,3		21,0	18,4		15,7	15,1	
	rad-ulnar inclination		8,7	5,4	*	7,1	7,1		10,3	6,0		6,3	6,1	
elbow	fl ext		16,2	16,3		13,6	13,6		13,9	12,6		34,1	36,4	
	pro-supination		39,0	29,0	*	57,7	57,7		34,4	30,2		23,6	26,1	
gleno humeral	plane of elevation		25,2	26,1		30,8	19,5		36,1	43,3		75,8	74,7	
	elevation		90,9	96,6		98,4	91,5		12,1	14,6		32,5	23,0	*
	axial Rotation		45,1	61,6	**	27,6	43,7		14,1	11,7		27,6	30,0	
shoulder (thoraco humeral)	plane of elevation		64,0	62,4		34,6	34,6		47,8	53,6		99,9	97,0	
	elevation		136,2	136,6		140,4	140,4		27,7	23,0		125,7	115,0	
	axial Rotation		100,2	108,3		71,1	71,1		19,0	20,1		164,3	155,9	
scapula	ant-post tilt		34,2	30,7		25,8	18,8		14,1	11,1		15,7	16,2	
	med-lat rotation		48,1	42,1		44,0	34,7		8,6	8,7		21,1	16,1	
	pro-retraction		22,8	26,8		17,3	16,6		14,5	21,0	**	65,7	62,7	
trunk	fl-ext		17,8	15,8		10.6	10.5		13,0	7,4	*	11,4	9,1	
	lat tilt		11,3	9,4		16.5	12.5	*	8,5	5,7		12,8	8,9	
	rotation		11,2	8,2		7.2	6.9		21,1	14,8		56,3	32,2	**

		external rotation			RTG			HTS			HTH		
		ND (N=11)	UI (N=12)	p	ND (N=11)	UI (N=12)	p	ND (N=11)	UI (N=10)	p	ND (N=11)	UI (N=11)	p
start angle													
wrist	fl-ext	19,7	11,1		-6,7	-7,4		-8,1	-2,4		-3,7	-5,6	
	rad-ulnar inclination	-9,4	-18,4	*	-6,0	-10,2		-6,9	-10,8		-6,7	-11,2	
elbow	fl ext	90,2	81,6		21,2	34,3		22,0	18,4		22,7	20,0	
	pro-supination	110,5	118,8		103,4	105,1		103,7	95,0		104,8	96,9	
GH	plane of elevation	-24,1	-28,3		6,9	11,9		6,5	9,3		8,1	8,2	
	elevation	-44,1	-48,4		-12,3	-14,0		-11,1	-13,3		-11,6	-13,2	
	axial Rotation	-18,2	-11,7		-30,7	-25,0		-28,7	-23,2		-28,2	-21,7	
shoulder (thoraco humeral)	plane of elevation	-7,4	-12,1		-3,0	6,6	*	-3,3	2,6		-2,9	1,0	
	elevation	-72,3	-71,6		-10,6	-9,4		-11,3	-9,6		-11,2	-9,3	
	axial Rotation	16,8	19,6		1,9	9,3		1,7	7,2		2,2	8,7	
scapula	ant-post tilt	-24,0	-18,5		-15,6	-12,0		-16,1	-12,0		-16,6	-12,4	
	med-lat rotation	-10,1	-5,9		4,4	2,1		2,1	3,0		2,7	4,0	
	pro-retraction	34,4	30,6		29,8	31,9		28,0	28,1		27,4	28,0	
trunk	fl-ext	6,7	6,4		5,5	9,3		4,8	10,3		4,6	8,2	
	lat tilt	-9,1	10,4	****	-0,3	2,5	*	-0,4	0,7		-0,5	2,0	*
	rotation	0,3	-2,0		0,8	-4,1	*	2,3	-3,0		2,0	-3,3	*

PTA angle												
wrist	fl-ext	-47,6	-45,5		-22,2	-23,9		-10,6	-5,7		-2,2	-4,0
	rad-ulnar inclination	-13,1	-17,1		-19,1	-18,5		-9,7	-14,4	*	-13,3	-12,4
elbow	fl ext	103,9	91,6		55,5	46,4		118,3	125,2	*	118,7	121,9
	pro-supination	91,7	88,0		94,2	98,4		45,6	50,3		36,1	39,6
GH	plane of elevation	1,2	-7,4	*	30,4	31,1		50,4	42,2	trend	21,2	17,7
	elevation	-39,1	-41,3		-36,7	-41,2		-25,9	-30,8		-70,9	-68,4
	axial Rotation	-79,3	-65,2	**	-42,5	-43,4		-15,8	-16,6		-73,7	-66,6
shoulder (thoraco humeral)	plane of elevation	10,0	2,8	*	38,6	48,3	*	52,2	53,6		44,0	36,8
	elevation	-67,6	-69,0		-15,3	-20,8		16,2	25,9	*	-113,9	-107,6
	axial Rotation	-80,2	-73,4		10,2	7,4		70,0	50,5	trend	-80,8	-79,0
scapula	ant-post tilt	4,9	13,2	*	-14,5	-10,9		-15,8	-8,5		-3,2	4,6
	med-lat rotation	-27,9	-27,9		-4,5	-9,3		-23,4	-18,0		-38,2	-32,4
	pro-retraction	5,6	0,4		42,8	44,1		53,2	45,1		25,6	22,3
trunk	fl-ext	-7,4	-5,3		5,3	9,2		2,9	7,5		-1,5	1,5
	lat tilt	-8,4	9,7	****	0,1	0,1	*	0,2	0,7		-3,8	5,3 ****
	rotation	-6,3	3,8	***	11,7	11,7	****	8,0	-2,1	***	1,6	-2,4
ROM angle												
wrist	fl-ext	71,4	58,7		32,0	37,4		28,1	29,5		28,2	31,3
	rad-ulnar inclination	11,7	7,0		16,7	13,2		10,6	8,2		13,6	13,1

elbow	fl ext	25,8	20,4	61,8	64,2		100,4	108,9		99,2	107,2
	pro-supination	40,6	35,5	28,3	27,2		60,5	49,4		72,4	62,1
GH	plane of elevation	26,3	21,6	26,6	24,5		44,7	34,2	**	17,4	18,6
	elevation	11,4	13,0	26,3	29,8		24,3	23,0		59,6	56,1
	axial Rotation	61,8	53,8	14,8	22,1	*	22,5	18,1		46,5	46,2
shoulder (thoraco humeral)	plane of elevation	19,4	16,7	45,0	46,3		58,0	53,2		49,3	42,2
	elevation	10,6	8,9	14,1	19,1		38,3	25,9	*	103,6	99,3
	axial Rotation	97,1	93,1	20,6	24,3		74,9	53,5	**	84,6	89,0
scapula	ant-post tilt	29,4	32,1	4,2	6,0	*	7,7	-8,5		15,0	18,0
	med-lat rotation	20,1	23,0	10,8	13,2		26,2	-18,0		41,9	37,7
	pro-retraction	29,3	30,8	15,1	15,6		27,0	45,1		11,0	11,9
trunk	fl-ext	14,8	12,1	2,5	2,6		3,0	*3,4*		6,4	6,9
	lat tilt	4,4	3,1	2,1	1,9		2,4	*2,0*		4,3	3,9
	rotation	7,7	6,4	11,4	8,3	*	7,8	*4,5*	*	4,0	4,0

Appendix 1 : Mean of the discrete joint angles of the non dominant side of typically developping children and unimpaired side of children with OBPP

ND : non dominant, N : number of children, UI : unimpaired

Fl-ext : flexion extension, pro-supination : pronation-supination, ant-post tilt : anterio-posterior tilt, med-lat rotation : medial-materal rotation, pro-retraction : protraction-retraction, lat tilt : lateral tilt

RTG : reach to grasp, HTS : hand to shoulder, HTH : hand to head

			Sh_Plane	Sh_Elev	Sh_Rot	El_Fl	El_Supi	Wr_Fl	Wr_Devia	Scap_Prot	Scap_Rot	Scap_Tilt	Tr_Fl	Tr_Lat	Tr_Rot	APS
Abduction	ND (n= 11)	moyenne	7,76	16,11	12,94	7,62	13,47	8,47	5,84	7,61	8,61	9,76	5,25	3,85	5,16	10,36
		SD	*1,94*	*5,43*	*5,17*	*4,18*	*4,60*	*4,91*	*3,13*	*3,54*	*4,93*	*5,25*	*2,06*	*1,32*	*2,43*	*2,29*
	UI (n=12)	moyenne	8,52	12,86	13,43	12,44	26,66	11,69	9,67	14,49	10,04	15,08	8,26	15,22	6,32	15,86
		SD	*3,99*	*3,06*	*3,60*	*20,08*	*30,24*	*5,93*	*11,36*	*8,78*	*3,75*	*11,98*	*4,22*	*3,81*	*4,30*	*8,75*
	p									*			*	****		*
H Adduction	ND (n=9)	moyenne	14,28	21,84	23,76	9,99	16,51	11,14	4,53	7,53	8,53	10,67	5,89	4,56	12,48	14,16
		SD	*6,88*	*8,24*	*8,24*	*5,36*	*8,84*	*6,15*	*1,77*	*2,97*	*3,85*	*4,16*	*2,44*	*1,99*	*6,34*	*3,05*
	UI (n= 12)	moyenne	20,47	31,67	36,59	14,98	24,31	14,71	7,84	11,81	7,90	13,56	7,86	15,02	27,46	22,40
		SD	*10,67*	*19,01*	*18,76*	*13,49*	*21,15*	*10,62*	*5,36*	*4,86*	*3,13*	*3,35*	*3,84*	*4,69*	*3,97*	*6,78*
	p				*					*				***	***	**
Flexion	ND (n= 11)	moyenne	13,91	22,23	18,66	8,84	12,21	10,62	5,51	9,63	9,28	12,28	6,96	3,01	5,26	12,71
		SD	*3,87*	*6,78*	*7,44*	*4,53*	*4,75*	*7,72*	*2,47*	*6,34*	*3,40*	*6,76*	*2,93*	*1,25*	*1,70*	*3,01*
	UI (n=12)	moyenne	12,05	15,98	16,80	8,71	20,46	11,02	6,11	10,41	9,86	10,97	10,32	8,99	9,47	13,48
		SD	*3,20*	*5,32*	*4,58*	*5,37*	*12,20*	*4,73*	*3,26*	*4,63*	*3,30*	*6,08*	*4,45*	*3,40*	*3,37*	*2,04*
	p			*			*						*	****	***	
Extension	ND (n= 11)	moyenne	10,16	9,04	12,21	6,97	14,30	12,17	5,59	5,78	5,26	8,35	6,58	3,72	7,86	9,65
		SD	*3,52*	*5,29*	*5,91*	*4,79*	*5,36*	*9,00*	*2,93*	*2,42*	*2,76*	*4,95*	*2,26*	*1,75*	*2,79*	*3,39*
	UI (n=12)	moyenne	10,47	8,38	15,50	7,51	20,64	9,11	8,54	7,61	6,08	9,34	13,79	6,32	14,59	12,92
		SD	*4,49*	*5,74*	*9,20*	*3,28*	*12,31*	*4,95*	*5,46*	*3,23*	*3,76*	*5,98*	*6,79*	*3,45*	*4,03*	*2,79*
	p												*		***	**
Ext Rotation	ND (n= 11)	moyenne	7,83	5,91	13,87	10,85	16,23	17,32	6,89	8,78	5,97	8,50	5,69	3,80	5,23	10,68
		SD	*3,71*	*2,28*	*3,57*	*6,14*	*7,62*	*9,75*	*2,58*	*4,04*	*2,29*	*2,66*	*1,90*	*1,53*	*2,45*	*2,45*
	UI (n=12)	moyenne	9,23	6,59	16,41	14,45	16,51	19,15	8,84	9,13	9,12	9,42	7,66	15,67	6,51	13,42
		SD	*3,22*	*3,77*	*6,64*	*6,18*	*7,34*	*7,08*	*5,00*	*3,16*	*4,70*	*4,59*	*3,38*	*4,59*	*3,84*	*1,91*
	p													****		**
Hand to Shoulder	ND (n= 11)	moyenne	10,58	8,62	12,02	13,87	14,10	10,29	4,89	5,82	6,21	8,33	6,68	1,60	3,85	9,80
		SD	*5,47*	*4,58*	*5,61*	*6,88*	*3,17*	*5,17*	*2,11*	*2,92*	*4,58*	*2,93*	*5,64*	*0,76*	*1,85*	*2,63*
	UI (n=10)	moyenne	10,06	10,17	15,09	14,86	17,77	13,55	7,20	6,27	7,86	8,47	10,65	2,65	6,91	12,10
		SD	*3,00*	*6,03*	*4,68*	*7,01*	*8,81*	*7,01*	*4,25*	*3,28*	*6,19*	*3,95*	*5,04*	*1,72*	*2,13*	*2,06*

	p														**	*
Hand to Head	ND (n= 11)	moyenne	10,18	13,00	9,70	15,90	16,27	11,83	6,48	6,11	6,76	7,80	5,44	2,55	3,86	10,75
		SD	*5,12*	*5,72*	*3,61*	*9,29*	*6,74*	*3,94*	*2,80*	*2,21*	*3,29*	*4,41*	*3,49*	*1,32*	*2,75*	*2,94*
	UI (n=10)	moyenne	15,37	15,02	17,40	14,62	20,16	15,41	6,98	7,50	8,36	9,71	7,78	5,26	5,33	13,66
		SD	*7,01*	*9,62*	*9,84*	*6,24*	*7,98*	*5,08*	*2,68*	*4,96*	*5,32*	*5,97*	*4,27*	*3,07*	*3,09*	*2,80*
	p				*									*		*
Reach to Grasp	ND (n= 11)	moyenne	7,00	5,67	9,84	8,94	12,05	14,37	6,55	4,05	4,19	6,00	4,43	1,45	4,32	8,43
		SD	*4,14*	*2,72*	*3,92*	*2,83*	*4,65*	*6,66*	*2,85*	*2,19*	*4,10*	*3,53*	*3,52*	*0,81*	*2,30*	*2,10*
	UI (n=10)	moyenne	13,33	8,07	12,58	18,21	16,32	15,70	7,36	5,41	7,65	5,50	9,18	3,93	11,19	12,55
		SD	*9,92*	*5,86*	*5,52*	*12,97*	*9,71*	*8,93*	*2,68*	*2,39*	*5,07*	*3,26*	*6,73*	*2,24*	*3,00*	*4,41*
	p					*					*		*	*	***	**

Appendix 2: Arm profile score, unimpaired side of children with OBPP (I OBPP), non dominant side of TD children (ND TDC)
*p<0.05

IX Communications

Articles dans des revues internationales

- Im HS, Alter KE, Brochard S, Pons C, Sheehan FT. In vivo pediatric shoulder muscle volumes and their relationship to 3D strength. J Biomech. 2014 Aug 22; 47(11):2730-7.
- Pons C, Sheehan FT, Im HS, Brochard S, Alter KE. Relating shoulder muscle atrophy to strength loss in Obstetrical brachial plexus palsy. Clin Biomech (Bristol, Avon). 2017 Oct;48:80-87. doi: 10.1016/j.clinbiomech.2017.07.010. Epub 2017 Jul 27.
- Pons C; Borotikar B, Garetier M, Burdin V, Ben Salem D, Lempereur M, Brochard S. Quantifying skeletal muscle volume and shape in humans using MRI: a systematic review of validity and reliability. Accepté dans Plos One.
- Christelle Pons; Dauphou Eddi; Grégoire le Gal; Marc Garetier; Douraied Ben Salem; Laetitia Houx; Franck Fitoussi; Nathaly Quintero; Sylvain Brochard; and the POPB-TOX Group (Marianne Alison, Madeleine Aslan, Jennifer Bastien, Gilles Dautel, Floriane Colin, Marion Delpont, Bruno Dohin, Marie Agnes Galloy, Vincent Gautheron Salem Hassan Al Khoury, Pascal Jehanno , Mélanie Kaas, Olivier Prodhomme, Mélanie Porte, Anne Gaelle Py, Helène Rauscent, Emilie Rumilly, Katherine Sanchez Barr , Catherine Tréguier, and Philippe Violas). Effectiveness and safety of early intramuscular botulinum toxin injections to prevent shoulder deformity in babies with obstetrical brachial plexus palsy (POPB-TOX), a randomized controlled trial: study protocol. Soumis dans BMJ Open.
- Pons C, Lempereur M, Alter K, Damiano D, Brochard S. Three-dimensional upper limb movement characteristics in children with brachial plexus birth palsy. En préparation pour Gait and Posture.
- Conze PH, Pons C, Burdin V, Sheehan FT, Brochard S. Healthy versus pathological learning transferability on shoulder muscle MRI segmentation using deep convoltional encoder-decoders. En préparation pour Transactions on Biomedical Engineering.

Communications lors de congrès internationaux

- Pons C; Borotikar B, Garetier M, Burdin V, Ben Salem D, Lempereur M, Brochard S. Quantifying skeletal muscle volume and shape in humans using MRI: a systematic review of validity and reliability. Poster, *ISPRM congress*, jul 2018, Paris
- Pons C, Borotikar B, Burdin V, Lempereur M, Brochard S. Validity and reliability of MRI methods to asses muscle volumes. Accepted (oral presentation), *European Congress of Physical Medicine and Rehabilitation,* May 2018, Vilnius
- Pons C, Le Corre T, Fitoussi F, Brochard S, Quintero N. Effectiveness of botulinum toxin injections on upper limb motor function of children with obstetrical brachial plexus palsy. Accepted (oral presentation), *European Congress of Physical Medicine and Rehabilitation,* May 2018, Vilnius
- Pons C, Brochard S. Biomechanical and morphological factors of the shoulder pathology in children with obstetrical brachial plexus palsy: impact on rehabilitative therapeutics. MRT 180sec, *European Congress of Physical Medicine and Rehabilitation,* May 2018, *Vilnius*
- Pons C, Sheehan FT, Alter KE, Im HS, Brochard S. Relating shoulder muscle atrophy to strength loss in Obstetrical brachial plexus palsy. Poster, *29th Annual Meeting of the European Academy of Childhood Disability (EACD)*, Amsterdam 2017.
- Pons C, Sheehan FT, Alter KE, Im HS, Brochard S. Shoulder muscle atrophy and its relation to strength in children with brachial plexus birth palsy. Poster, *7th World Congress of Biomechanics*, Boston, July 2014.

Communications lors de congrès nationaux

- Pons C, Brochard S et al. Safety and effectiveness of early intramuscular botulinum toxin injections to prevent shoulder deformity in babies with obstetrical brachial plexus palsy: presentation of a multicentre randomised double blind placebo-controlled trial. Poster, *31ième Congrès de la société de médecine physique et de réadaptation* (SOFMER), St Etienne, Oct 2016.
- Pons C, Sheehan FT, Alter KE, Im HS, Brochard S. Caractérisation tridimensionnelle de l'atrophie musculaire et de ses conséquences sur la force produite par l'épaule des enfants avec paralysie obstétricale du plexus brachial. Oral presentation, *28ième Congrès de la société de médecine physique et de réadaptation* (SOFMER), Reims, Oct 2013.

Ma thèse en 180 secondes

Travaux scientifiques publiés dans des revues internationales en dehors du cadre de la thèse

- Pons C, Rémy-Néris O, Médée B, Brochard S. Validity and reliability of radiological methods assessing the proximal hip geometry in children with cerebral palsy : a systematic review. Dev Med Child Neurol. 2013 Dec; 55(12):1089-102.
- Bourseul JS, Brochard S, Houx L, Pons C, Buée M, Manesse I, Ropars J, Guyader D, Le Moine P, Dubois A. Care-related pain and discomfort in chidren with motor disabilities in rehabilitation centres. Ann Phys Rehabil Medd. 2016 Jun 14.
- Pons C, Brochard S, Gallien P, Nicolas B, Duruflé A, Roquet M, Rémy-Néris O, Garlantezec R. Medication, rehabilitation and health care consumption in adults with cerebral palsy : a population based study. Clin Rehabil. 2016 Aug 9.
- Bourseul JS, Lintanf M, Houx L, Pons C, Chaléat-Valayer E, Brochard S. Botulinum toxin injection in children younger than 2 years old : what safety and effectiveness ? Actualités en MPR. Dec 2016.
- Bourseul JS, Molina A, Lintanf M, Houx L, Chaléat-Valayer E, Pons C, Brochard S. Early Botulinum Toxin Injections in Infants With Musculoskeletal Disorders: A Systematic Review of Safety and Effectiveness. Arch Phys Med Rehabil. 2017 Dec 27. pii: S0003-9993(17)31422-3. doi: 10.1016/j.apmr.2017.11.013.
- Lintanf M, Bourseul JS, Houx L, Lempereur M, Brochard S, Pons C. Effect of ankle-foot orthoses on gait in children with cerebral palsy: a systematic review and meta-analysis. Clin Rehabil. 2018 Apr 1:269215518771824. doi: 10.1177/0269215518771824. PMID: 29714066
- Paradis J, Arnould C, Thonnard JL, Houx L, Pons-Becmeur C, Renders A, Brochard S, Bleyenheuft Y. Responsiveness of the ACTIVLIM-CP questionnaire measuring global activity performance in children with cerebral palsy. Dev Med Child Neurol. 2018 Jun 4. doi: 10.1111/dmcn.13927.
- Roquet M, Garlantezec R, Houx L, Sacaze E, Gallien P, Pons C, Brochard S. From childhood to adulthood: survey of healthcare use in individuals with cerebral palsy. Dev Med Child Neurol.2018 Aug 31. doi: 10.1111/dmcn.14003

UNIVERSITE BIOLOGIE BRETAGNE SANTE LOIRE

UBO Université de Bretagne Occidentale

Titre : Analyse morphologique et biomécanique de l'épaule et du membre supérieur des enfants avec une paralysie obstétricale du plexus brachial: impact sur les thérapeutiques

Mots clés : biomécanique, épaule, membre supérieur, paralysie obstétricale du plexus brachial, thérapeutique

Résumé : La paralysie obstétricale du plexus brachial (POPB) est une parésie d'un ou des membres supérieurs causée le plus souvent par un étirement excessif des racines nerveuses à la naissance. Les enfants sans récupération complète garderont des séquelles à vie, comprenant une diminution de force et des mouvements, des déformations osseuses, impactant leurs activités quotidiennes. L'atteinte de l'épaule est la principale cause de morbidité.
Les muscles gléno-huméraux sont au cœur de la pathologie de l'épaule. L'IRM permet l'évaluation de l'atteinte des muscles de l'épaule. Les volumes musculaires, intéressants du fait de leur corrélation avec la force, peuvent être obtenus par différentes techniques de segmentation dont les propriétés métrologiques sont inégales.
Chez l'enfant avec POPB, l'utilisation d'une technique de segmentation sur un grand nombre de coupes a montré une atrophie variable des muscles gléno-huméraux menant à des déséquilibres musculaires dans les trois plans de l'espace. Des corrélations entre les volumes musculaires et la force, significatives mais plus faibles que chez les enfants à développement typique étaient retrouvées.
Du fait de l'atteinte osseuse et musculaire, la mobilité de l'articulation gléno-humérale est limitée. Dans une étude utilisant l'analyse quantifiée du mouvement, cette limitation, majeure en rotation externe d'épaule ainsi que des compensations au niveau de l'ensemble du membre supérieur ont été objectivées. La performance du mouvement était bonne.
A partir des résultats obtenus différents objectifs et cibles thérapeutiques sont discutés. La lutte contre le déséquilibre musculaire rotateurs internes-externes apparaît comme une priorité.

Title : Morphological and biomechanical analysis of the shoulder and upper limb of children with obstetrical brachial plexus palsy: impact on therapies

Keywords : biomechanics, shoulder, upper limb, obstetrical brachial plexus palsy, therapeutics

Abstract : Obstetric Brachial Plexus Palsy (OBPP) is the paralysis of one or both upper limbs. It is most often caused by excessive traction on cervical nerve roots during a difficult birth. The children without incomplete recovery will have long-term impairment, including loss of active and passive mobility, loss of strength, bony deformities, activity limitation and participation restriction. The loss of shoulder function is the main cause of morbidity in this population.
Glenohumeral muscles involvement is a key element of the pathology of the shoulder. MRI allows evaluation of the shoulder muscle involvement. Muscle volumes in particular, well correlated with muscle strength, can be modified by different segmentation techniques whose metrological properties are unequal.
In children with OBPP, the use of a segmentation technique on a large number of slices has shown a variable atrophy of the gleno-humeral muscles leading to three-dimensional muscular imbalances. Correlations between muscle volumes and strength were significant but lower than in children with typical development.
Because of the bone deformity and muscle involvement, the mobility of the glenohumeral joint is limited. In a study using 3D motion analysis of the movement, this limitation, which is large in external shoulder rotation, as well as compensations on the whole upper limb, were shown. The performance of the movement was good.
From these results, different objectives and therapeutic targets are discussed. Internal-external rotator muscular imbalance correction appears as a priority.